Active corrosion protection of aerospace aluminium alloys by lithium-leaching coatings

Visser, Peter

DOI
10.4233/uuid:dcf9932a-3391-480a-a900-b2697d796d9e

Publication date
2019

Document Version
Final published version

Citation (APA)
Visser, P. (2019). *Active corrosion protection of aerospace aluminium alloys by lithium-leaching coatings*. [Dissertation (TU Delft), Delft University of Technology]. https://doi.org/10.4233/uuid:dcf9932a-3391-480a-a900-b2697d796d9e

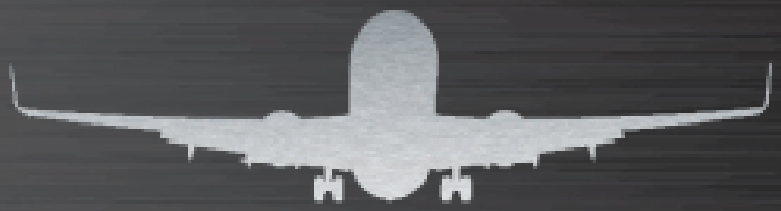

ACTIVE CORROSION PROTECTION OF AEROSPACE ALUMINIUM ALLOYS BY LITHIUM-LEACHING COATINGS

PETER VISSER

ACTIVE CORROSION PROTECTION OF AEROSPACE ALUMINIUM ALLOYS BY LITHIUM-LEACHING COATINGS

PhD thesis

Peter Visser

This research was performed in Delft University of Technology
Department of Materials Science and Engineering
Mekelweg 2, 2628 CD Delft,
The Netherlands

The cover represents the protective layer on the aluminium alloy generated from lithium-leaching coatings.

ACTIVE CORROSION PROTECTION OF AEROSPACE ALUMINIUM ALLOYS BY LITHIUM-LEACHING COATINGS

Proefschrift

ter verkrijging van de graad van doctor
aan de Technische Universiteit Delft,
op gezag van de Rector Magnificus prof.dr.ir. T.H.J.J. van der Hagen
voorzitter van het College voor Promoties,
in het openbaar te verdedigen op woensdag 10 april 2019 om 12:30 uur

door

Peter VISSER
HBO ingenieur Hoger Laboratorium Opleiding
Hogeschool Rotterdam & Omstreken, Delft, Nederland
geboren te Vlaardingen, Nederland

Dit proefschrift is goedgekeurd door de promotoren:
Prof. dr. ir. J.M.C Mol
Prof. dr. ir. H. Terryn

Samenstelling promotiecommissie bestaat uit:

Rector magnificus	voorzitter
Prof. dr. ir. J.M.C. Mol	Technische Universiteit Delft, promotor
Prof. dr. ir. H. Terryn	Vrije Universiteit Brussel, België/Technische Universiteit Delft, promotor

Onafhankelijke leden:

Prof. dr. R.G. Buchheit	University of Kentucky College of Engineering, USA
Prof. dr. M. L. Zheludkevich	Helmholtz-Zentrum Geesthacht, Germany
Prof. dr. ir. J. Sietsma	Technische Universiteit Delft
Dr. M. Beneke	Airbus Operations GmbH, Germany
Prof. dr. U. Staufer	Technische Universiteit Delft, reservelid

Overig lid:

Prof. dr. S.B. Lyon	University of Manchester, United Kingdom

This research was carried out under a research collaboration agreement between AkzoNobel and Delft University of Technology in the Netherlands.

Keywords: Aluminium, Cr(VI)-free, Lithium, Active Protective Coatings, Corrosion Protection, Leaching.

ISBN 978-94-6380-267-3
Coverdesign by: SVDH MEDIA
Printed by: ProefschriftMaken || www.proefschriftmaken.nl

“Look up at the stars and not down at your feet.
Try to make sense of what you see and
wonder about what makes the universe exist.
Be curious……”

Stephen Hawking

Table of Contents

Summary

For decades, scientists and engineers are searching for a safe and environmentally friendly alternative for the toxic chromate corrosion inhibitors in active protective coatings for the protection of aerospace aluminium alloys. In this search many different compounds have been investigated as leachable corrosion inhibitor, but no alternative with equal or better performance compared to chromates has been found yet. In 2010 it was discovered that organic coatings loaded with lithium-salts (Li) as leachable corrosion inhibitor provided very effective and promising corrosion inhibition on aluminium alloys when exposed to industrial accelerated corrosion tests. Initial investigations showed the formation of a corrosion protective layer on the aluminium alloy in a defect area, which appears to be a key feature of these Li-leaching coatings.

The scientific objective of this PhD thesis was to gain a deep understanding of the layer formation mechanism and to link its chemical and physical properties with the corrosion protective performance of these layers when generated in a defect area from Li-leaching coatings. The knowledge and understanding of this mechanism is essential for the future industrial development and implementation of this novel active protective coating technology for the protection of aluminium alloys in the aerospace industry.

The active protective properties of the Li-leaching coating technology were investigated using a combined approach of surface analytical and (local) electrochemical techniques. The study can be divided in three parts: (I) characterization of the chemical composition and morphology of the protective layer, (II) the mechanism of formation, (III) performance properties of the corrosion inhibiting layer. The first part of the investigation involved the characterization of the corrosion protective layer generated in a coating defect when Li-salts are used as leachable corrosion inhibitor in organic coatings. Cross-sectional scanning electron microscopy (SEM) of the protective layer revealed a characteristic three-layered morphology comprising a dense layer near the aluminium substrate, a porous middle layer and a columnar outer layer. High-resolution transmission electron microscopy (TEM) and electron energy loss spectroscopy (EELS) showed that the protective layer mainly consisted of aluminium and oxygen. Lithium was distributed throughout the layer indicating that lithium leached from the coating matrix and was involved in the formation of the protective layer. Based on the characterization a possible mechanism for the formation of such a protective layer was proposed.

With this hypothesis, a combined approach of electrochemical and surface analytical investigations was used to study the formation mechanism of the protective layer in a coating defect when exposed to corrosive conditions and under controlled conditions in an electrochemical cell. Results showed that the formation mechanism of this protective layer have the characteristics of a conversion coating, involving three stages: (I) oxide thinning in the early stages due to the exposure to the corrosive environment (II) anodic dissolution of

aluminium from the matrix and the formation of an aluminium hydroxide gel film on the substrate, followed by (III) film growth through a competitive growth-dissolution process.

The development of the electrochemical properties of the protective layers were studied during the formation and an electrochemical analysis provided a quantitative link between the electrochemical behaviour and the physical model of the protective layer at the different stages of the formation. This study revealed that the corrosion protective properties of the layer originate from the dense inner layer near the aluminium substrate. Complementary analysis with (local) electrochemical techniques demonstrated that the Li-leaching coatings provide fast, effective and irreversible corrosion inhibition resulting in long-term corrosion protection.

The chemical throwing power or the distance over which an inhibitor is able to effectively protect a defect was investigated for the Li-leaching coatings. Coatings with different Li-inhibitors and leaching behaviours were applied on samples with increasing defect widths. Time-of-flight secondary ion mass spectrometry (ToF-SIMS) was applied to investigate the lateral Li-spread and chemical composition of the corrosion protective layers in the defect areas. The results demonstrated that Li-leaching coatings were able to effectively protect defect areas up to about 6mm in neutral salt spray tests. Lithium was detected throughout the protected defect areas. Furthermore, it was found that the surface composition of the protective layer is related to the of lithium-release rate of the coating and the width of the defect. It was demonstrated that only a low amount of leached li-ions is needed to obtain effective corrosion inhibition

Furthermore, the active protective properties of the Li-leaching coatings were investigated on different aluminium alloys with a different electrochemical activity. It was demonstrated that the Li-leaching coatings effectively provided corrosion inhibition on a range of aluminium alloys despite their different physical metallurgy and electrochemical activity by the formation of the protective layer in the defect area.

In this thesis it was demonstrated that Li-leaching coatings possess all the key criteria, such as inhibitor solubility, fast, irreversible and effective corrosion inhibition. The results demonstrate that Li-salts are promising corrosion inhibitors which potentially can become a new class of corrosion inhibitors for the chromate-free protection of aluminium alloys.

Samenvatting

Al tientallen jaren zoeken wetenschappers en ingenieurs naar een veilig en milieuvriendelijk alternatief voor de giftige chromaathoudende corrosie-inhibitoren die worden toegepast in actief beschermende coatings voor aluminium legeringen in de vliegtuigindustrie. In deze zoektocht zijn al veel verschillende verbindingen onderzocht voor de toepassing als uitloogbare (leaching) corrosie-inhibitor, maar tot nu toe is er nog geen geschikt alternatief gevonden met een gelijke of betere corrosiewerende werking als de chromaathoudende corrosie inhibitoren. In 2010 werd ontdekt dat organische coatings geladen met lithium zouten als uitlogende corrosie-inhibitor een zeer effectieve en veelbelovende corrosiebescherming opleverden wanneer aluminiumlegeringen met deze coatings werden blootgesteld aan industriële versnelde corrosietesten. Verkennend onderzoek toonde aan dat er een corrosiewerende laag was gevormd op het aluminium van een beschadigde coating. Deze laagvorming blijkt een kenmerkende eigenschap te zijn van deze lithium-leaching coatings.

Het wetenschappelijke doel van dit proefschrift was om een beter begrip te verkrijgen van het mechanisme van de laagvorming en tevens om een verband te leggen tussen de chemische en fysische eigenschappen en de corrosiewerende werking van deze lagen, gedurende de vorming op het aluminium substraat in een coating defect vanuit de lithium-leaching coatings. De kennis en het begrip van dit vormingsmechanisme is essentieel voor de toekomstige industriële ontwikkeling en implementatie van deze nieuwe actief beschermende coatingtechnologie voor de bescherming van aluminiumlegeringen in de luchtvaartindustrie.

De actief beschermende eigenschappen van deze lithium-leaching coatings zijn onderzocht middels een gecombineerde benadering van oppervlakteanalyses en (lokale) elektrochemische technieken. In algemene zin kan het onderzoek van dit proefschrift in drie delen worden verdeeld: (I) karakterisering van de chemische samenstelling en morfologie van de beschermende laag, (II) het mechanisme van de vorming van de laag, (III) de corrosiewerende eigenschappen van de gevormde laag.

Het eerste deel van het onderzoek richt zich op de karakterisering van de corrosiewerende laag die in een coatingdefect wordt gevormd wanneer lithium zouten worden gebruikt als leaching corrosie-inhibitor in organische coatings. De analyse van dwarsdoorsnedes van de corrosiewerende laag met een scanning elektronen microscoop (SEM) onthulde een karakteristieke morfologie met drie lagen, een laag met een dichte morfologie nabij het aluminiumsubstraat, een poreuze middenlaag en een kolomvormige morfologie aan de buitenzijde van de laag. Met behulp van hoge resolutie transmissie-elektronen microscopie (TEM) gekoppeld met electron energy loss spectroscopy (EELS) was het mogelijk om aan te tonen dat de corrosiewerende laag voornamelijk bestond uit aluminium, zuurstof en lithium. Het lithium was door de hele laag verdeeld, wat erop wijst dat lithium uit de coatingmatrix is geloogd en betrokken was bij de vorming van de

beschermende laag. Op basis van deze karakterisering en observaties werd een mogelijk mechanisme voor de vorming van een dergelijke beschermende laag voorgesteld.
Met deze hypothese is het vormingsmechanisme van de laag bestudeerd met behulp van elektrochemische en oppervlakte-analytische technieken. Eerst werd de vorming van de corrosiewerende laag bestudeerd in een coatingdefect als gevolg van blootstelling aan de corrosieve omstandigheden van een versnelde corrosie test. Tevens werd de vorming bestudeerd onder gecontroleerde omstandigheden in een elektrochemische cel. De resultaten tonen aan dat de vorming van de corrosiewerende laag de karakteristieken heeft van een conversie coating en in het algemeen drie stappen omvat: (I) in het vroege stadium van het proces, het oplossen en dunner worden van de oxide laag als gevolg van de blootstelling aan de corrosieve omgeving (OH^- en Cl^-), (II) anodische oplossing van aluminium van de matrix en de formatie van een aluminium hydroxide gel conversie laag op het substraat, gevolgd door (III) groei van de conversielaag door een competitief groei en oplossingsproces.

De ontwikkeling van de elektrochemische eigenschappen van de corrosiewerende conversie laag werd gevolgd tijdens de formatie en met behulp van elektrochemische analyse was het mogelijk om een kwantitatief verband te leggen tussen het elektrochemische gedrag en het fysieke model van de corrosiewerende laag gedurende de verschillende stadia van de formatie. Deze studie onthulde dat de corrosiewerende eigenschappen van de laag zijn toe te schrijven aan de dichte binnenlaag nabij het aluminium substraat. Complementaire experimenten met (lokale) elektrochemische technieken toonden aan dat de lithium-leaching coatings zorgen voor een snelle, effectieve vorming van een irreversibele corrosiewerende laag resulterend in een langdurige corrosiebescherming.

De chemische throwing power oftewel, de afstand waarover een corrosie-inhibitor een defect effectief kan beschermen, werd onderzocht door formuleringen van de lithium-leaching coatings met verschillende lithium zouten en verschillend uitlooggedrag aan te brengen op panelen en deze te voorzien van defecten met een toenemende breedte. Met behulp van Time-of-flight secundaire ionen massaspectrometrie (ToF-SIMS) was het mogelijk om de laterale lithium distributie en de oppervlakte chemie van de corrosiewerende lagen in de coating defecten te onderzoeken. De resultaten na blootstelling aan de neutrale zoutsproeitest tonen aan dat lithium-leaching coatings in staat zijn om defecten tot een breedte van ongeveer 6 mm effectief te beschermen. Daarnaast werd er lithium gedetecteerd in alle defecten waar de corrosie-werende laag was gevormd. Bovendien is uit dit onderzoek gebleken dat de oppervlaktechemie van de corrosie-werende laag gerelateerd is aan de hoeveelheid lithium die uit de coating kan logen en de breedte van het defect. Uiteindelijk is aangetoond dat er slechts een lage hoeveelheid of concentratie lithium-ionen nodig is om effectieve corrosie-inhibitie te verkrijgen

Tevens werden de actief beschermende eigenschappen van lithium-leaching coating technologie onderzocht op diverse aluminium legeringen met een verschillende fysische metallurgie en elektrochemische activiteit. Hierbij werd aangetoond dat de lithium-leaching coatings in staat zijn om een reeks aluminiumlegeringen effectief te beschermen door de

vorming van de corrosie-werende laag in het coating defect ondanks de verschillende fysische metallurgie en elektrochemische activiteit van deze legeringen.

Dit proefschrift toont aan dat de lithium-uitlogende coatings alle belangrijke criteria bezitten voor actief beschermende coatings, zoals de oplosbaarheid van de inhibitor, snelle, effectieve en irreversibele corrosiebescherming in het coating defect. De resultaten van deze studie laten zien dat lithium-zouten veelbelovende corrosie-inhibitoren zijn die mogelijk een nieuwe klasse van corrosie-inhibitoren kunnen worden voor de bescherming van aluminium legeringen zonder het giftige chromaat.

Abbreviations and acronyms

AA	Aluminium Alloy
AAS	Atomic Absorption Spectrometry
AES	Auger Electron Spectroscopy
at.%	Atomic percent
BE	Binding Energy
BSAA	Boric-Sulphuric Acid Anodising
BTA	Benzotriazole
CAA	Chromic Acid Anodising
CIC	Corrosion Inhibiting Compound
Cr(VI)	Hexavalent chromium
EELS	Electron Energy Loss Spectroscopy
EIS	Electrochemical Impedance Spectroscopy
EC	Electrical Equivalent Circuit
EDS	Energy Dispersive X-ray Spectroscopy
FWHM	Full-width at Half-Maximum
HVLP	High Volume Low Pressure
ISO	International Organization for Standardization
Li	Lithium
Li-LDH	Lithium based Layered Double Hydroxide
Li-PB	Lithium mixed Pseudo Boehmite
MVA	MultiVariate Analysis
NMF	Non-negative Matrix Factorization
MRO	Maintenance Repair and Overhaul
NSS	Neutral Salt Spray test
OEM	Original Equipment Manufacturer
PAA	Phosphoric Acid Anodizing
PB	Pseudo Boehmite
PSA	Phosphoric-Sulphuric Acid anodizing
PVC	Pigment Volume Concentration
R&D	Research and Development
REACH	Registration, Evaluation, Authorization and Restriction of Chemicals
RT	Room Temperature
SAA	Sulphuric Acid Anodizing
SEM	Scanning Electron Microscopy
TEM	Transmission Electron Microscopy
ToF SIMS	Time-of-Flight Secondary Ion Mass Spectrometry
TSA	Tartaric Sulphuric Acid anodizing
VOC	Volatile Organic Compound

Vol. %	Volume percent
Wt. %	Weight percent
XPS	X-ray Photoelectron Spectroscopy
2-MBT	2-mercaptobenzotiazole

Chapter 1

Introduction

1.1 Background and industrial relevance

Aluminium is the most dominant material used in current structural aircraft design because of its lightweight properties and high strength-to-weight ratio. The mechanical, physical and chemical properties of aluminium alloys depend on their composition and microstructure. The desired properties for the intended application can be achieved by the addition of alloying elements in combination with specific mechanical and thermal treatments (tempering).[1] The structural designs of today's aircraft make extensive use of high-strength aluminium alloys such as AA2024-T3 and AA7075-T6. However, the alloying elements used to provide the good mechanical properties also render these alloys susceptible to localized corrosion.[2] Therefore, a corrosion protective scheme is an important element of the aircraft design to prevent corrosion of these alloys and ensure the structural integrity during the service life of an aircraft.[2] The corrosion protective scheme for aerospace aluminium alloys consists of multiple layers, which typically involve a pre-treatment and an organic coating system (Figure 1.1).[3] The corrosion protective scheme forms a physical-chemical barrier between the alloy and the corrosive environment during aircraft operations, i.e. passive protection. However, in case of a damage, the corrosion protective scheme needs to provide active corrosion protection as well.

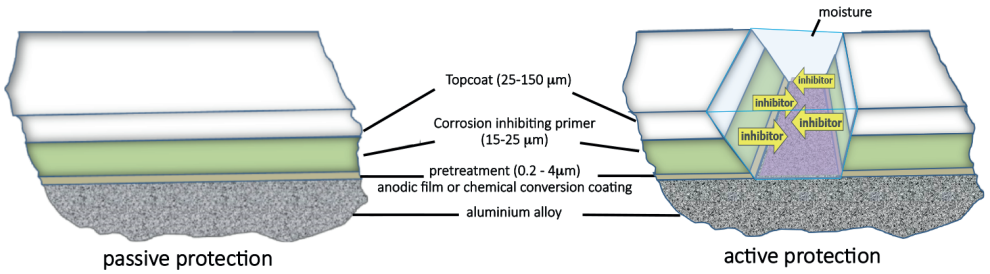

Figure 1.1 *Schematic illustration of the corrosion protective scheme for aerospace aluminium alloys with passive and active corrosion protection*

Leaching is the main active protective mechanism of corrosion inhibiting primers in the aerospace industry. These primers are loaded with sparingly soluble salts to provide a reservoir of corrosion inhibiting ions, which can be released when the coating is subjected to humid conditions. The aerospace industry has been, and still is using hexavalent chromium-based compounds (chromates) as the active corrosion inhibiting material in the corrosion protective scheme.[4] Strontium chromate is a highly effective corrosion inhibitor and therefore widely used as leachable corrosion inhibitor in primers used on the structure and exterior aircraft areas with excellent performance.[5] In case of a defect, the coating will be exposed to the environment and absorb moisture, the chromate inhibitor will be dissolved and released from the coating matrix into the coating defect (Fig. 1.1).[6]

The soluble chromate-ion (CrO_4^{2-}) interacts with the aluminium substrate and suppresses the oxygen reduction reaction and inhibits the corrosion process.[7] However, these hexavalent chromium compounds are toxic and known carcinogens, and need to be replaced by environmentally friendly alternatives. Recent strict international regulations and legislations are putting increasing pressure on the industry to find alternative solutions.[8-10]

The unique properties of hexavalent chromium make the replacement of these chromate inhibitor pigments in organic coatings a very difficult task.[5, 11] Since the early 1990s, many different compounds have been investigated to find a suitable replacement for chromates as leachable corrosion inhibitor in organic coatings.[5, 12] Ideally, these compounds should have at least an equivalent or better performance as chromates. Whilst many approaches have been attempted to achieve acceptable alternatives, no system has demonstrated similar effectiveness as leachable corrosion inhibitor compared to the chromate containing systems. Therefore, the search for suitable alternatives for chromates continues.

In 2010, Visser and Hayes proposed to use Li-salts as a leachable corrosion inhibitor for the potential replacement of chromates in organic coatings for the protection of aluminium alloys.[13] This novel inhibitor-leaching coating technology exhibits a promising performance in industrial laboratory corrosion testing (Fig. 1.2) and might provide a new paradigm for the active protection of aluminium alloys.[14] However, before such a new corrosion inhibiting technology is accepted in the aerospace industry, more fundamental knowledge and understanding about the corrosion inhibition mechanism is of critical importance.

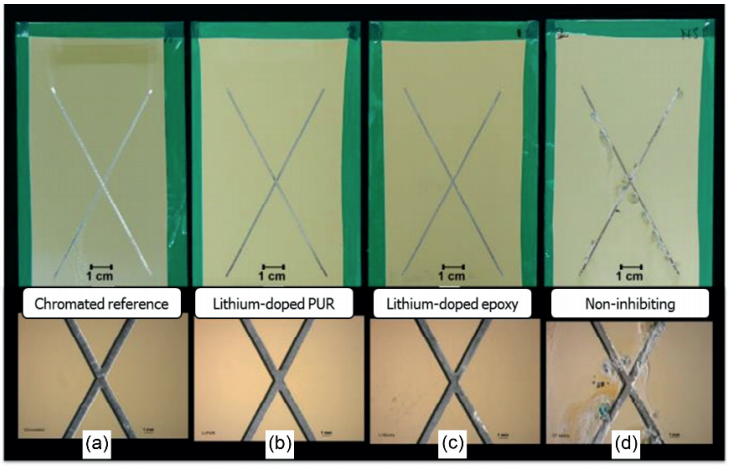

Figure. 1.2 *Optical images of aluminium alloy AA2024-T3 coated with industrial coating concepts after 3000 h neutral salt spray exposure (ASTM B-117). Top: entire panel; bottom: magnification of the defect area: (a) epoxy-amine based chromate-leaching primer, (b) polyurethane based Li-leaching primer (c) epoxy-amine based Li-leaching primer, (d) epoxy-amine based non-inhibiting primer.*

1.2 Lithium and the protection of aluminium alloys

The use of Li-salts for the protection of aluminium alloys is not unknown but has not been studied extensively. Li-salts became of interest for corrosion protection of aluminium after the reports of unexpected passivity of aluminium in alkaline Li-solutions by Gui and Devine in the late 1980s.[15] It was found that, whereas aluminium normally shows a high dissolution rate in alkaline solutions, it surprisingly showed passive behaviour due to the formation of a continuous polycrystalline layer on the aluminium surface.[16-19]

These observations were the basis for the development of a chromate-free chemical conversion coating for aluminium alloys by Buchheit et al. in the 1990s.[19] They suggested that the protective properties of the Li-based conversion layers originate from the Li-aluminium-hydroxide-carbonate-hydrate layer (layered double hydroxide - LDH) generated on the aluminium alloy.[17] Lithium is the only monovalent cation that is known to intercalate in aluminium hydroxide to form these LDHs.[20] This layer greatly increased the corrosion resistance of a range of aluminium alloys. Despite the promising results, the research of these Li-based chemical conversion layers stalled in 2004.

In 2010, Visser and Hayes observed passivation of aluminium alloys in coating defects under corrosive conditions when Li-salts were incorporated as leachable corrosion inhibitor in organic coatings.[13] Similar to Li-based chemical conversion coatings, the corrosion protective properties seem to be provided by the formation of a layer on the exposed aluminium in the defect area (Fig. 1.3)

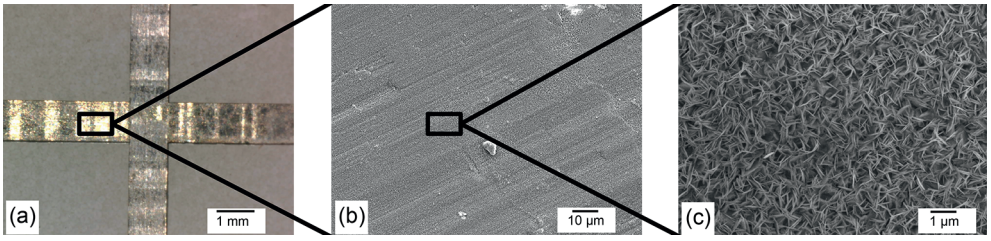

Figure 1.3 *Corrosion protection by Li-leaching coating technology after 168 h NSS exposure: (a) overall visual appearance of the defect area; (b) low-magnification scanning electron micrograph of the surface in defect area; (c) high-magnification scanning electron micrograph of the protective layer in the defect area*

This observation could well be the discovery of a new class of leachable corrosion inhibitors and marks a new episode for Li-salts and the protection of aluminium alloys. Fig. 1.4 illustrates the main stages of the evolution from the first observation of passivity in the late 1980s to the development of Li-leaching coating technology of today. Although, some studies have been performed on the Li-based chemical conversion coatings using electrochemical approaches and corrosion tests, only limited studies have been carried out focusing on detailed morphological and chemical information or corrosion protective properties linked with the layer formation mechanism.

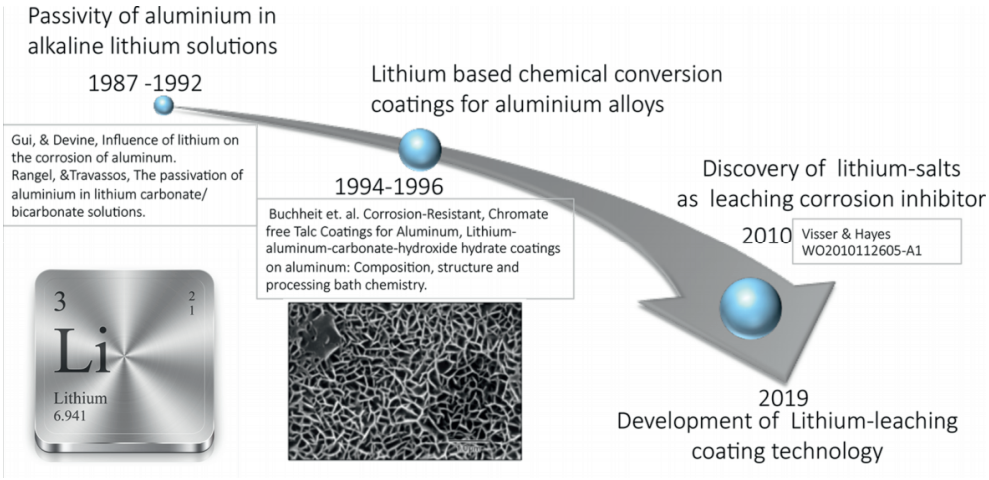

Figure 1.4 *Evolution of the Li-leaching coating technology.*

1.3 Research objective and experimental approach

The overall scientific objective of the research is to investigate the mechanism that provides the Li-leaching coating technology its active protective properties. The obtained knowledge and understanding of this mechanism is essential for the future industrial development of the Li-leaching coating technology and should contribute to the confidence of the aerospace industry to implement this new active protective coating technology and replacing the toxic chromate-leaching coating technology.

The work presented in this thesis addresses the following research questions to provide an enhanced insight into the active protective mechanism and performance of the Li-leaching coating technology:

1. What is the composition of the protective layer?
2. What is the mechanism involved to form the protective layer?
3. What are the protective properties of the generated protective layer?
4. What is the chemical throwing power of Li-leaching coating technology?
5. What is the behaviour of the Li-leaching coating technology on other aluminium alloys?

The investigations of the thesis can be divided in three parts: the *characterization* of layers generated by the Li-leaching coatings, focusing on the corrosion inhibiting ability of Li-salts; the study of the *mechanisms* involved in terms of the inhibition mechanism and the stages of formation of the protective layer and finally the *performance* from coatings investigating the effects of the active protective properties, linking the corrosion protective properties with the physical model of the layer, the chemical throwing power of the Li-inhibitors related

to the leach rate from the coating, and finally the active protective properties on other aluminium alloys than AA2024-T3.

The protective layers were generated using Li-salt solutions under controlled conditions in an electrochemical cell or by exposing Li–leaching model coatings with an artificial coating defect in a corrosive environment such as the neutral salt spray test (ASTM B-117). The generated protective layers were studied with (local) electrochemical, microscopy and surface analytical techniques at different stages of the formation process. This combined approach provided pivotal insights in the active corrosion protection of aluminium alloys by Li-leaching coatings.

1.4 Outline of the thesis

The outline of the thesis is shown in a graphical illustration in Fig. 1.5. An introduction to the background of the research questions and the research approach is presented in Chapter 1. Chapter 2 is the literature review discussing the state of the art of active protective coatings for the protection of aluminium alloys in the aerospace industry. Chapter 3 discusses the first studies and observations of the corrosion inhibiting effect of Li-leaching coatings. The protective layer, formed in a defect from Li-leaching coatings, was characterized in terms of physical morphology, thickness and chemical composition. Based on these observations a possible mechanism was proposed which was the basis for the further investigations presented in this thesis. Chapters 4, 5, and 6 present the studies on the involved mechanisms of the Li-leaching coating technology. Chapter 4 presents a comparative study of the performance of the Li-leaching coatings and organic corrosion inhibitors revealing an essential difference in corrosion protective properties. Chapter 5 focuses on the formation of the protective layer in a defect from a model coating loaded with leaching Li-salts and chapter 6 presents the formation of these protective layers studied in an electrochemical cell under controlled conditions. Chapters 7, 8, and 9 focus on the performance related items of the Li-leaching coating technology. Chapter 7 focuses on the development of the protective properties of the layers in a coating defect during the formation. Chapter 8 discusses the chemical throwing power of the Li-leaching coating technology. Chapter 9 discusses the performance of the Li-leaching inhibitor technology on other aluminium alloys with a different physical metallurgy and electrochemical activity in terms of formation of the protective layers and the protective properties provided. Finally, a general overview, conclusions and recommendations based on the research presented in this thesis are provided in Chapter 10.

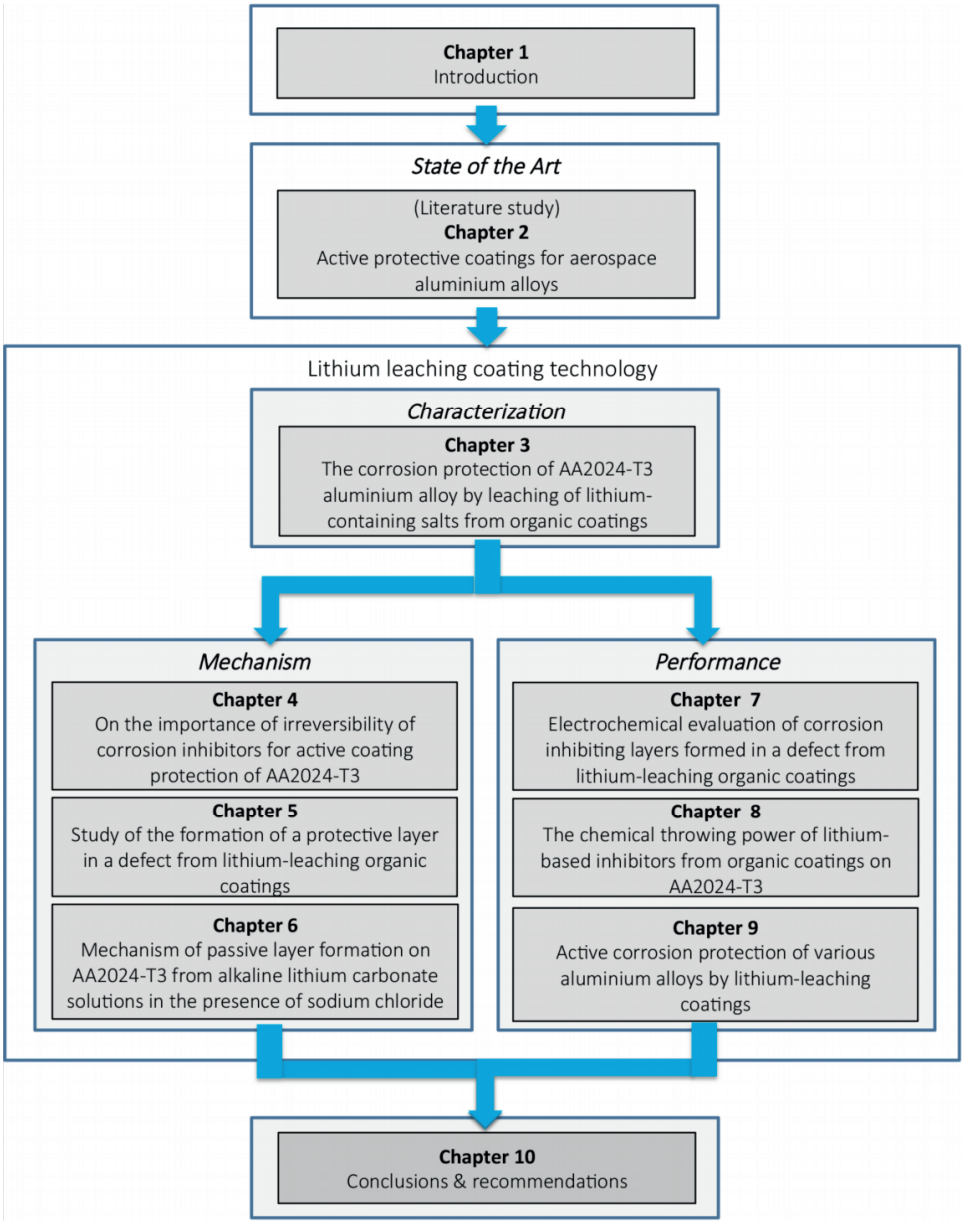

Figure 1.5 Graphic representation of the thesis outline

References

1. J. G. Kaufman, *Introduction to aluminum alloys and tempers*, ASM International, 2000.
2. S. Benavides, *Corrosion Control in the Aerospace Industry*, Woodhead Publ Ltd, Cambridge, 2009.
3. G. Bierwagen, Next generation of aircraft coatings systems, *Journal of Coatings Technology*, 2001, 73, 45-52.
4. A. K. Chattopadhyay and M. K. R. Zentner, *Aerospace and Aircraft Coatings*, Federation of Societies for Coatings Technology, 1990.
5. J. Sinko, Challenges of chromate inhibitor pigments replacement in organic coatings, *Progress in Organic Coatings*, 2001, 42, 267-282.
6. F. H. Scholes, S. A. Furman, A. E. Hughes, T. Nikpour, N. Wright, P. R. Curtis, C. M. Macrae, S. Intem and A. J. Hill, Chromate leaching from inhibited primers. Part I. Characterisation of leaching, *Progress in Organic Coatings*, 2006, 56, 23-32.
7. G. O. Ilevbare and J. R. Scully, Oxygen Reduction Reaction Kinetics on Chromate Conversion Coated Al-Cu, Al-Cu-Mg, and Al-Cu-Mn-Fe Intermetallic Compounds, *Journal of The Electrochemical Society*, 2001, 148, B196-B207.
8. M. Costa and C. B. Klein, Toxicity and carcinogenicity of chromium compounds in humans, *Critical Reviews in Toxicology*, 2006, 36, 155-163.
9. P. National Toxicology, NTP 12th Report on Carcinogens, *Report on carcinogens : carcinogen profiles / U.S. Dept. of Health and Human Services, Public Health Service, National Toxicology Program*, 2011, 12, 106 - 109.
10. U. P. H. Service, Toxicological Profile for Chromium, *Report No. ATSDR/TP 88/10*, 1989.
11. M. W. Kendig and R. G. Buchheit, Corrosion inhibition of aluminum and aluminum alloys by soluble chromates, chromate coatings, and chromate-free coatings, *Corrosion*, 2003, 59, 379-400.
12. R. L. Twite and G. P. Bierwagen, Review of alternatives to chromate for corrosion protection of aluminum aerospace alloys, *Progress in Organic Coatings*, 1998, 33, 91-100.
13. P. Visser and S. A. Hayes, Low-temperature-curable coating composition useful as anticorrosive primer coating for non-ferrous metal substrates, particularly aluminum or aluminum alloy, comprises film-forming resin, curing agent, and lithium salt, *patent nr. WO2010112605-A1*, 2010.
14. P. Visser, Y. Liu, H. Terryn and J. M. C. Mol, Lithium salts as leachable corrosion inhibitors and potential replacement for hexavalent chromium in organic coatings for the protection of aluminum alloys, *Journal of Coatings Technology and Research*, 2016, 13, 557-566.
15. J. Gui and T. M. Devine, Influence of lithium on the corrosion of aluminum, *Scripta Metallurgica*, 1987, 21, 853-857.
16. C. M. Rangel and M. A. Travassos, The passivation of aluminium in lithium carbonate/bicarbonate solutions, *Corrosion Science*, 1992, 33, 327-343.
17. C. M. Rangel and M. A. Travassos, Li-based conversion coatings on aluminium: An electrochemical study of coating formation and growth, *Surface & coatings technology*, 2006, 200, 5823-5828.
18. R. G. Buchheit, Bode, M.D., Stoner, G.E., Corrosion-Resistant, Chromate free Talc Coatings for Aluminum, *Corrosion*, 1994, 50, 205-214.
19. C. A. Drewien, Eatough, M.O., Tallant, D.R., Hills, C.R., Buchheit, R.G., Lithium-aluminum-carbonate-hydroxide hydrate coatings on aluminum: Composition, structure and processing bath chemistry, *Journal of material research*, 1996, 11, 1507-1513.
20. M. Frenkel, A. Glasner and S. Sarig, Crystal modification of freshly precipitated aluminum hydroxide by lithium ion intercalation, *The Journal of Physical Chemistry*, 1980, 84, 507-510.

Chapter 2

Active Protective Coatings for Aerospace Aluminium Alloys

Chapter 1 introduced the research questions related the use of Li-salts as leachable corrosion inhibitor in organic coatings for the protection of aluminium alloys. Corrosion control is an important aspect in the aerospace industry. Therefore, active protective coatings are an important part of the corrosion protection scheme within the aircraft design. This chapter provides an overview of the state of the art in the field of aerospace coatings. It discusses the different types of coatings and their role in the corrosion protection scheme. Active corrosion protection is a key feature of these coatings. Today, the industry is facing an enormous challenge because the toxic chromates need to be replaced by environmental-friendly alternative corrosion inhibitors. This chapter provides a review of the challenges and developments towards hexavalent chromium-free coating systems and it provides insight in the current status and trends in the industry of aerospace coatings and discusses the new approaches and corrosion inhibiting strategies towards chromate-free active protective coating systems.

This chapter was published as a book chapter:
P. Visser , H.A. Terryn, J.M. Mol, Aerospace Coatings, in: A.E. Hughes, J.M. Mol, M.L. Zheludkevich, R.G. Buchheit (Eds.) Active Protective Coatings, New-Generation Coatings for Metals, Springer, Netherlands, 2016, pp. 315-372

Abstract

Aircraft are complex multi-material structures that are optimized for strength to weight ratio, fatigue properties and operational performance. Corrosion control is an important aspect in the aerospace industry. Therefore, active protective coatings are an important part of the corrosion protection scheme within the aircraft design. This chapter provides an overview of the field of aerospace coatings, the different types of coatings and their role in the corrosion protection scheme. Active corrosion protection is a key feature of these coatings. For decades, the aerospace industry has been relying on hexavalent chromate as active corrosion inhibiting species. The industry is facing an enormous challenge because this toxic material needs to be replaced by environmental-friendly alternatives. This chapter provides a review of the challenges and developments towards hexavalent chromium free coating systems and it provides insight in the current status and trends in the industry of aerospace coatings and discusses the new approaches and corrosion inhibiting strategies towards chromate-free active protective coating systems

2.1 Introduction

Since the first flight of Orville and Wilbur Wright on Dec. 17, 1903, the aviation industry evolved from pioneers that wanted to fly, into a global high-tech engineering industry that enables transport and travel around the world, with an impressive safety record. Aviation has become an integral part of society; it brings people closer together, contributes to economic growth, and plays an important role in today's global economy. As air travel continues to grow and new business models expand, the evolution of the industry continues and provides new aircraft designs and construction materials. Over the years, aircraft design evolved from wooden structures covered with fabric into complex multi-material models optimized in terms of strength to weight ratio, fatigue, aerodynamics and operational performance.

Aerospace coatings play an important role in aircraft design. They have a decorative role, but an active protective function as well. Coatings for aircraft must cope with extreme conditions. In daily service they have to withstand rapid temperature changes when taking off for example from the desert at +50°C, and climbing to a cruising altitude of 10 kilometre with temperatures as low as -55°C and high levels of UV irradiation. On the other hand these coatings need to withstand repeated dry and wet cycles due to condensation, erosion and impact effects, the vibrations of the engines and structural flexing due to turbulence, pressurizing effects and wing movements. In addition to this, the coating systems are from time to time exposed to various fluids and chemicals, such as de-icing fluids, aviation fuel, cleaning chemicals, and hydraulic fluids. Last but not least, other environmental stresses such as accumulated dirt and potentially corrosive salts from coastal and maritime environments, and acids formed by industrial air pollution and volcano eruptions have a detrimental effect on the coating system integrity.[1]

Each aircraft is exposed to unique conditions during its operational life. For example, long haul with low cycles or regional service with many cycles and the operational route (transatlantic or continental, northern hemisphere or southern hemisphere) and geographical areas (Europe or South-East Asia). Whereas commercial aircraft may fly up to 4000 hours per year, defence aircraft or business jets can have only limited flight time. Some aircraft are even parked in the desert for a significant period of time. Despite all these factors and impacts originating from the in-service environment the aircraft needs to be colourful and glossy on the outside and the coating systems should protect the structure against corrosion for the entire service life. Aerospace coatings have been designed to address these specific needs of this highly regulated and demanding industry.

2.2 Aerospace market

The Aerospace coatings market can be divided in four segments: commercial passenger aircraft, defence aircraft, general aviation and space. The first two markets account for most of the sales and volume of the market. The commercial segment is a growing segment whereas the military and defence market is expected to decline over the coming years.[2] The general aviation market produces private and business jets and depends strongly on the economical climate and is slowly recovering after production dropped from 4277 units in 2007 to about 2100 per year in 2012.[3]

According to the long-term outlook of large commercial aircraft manufacturers, air travel will keep growing together with the expansion of the world's aviation network and connectivity and more capacity between major populations centres. Based on this, they produce between 27000 and 34000 commercial aircraft in the coming 20 years.[4, 5] The in-service fleet of 20.341 commercial aircraft with a capacity of more than 100 passengers is expected to grow an average of 3.6 % per year to double its size to more than 41.000 aircraft by 2032. Growth of passenger travel in Asia and Middle East and the need for more fuel-efficient aircraft are driving this growth. Over a 23-year period the 7-year moving average of aircraft deliveries grew from 500 to more than 1000 in 2013 and is expected to grow even further.[2]

The aerospace coatings business has evolved to a global business. All segments have their Original Equipment Manufacturers (OEM's) and Maintenance, Repaint and Overhaul (MRO) facilities. In addition to their final assembly lines, OEM's have an extensive network of contractors and subcontractors all over the world that supply a variety of parts and assemblies. These suppliers must apply coatings specified by the OEM's. Most airlines repaint their aircraft every 5 to 7 years of service during maintenance intervals or for rebranding purposes. Considering the average service life of an aircraft being more than 20 years, the volume of paint for this MRO business is significant.[6]

Historically, the final assembly lines of the OEM's were concentrated in Europe and North America. Now, manufacturing and maintenance operations are moving to Asia and South America to take advantage of the lower labour costs. In particular the aerospace industry of China is growing rapidly in terms of airline operations, maintenance and aircraft production.[7]

2.3 Corrosion control in the aerospace industry

Air transport plays an important role in the world's economic activities. Safety is a key element next to efficient and environmentally sustainable operations on regional and global level. Due to many safety management programs and systems that are based on risk management principles, the safety record of the industry dramatically improved, with 2013, as the safest year ever in terms of fatalities for scheduled international air transport

operations.[8] Despite this achievement corrosion control remains a very important aspect of the aerospace industry. The cost of corrosion is a significant percentage of the total aircraft maintenance costs.[9] In addition to this, corrosion impacts safety and aircraft availability. Corrosion compromises the structural integrity of aircraft structures and in the event of corrosion consequences can be dramatic. In the design phase of an aircraft many requirements such as weight, aerodynamics, fatigue and fuel properties are determined. An aircraft design comprises many dissimilar metals, complex geometrical structures, joining techniques and many difficult-to-inspect areas. Corrosion is a very important but difficult parameter to take into account because the prediction of corrosion initiation and extent of structural damage is hard to determine. Despite advances in corrosion knowledge, computational design capabilities, maintenance data analysis and simulations, there is no reliable model for predicting corrosion.[10]

Aircraft structures are exposed to a number of stresses and conditions depending on the operating environment of the aircraft. The aircraft is designed to resist various types of corrosion through selection of the proper materials, alloys, tempers, pre-treatments, coating systems (defined as the corrosion protective scheme), and the use of drainage points, sealants and corrosion inhibitors. These designs are based on knowledge and experience of what causes corrosion and the types of corrosion that occur in airplane structures. In addition to this design, a corrosion control program is needed throughout the service life of the aircraft. This is essential to control corrosion to a predictable, manageable level that does not degrade structure or jeopardize the ability of the airplane to carry its intended design loads. The use of the current corrosion schemes and corrosion management programs it has made it possible for aircraft to operate beyond their designed life without compromising safety performance.

2.3.1 Introduction to the corrosion protection scheme

The corrosion protection scheme is a key element of the aircraft design. Each part of the structure has several protecting layers to ensure the structural integrity during the service life. In general it can be stated that the 'state of the art' corrosion protection scheme is applied on top of the substrate, commonly aerospace aluminium alloys, and consists of two or three layers, which typically is a pre-treatment and a coating system. The pre-treatment can be a chemical conversion coating, wash-primer or an anodic film (anodising layer). Whereas, the second layer is an organic coating, which can be a primer or a primer-topcoat system. The main function of such a corrosion protection scheme is to act as a barrier between the alloy and the operating environment (passive protection). In addition, the corrosion protection scheme needs to provide active corrosion protection, by the ability to release an inhibitor (leaching mechanism) to provide corrosion protection in case this barrier is damaged. Today, this leaching mechanism is a key feature in active corrosion protection mechanism of the state of the art corrosion protective scheme. This means, when the corrosion protective scheme is damaged and the substrate is exposed to the environment, the inhibitor dissolves from the coating due to moisture ingress and will be transported to

the exposed or damaged area and forms a new barrier layer and protects the alloy from the aggressive environment and corrosion.

For decades, the aerospace industry has been, and still is relying on hexavalent chromium-based (Cr (VI)) compounds (chromates) as active corrosion inhibiting material for the corrosion protection of the structures. These hexavalent chromium compounds are used in many processes such as: deoxidizers, anodizing processes, conversion coatings, sealants and organic coatings. The corrosion inhibition mechanism of these compounds has been studied extensively.[11] Their solubility combined with the ability to act as both an anodic or cathodic inhibitor and the complex oxidation/reduction chemistry, provide them with unique properties to inhibit corrosion on ferrous and non-ferrous metals at low concentrations and over a wide pH range. Chromates have a proven track record for many years. They are not perfect, but over the years, the industry has based all the designs, specifications, processes, and corrosion management programs around the solid performance of this class of inhibitors. Unfortunately, these hexavalent chromium compounds are toxic and proven to be carcinogenic.[12] Hence, elimination of these compounds has been an important topic for more than 20 years.[13]

Aluminium alloys used in aerospace

Aluminium is the most dominant substrate in aircraft design, because of its lightweight properties and high strength-to-weight ratio. The mechanical, physical and chemical properties of aluminium alloys depend on the composition and microstructure. The addition of selected alloying elements in combination with the mechanical and thermal treatments (tempering) provide the desired properties for the intended application of the aluminium alloy.[14] Wrought alloys such as AA2024 and AA7075 are most commonly used for the legacy aircraft. The first digit of the alloy indicates the major alloying element. This is copper for AA2024 and zinc for AA7075. The second digit indicates modifications from the original alloy and the last two digits identify the specific alloy. The alloy designation is followed by a temper designation, for example T3 or T6. This designates the heat treatment used. T3 is solution heat treated, cold worked, and naturally aged. The T6 temper is solution heat treated and artificially aged.[15-17] AA2024 is mainly used for the fuselage skin and frame along with other structural parts; AA7075 is often used for a wide variety of structural parts.

The addition of alloying elements such as copper and zinc to aluminium has significant benefits for the strength-to-weight ratio but it also reduces the corrosion resistance. The heterogeneous microstructure of these aluminium alloys, crystallography, grain size and shape residual stresses and intermetallic particles, plays an important role in the reduced corrosion resistance of these alloys. In recent years, understanding of the microstructure and the influence on corrosion of high strength aluminium alloys advanced significantly.[18]

Weight reduction is one of the most important driving forces in new aircraft design.[19] Reduced weight improves fuel consumption, increases payload and range. New construction materials should also provide improved and optimised mechanical properties to increase maintenance intervals and reduced repair costs. Reduction of the material density is the

most effective way to reduce the weight of the aircraft. Hence, composites and fibre metal laminates (GLARE) have been introduced and new alloys are being developed. Although, the use of composite in new aircraft models reduced the role of high strength aluminium alloys to some extend, the aluminium alloys remain important in the aircraft design due to their low cost, lightweight properties and easy low cost workability. Besides the 2000 and 7000 series, the 3rd generation aluminium-lithium (Al-Li) alloys are finding their application in the new aircraft designs. This new generation of alloys provides weight savings, but also higher strength and improved fracture toughness. Al-Li 2199 is used for the fuselage and lower wing applications. Al-Li 2099 is used for extrusions for the internal structure.

Table 2.1: Chemical composition of some Aluminium alloys.[19]

Alloy	Cu	Zn	Li	Mg	Mn	Fe	Si	Cr	Zr	Ti	Al
2024	4.4	-	-	1.5	0.6	≤0.5	≤0.5	0.1		0.15	Balance
7075	1.2-2.0	5.1-6.1	-	2.1-2.9	0.3	0.5	0.4	0.18-0.28	-	0.2	Balance
2099	2.4-3.0	0.4-1.0	1.6-2.0	0.1-0.5	0.1-0.5	0.07	0.05	0.1-0.5	0.05-0.12	0.1	Balance
2199	2.0-2.9	0.2-0.9	1.4-1.8	0.05-0.4	0.1 -0.5	0.07	0.05	-	0.05-0.12	0.1	Balance

Surface treatment of aluminium

The surface treatment is the first step of the corrosion protective scheme after the selection of the alloy. These treatments are the first defensive layer to protect the substrate from the environment and are the foundation for the second step, application of the organic coating. Typically, three types of treatments are being used in the aerospace coatings industry, chemical conversion coatings, anodising and wash primers. Each of them has its specific characteristics and application properties. Their use has been specified in specifications and application manuals. These treatments are mostly used in combination with a coating but provide stand-alone corrosion protection as well.

Chromated chemical conversion coatings have been an important part of the corrosion protective scheme for commercial and military aircraft for many decades. These coatings provide a thin protective layer on the substrate generated by a chemical reaction of the chemical conversion solution and the metal. The layer is a very good base for paint adhesion and it provides good stand-alone corrosion protection. Chemical conversion coatings can be applied by dipping, spraying and no-rinse processes.

The chromated chemical conversion process has been studied extensively to resolve the mechanism.[20] When the chemical conversion solution is applied on the aluminium, a redox process forms the chemical conversion film. In this process aluminium is oxidized and hexavalent chromium (Cr^{6+}) is reduced to Cr^{3+} and the coating formation evolves by hydrolysis, polymerization, and condensation of Cr^{3+}, triggered by the pH increase near the surface of the aluminium alloy.[21, 22] Fluoride species are added to the conversion solutions to activate the aluminium and to prevent re-passivation of the surface. Higher concentrations of fluoride (F^-) activate the surface faster and results in a thicker conversion coating in the same time.[23] Studies demonstrated the inclusion of Cr^{6+} in the chemical conversion coating.[22, 24] This inclusion is thought to be the reason for the excellent corrosion protective properties and the "self-healing" nature of these chromated chemical conversion coatings.

The model for self-healing activity assume the leaching or diffusion of Cr^{6+} species from the chemical conversion film to cracks or other damages whereas it forms a chromate corrosion product consisting of an Al^{3+} and Cr^{3+} mixed oxide which repassivates the damaged area.[25] This storage, release, diffusion and inhibition are essential to the excellent corrosion protective properties of these chromated chemical conversion coatings.

Anodising of aluminium alloys is another common treatment in the aerospace industry.[26] This electrochemical process converts the surface of the aluminium surface to a strong and stable aluminium oxide with a porous morphology. These porous aluminium oxide films provide very good corrosion protection and wear properties. Also, it serves as a good foundation for adhesive bonding and adhesion of organic paint films.

Such an anodic layer is typically 2-5 μm thick and consists of millions of pores per cm^2. The film has a thin non-porous barrier layer of 10-50 nm thick. On top of this layer there is the porous structure with a close packed hexagonal (honeycomb) cell arrangement, each cell consists of an amorphous anodic alumina with a central pore. The pore and cell dimensions can be influenced by selection of the anodizing electrolyte and the anodizing parameters, such as pH, time, temperature, current density, and voltage etc.[27] The desired morphology and anodic film characteristics depend on the properties needed for the application, for example adhesion bonding, painting or stand-alone corrosion protection.

There are many types of anodising processes. In the aerospace industry, chromic acid and sulphuric acid electrolytes are widely used for the protection of aircraft parts. Chromic Acid Anodising (CAA) provides excellent corrosion protection with a relative thin coating and without significant fatigue loss of the material.[28] Sulphuric Acid Anodising (SAA) and Phosphoric Acid Anodising (PAA) are frequently used as well. Boric sulphuric acid electrolytes have been introduced to overcome the fatigue issues, which has been the main drawback of the tradition sulphuric acid anodising processes. Tartaric Sulphuric acid (TSA) and Boric Sulphuric acid anodising (BSAA) have been introduced as a replacement of the hexavalent chromium CAA process.

In some cases, anodised parts are subjected to a sealing procedure. Sealing in hot water or hot dilute dichromate solution will convert the amorphous aluminium oxide to a monohydrate. This process partially or fully closes the pores and enhances the corrosion resistance. However, sealed anodized layers are not very suitable for adhesive bonding or coating adhesion. If painting or bonding is required, the sealing step must be eliminated or carefully controlled to ensure good adhesion. Anodising is much more expensive than a chemical conversion process and not suitable for all types of parts. Critical structures are often anodized for maximum corrosion protection.

Wash primers, also known as etch primers, have been used as metal conditioner and alternative to the “wet” chemical conversion process. Polyvinyl butyral based wash primers have been used extensively on military and commercial aircraft. The reactions of a curing chromated wash primer are complex. They are available in two component and one-pack systems. A typical two-component wash primer consists of a base component and an

activator. The base component contains: polyvinylbutyral, zinc tetraoxychromate, talc, and solvents such as isopropanol and butanol. The activator is a solution of water isopropanol and phosphoric acid.[29] Upon mixing of the base with the activator many different reactions take place that are unique for this chemistry and make it very difficult to develop alternative chromate free formulations. Wash primers were mainly used in repair schemes and in the maintenance area for the repainting of commercial aircraft using chromated or chromate-free epoxy or urethane intermediate primer over it. Various wash primer systems are qualified according to maintenance specifications. However, the use of wash primers has declined over the recent years due to the introduction of new pre-treatments and coating solutions.

Organic coatings

The organic coatings are the last part of the corrosion protection scheme. They act as the first barrier against the environmental conditions and need to fulfil a wide range of functions. Secondly, they have to be able to actively protect the substrate when a damage, crack or delamination occurs. Typically, the organic coating is applied in one (primer only) or two (primer/topcoat) layers. The primer is designed to maintain adhesion on the various treatments and contains corrosion inhibitors for active corrosion protection. Their composition has been carefully formulated to ensure the performance throughout the service life of the aircraft. In other cases, a second layer (top coat) is applied to the corrosion protective scheme. This topcoat can have a decorative or an additional protective function. Together with the pre-treatment, the coating system protects the substrate or alloy against environmental effects. There are many different coating systems specified in an aircraft design. For example, a fuel tank coating system has a different build-up and requirements differ compared to exterior decorative systems. The specific requirements of each coating system are defined in specifications.

2.3.2 Types of corrosion and failures

Corrosion occurs in many forms on the aircraft structure. These complex phenomena, although mechanistically different, are similar in terms of their potential effects in reducing the structural integrity. The corrosion processes of the aluminium in the aerospace industry are electrochemically driven. The local electrochemical potential differences at the alloy surface create the driving force for corrosion initiation.[30-32] Active spots become anodes, whereas the more noble areas act as a cathode. The form of corrosion is influenced by factors such as alloy and temper used, environmental conditions, corrosive agents present, geometry, design, and mechanical loading. The various types of corrosion are briefly discussed below.

Filiform corrosion is a very common type of corrosion in aircraft structures. This worm-like type of corrosion occurs between the metal and the polymeric coating. It initiates at a crack or rupture around a rivet head or lap joint under acidic, chlorine- rich and humid conditions. Once initiated, the propagation is determined by anodic undermining.[33] In

addition to the environmental effects, filiform corrosion is also affected by the microstructure of the aluminium alloys and the properties of the applied coating system.[34]

Pitting corrosion is another type of corrosion that occurs frequently in aerospace structures. It is different from general corrosion because of the absence of measurable material thinning. This is an extremely localized form of corrosion that results in holes and pits that penetrate in the structure and leads to degradation of the structural capabilities. The typical 2000 and 7000 series aluminium alloys used in the aerospace industry are susceptible to pitting corrosion and therefore have been widely studied.[35-41] These studies have led to improved knowledge on the nucleation of pits on high strength alloys such as 2024. However, the establishment and propagation of stable pits is still being investigated.

Intergranular corrosion and to a greater extent *exfoliation* corrosion typically occurs on 2000 and 7000 series high strength aluminium alloys.[42-44] Especially, the aluminium alloy 7075 is susceptible to intergranular and exfoliation corrosion, this alloy contains both significant levels of copper and zinc. Due to processing and heat treatments copper and/or zinc accumulate at the grain boundaries. These grain boundaries preferentially corrode because of the galvanic couple between the grain bodies and boundaries and the anodic behaviour of aluminium towards copper. Intergranular corrosion can start at a pit, second phase intermetallic particle or at grain boundaries at the surface and it penetrates much faster into the alloy compared to pitting corrosion. Exfoliation corrosion has a very characteristic appearance of leafing aluminium layers due to corrosion of a very elongated and flattened grain structure parallel to the alloy surface due to the rolling. Exfoliation corrosion originates from intergranular corrosion at the edges of riveted and bolted aircraft components. The susceptibility to exfoliation corrosion can be reduced by the modification of the annealing process to obtain a more favourable distribution of precipitates.[45, 46]

Stress corrosion cracking (SCC) or environmental assisted stress corrosion can be one of the most destructive types of corrosion.[47-49] This form of corrosion causes a loss of load-carrying capability from the combined effect of tensile stress and corrosion. There are two forms of SCC: intergranular and transgranular SCC. Aluminium alloys typically show intergranular SCC. Under corrosive conditions (humid environments with chloride) stress corrosion is initiated rapidly and follows the grain boundaries in aluminium alloys. There are two mechanisms proposed for SCC: anodic dissolution and hydrogen embrittlement. However, the exact mechanisms have not been resolved yet, despite extensive work in modelling of SCC and elucidating microstructural features along grain boundaries that influence stress assisted corrosion. The most effective way to control this kind of corrosion is to use materials that are not susceptible to SCC at design stress levels and protection from corrosion initiation by coatings and excluding electrolytes.

Crevice corrosion or concentration cell corrosion is the most common type of corrosion in aircraft.[47] It occurs when moisture is trapped between surfaces. This can be at fasteners, delaminated paint, and unsealed joints or within a delaminated bond line. This type of corrosion is aggressive and can initiate pitting and exfoliation corrosion depending on the alloy, temper and form of the material that is affected. It is driven by a differential

concentration mechanism.[50] The most effective way to prevent crevice corrosion is to avoid water penetration by the application of sealants and water-displacing corrosion inhibiting compounds.[51]

The aircraft design does not only contain aluminium alloys but also many dissimilar materials like: titanium, magnesium, stainless steel and composites. Without proper protection the combination of these dissimilar materials can lead to *galvanic corrosion*. This occurs when two dissimilar materials are connected in the presence of an electrolyte. Recent aircraft designs use more and more carbon-reinforced plastics. These composite materials can induce galvanic potential differences due to the very conductive carbon fibres in the material. When joined to the aluminium structure, composite materials can act as cathodes and accelerate the electrochemical dissolution of the aluminium. The rate of corrosion depends on the surface ratio between the cathode and the anode design geometry. A large cathode surface area with respect to the anode surface area can lead to fast and severe corrosion. The only one way to prevent galvanic corrosion is to prevent direct contact of the dissimilar metals and the ingress of moisture (electrolyte). This can be done with the use of a physical barrier in the form of a coating, sealant and/or corrosion protection compounds (CPC's).

2.3.3 Corrosion protection and design

Corrosion can be initiated by many sources and affect the aircraft structure. These sources can be identified at the manufacturer and operator levels.[50] The basic design combined with manufacturing and processing are the most important factors in corrosion protection at the manufacturing level. At the operator level there are different factors that potentially could initiate corrosion of the structure, among them improper maintenance, deterioration of the coating system, operational environment, accidental contaminations, and the environmental conditions in the aircraft.
Corrosion can initiate when the following three parameters are present:

- A cathode and an anode
- A metallic connector between the anode and cathode
- An electrolyte (water)

Elimination of these three conditions is limited by feasibility, practicality, and functionality. Each part of the aircraft is designed to withstand the stresses and operating environment for the service life of the aircraft.

Therefore, 6 key elements need to be considered when designing for corrosion control:

- Selection of materials
- Coating system
- Sealants
- Corrosion inhibiting compounds
- Avoidance of contact between dissimilar metals
- Drainage
- Access for maintenance

For the *material selection*, the design considers many parameters such as, alloy, shape, weight to strength ratio strength, durability and fatigue properties. Whereas the high-strength aluminium alloys are used most widely in the aircraft design, coupling to other materials like Titanium (6-AL-4V), Magnesium, Stainless steel, low alloy, high strength carbon steel, and increasing amounts of Carbon Fibre-Reinforced Plastics (CFRP) can set up galvanic corrosion cells which need to be eliminated in the design stage.

The *coating system* is a key element to protect the selected material from the operating environment. This barrier typically consists of multiple layers. This may include anodised layer or chemical conversion coatings that are coated with corrosion inhibiting primers. Exterior surfaces and some structural areas are coated with chemical resistant topcoats. Titanium alloys are anodized or coated and stainless steel is most commonly cadmium plated before being primed. The active protective primers are a key element in the protection scheme and will be discussed in more detail.

It is not always possible to avoid dissimilar metal contact, crevices and the use of specific alloys because of weight, cost, and functional issues. However, the potential for corrosion can be minimized by using polysulfide *sealants* that are typically applied to faying surfaces of the joints to prevent moisture ingress leading lap joint or crevice corrosion or to prevent dissimilar metal contact. They are applied at many connections like stringer to stringer and skin-to-shear tie joints, skin splices and skin doublers and pressure bulkhead In addition to this, exterior fasteners and fasteners that penetrate pressurized areas are installed with a sealant.

Moisture cannot be eliminated during operations. Therefore, it needs to be controlled by *drainage* and *corrosion-inhibiting compounds* (CIC's). Drainage of the aircraft structure by the use of drain paths, drain holes is important to prevent entrapment of moisture and corrosive fluids in crevices and lower fuselage area. The design is optimized to direct the fluids towards the drain holes. CIC's are used to provide additional corrosion protection. These CIC's are petroleum based water-displacing compounds with corrosion inhibitors and are sprayed on the structure to penetrated faying surfaces. The CIC's are applied in areas that are prone to corrosion (lower fuselage). Low viscosity CIC's are able to penetrate crevices and displace water, whereas viscous CIC's will act as a coating.

The features discussed above must ensure a safe and economical service life. However, the aircraft design must ensure easy access for maintenance and corrosion inspections as part of a *corrosion management/maintenance program*. Corrosion cannot be eliminated but, timely inspections will help to detect corrosion, trapped moisture, plugged drain-holes, and chipped or missing paint at an early stage and combined with sealant and CIC's applications much corrosion can be prevented.

2.4 Introduction into aerospace coatings

Aerospace coatings serve as decorative and protective layers for all types of passenger, freight and military aircraft. The systems evolved over the years from very simple formulations into complicated materials with specific functions and an important role in the corrosion protective scheme of today's aircraft industry. Three types of coating systems can be recognized. The exterior decorative system, which provides image and recognisability, Structural coatings that are an integral part of the corrosion protection scheme, and finally the special purpose systems. Each of these coating systems has their own requirements and must be able to withstand a wide range of stresses during their operational life.

2.4.1 History of aerospace coatings

In the early days, 1910, the first aircraft were painted with colourless single component cellulose lacquers to provide tension to the linen (fabric). Around 1915, pigmented or coloured coatings were introduced to provide camouflage for military aircraft during World War I. Up to 1935, aircraft were mainly constructed from wood, linen and steel. Cellulose lacquers and alkyd enamels were mainly used as coatings for the protection of these aircraft. Around 1935, the first metal aircraft were designed. New coatings were developed to protect these aircraft from corrosion, such as zinc chromate alkyd primers and chromated chemical conversion coatings (CCC), wash or etch primers, acrylic lacquers and alkyd enamels. The products were used on commercial as well as on military aircraft. In 1960, the first generation of jet engine powered aircraft, McDonnell-Douglas DC-8 and the Boeing B-707, were introduced. New highly chemical resistant coatings were required to withstand the hydraulic fluids that were introduced with these new aircraft. These developments are the basis of the coating technologies used today. Two component paint systems were developed such as epoxy -amine or -amide primer technology and polyurethane (polyester / isocyanate) topcoats. In the mid 1980's clear coat technologies were introduced because atmospheric acidification due to volcano eruptions (Mt Pinatubo) caused severe damage to the paint systems. In the mid 80s environmental awareness started to influence the aerospace coatings industry. Toxic materials such as lead and cadmium were removed from the coatings and the quest for the replacement of carcinogenic hexavalent chromium was started. Solvent emissions needed to be reduced. This led to the introduction of high solid primers and topcoats and water-based coatings. Benzyl alcohol based paint removers replaced

methylene chloride and phenol containing paint removers. These can be neutral, acid or hydro peroxide activated. This initiated the introduction of selective strippable paint systems. In early 2000, developments were focused on efficiency improvements like super durable topcoats, weight reduction, less layers, easy application fast curing systems. This led to the introduction of base coat / clear coat systems for the aerospace industry. Over the years aerospace coatings evolved into high performance coatings that are able to withstand aggressive environments. Currently the aerospace coatings industry is facing new challenges with the introduction of all composite fuselage designs and the replacement of hexavalent chromium for structural applications.

2.4.2 Aerospace coating systems and their requirements

The main reasons for painting aircraft are corrosion protection, airline identification, appearance and survivability. The paint system on the aircraft protects the metal and composite structures from the environment. Many aircraft components are designed for structural and fatigue performance and are not very resistant to the atmospheric exposure. Aerospace coatings systems have cope with extreme in-service conditions. Because of this, the systems evolved over the years in terms of chemical and fluid resistance, corrosion resistance and exterior durability. Many different systems were developed to protect the various areas of the aircraft. In general, aerospace coating systems can be categorized in three main groups: exterior systems, structural systems, and special purpose systems.

Exterior systems

Exterior coating systems are applied on the fuselage and other exterior areas of the aircraft. The systems reflect the identity and image of the airlines. Historically aircrafts were mainly white. Today, aircraft liveries have to be glossy and feature vibrant colours and are used as a marketing tool (Fig. 2.1). These exterior systems have to be able to withstand a wide range of environmental stresses like temperature changes, high levels of UV irradiation, humidity exposure, erosion and exposure to aggressive media including fuel, de-icing fluids, hydraulic fluids, potentially corrosive salts due to maritime areas and acidic aerosols in the atmosphere due to volcano eruptions and industrial pollution. These stresses combined with the vibration effect of the powerful engines and structural flexing due to by pressurizing and turbulence put the coatings under severe stress.

Figure 2.1 *Exterior coating systems are used for identity and marketing.*

A typical exterior coating system is a multi-layered system and consists of a pre-treatment layer (anodized layer, chemical conversion coating), and a primer layer of 15 to 25 µm, which is covered with a pigmented decorative topcoat of 60 to 120 µm (Fig. 2.2). The airline livery is applied with the decoration colours on top of this basic topcoat layer.

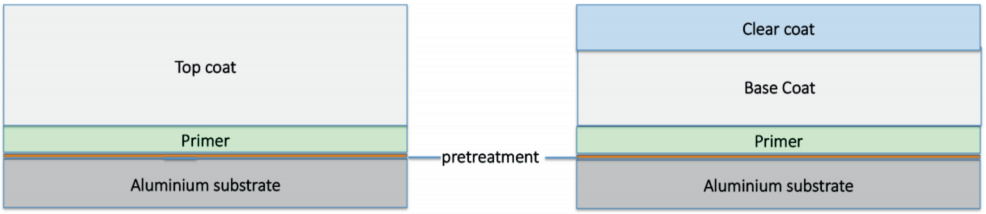

Figure 2.2 *Generic system build-up of an exterior coating systems.*

Recently, the base coat / clear coat topcoat philosophy has been introduced in the aerospace market. In this philosophy the decorative topcoat is replaced by a fast-drying, highly pigmented coloured base coat making it possible to reduce the process time of painting an aircraft, particularly complex liveries. Once all the colours are applied, the clear coat is applied providing an improved gloss and colour retention, thus longer durability.
Typical failures of external systems during aircraft operation are gloss reduction, loss of adhesion (rivet rash), cracking, and filiform corrosion.

Structural coating systems

Structural coating systems are designed to protect the structural parts of the aircraft. These systems are applied on small parts and sub-assemblies before the final assembly (Fig. 2.3).

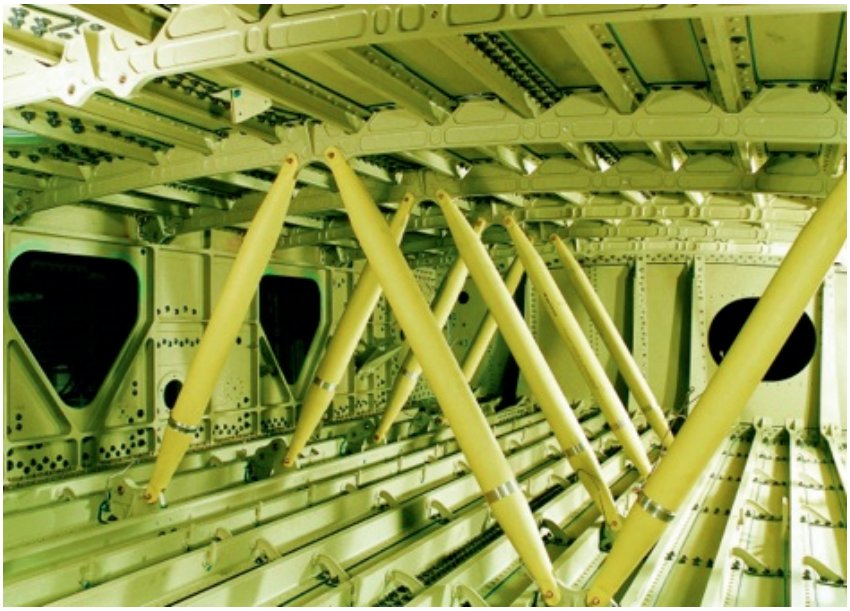

Figure 2.3 *impression of the structural coating system.*

Usually the system consists of a pre-treatment layer, which can be a chemical conversion coating or an anodic film, coated with 15 to 20 µm of structural primer. In some areas of the aircraft, for example in lower areas (bulge area) and cargo area, an additional 20 µm epoxy or polyurethane topcoat is applied for additional protection (Fig. 2.4). Structural coating systems are usually not stripped at regular maintenance intervals and are applied in areas that cannot be inspected. The system needs to provide passive and active corrosion protection for the entire service-life of the aircraft. Therefore these systems are developed excellent barriers and provide long-term corrosion protection, excellent adhesion to a wide variety of substrates. During the operational life of aircraft these coatings are exposed to many different stresses and wet and dry cycles.[52]

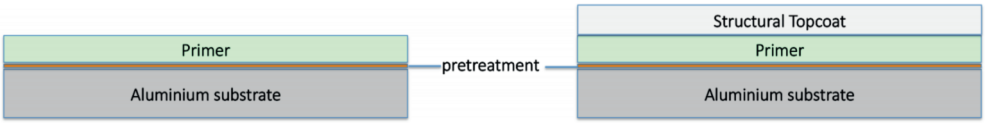

Figure 2.4 *General build-up of a structural coating system*

Special purpose coating systems

In addition to these generic coating systems, specific area's of the aircraft need specific coatings. Examples are composite areas, the fuel tank and wings. But as well, there are many different types of coatings with specific purposes. Amongst them: coatings for non-slip, conductivity, selective strip-ability, heat resistance, abrasion resistance, solar heat-reflective coatings, fuel vapour barrier, and camouflage (Infra-red absorption or reflection).

Coating system requirements and specifications

The requirements for coating systems used in the aerospace industry are controlled by a large number of specifications. Various specifications can be considered: MIL- Specifications issued by the US Government for military aircraft, OEM specifications of commercial Aircraft manufacturers and maintenance specifications defined and controlled by the SAE group. These specifications describe the general properties and performance requirements of coating system for a specific purpose like structural primer, fuel tank primer, exterior paint system, paint system for composites, and wing coating. The requirements are based on critical properties that are needed for a coating to demonstrate its intended function. Commercial aircraft manufacturers, governmental research laboratories or certified private testing institutes perform tests on submitted coating products to determine whether it complies with the requirements of a particular specification. Once the product meets the specification requirements, it will be added to the Qualified Product List (QPL) of the specification. Specifications of commercial aircraft manufacturers are usually not public documents, whereas military specifications that are managed by governments are publicly available.

Specifications are designed for each specific coating. They describe a variety of tests that ensure that application, appearance, and performance characteristics of the coating are fitting the intended use. The tests listed in these specifications often follow ISO, or ASTM standards. Specifications describe qualification and quality control tests that coatings must pass in order to be approved for use in the industry. The specifications contain a list of requirements for wet paint properties, application, appearance, and the dry film properties. Quality control tests describe which tests must be performed to ensure that the batch has been manufactured correctly. Some of the typical test for aerospace coatings are described below.[53]

Wet paint properties

Properties such as *viscosity, pot life* and *dry-time* are typical application related properties. The paint viscosity influences the atomization, substrate wetting, flow, levelling, and sagging resistance. Usually, the paint viscosity is measured with a flow cup. Coatings with thixotropic and pseudo-plastic behaviour need more sophisticated techniques such a Brookfield viscometer. Most aerospace paints are two-component chemically curing systems. These systems have a so-called "pot life". This important property can be defined as the period of time in which the product can be applied with the required finish quality (appearance) and

final dry film is performing according to the specification. Viscosity increase is an important measure for this property. In addition to this, dry-time is an important factor in the aerospace industry. The curing profile is an important characteristic when developing an aerospace formulation. Various dry times can be identified as relevant for the aerospace business. Set to touch time, Dust free time, tack free time, dry to stack-time, dry to tape time, dry hard time and dry to recoat.

Appearance and durability

Gloss and *colour retention* are the most important appearance related properties for exterior coatings. Gloss can measured at various angles (20, 60 and 85 degrees) with a gloss meter. Colour retention and colour accuracy is very important to the aerospace business. Colour is usually measured with a spectrophotometer using the CIELAB colour system and compared with colour standards.[54] Exterior systems need to retain their gloss and colour during their service life. Aerospace coatings are exposed to high levels of ultraviolet light, which has a detrimental effect on the binder system and colour retention of the pigments. Thermic cycling and moisture from humidity, condensation and rain accelerate this degradation. Artificial weathering tests are used to simulate these degradation phenomena. UVCON and Xenon Weather-O-Meter are the regularly used methods for accelerated weathering. Unfortunately, both are not representative to real life conditions. Alternatively, south Florida exposure is used as another reference exposure for durability.

Dry film properties

There are many properties that should be considered when evaluating the performance aerospace coating systems. *Adhesion* is one of the prime properties and can be tested by scribing the coating with a knife, followed by the application, and removal of a pressure sensitive tape. Pass or fail is specified by the amount of coating that was removed by this test. The scribe pattern and tape are specified in the specification. Adhesion tests are normally executed before and after water or *fluid immersion*. During operation of the aircraft, the coating will be exposed to several kinds of fluids like hydraulic fluids, kerosene, lubricating oil, toilet fluids, and de-icing fluids. Both primers and topcoats are designed to withstand these fluids and their resistance is tested by immersion in these fluids for a specific duration at a specific temperature. After immersion the system is tested for adhesion, softening, and blistering. Aerospace systems are exposed to a range of fast and slow deformation to test their *flexibility and impact resistance.* Therefore, the systems are subjected to various flexibility tests with conical and cylindrical mandrels at ambient and low temperature (-55°C). Impact tests are typical fast deformations using a specified force and or shape. Impact resistance is reported in different ways varying from pounds per inch, elongation or degree of cracking with fixed deformation and mass. After impact the coating is evaluated for cracks and adhesion. During the service-life of an aircraft, the exterior paint system will be removed and re-applied a number of times. Reasons for such strip and re-paint exercises are the periodically maintenance, inspection and overhaul schedules but as

well changing aircraft owners and new liveries (re-branding). In order to ensure adequate and efficient strip ability process, the system needs to be tested for *strippability* using aerospace qualified chemical paint removers.

Corrosion resistance

In aerospace coatings a number types of corrosion testing are used. *Salt spray* and *filiform corrosion testing* are the most common applied corrosion tests. In these tests coated panels, primer only or primer – topcoat, are scribed through the coating into the bare metal and subjected to the corrosion test. In neutral salt spray, panels are positioned in a slight inclined vertical position and exposed to a 5% sodium chloride solution up to 3000 hours. After this exposure the panels are evaluated for corrosion extended along the scribe and blistering. In addition to this regular neutral salt spray, some specifications require acidified salt spray. Whereas in salt spray, corrosion develops under a continuous salt fog, filiform develops under high temperature and humid conditions in the presence of chloride ions. Therefore, the scribed paint systems are exposed first to the fumes of concentrated hydrochloric acid for one hour and then immediately placed in elevated temperature (30-42°C) and high-humidity (85-95%) environment for 1000 hours. Although, these accelerated corrosion tests do not represent the in-service conditions, these are currently the only way to assess the corrosion protective properties of the active corrosion protective mechanism of the coatings.

2.4.3 Coating chemistry

Several reviews on protective coatings for aerospace applications can be found in the literature.[55, 56] The organic coatings that are applied in the aerospace industry are complex materials. These heterogeneous materials are the basis for the corrosion protection scheme of aircraft structures. The complex resin matrix contains pigments, fillers, solvents, and additives. Each type of coating is carefully designed to meet the industry standards. In the 1970's, the fundament of today's generation of coatings and the protection of aerospace structures was set with the development of hexavalent chromium containing, hydraulic fluid resistant epoxy/amine primers, together with the development of flexible but chemical resistant polyol/isocyanate polyurethane topcoat technology.

This section discusses the different coating technologies, primer and topcoat chemistries in the marketplace and the active protective mechanism used to provide long term corrosion protection.

Coating technologies

There are many different types of coatings in the aerospace industry. Over the years, many coating technologies have been developed due to pressure to reduce solvent emissions of coatings. The regulations for Volatile Organic Compounds (VOC) vary all over the world but in general the current limits for VOC are 350 grams per litre for primers and 420 grams per litre for topcoats. Currently, there are 4 different types of coatings in the market place:

- Conventional coatings
- VOC exempt coatings
- High Solid coatings
- Water Based coatings

Together with this pressure to reduce VOC in the coatings many different resin technologies were developed to maintain the application properties and performance of the aerospace coating systems. Whereas in conventional coatings solid resins were used, high solid coatings are based on liquid resins. In some instances the solvent reduction in grams per litre seems limited, Fig. 2.5 shows the real solvent emission reduction per applied surface area when replacing conventional coatings by low VOC coating technologies.

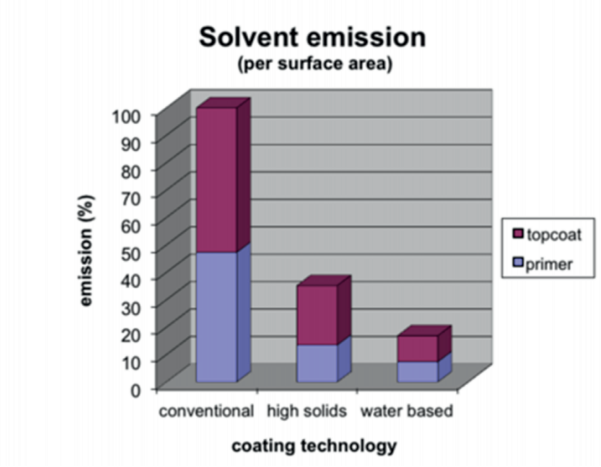

Figure 2.5 *Relative solvent emission reduction by introduction of high solids and water based coating technology.*

Conventional aerospace coatings contain typically 550-650 grams of solvent per mixed litre (g/L) paint. The coatings are often formulated with high molecular weight resins. In addition to their physical properties and the ability to comply with the aerospace applications, these systems have very favourable application properties such as: long pot life, fast physical drying properties, good film thickness control and a smooth appearance.

VOC exempt coatings are applied as a low VOC (340 g/L) alternative in primer technology. Some VOC's have a negligible atmospheric photochemical reactivity and are considered as

exempt solvents and therefore these solvents are not considered a VOC. Examples of such solvents are acetone and parachlorobenzotrifluoride. The use of exempt solvents offers many advantages to the coating formulator to formulate low VOC coatings with similar resin technologies as conventional coatings but maintain low viscosity and the application characteristics.

Today, new technologies are often based on high solid coating technology is another common approach to formulate VOC compliant primers and topcoats. Respectively they have a VOC of 350 and 420 g/L. High solid coating technology is based on crosslinking low viscosity resins with low viscosity curing agents. These resins are much lower in molecular weight compared to the conventional resins and have a higher reactivity. The drying time depends on how fast a high molecular weight network requires to become tack-free. However, a fast tack–free time is in contradiction to a long pot life. Therefore, formulators have to find the right balance between these properties. Additionally, low molecular resins and curing agents provide very highly cross-linked systems. This is very beneficial for a good chemical resistance but can be detrimental to the flexibility. Usually high solids coating formulations are blends of various resins and curing agents to find the right balance between the dry film and application properties.

Progress in the resin industry has helped the industry to develop water-based coating technologies for aerospace applications. In the late 1980's, the first water reducible primers were introduced for military aircraft. Today, there are multiple water based primer technologies available for structural applications. Water-reducible coatings are based on high solid resins made in solvents that form a dispersion of resin in water when reduced with water. Modern water-based systems are based on dispersions and emulsions of resins that easily mix and can be used without the addition of additional water. These systems provide a further reduction of solvent emissions (250 g/L excluding water) and applications properties of conventional coating systems such as fast cure, good film thickness control.

Aerospace primer coating technologies

Primers are used for exterior and structural protection of the aircraft. They provide active corrosion protection towards the substrate and provide adhesion to the topcoats. These primers have to comply with many criteria. These include:

- Room temperature cure
- Excellent adhesion to multiple substrates
- High chemical resistance
- Sufficient flexibility
- Long term corrosion resistance
- Good compatibility with the topcoat
- Applicable under various climatic conditions

Epoxy primer technology

The majority of the primers in the aerospace coatings market are 2 component epoxy/ amine primers. The base component comprises a mixture of epoxy resins, pigments, corrosion inhibitors, extenders, additives, and solvents. The second component, the hardener or curing solution, contains curing agents (amine or poly amide) and solvents. Corrosion inhibitors such as barium chromate and strontium chromate have been and are still most commonly used as corrosion inhibitor. Epoxy primer technology is used because of its very versatile properties. It has good adhesion to many substrates, good corrosion resistance, and can be formulated to find a balance between the chemical resistance, flexibility, impact resistance and hardness requirements of the aerospace industry. On the other hand, epoxy amine primers are difficult to strip, have relative long drying times and limited exterior durability.

Epoxy resins

There is a wide range of epoxy resins available. The majority of the epoxy resins are derived from the reaction between epichlorohydrin and diphenylol propane (Bisphenol A).[57] There are mainly 4 groups of epoxy resins (Fig. 2.6):

- Bisphenol A epoxy resins
- Bisphenol F epoxy resins
- Epoxy Novolacs
- Epoxy functional diluents and modifiers

Each type of resin has a range of variations in molecular weight and functionality. The selection of an epoxy resin depends on for which specification or application the coating needs to be developed. Many products contain mixtures of epoxy resins to obtain the specific coating properties needed for aerospace applications. High functional resins are blended with flexible epoxies for increased elongation properties whereas solid high functional resins are blended for fast physical drying and chemical resistance. Bisphenol A and F resins are blended to adapt the cure speed and epoxy functional reactive diluents are added to reduce viscosity and increase flexibility.

Epoxy Curing agents: There are many possibilities to cross-link epoxy resins (amines, thiols, carboxylic acids) via an addition reaction (some examples are provided in (Fig.2.7). In aerospace coatings, most epoxy primers are formulated with amine functional curing agents. Epoxy resins react under ambient conditions with the primary and secondary amines. The reaction rates depend on the epoxy and amine structures.

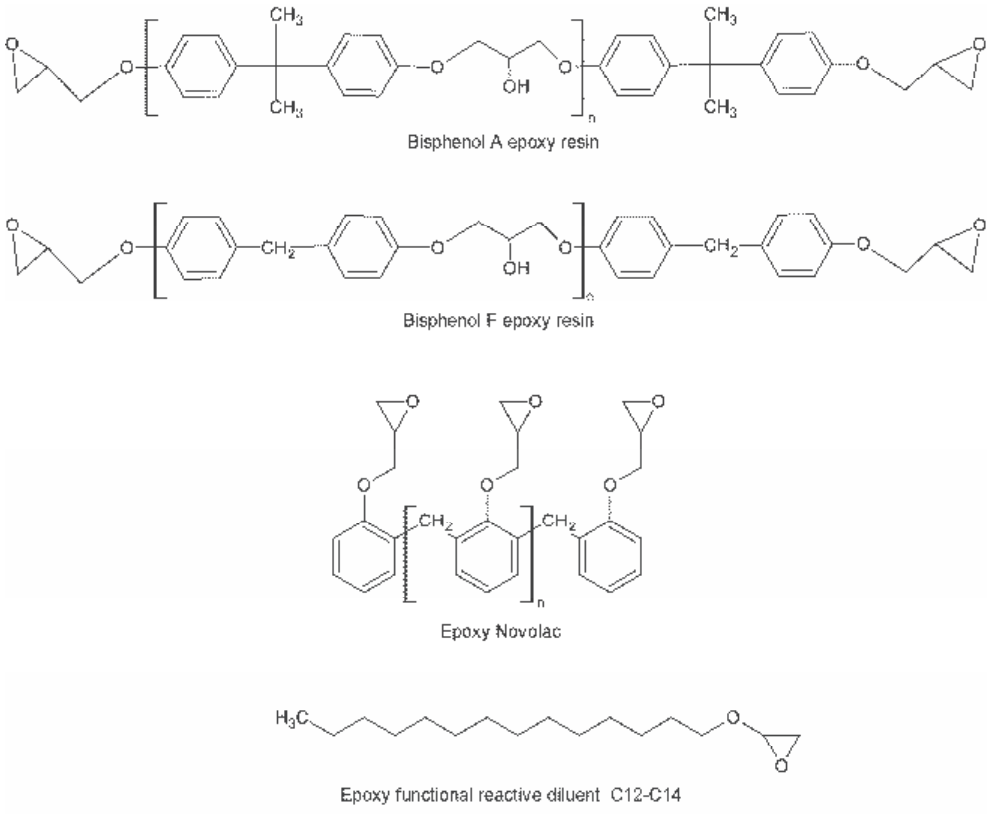

Figure 2.6 *Types of epoxy resins.*

Terminal epoxy groups are more reactive than internal and more sterically hindered epoxy groups. Reactivity of amines tends to increase with base strength and decreases with steric hindrance. Cycloaliphatic amines have reduced reactivity; the second reaction of such an amine is particularly slow. Aliphatic amines are less basic than aromatic amines and therefore more reactive. The epoxy amine reaction is catalysed by water, alcohols, tertiary amines, and weak acids (e.g. phenols), which promote ring opening by proton complexation with the epoxide oxygen.

The selection of epoxy resins and curing agents depends on the desired coating properties. Most commonly the formulation will consist of a mixture various epoxy resins reactive diluents of aliphatic or cyclo-aliphatic amines blended with polyamides. This all to adjust the various coating properties for adhesion, flexibility, chemical resistance, pot life, and cure speed needed for its specific application and specification.

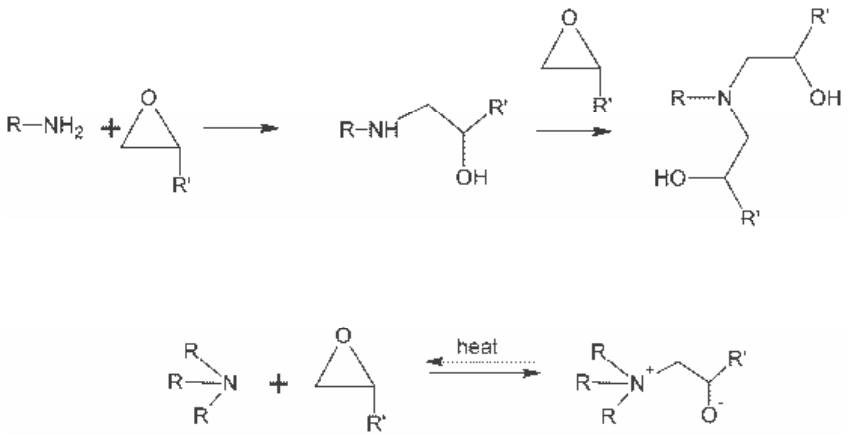

Figure 2.7 Epoxy curing reactions.

The selection of epoxy resins and curing agents depends on the desired coating properties. Most commonly the formulation will consist of a mixture various epoxy resins reactive diluents of aliphatic or cyclo-aliphatic amines blended with polyamides. This all to adjust the various coating properties for adhesion, flexibility, chemical resistance, pot life, and cure speed needed for its specific application and specification.

Aerospace topcoat technologies

Aerospace topcoats are applied both in structural and exterior applications. Although, both with a different purpose. Epoxy topcoats are applied for structural applications due to their good adhesion and excellent fluid resistance to ensure the good corrosion protection properties of the coating system. The basic chemistry of epoxy topcoats is similar to the primer technology. Epoxy topcoat technology is used for structural parts since they are not durable enough for exterior applications.

Since the late sixties, polyurethane topcoats have been applied in the aerospace industry due to their very good exterior durability combined with excellent flexibility and good fluid resistance. Polyurethane topcoats are based on 2K formulations of which one part contains a polyol (polyester or acrylate resin) that is cured with the other part that contains aliphatic isocyanates. Sometimes, a third part that contains a catalyst is added to adjust the cure rate for different application conditions.

The polyurethane coating technology is based on the main reaction between primary and secondary hydroxyl groups of the polyol and isocyanates forms urethane crosslinks[57]. On the other hand urea crosslinks are formed by the reaction of atmospheric water with isocyanates (Fig. 2.8). This secondary reaction is somewhat slower than the reaction with a secondary hydroxyl group but it is an important aspect of formulating with polyurethane coating technology.

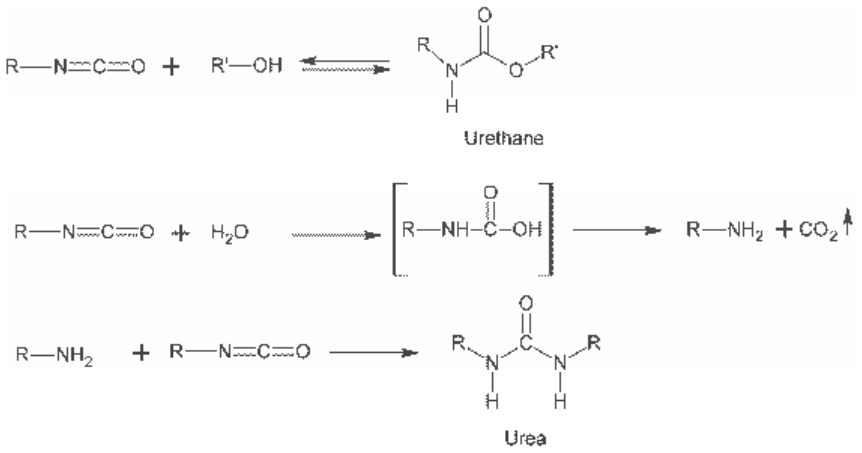

Figure 2.8 *Isocyanate reactions.*

The properties of polyurethane coatings depend on the polyol structure, type of isocyanate and the stoichiometric ratio of the isocyanate and hydroxyl groups (NCO/OH ratio). The chemical or fluid resistance of the coating depends on the crosslink density. Polyols with high hydroxyl functionality will increase crosslink density and provide more chemical resistant but less flexible films. Aerospace finishes are often formulated with a higher NCO/OH ratio to increase fluid resistance especially hydraulic fluids. Over-indexing with isocyanate minimizes the amount of unreacted hydroxyl groups and the excess isocyanate groups react with water to form the urea groups resulting in a more resistant coating with a higher T_g. Hydroxy-terminated polyester and hydroxy-substituted acrylic resins are most commonly used polyol resins in aerospace exterior topcoats. Polyesters permit higher solids and give films with greater solvent resistance. Acrylics provide faster dry, higher gloss and better exterior durability, resulting from superior hydrolytic and photochemical stability. Therefore, polysesters are used for solid colour topcoats and acrylics are used for clear coat applications.

Aliphatic isocyanates such as hexamethylene diisocyanate and isophorone diisocyanate are commonly used in the aerospace topcoats. Because of their toxic nature, these diisocyanate monomers are converted into high molecular weight trimers (triisocyanurates) with a very low concentration of monomeric isocyanate. These high molecular isocyanates are available as low viscosity resins with a 100% solid content.

Aerospace coatings are designed for cure at room temperature conditions. However, the reaction between primary or secondary hydroxyl groups and the aliphatic isocyanate are slow at room temperature conditions and therefore needs to be catalysed. Tertiary amines (diazabi- cyclo [2.2.2] octane (DABCO)) and organometallic compounds, such as dibutyltin dilaurate (DBTDL), or carboxylic acid salts, are the most commonly used catalysts for these 2 component polyurethane coatings. The type of the catalyst and the amount used in the formulation is critical to the balance of pot life, application properties and the drying time of the coating. Extended pot life in combination with rapid cure can be obtained using organotin

catalyst (DBTL) in combination with 2,4-pentanedione (acetyl acetone) or volatile carboxylic acids (formic acid or acetic acid).

The majority of the polyurethane technology is used for exterior applications. Therefore exterior durability is a key element for these formulations. Exterior durability is referred to the resistance to withstand degradation processes when exposed to the environmental conditions and the ability to maintain the aesthetic and functional properties of the coating. Chemical processes such as hydrolysis and photo-oxidation resulting from exposure to the environmental conditions cause coating degradation. UV radiation from sunlight can initiate photo-oxidation processes in the resin system. In addition to this, environmental conditions such as acid rain due to air pollution or atmospheric degradants (e.g. ozone) can initiate hydrolytic degradation processes in the coating. Temperature and adhesion also can affect these processes. These degradation processes may lead to loss of gloss, discoloration or even to cracking, delamination that can provide an access point for the environment to reach the substrate and cause corrosion. The resins for exterior applications are optimized for hydrolytic stability and are stable against photo-oxidation. Another critical factor for exterior durability is the selection of pigments. The quality and after-treatment of pigments can have a significant effect on the colour stability and gloss of the coating. Photo stabilization additives, such as UV absorbers, and radical scavengers hindered amine light stabilizers (HALS) and anti-oxidants, provide an additional protection against photo initiated oxidative degradation.

2.4.4 Active corrosion protection and leaching

Organic coatings provide protection to the metallic substrates by passive inhibition mechanisms such as barrier function and adhesion to the substrate; this protects substrates against corrosive species from the operating environment. However, passive inhibition is not sufficient for aerospace coatings and therefore these coatings require an active protective mechanism as well. This active protection is achieved by the addition of corrosion inhibitors. Hexavalent chromate pigments (strontium chromate) loaded primers are widely used in the aerospace industry and have demonstrated excellent performance and long-term corrosion resistance.[58, 59] These coatings provide active corrosion protection by means of a leaching mechanism (Fig. 2.9). This is initiated by the ingress of water into the coating via a crack, void or other damage. This will be followed by the dissolution of the corrosion inhibitor particles and transportation of these inhibitors to the damaged area that is exposed to the corrosive environment and inhibit the corrosion process. The rate of inhibitor leaching has an influence on the immediate and long-term corrosion protection.

Ideally, coating systems would release inhibitors quickly for fast and effective corrosion protection as well as slow release to ensure long-term protection. The performance of active protective coatings depends on many parameters like the binder system [58] and solubility of the inhibitor, pH, coating composition, pigment volume concentration (PVC) and finally the inhibitor loading. Corrosion inhibiting primers usually are highly loaded coatings with a PVC

between 25 and 32%. The amount of hexavalent chromate pigment depends on the leach rate necessary for the specific application.

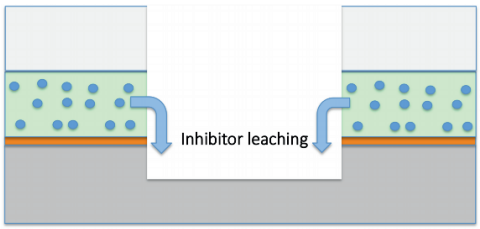

Figure 2.9 *Inhibitor leaching from the coating as active corrosion inhibition mechanism.*

Although the corrosion protection of hexavalent chromium systems is very good, their leaching properties have been studied only since early 2000. Scholes *et al.* characterized the leaching properties of chromate from primers[60] and Furman *et al.* found that the inhibitor release is not controlled by a Fickian diffusion process.[61] However it must be considered that every coating composition is different and leach rates can differ significantly which each different coating. Studies are continuing to improve the understanding of the leaching process Sellaiyan *et al.* studied the leaching process using radioactive tracers demonstrating water ingress complete dissolution of the chromate inhibitor and the generation of small voids, which can further enhance the leaching of the inhibitors.[62] Knowledge and understanding of the leaching process are important to understand the leaching mechanisms. Computed tomography techniques are becoming more and more common in corrosion[63, 64] and paint research.[65] These techniques make it possible to study microstructural changes in a paint film. For example, Hughes *et al.* studied the transport pathways of a chromate inhibitor loaded model primer using Quasi 4D computed tomography and demonstrated that there is no chromate transport through the epoxy resin matrix itself.[66] However, the chromate release occurs via direct dissolution of chromate clusters, which are in contact with the electrolyte at the surface and at a later stage through the micro-capillaries and voids left after the dissolution of the inhibitor pigment. This work defines a model that considers fast initial release due to dissolution and a slower release mechanism of inhibitor dissolution and transport through the fractional network. Clusters that were not connected to the electrolyte were not dissolved and are considered inhibitor reservoirs in case of any further local damage. These inhibitor transport studies and models are important for the development of new hexavalent chromium free systems to tailor the release of alternative inhibitors for immediate and long term protection.[67] All corrosion inhibiting primers in the aerospace industry use this leaching mechanism for the active protection mechanism. The unique solubility and corrosion inhibiting properties of these chromated primers is the basis for the track record and confidence of the chromated primer technologies for the protection of aircraft structures.

2.4.5 Application

Today, most aerospace coatings are applied with hand-held spray equipment. The large variety of parts that need painting before assembly and the dimension and shape of the aircraft have made automation difficult. Especially, the exterior painting process is still a labour-intensive job due to the pre-treatment steps and the masking and de-masking processes involved prior to and during the painting process (Fig. 2.10). In addition to this, there are several other factors that influence the painting process. Hangar conditions can vary from 23°C and 55% Relative humidity (RH) in climatized hangers to severe conditions with high temperatures and high humidity (35°C/90 % RH) or low temperature conditions with very low humidity conditions. Some hangars are equipped with movable platforms and others have fixed scaffolding. Under these varying conditions, the quality of the finish depends on factors like, teamwork, experience, and skills of the painters. Another important factor is the application equipment.

Figure 2.10 *Aircraft painting*

Equipment

There are many different types of equipment for the application of aerospace coatings. The most conventional type is the air-atomized spray. This type of spray guns uses air to atomize the paint in very small droplets that results in a very smooth finish. The equipment is not expensive, easy to clean and is easy to maintain. Although, it has a low transfer efficiency of approximately 20-30 % and is not suitable for large area application. Over the years several alternative types of air atomized spray guns have been developed to improve the transfer efficiency. Examples are HVLP (High-Volume Low-Pressure) and HR/RP (High Return /

Reduced Pressure) spray guns. Air Less spray equipment uses hydraulic pressure instead of air to atomize the paint. The paint is forced through the nozzle with 100-150 bar of pressure to atomize the paint. The velocity of the atomized droplets is less compared to air atomized spray, which results in a higher transfer efficiency. The equipment has a high flow rate providing a faster application speed. Airless air assisted spray equipment combines both of both worlds in air atomized and airless spray. Another way to reduce overspray and increase transfer efficiency is the use of electrostatic spray equipment. The atomized droplets are charged using a high voltage (60-90kV)/low current generator and attracted to a grounded conductive object. Transfer efficiencies of 70% are possible. This transfer efficiency depends on the coating formulation. This type of equipment is most frequently in OEM and MRO paint shops.

Plural component spray equipment is becoming more common in the structural coatings market but as well for exterior aircraft painting. The equipment mixes the components (base, hardener and activator) at the desired mixing ratios just before or at the spray gun. This equipment reduces the pot-life factor of 2 component paints and reduces the amount of waste from unused mixed paint.

Paint automation for exterior and structural painting

The use of paint automation in commercial aircraft production is being studied to reduce process cycle times, provide a higher quality paint finish, lower emissions, increased transfer efficiency and increase process consistency.[68] Increasing production rates and the need for increased capacity in the current hangers is driving this need for automation and use of new coating technologies. However, there are differences between aerospace and automotive applications such as paint cure times, number of paint colours, environment control, and part size considerations are some of the issues that make aerospace application of coatings more difficult than automotive applications. Understanding the unique factors involved in the robotic application of commercial aerospace coatings is important for future advancements in application technology, gains in aircraft paint hangar capacity, delivering quality coating finishes, and lowering environmental footprint. In structural painting automation has been introduced. Small parts are applied on conveyer belt systems and robotized paint lines have been introduced on the subcontracting level e.g. for the wing sections and stringer painting.

Application of an exterior paint system

Painting aircraft is a labour-intensive, multi-step process that requires a significant amount of handwork and attention to detail. Fig. 2.11 illustrates the different steps required for exterior painting. The aircraft is washed and moved into hanger, all the at-risk components (composite parts) and flight controls are covered or removed. Then the chemical stripper is applied to remove the old paint film. After this, the aircraft is cleaned and inspected, flaws are removed, corrosion is treated, and necessary repairs made. Then the aircraft is pre-

treated for application using an alkaline soap wash, the aluminium surfaces are etched or abraded prior to the application of the chemical conversion coating, or wash primer. Within the recommended application window the protective primer will be applied followed by the base colour topcoat for the aircraft. With use of decals, the paint scheme will be laid out on the aircraft and the rest of the aircraft is masked and the decoration colours are applied. When the paint scheme is completed, there is the final inspection and the aircraft will be released for service.

Figure 2.11 *Steps required for aircraft painting (images kindly provided by Airbus and Emirates Airlines).*

2.4.6 Trends in aerospace coatings

The aerospace market is focused to increased efficiency, reduced operational and maintenance costs.[69] There are two important drivers that influence the aspects of innovation in the in the market for aerospace coatings. First, there is the drive for more environment friendly coating systems and second, there is the need for increased efficiency.

When considering efficiency, there is a drive towards reduced weight, faster application times for coatings, longer service life and increased functionalities. Fuel costs are a significant part of the operational costs, airlines and aircraft manufactures need to consider ways to save money. One way to achieve this is to reduce weight by selecting new materials in design or reduction of the weight of the paint system. The weight of the paint film can be reduced in different ways like, the reduction of the dry film density of the coating, reduction of thickness of the paint system or using fewer layers in the paint film.

The second efficiency driver is the time of the paint process. Airlines merge and rebrand their liveries; therefore there is an increased need for repainting. In addition to this, the market is growing; build rates at the OEM's are increasing to keep up with the demand from the market. Therefore the cycle time of paint process needs to be reduced to get the aircraft back in service quicker to create revenue for the airline and to ensure final assembly line throughput at the OEM's. The livery and interior of the aircraft are part of the airline's brand and image. A clean and glossy appearance with vibrant colours is a key aspect of the branding strategy of an airline. To support this, basecoat/clear coat paint systems have been introduced into the market. These fast curing collared basecoats are covered with a clear coat to ensure long-term durability (gloss and colour). In addition to this, the industry is looking for increased coating functionalities in the coating. Examples of such functionalities are: drag reduction, anti-icing, solar hear reflection / heat dissipation, and self-healing abilities.

The other important aspect is the environmental impact of the coatings. Terms such as Eco-efficiency, sustainability, and carbon footprint are an integral part of the development of new products for the aerospace industry. Not only for the coating manufacturers, but for the entire supply chain from raw material to end-user. Moreover new legislations such as REACH (Registration, Evaluation, Authorization, and Restriction of Chemicals) and regulations from governmental institutions as the Environmental Protection Agency (EPA) and Occupational Safety and Health Administration (OSHA) are applying enormous pressure to develop more sustainable products with a lower environmental impact. The REACH legislation targets the ban of all chemicals that may be considered hazardous. Over the years, this has resulted in the replacement of many hazardous materials with more acceptable alternatives and solvent emissions have been reduced

In the field of aerospace coatings there have been many advances.[70] Today, solvent emissions can be reduced significantly. Conventional coatings, with low solids and high solvent content can be replaced by high solids or water-based coatings. Water based cleaners and pre-treatments have been introduced and environmentally friendly paint removers were developed. The elimination of hexavalent chromium or chromate from the protective coatings and coating processes is a key topic for the aerospace industry, which will be discussed below.

2.5 Developments towards a chromate-free corrosion protective scheme

For more than 50 years the aerospace industry has been using hexavalent chromium as corrosion inhibiting compounds for the protection of the aircraft structure in many processes and products. However, the health issues associated with the use of these chromate materials and new regulations and legislations are putting pressure on the industry to find alternative solutions.[12, 71, 72] The European REACH (Registration, Evaluation, Authorization and restriction of Chemicals) regulation (EC N° 1907.2006), hexavalent chromium compounds have been identified as a Substances of Very High Concern (SVHC) and are subject to a formal and time limited Authorization for use. This means that they cannot be used after the "sunset date" unless there is an authorization. In the USA, the Occupational Safety and Health Administration (OSHA) reduced the employee permissible exposure limits (PEL) to hexavalent chromium from 52 $\mu g/m^3$ to 5 $\mu g/m^3$ inducing strict expose controls of these chemicals.

Through significant efforts in the different areas of the industry various chromate free alternatives have been developed and qualified to aerospace standards and specifications, and introduced to the market place.[13, 73-79] Examples of this are chromate free anodizing, acid pickling, conversion coatings, sealants and coatings. This part of the chapter provides an overview of the developments in chromate free coating technology from pre-treatments, coatings and some more innovative approaches which should lead eventually towards a fully chromate free corrosion protective scheme for the protection of the aircraft structures.

2.5.1 Chromate-free pre-treatments

Various processes can be utilized prior to the application of the organic coating. The specific process used depends on the substrate, and the performance characteristics required for the protective system. Typically, a process will start with a cleaning step to remove organic contaminations. This will be followed by a deoxidation or pickling step and the application of a surface treatment for corrosion protection and paint adhesion.[80, 81] The use of non-chrome processing solutions for cleaning, deoxidation, desmutting, etching has increased over the recent years. In addition to this, several alternative solutions for surface treatment have been developed and introduced to the market place. These hexavalent chromate free surface treatments are the new base for the future hexavalent chromate free corrosion protective scheme.

Chemical Conversion coatings

Significant effort has been spend to develop a suitable alternative to the chromated chemical conversion coatings. The coatings developed from chromate solutions have a robust performance in processing, corrosion protection and adhesion performance. A wide range of technologies has been investigated, demonstrating the array of alternative chemistries available for aluminium. These include molybdates, vanadates[82], permanganate[83-85],

phosphates, silanes, sol-gels, self-assembling monolayers, hydrotalcite[86-91], and rare earth (cerium) based chemistries.[92] Only a few chemistries have been able to come close or meet the corrosion protection requirements of aluminium according to the MIL-DTL-81706/5541 specification. Examples of this are conversion coatings based on trivalent chromium processes (TCP) and cerium. Both these approaches are commercially available and found their application as part of a coating system.[81]

Rare earth based salts are promising options for chromate replacement in chemical conversion coatings for the protection of aluminium alloys. Several rare earths have been identified as cathodic inhibitors.[93, 94] These materials tend to precipitate as metal hydroxide at local areas that are associated with a pH increase due to the oxygen reduction reaction at the cathode.[95] This results in the deposition of a hydrated oxide layer on the aluminium surface.[96-98] Unfortunately, most rare earths are too costly for commercial use. However, cerium is the most active rare and has been studied extensively since the early 1990's.[93] A review by Harvey is the most recent that covers specifically cerium-based conversion coatings.[92] Several cerium-based chemical conversion coating have been developed and commercialised.[99-102]

On the other hand, trivalent chromium processes have been developed as alternative to hexavalent chromium pre-treatments. The Naval Air Systems Command (NAVAIR) has developed and patented a range of processes using trivalent chromium and zirconium fluoride.[103] This process has been approved according to MIL-PRF-81706/5541 and has been licensed to various parties. These trivalent chromium conversion coatings have been introduced into the hexavalent chromium free surface finishes of the US Navy.[104-106] and slowly finds it way to the civil aviation. There have been many studies on this Trivalent Chromium Process (TCP). Guo and Frankel studied the conversion layers and the self-healing or active corrosion inhibition properties of TCP.[107, 108] On the coating surface a dense layer of 40-120 nm was found. The protective barrier layer provides corrosion protection by suppression of the oxygen reduction reaction. Moreover, the TCP coating is able to release chromium from the coating proving self-healing or active corrosion inhibition properties. No hexavalent chromium has been detected in these coatings after deposition and corrosion testing.[109, 110]

The performance of these new chemical conversion coatings is not at the same level as the hexavalent chromated conversion coatings. Although, these chromate free chemical conversion coatings are finding their place in the aerospace industry and potentially are the new base for the chromate free coatings systems.

Anodising

Traditionally, the anti-corrosion performances were achieved by chromic acid anodizing (CAA), followed by painting. However, environmental issues and associated costs for the disposal of chromate wastes, require the development of new approaches for anodizing of aluminium alloys. Phosphoric acid anodising (PAA) and sulphuric acid anodising (SAA) have been available to the industry but were not suitable chromate free alternatives to CAA

because of degradation of fatigue life, corrosion resistance adhesive bonding or paint adhesion. Boric sulphuric acid (BSA) and tartaric sulphuric acid (TSA) electrolyte anodising processes have been developed and introduced as suitable alternatives to CAA for corrosion protection.[111-113] Phosphoric Sulphuric acid (PSA) anodizing is used for structural bonding. These processes have been optimized balancing three criteria: Adhesion, corrosion resistance and fatigue properties. The new processes provide anodic film with a similar thickness as the conventional chromate containing process and a regular open structure using lower anodizing temperatures, shorter process times and reduced voltages.

Further research is focused to improve and understand the chromate free anodising processes and their performance even further.[114, 115] Reduction of energy costs [116] modification of film morphologies.[117] Potentiodynamic anodising is a new tool that allows fundamental and practical investigations of the anodising process. It is suitable to compare different electrolytes and to determine the optimum parameters to obtain porous anodic films. These parameters include current-potential relationship, maximum anodizing potential and current as a function of electrolyte concentration or temperature.[118] Dichromate sealing processes are commonly used after the anodising process to improve the corrosion resistance of the anodic film. Numerous studies were performed to investigate the effect of the addition of inhibitive species to the anodizing electrolyte or as sealing process to improve the anodic film or to replace this dichromate-sealing step. Proposed alternatives are species like cerium nitrate, molybdate, permanganate, phosphates, or hydrophobic carboxylic acids.[119-122]

Pre-treatments

The need for hexavalent chromate free chemical conversion coatings stimulated the development of several alternative chromate free pre-treatments. An example of such an alternative is a sol-gel based pre-treatment. This coating has a specific formulation of components that provides a sol-gel hybrid network. The formulation is based on a reactive mixture of an organo-functionalized silane with a stabilized zirconium complex and forms a covalently bonded film on the metal surface (Fig. 2.12) and strong and durable bonds with paints adhesives and sealants.[123] The sol-gel pre-treatment does not contain any corrosion inhibitors and has no significant “stand-alone” corrosion protection.

However, it is compliant to the aerospace specifications when used in combination with appropriate paint systems. In 2008, this pre-treatment was introduced to the OEM end lines for exterior painting. Since then it was licensed to several parties and is currently used in OEM and the MRO sector as part of chromated and chromate free coating systems. In addition to the environmental and health, and safety benefits, in-service flight data demonstrated that the sol-gel pre-treatment reduced the occurrence of “rivet rash” adhesion failures, which has been a serious issue for many years.

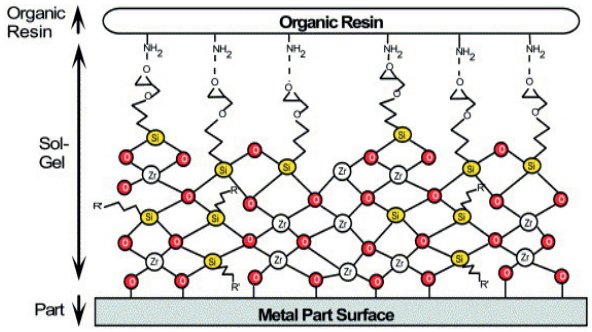

Figure 2.12 Representative structure of a sol–gel coating [124].

The material can be applied by spray, brush or flooding. This pre-treatment did not only eliminate the use of hexavalent chromium in the conversion coating step but, it simplified the application process, reduced drying times, water consumption and, the time required to paint an aircraft.[81, 125] In addition to the sol gel technology, other chromate-free pre-treatment technologies were introduced into the marketplace. These products do not only eliminate hexavalent chromium from the pre-treatment step but as well acid brighteners, solvents and alkaline washes[126]. These particular pre-treatments clean the surface to be painted and deposit a molecular layer that bonds to the metal. This layer improves the adhesion of the coating system to the metal, but do not have any stand-alone corrosion protection. However, they provide an environmentally friendly alternative to the hexavalent chromate containing chemical conversion coatings in combination with aerospace qualified coating systems.[73, 77]

2.5.2 Developments in chromate free organic coatings

The hexavalent chromate free surface treatments as discussed above provide the first basis of the corrosion protective scheme. Today, the majority of these environmental friendly surface treatments are coated with chromate containing organic coatings (primers). On the other hand, there is an enormous effort on going to find suitable alternatives for hexavalent chromium in coatings for the aerospace industry. Many inhibitors were evaluated over the years, however with limited success.[58, 127] For a long time the objective was to mimic the activity of chromates which are very effective in low concentrations and in a wide pH range.[128] Many inhibitors were identified in electrochemical studies but more than often these were out- performed by the unique properties of hexavalent chromium or they needed the support of chromated chemical conversion coatings, wash primers or anodising. The quest has not yet been resolved but, there has been promising progress in chromate free coatings development and total chromate free coating systems are being introduced into the market place for exterior painting. With this achievement, the industry will realign its focus to the elimination of hexavalent chromium from the structure of the aircraft.

Corrosion inhibiting strategies

Multiple corrosion inhibiting strategies have been developed for chromate free active protective coatings. First, there is the traditional "leaching" process, whereas a corrosion inhibitor is incorporated in a paint film and moisture dissolves the corrosion inhibitor and transports it to the damaged area as discussed in 2.4.4. Second, there is the mechanism of galvanic inhibition, this inhibiting strategy is based on sacrificial oxidation (cathodic protection) using metallic particles which are electrically connected and more anodic (reactive) than the substrate in the electrochemical series and last, there are the smart-coating approaches with inhibition through self-healing properties and on-demand inhibitor release. The leaching and galvanic inhibition strategies have been introduced to the market place[129] and the smart-coating approaches are still under development.

Inhibition through leaching

The traditional leaching-mechanism is the fundament of current aerospace specifications for active protective coatings in the aerospace industry. The performance of hexavalent chromium corrosion inhibiting pigments provided a proven track record and is currently the benchmark for all new chromate free active protective coatings. The leaching inhibitors need to provide active corrosion inhibition when the measures of the corrosion protection scheme are failing (substrate, pre-treatment, sealant, drainage) and the system is damaged by means of a crack, drilling hole or, scratch. At this stage, moisture ingresses into the crack or system, the inhibitor should be dissolved and transported to the damage. Where chromates were unrivalled for a long time, chromate free alternatives are being introduced into the market place.

Leaching inhibitors have to be versatile and it is the question whether it is possible to find the complete package (like chromates) all in a single inhibitor. There are many chromate-free inhibitors that demonstrate activity but do not perform when incorporated in to a coating due to various reasons like: solubility, efficacy, or compatibility with the binder system. Therefore the leaching capabilities should be considered from coating / inhibitor perspective and have adequate solubility and leaching characteristics, fast and effective formation of an irreversible protective layer in the damaged area, underneath the coating and, maintain a good coating integrity (adhesion and barrier function). Many inhibitors have been developed and investigated in the academic environment but as well in the industry. Many patents have been filed and published on a range of corrosion inhibiting materials. Several of them have been introduced to the market place but none of them can be really considered as the true replacement and alternative to hexavalent chromium. Some examples are mentioned below.

Most of the inhibitors are based on inorganic materials, among them inhibitors based on rare earths (Cerium and praseodymium), molybdates, and vanadates.[130, 131] Praseodymium has received considerable attention as well. Stoffer *et al.* claim a corrosion inhibiting coating composition based on a rare earth compound (praseodymium oxide) and a neutral to acidic generating extender (Calcium Sulphate).[132] Pr_2O_3 provides the best protection across a pH

range from 5 to 8. Praseodymium-rich species leach from the coating and precipitate as hydroxy carbonates in the damaged area near cathodic sites.[133] Pipko and Vitner developed and claimed compositions of oxyaminophosphate salts of magnesium as leaching inhibitors. These slow releasing materials were found to form stable magnesia layers on the metal surface.[134, 135] Yu *et al.* claimed a non-carcinogenic corrosion-inhibiting additive comprises an anodic corrosion inhibitor and/or a cathodic corrosion inhibitor. This leaching inhibitor uses a molybdate salt as anodic inhibitor, cerium as cathodic inhibitor and citrate as a metal-complexing compound.[136, 137] Walters and Schneider claim a coatings composition utilizing nano-sized Magnesium oxide particles as alternative to hexavalent chromium.[138] Visser and Hayes propose Li-salts as corrosion inhibitor for 2024 T3 aluminium alloys.[139] Whereas, organic inhibitors and rare earth species are active in on active copper intermetallic (cathodes)[140], leaching of Li-species from organic coatings results in the formation of a protective layer with a characteristic three-layered morphology on the aluminium in the damaged area.[141] Boocock used a composition with amorphous zirconium vanadium oxide/hydroxide for the protection of high strength aluminium alloys[142], and Becker *et al.* proposed a coatings composition containing a corrosion inhibitor and at least one quaternary ammonium compound.[143]

In addition to the inorganic inhibitors, there are many organic inhibitors that are and have been investigated. Harvey *et al.* investigated the effect of the inhibitor structure on the corrosion of AA2024 and AA7075 and found good inhibitor efficiencies for most of these well-known "copper" inhibitors, Among them benzotriazole, 2-mercaptothiazole, dithiocarbamates, and dimercapto thiadiazoles.[144] Sinko designed different hybrid organic-inorganic corrosion-inhibiting micro composite pigment grades that contain 2,5 dimercapto-1,3,4-thiadiazole, zinc oxide, zinc phosphate, and zinc cyanimide.[145-147]

Furthermore, together with Kendig, Sinko proposed a guest–host pigment (hydrotalcite based) that can be loaded with an organic inhibitor.[148, 149] Hayes *et al.* proposed a pigment comprising a neutralized metal salt of a corrosion inhibiting organic anion, wherein 2.5% by weight aqueous mixture of the dry salts has a pH above 6 and below 8.[150]

Other researchers try to find viable alternatives for hexavalent chromium combining the best of both inorganic and organic inhibitors. Examples are cerium salts of organic inhibitors cerium cinnamate[151], Cerium dibutylphosphate[152, 153] and cerium or praseodymium mercapto acetate.[154]

Galvanic inhibition

Cathodic protection or galvanic inhibition is a method that is extensively used for the protection of steel structures. The protection is based on a sacrificial mechanism. In the case of steel, zinc (Zn) is used because it is more reactive (anodic) compared to Iron (Fe), which is the main constituent of steel in the electrochemical series. Using this principle metal rich coatings have been developed for the protection of the aluminium structures of aircraft.

There are some basic principles that need to be taken into account to provide cathodic protection. The coatings are composed of organic or inorganic film forming resins and are

pigmented with particulate metal particles in either spherical or flake form. The metallic particle selected must be must be more anodic compared to the metal/substrate that needs to be protected. As already mentioned, for steel this is most commonly Zinc. The pigment volume concentration (PVC) of the metal particles in the coating needs to be close to or exceed the critical pigment volume concentration (CPVC) enabling mutual contact between the particles and the underlying substrate. The resin matrix of the coating must be able to withstand the alkaline environment created by the oxidation of the metal pigment. Good adhesion to the substrate under corroding conditions is another essential parameter. In order to preserve the inhibitive capacity, the sacrificial primer needs to be covered by a topcoat ensuring good barrier for the structure to the environment and protection in case of damage.[155]

In 2004, Nanna and Bierwagen proposed the Magnesium-Rich Primer technology (MgRP) as a new paradigm for chromium free corrosion protection for aerospace aluminium alloys.[156, 157] This was an entirely different approach compared to the traditional chromated leaching technology. Aluminium is at the bottom of the galvanic series, and magnesium has an even more positive potential.[158] Therefore magnesium can act as a sacrificial element for the protection of aluminium alloys. The magnesium rich coating has the same features as a zinc rich primer. The magnesium particles are connected to each other and the metal substrate (Fig. 2.13).[159] Therefore the primer is loaded with magnesium particles to a level close to the critical pigment volume concentration (CPVC). When the MgRP is applied over aluminium alloy, the steady state potentials (OCP) are corresponding to the potential of the galvanic couple of the substrate and magnesium (Fig. 2.14).

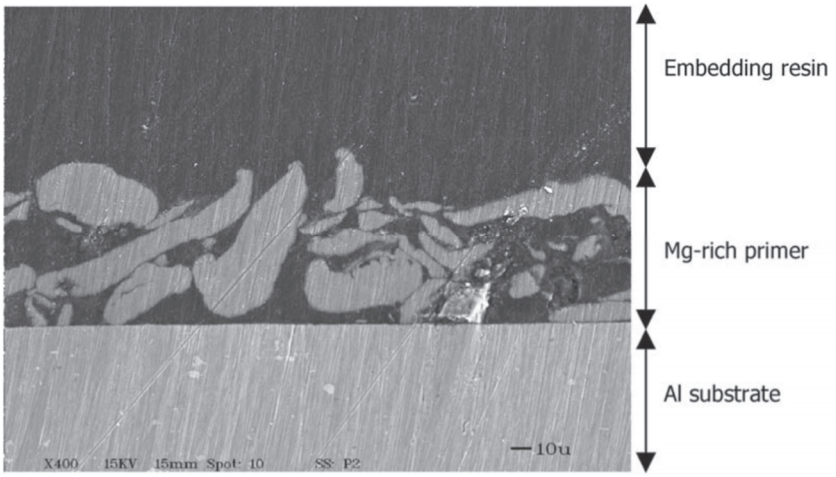

Figure 2.13 *Cross-section micrograph of Mg-rich primer on aluminium alloy substrate.*[160]

Magnesium polarizes the system cathodically, shifting the system potential below pitting corrosion potential. This polarization prevents pit nucleation at exposed or damaged areas or inhibits pit growth for nucleated pits. In addition to this electrochemical protection, a precipitation effect has been postulated due to precipitation of magnesium oxides in damaged areas.[160] The technology was licensed and developed to a mature product that meets aerospace specifications and is currently used in the aerospace industry.[161, 162] Research on this inhibitor continued, addition of metal salts (Li_2CO_3 and $Mg(NO_3)_2$ enabled the reduction of Magnesium metal in the coating while improving the overall corrosion protection.[163]

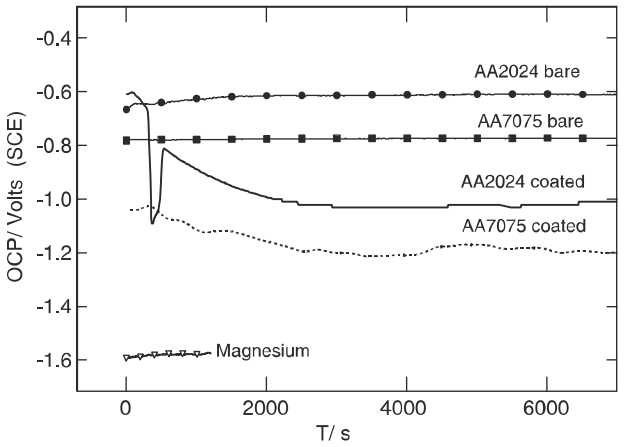

Figure 2.14 *Open circuit potential of the bare substrates, of the magnesium-rich primer coated substrates and of magnesium, in 0.1% NaCl.* [160]

Similar approaches with different alloys have been investigated since the introduction of the magnesium rich technology. Xu *et al.* [164] evaluated magnesium alloys to understand the effects of particle shape, particle size, particle size distribution, and metal alloy chemical composition whereas, Plageman *et al.* [165] investigated the effect of spherical zinc and zinc alloys to use the benefits of both zinc and magnesium by alloying. Magnesium would still provide cathodic protection, whereas the zinc would provide a lower reactivity of the particle. In addition, the zinc magnesium particles would lead to more voluminous corrosion products and a densification within the coating and improving the barrier properties of the coating. The alloy with 74% zinc and 26% magnesium demonstrated to be effective in accelerated corrosion testing. Thin film zinc rich primers (10-20 μm) were successfully tested on laboratory scale and by flight trials.[166]

Smart and self-healing coating technologies

Self-healing and smart coatings have become a growing and important concept for coatings for the protection of metals and alloys. One of the strategies is to detect and heal damages in a coating and to recover the initial functionality of the coating system. Since this pioneering

work of White *et al.*[167], self-healing or smart coatings discipline took a flight and resulted in a rapid increase of approaches. The main self-healing strategies are aesthetics and barrier recovery (gap filling) and active corrosion inhibition.[168] The strategies include the release of liquid reactive healing agents from capsules due to a mechanical damage, expansive phases, flow and reflow of material followed by a chemical reaction or restoration of physical bonds. The other approach is the release corrosion inhibitors or surface reactive compounds from microcapsules. Inhibitor release from these capsules can be triggered by mechanical damage, diffusion, ion exchange or change of pH. In 2011 Zheludkevich provided a comprehensive review of these smart and self healing technologies.[169] Since then, new approaches have been proposed. Garcia *et al.* proposed a self-healing concept based on an encapsulated water reactive silyl ester that is based on wetting and a reaction with ambient humidity and the metallic surface and it finally forms a hydrophobic layer to extend corrosion protection.[170] Other micro-capsule approaches proposed including: inhibitor impregnated $CaCO_3$ micro beads[171], TiO_2 nano-containers loaded with 8-hydroxyquinoline[172], Silica nano-containers with a regular shape and diameter between 100 and 150 nm loaded with 2-mercaptobenzothiazole[173], EDTA loaded Layered double hydroxides[174], and Cerium and diethyldithiocarbamate (DEDTC) double doped zeolites.[175] Also some patents have been filed to claim the use of such strategies for the protection of aluminium structures for Aerospace. Gammel *et al.* propose a coating with embedded micro-capsules containing 2-mercaptobenothiazole.[176] Barbe *et al.* claim a coating composition that comprises ceramic particles with a releasable active material homogeneously distributed in each particle.[177]

Another approach is the use of conducting polymers. Tallman *et al.* reported corrosion protective properties of conductive polymer coatings.[178, 179] Most of the investigated conductive polymers are based on polyaniline (Pani). The galvanic interaction between the oxidized and conducting form of Pani, the Emeraldine Salt (ES) and the aluminium substrate leads to positive polarization of the aluminium substrate and the reduction of Pani ES to the leucoemeraldine base (EB) of Pani and the release of a dopant anion.[180] The dopant can play a role in the corrosion protection due to the formation of a metal-dopant interface, Kendig *et al.* proposed to dope Pani ES with specific anions that could work as cathodic inhibitors and reduce the oxygen reduction reaction at copper-rich intermetallic particles.[181, 182] However, the exact protective mechanism for aluminium alloys has not been resolved yet.[183, 184] Concepts of such 'smart' conductive coatings have been developed by Kinlen and Kendig *et al.*[185, 186], and the first field testing studies, as an alternative to chromated chemical conversion coatings, have been reported [187].

Both the self-healing and conductive coating approaches are still under development and do not provided the industry with a drop-in alternative for hexavalent chromium, however the knowledge that is generated from this work can provide future tools for chromate free corrosion protection of aircraft structures.

Alternative coating techniques

The aerospace industry has been rather conservative in terms of accepting alternative coating technologies. The coating systems have been improved incrementally over the years and no real new coatings concepts have been introduced. However, with the current demands of the industry in terms of productivity and environmental impact, alternative coating techniques can be considered. Examples of such alternative coating techniques are electro deposition paints, powder coatings and UV curable coatings.

Electro deposition primers are widely used in the automotive industry. However, it was not introduced in the aerospace industry because of bath stability issues, coating thickness, high curing temperature and large capital investment. Recent developments make it possible to coat small parts with a chromate free electro deposition process.[188] In this efficient coating process, an electrical field is applied and water dispersed paint particles will be negatively charged and move to the anode. When the surface is coated, the part will be rinsed and thermally cured. Introduction of this technology will increase transfer efficiency and reduce over spray and solvent emissions, waste, and improved layer thickness control. The technology is based on anaphoretic paint deposition, which cures below 120°C. An Electro deposition coating provides anodisation and coating application in the same step. An interfacial oxide layer is formed during the anaphoretic paint deposition.[189] The oxide layer is composed of a dense sub-layer at on the substrate with oxide filaments interpenetrating in the coating with a film thickness of 20 μm. The technology is being introduced to the aerospace industry.[190]

Since the early 1980's there have been developments on powder coatings for aerospace applications.[191] This technology would eliminate solvent emissions, hazardous air pollutants, and reduce waste. In addition, it can provide improved efficiency due to faster curing, no pot life issues, and high transfer efficiency. The main issue of powder coatings has been the high temperatures needed to get a full cure of the system. These high curing temperatures, 220°C and higher, might affect the strength of the aluminium alloy. Research has resulted in low temperature and UV curable approaches, but the technology in not widely used in the industry.[192, 193]

Ultraviolet (UV) curing is the other alternative technology that can be used in coatings. These coatings can be formulated as 100% solids, without the use of VOC and hazardous air pollutants and can be polymerized, cross-linked in a matter of seconds and provides films that are decorative and functional. The UV curing mechanism is a photo- chemical process by which a liquid coating is completely cross-linked to solid polymer through exposure to UV radiation without the need for isocyanate cross-linking agents. There are two classes of UV curing technology, based on the nature of photo initiators and resin chemistry: free radical (mostly acrylate) and cationic (epoxy). Acrylate self-priming topcoat approaches were proposed for the protection of aerospace aluminium alloys. Although the approach was over chromated conversion coating, energy savings and solvent emission reductions were additional benefits to the reduction of chromates in the total paint system.[194, 195] Moreau *et al.* designed UV-curable hybrid sol-gel formulations based on both organic and inorganic

photo polymerization.[196] This process is based on the liberation of photo acids by the UV decomposition of iodonium salt. This triggers simultaneously the sol-gel process and epoxy cationic polymerization.[197] The one-step UV-curing process hybrid sol-gel coatings can provide high corrosion resistance on metallic substrates and protection of composites.

2.5.3 New approaches towards chromate free coatings technology

Chromate-free coatings technology is evolving rapidly. Over the years many inhibitors have been tested. However, corrosion testing is one of the bottlenecks in the coating development process. There is a need for faster and more accurate screening of new chromate free candidates. Inhibitors need to be tested for synergistic performance or activity over a wide pH range. In addition to this, chromate-free corrosion inhibiting coating technologies became better and therefore it becomes more difficult to discriminate between the current technologies and possible improvements, resulting in longer testing. Evaluation of corrosion results is still rather old fashioned and difficult to get absolute numbers. High throughput experimentation and imaging techniques are two examples of tools that can be used to accelerate the development of new chromate free inhibiting technology

High throughput experimentation

Corrosion performance has been historically evaluated using electrochemical techniques, accelerated corrosion testing, or even outdoor exposure. These methods require testing times ranging from hours to years. Advances in material science have broadened in the scope for the discovery of new corrosion inhibitors. Recent developments consider the combination of two or more inhibitor technologies (i.e. anodic and cathodic inhibitors) to obtain multifunctional or synergistic performance.[198, 199] There has been a considerable effort to develop high throughput experimentation techniques to increase the rate of new inhibitor screening and to find combinations for synergistic and antagonistic effects. High throughput combination and electrochemical characterization have provided new tools for the exploration and understanding of new corrosion inhibitors. Chambers *et al.* investigated the inhibition characteristics of 50 different chemistries within 9 hours using a direct current (DC) polarization between two AA2024 wire electrodes and a multiple –electrode-testing system.[200] Garcia *et al.* used a multi-metal electrode set-up to identify inhibitor efficacy to different metals simultaneously.[201] White *et al.* designed a multi-channel array for screening aqueous corrosion inhibitors on aluminium AA2024-T3. This method allows solutions to flow over the surface of the alloy. Inhibitor efficiency can be compared visually and quantitatively via solution analyses.[202] Another approach of White et al. is the use of a multi-well plate that can be filled with a range of solutions and the inhibitor performance is quantified with a computerized optical analysis method.[203] Further high throughput techniques are summarized in a review of Muster *et al.*[204]

Imaging techniques for corrosion evaluation

Quantification of corrosion during and after corrosion testing is another issue in corrosion research. Today, corrosion evaluation of coated panels for specification testing is still a visual process which is supported by a ruler and a camera to capture a value for the maximum corrosion, creep or undercutting from the scribe edge and sometimes a corrosion density. Many specifications have only maximum creep from scribe requirements. In addition corrosion progresses after testing making storage of after corrosion testing for future reference more or less useless. Imaging techniques have been proposed to improve the quantification of corrosion during and after corrosion testing.[205, 206] The quantification of corrosion is potentially valuable because it provides researches with absolute numbers, which can be used to discriminate between different inhibitor technologies. Corrosion is dissipating over a certain area and hence using maximum creep values is not providing the real value. The filiform analysis (Fig. 2.15) method can analyse data over a larger area, and it provides values that potentially can be used for corrosion rate or corrosion kinetics calculations. Moreover, the values can be used for corrosion rate and corrosion. Imaging has been used in the analysis of coatings with different corrosion inhibitors during the filiform corrosion test, large differences are obvious and can be easily observed. On the other hand, the other systems perform alike according the longest filament evaluation. However, evaluation of the total corrosion area provides a different perspective and it is easier to discriminate the systems that perform better and have a lower corrosion rate.

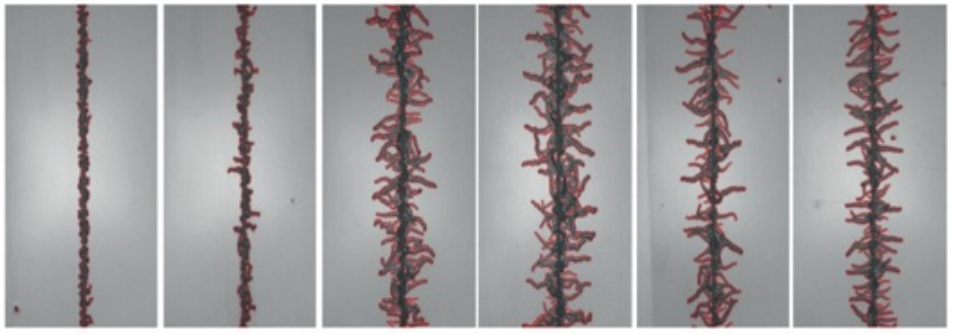

Figure 2.15 *Imaging of filiform corrosion.*

Another challenge for the engineers that develop or qualify new corrosion inhibiting systems is the evaluation of panels that have been exposed to salt spray exposure (ASTM B-117). It is very complicated to assign absolute numbers to these panels. Moreover, the time to discriminate between better performing technologies is increasing and limits fast developments. A method has been developed to evaluate the degree of pitting corrosion during and after accelerated corrosion testing. The method involves a surface roughness measurement of the exposed damaged area with the use of white light interferometry (Fig. 2.16).

Especially on AA2024, the method demonstrated the ability monitor the increase of the surface roughness of the damaged area (scribe) due to corrosion phenomena at the early stages of exposure and after longer-term exposure to the corrosive environment. With the use of imaging software it is possible to quantify the surface roughness of the area, increase in surface area, and the amount of areas or pits deeper than a certain threshold value. These values can be related to a degree of pitting.[129]

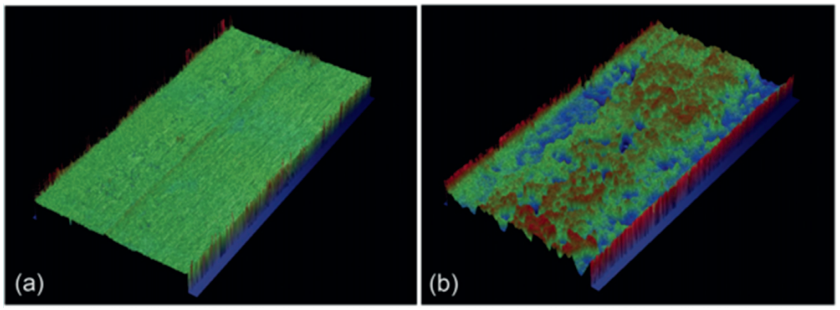

Figure 2.16 *White light interferometry analysis before (a) and after (b) Neutral Salt spray (ASTM B117) exposure reveals the change in surface roughness due to pitting corrosion on AA2024-T3.*

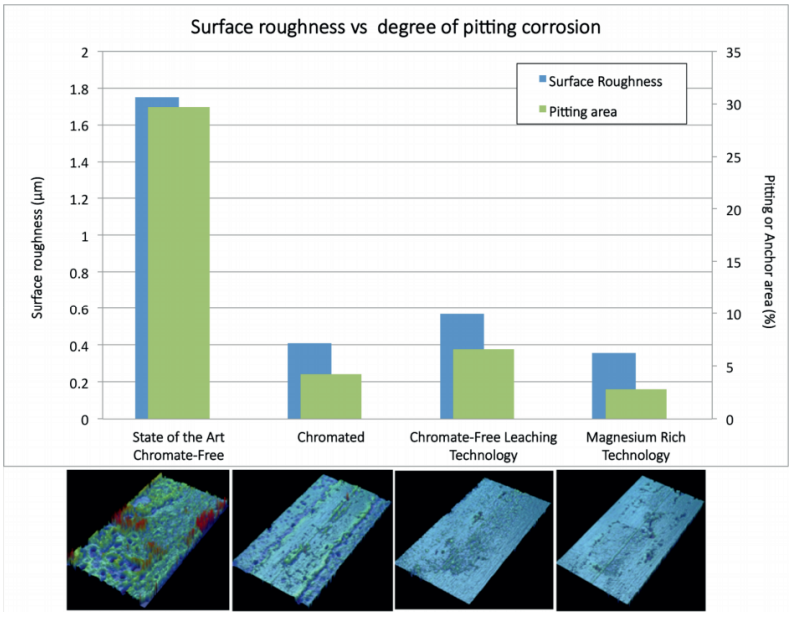

Figure 2.17 *Relation between surface roughness and pitting area for various corrosion inhibiting coating technologies after 3000 h neutral salt spray (ASTM B-117) exposure.*[129]

The technique enables the determination and quantification of the performance of corrosion inhibiting technologies before the human eye is able to detect the differences, and support engineers to make decisions based on values rather than opinions. A practical example can be found in Fig. 2.17. This figure compares three chromate-free coatings and a chromated coating. It shows that the surface roughness and degree (%) of pitting corrosion are closely related and that both new two chromate free coatings are demonstrating good corrosion protection with a low degree of pitting alike the traditional chromated coating.

2.6 Remaining challenges for chromate replacement

The replacement and elimination of hexavalent chromium based processes and inhibitors is an enormous challenge for the aerospace industry. The corrosion control requirements in the aerospace industry have been developed and are based on the performance of hexavalent chromium (chromates). All designs, specifications, testing data and in-service experience are based on this versatile and unique inhibitor. The track record of chromates is impressive. However, legislative pressure pushes the industry to look for suitable alternatives for this unique material. A tremendous amount work is on going and over the recent years the progress has provided the industry with a number chromate free options for pre-treatments, and coatings. Despite this progress, there are many challenges for the industry. Processes and mechanisms need to be reviewed or reconsidered and possibly changed to provide the industry with confidence to eliminate hexavalent chromium. Chromate free coating technology evolved and chromate free systems are being qualified at the major aircraft manufacturers for external applications. Nevertheless, it is clear that the current efforts did not result in the perfect replacement and a lot of work is needed to provide confidence to apply these systems.

Multiple chromate free alternative processes have been introduced to the industry.[80, 106] Especially on pre-treatment level, alternative solutions were introduced but still to be used in combination with chromated coating systems Therefore, many challenges have to be overcome before hexavalent chromium and chromates can be eliminated from the aerospace industry. These challenges are:

- Technical performance
- Processes and requirements
- Industry confidence
- Service life prediction

First, the primary challenge is to find suitable alternative inhibitors and coating systems that demonstrate an equal or better technical performance compared to the hexavalent chromium. The superior inhibiting efficiency and versatile behaviour of chromates and hexavalent chromium materials make it very difficult to replace it by a single drop-in material. Chromate inhibition mechanisms have been studied[20], but mimicking chromates has not

been very successful and possibly new approaches are necessary to provide a similar protection. Nevertheless, in recent last years many inhibitors were identified and tested extensively. Some are promising candidates and some are very close to the performance of chromates in accelerated corrosion tests. However, the performance in service is still unclear.

The second challenge concerns the processes and requirements of the aerospace industry. Hexavalent chromium is the primary corrosion control material. It is embedded in all parts in aerospace industry, from the smallest clip to the largest stringer, fasteners and sealants, coatings and pre-treatments. Chromate containing products processes are specified by material specifications for new aircraft but as well in the maintenance manuals of legacy aircraft currently in service. The replacement of chromates will be a long process with many hurdles.

Industry confidence is the third challenge. First of all, are the performance of the new chromate free technologies and the confidence of the industry sufficient enough to make a switch to total chromate free aircraft when legislation and regulations ban the use of these carcinogenic materials? Today, alternative solutions have been introduced, these solutions passed the material specification requirements but still are not as good or robust as chromated technology. When these individual qualified materials are introduced in a system, it is possible that the total system does not always requirements. The laboratory performance of new systems is known, but the in-service behaviour and performance is unknown. Therefore, new chromate-free systems need to be tested extensively to provide confidence to the aerospace engineers to justify a switch to chromate free coating technology.

The final challenge is service-life prediction. Chromated systems have a proven track record of more than 50 years within the aerospace industry. The protection of aircraft structure has been ensured for more than 30 years. With the introduction of the chromate-free technology it is a brand new story. Developments demonstrate that it is possible to meet the aerospace specification requirements. However, it remains unclear how the system behaves under in-service conditions. The challenge is how to predict the long-term performance of a new chrome-free coating system so it protects the aircraft structure for more than 30 years. Reduced performance will lead to higher maintenance and depreciation costs.

2.7 Summary and conclusion

Aviation is an integral part of society of today. Air travel is increasing and the number of aircraft is expected to double over the coming 20 years. Aircraft are very complex designs with variety of metals and composite materials. With an expected service- life of about 30 years and the harsh operating environment with many flight cycles makes fatigue properties and corrosion protection important concerns.

Aluminium is the predominant construction material for aircraft. Especially, 2024 and 7075 are commonly used because of their favourable strength to weight ratio. However, these alloys are susceptible to various types of corrosion. Corrosion control is a key element next to efficient and environmental sustainable operations Coatings and surface treatments is one of the critical factors in the corrosion protection scheme to ensure the long- term protection of the aircraft structure.

Aerospace coatings are used on all types of commercial and military aircraft as protective and decorative finishes. These coatings are designed and formulated to withstand challenging operating conditions. The requirements and properties for aerospace coatings are controlled by specifications. There are 3 categories of aerospace coatings: structural systems, exterior systems and special purpose systems. They are usually applied with hand-held spray equipment and cured at ambient conditions.

Current aerospace coating systems are mainly based on a pre-treatment (e.g. Chemical Conversion Coating or anodising) on the aluminium alloy, a corrosion inhibiting epoxy-amine primer, and a protective or decorative polyurethane topcoat. Hexavalent chromium compounds are widely used coatings and pre-treatments; these materials have excellent anticorrosive properties and provided the foundation of the corrosion protection of today's aircraft structures. The hexavalent chromium compounds are the basis of the active protective nature of these coating systems. Next to the barrier function, these coatings have the ability to release the corrosion inhibitor from the coating by a leaching process.

The industry has been using hexavalent chromium inhibition since the introduction of the aluminium aircrafts. However, health issues and new legislations and regulations are putting pressure on the industry to find sustainable alternatives to replace hexavalent chromium compounds. Already since the 1980's fundamental and applied research has been searching for alternatives and resolving the inhibition mechanism of hexavalent chromium. The quest for chromate-free coatings systems that provides corrosion protection better than or equal to the chromated technology has resulted in a range of chromate free pre-treatments and coating systems. Several of them have been qualified and introduced into the market place. The research also provided new inhibition strategies like: cathodic protection, conductive polymers, self-healing approaches, high throughput technologies, and advanced corrosion assessment tools.

Despite the availability of chromate free materials and systems, it can be stated that there is no direct replacement for hexavalent chromium available to date. Therefore, research continues to meet the technical performance of chromated technology and to overcome the challenges associated chromate free inhibition systems for aerospace coatings and to provide the confidence to the industry to introduce the chromate free alternatives and eliminate hexavalent chromium compounds from the industry.

References

1. O. Guseva, S. Brunner and P. Richner, Analysis of the environmental parameters for aircraft coatings, *Macromolecular Symposia*, 2002, 187, 883-893.
2. Deloitte, 2013 Global aerospace and defense industry outlook,http://www.deloitte.com/aerospace&defense/2013a&doutlook, (accessed 12 march 2014, 2014).
3. G. A. M. A. (GAMA), 2012 General Aviation Statistical Databook & Industry Outlook, http://www.gama.aero/media-center/industry-facts-and-statistics/, (accessed 10 October 2013, 2013).
4. Airbus, Airbus Global Market Forecast 2012-2031,http://www.airbus.com/company/market/forecast/?, (accessed August 2013).
5. Boeing, Current Market Outlook 2013–2032, http://www.boeing.com/assets/pdf/commercial/cmo/pdf/Boeing_Current_Market_Outlook_2013.pdf,, (accessed august 2013).
6. H. Jiang, Key Findings on Airplane Economic Life, http://www.boeing.com/boeing/commercial/industry_info.page, (accessed 12 December 2013, 2013).
7. T. Wright, Aerospace coatings, *Coatings World*, 2010, 15, 28-31.
8. I. C. A. Organization, ICAO Safety Report 2014 Edition, http://www.icao.int/safety/Documents/ICAO_2014 Safety Report_final_02042014_web.pdf, (accessed 13 March 2014, 2014).
9. G. H. Koch, Cost of Corrosion Appendix P Aircraft, http://corrosionda.com/transportation/aircraft/index.htm, (accessed 13 March 2014).
10. J. A. DeRose, T. Suter, T. Hack and R. Adey, *Aluminium Alloy Corrosion of Aircraft Structures: Modelling and Simulation*, WIT Press, 2013.
11. M. Kendig, S. Jeanjaquet, R. Addison and J. Waldrop, Role of hexavalent chromium in the inhibition of corrosion of aluminum alloys, *Surface and Coatings Technology*, 2001, 140, 58-66.
12. P. National Toxicology, NTP 12th Report on Carcinogens, *Report on carcinogens : carcinogen profiles / U.S. Dept. of Health and Human Services, Public Health Service, National Toxicology Program*, 2011, 12, 106 - 109.
13. D. C. v. Beelen, P. Rouw, R. Boomgaard and K. Zabel, Aviox CF Primer: a new generation primer for aircraft maintenance, *Anti-Corrosion Methods and Materials*, 1997, 44, 28-33.
14. J. G. Kaufman, *Introduction to aluminum alloys and tempers*, ASM International, 2000.
15. J. R. Davis, *Corrosion of aluminum and aluminum alloys*, ASM International, 1999.
16. T. Richardson, B. Cottis, D. Scantlebury, R. Lindsay, S. Lyon and M. Graham, *Shreir's Corrosion*, Elsevier, 2010.
17. I. J. Polmear, *Light Alloys*, Elsevier Ltd, 2005.
18. A. E. Hughes, Birbilis, N., Mol, J.M.C., Santiago J. Garcia, S.J., Zhou, X., Thompson, G.E. , in *Recent Trends in Processing and Degradation of Aluminium Alloys*, ed. P. Z. Ahmad, *In Tech*, 2011.
19. T. Dursun and C. Soutis, Recent developments in advanced aircraft aluminium alloys, *Mater. Des.*, 2014, 56, 862-871.
20. G. S. Frankel, Mechanism of Al alloy corrosion and the role of chromate inhibitors final report, *STAR*, 2002, 40.
21. L. Xia and R. L. McCreery, Chemistry of a chromate conversion coating on aluminum alloy AA2024-T3 probed by vibrational spectroscopy, *Journal of the Electrochemical Society*, 1998, 145, 3083-3089.
22. J. H. Osborne, Observations on chromate conversion coatings from a sol-gel perspective, *Progress in Organic Coatings*, 2001, 41, 280-286.
23. P. Campestrini, G. Goeminne, H. Terryn, J. Vereecken and J. H. W. De Wit, Chromate Conversion Coating on Aluminum Alloys I. Formation Mechanism, *Journal of the Electrochemical Society*, 2004, 151, B59-B70.
24. L. Xia, E. Akiyama, G. Frankel and R. McCreery, Storage and release of soluble hexavalent chromium from chromate conversion coatings. Equilibrium aspects of CrVI concentration, *Journal of the Electrochemical Society*, 2000, 147, 2556-2562.
25. J. D. Ramsey and R. L. McCreery, In situ Raman microscopy of chromate effects on corrosion pits in aluminum alloy, *Journal of the Electrochemical Society*, 1999, 146, 4076-4081.
26. G. E. Thompson, H. Habazaki, K. Shimizu, M. Sakairi, P. Skeldon, X. Zhou and G. C. Wood, Anodizing of aluminium alloys, *Aircraft Engineering and Aerospace Technology*, 1999, 71, 228-238.
27. G. C. Wood and J. P. O'Sullivan, The anodizing of aluminium in sulphate solutions, *Electrochimica Acta*, 1970, 15, 1865-1876.
28. A. D. Juhl, Overview of anodizing in the aerospace industry, *Metal Finishing*, 2010, 108, 20-21.
29. H. Rosenboom, Chemistry of wash primers, *Industrial & Engineering Chemistry* 1953, 45, 2982.

30. R. G. Buchheit, A compilation of corrosion potentials reported for intermetallic phases in aluminum-alloys, *Journal of the Electrochemical Society*, 1995, 142, 3994-3996.
31. R. G. Buchheit, R. P. Grant, P. F. Hlava, B. McKenzie and G. L. Zender, Local dissolution phenomena associated with S phase (Al2CuMg) particles in aluminum alloy 2024-T3, *Journal of the Electrochemical Society*, 1997, 144, 2621-2628.
32. N. Birbilis and R. G. Buchheit, Electrochemical characteristics of intermetallic phases in aluminum alloys - An experimental survey and discussion, *Journal of the Electrochemical Society*, 2005, 152, B140-B151.
33. J. H. W. de Wit, New knowledge on localized corrosion obtained from local measuring techniques, *Electrochimica Acta*, 2001, 46, 3641-3650.
34. J. M. C. Mol, A. E. Hughes, B. R. W. Hinton and S. van der Zwaag, A morphological study of filiform corrosive attack on chromated and alkaline-cleaned AA2024-T351 aluminium alloy, *Corrosion Science*, 2004, 46, 1201-1224.
35. Z. Szklarska-Smialowska, Pitting corrosion of aluminum, *Corrosion Science*, 1999, 41, 1743-1767.
36. A. Boag, A. E. Hughes, A. M. Glenn, T. H. Muster and D. McCulloch, Corrosion of AA2024-T3 Part I: Localised corrosion of isolated IM particles, *Corrosion Science*, 2011, 53, 17-26.
37. A. E. Hughes, A. Boag, A. M. Glenn, D. McCulloch, T. H. Muster, C. Ryan, C. Luo, X. Zhou and G. E. Thompson, Corrosion of AA2024-T3 Part II: Co-operative corrosion, *Corrosion Science*, 2011, 53, 27-39.
38. A. M. Glenn, T. H. Muster, C. Luo, X. Zhou, G. E. Thompson, A. Boag and A. E. Hughes, Corrosion of AA2024-T3 Part III: Propagation, *Corrosion Science*, 2011, 53, 40-50.
39. A. Boag, R. J. Taylor, T. H. Muster, N. Goodman, D. McCulloch, C. Ryan, B. Rout, D. Jamieson and A. E. Hughes, Stable pit formation on AA2024-T3 in a NaCl environment, *Corrosion Science*, 2010, 52, 90-103.
40. S. T. Pride, J. R. Scully and J. L. Hudson, Metastable pitting of aluminum and criteria for the transition to stable pit growth, *Journal of the Electrochemical Society*, 1994, 141, 3028-3040.
41. M. B. Vukmirovic, N. Dimitrov and K. Sieradski, Dealloying and corrosion of Al alloy 2024-T3, *Journal of the Electrochemical Society*, 2002, 149, B428-B439.
42. C. Luo, X. Zhou, G. E. Thompson and A. E. Hughes, Observations of intergranular corrosion in AA2024-T351: The influence of grain stored energy, *Corrosion Science*, 2012, 61, 35-44.
43. X. Zhou, C. Luo, Y. Ma, T. Hashimoto, G. E. Thompson, A. E. Hughes and P. Skeldon, Grain-stored energy and the propagation of intergranular corrosion in AA2xxx aluminium alloys, *Surface and Interface Analysis*, 2013, 45, 1543-1547.
44. F. Andreatta, H. Terryn and J. H. W. de Wit, Corrosion behaviour of different tempers of AA7075 aluminium alloy, *Electrochimica Acta*, 2004, 49, 2851-2862.
45. T. Marlaud, B. Malki, C. Henon, A. Deschamps and B. Baroux, Relationship between alloy composition, microstructure and exfoliation corrosion in Al-Zn-Mg-Cu alloys, *Corrosion Science*, 2011, 53, 3139-3149.
46. M. Tanaka, C. Hénon and T. Warner, *Journal*, 2006, 519-521, 345-350.
47. R. T. Foley, Localized Corrosion of Aluminum Alloys - a Review, *Corrosion*, 1986, 42, 277-288.
48. R. Braun, Environmentally assisted cracking of aluminium alloys, *Materialwissenschaft und Werkstofftechnik*, 2007, 38, 674-689.
49. R. C. Newman, Elsevier, 2010, pp. 864-901.
50. D. Banis, A.J. Marceau, M. Mohaghegh, Design for corrosion control, http://www.boeing.com/commercial/aeromagazine/aero_07/corrosn.html - methods, (accessed 22 December, 2013).
51. O. M. Matarredona, K. Mach, M. M. Rieger and E. A. O'Rear, Alteration of wettability and inhibition of corrosion in narrow aluminium 7075 gaps by thin polymer films, *Corrosion Science*, 2003, 45, 2541-2562.
52. I. S. Cole, W. G. Ganther, P. Corrigan, S. Galea, P. Trathen and B. Hinton, Frequency and duration of wetness periods on surfaces in airframes, *Corrosion Engineering Science and Technology*, 2012, 47, 529-535.
53. J. V. Koleske, *Paint and Coating Testing Manual: Fourteenth Edition of the Gardner-Sward Handbook*, ASTM, 1995.
54. N. Ohta and A. R. Robertson, in *Colorimetry*, John Wiley & Sons, Ltd, 2006, DOI: 10.1002/0470094745.ch3, pp. 63-114.
55. A. K. Chattopadhyay and M. K. R. Zentner, *Aerospace and Aircraft Coatings*, Federation of Societies for Coatings Technology, 1990.
56. G. P. Bierwagen and D. E. Tallman, Choice and measurement of crucial aircraft coatings system properties, *Progress in Organic Coatings*, 2001, 41, 201-216.
57. Z. W. Wicks, F. N. Jones, S. P. Pappas and D. A. Wicks, *Organic Coatings: Science and Technology*, John Wiley & Sons, Inc., 2006.

58. J. Sinko, Challenges of chromate inhibitor pigments replacement in organic coatings, *Progress in Organic Coatings*, 2001, 42, 267-282.
59. M. W. Kendig and R. G. Buchheit, Corrosion inhibition of aluminum and aluminum alloys by soluble chromates, chromate coatings, and chromate-free coatings, *Corrosion*, 2003, 59, 379-400.
60. F. H. Scholes, S. A. Furman, A. E. Hughes, T. Nikpour, N. Wright, P. R. Curtis, C. M. Macrae, S. Intem and A. J. Hill, Chromate leaching from inhibited primers. Part I. Characterisation of leaching, *Progress in Organic Coatings*, 2006, 56, 23-32.
61. S. A. Furman, F. H. Scholes, A. E. Hughes and D. Lau, Chromate leaching from inhibited primers. Part II: Modelling of leaching, *Progress in Organic Coatings*, 2006, 56, 33-38.
62. S. Sellaiyan, A. E. Hughes, S. V. Smith, A. Uedono, J. Sullivan and S. Buckman, Leaching properties of chromate-containing epoxy films using radiotracers, PALS and SEM, *Progress in Organic Coatings*, 2014, 77, 257-267.
63. X. Zhou, C. Luo, T. Hashimoto, A. E. Hughes and G. E. Thompson, Study of localized corrosion in AA2024 aluminium alloy using electron tomography, *Corrosion Science*, 2012, 58, 299-306.
64. S. P. Knight, M. Salagaras, A. M. Wythe, F. De Carlo, A. J. Davenport and A. R. Trueman, In situ X-ray tomography of intergranular corrosion of 2024 and 7050 aluminium alloys, *Corrosion Science*, 2010, 52, 3855-3860.
65. A. Trueman, S. Knight, J. Colwell, T. Hashimoto, J. Carr, P. Skeldon and G. Thompson, 3-D tomography by automated in situ block face ultramicrotome imaging using an FEG-SEM to study complex corrosion protective paint coatings, *Corrosion Science*, 2013, 75, 376-385.
66. A. E. Hughes, A. Trinchi, F. F. Chen, Y. S. Yang, I. S. Cole, S. Sellaiyan, J. Carr, P. D. Lee, G. E. Thompson and T. Q. Xiao, The application of multiscale quasi 4D CT to the study of SrCrO4 distributions and the development of porous networks in epoxy-based primer coatings, *Progress in Organic Coatings*, 2014, 77, 1946-1956.
67. E. Javierre, S. J. García, J. M. C. Mol, F. J. Vermolen, C. Vuik and S. van der Zwaag, Tailoring the release of encapsulated corrosion inhibitors from damaged coatings: Controlled release kinetics by overlapping diffusion fronts, *Progress in Organic Coatings*, 2012, 75, 20-27.
68. P. E. Jennerjohn, Unique aspects involved in the robotic painting of commercial aircraft structures, *SAE Technical Papers*, 2011, DOI: 10.4271/2011-01-2790.
69. K. Pianoforte, Aerospace Coatings Market, http://www.coatingsworld.com/issues/2013-05/view_features/aerospace-coatings-market-316334/, (accessed 08 july, 2013).
70. G. Bierwagen, Next generation of aircraft coatings systems, *Journal of Coatings Technology*, 2001, 73, 45-52.
71. M. Costa and C. B. Klein, Toxicity and carcinogenicity of chromium compounds in humans, *Critical Reviews in Toxicology*, 2006, 36, 155-163.
72. U. P. H. Service, Toxicological Profile for Chromium, *Report No. ATSDR/TP 88/10*, 1989.
73. W. Robison, Pantheon's PreKote Surface Pretreatment Qualifies to AMS 3095A with Three Coatings Systems, http://www.reuters.com/article/2013/04/30/az-pantheon-enterprises-idUSnBw306717a+100+BSW20130430).
74. A. Davis, Boeing Delivers KLM 777-300ER in SkyTeam Livery, http://www.prnewswire.com/news-releases/boeing-delivers-klm-777-300er-in-skyteam-livery-62024167.html).
75. T. Pennington, PPG Aerospace Chromate-Free Primer First to be Qualified by Boeing, *Products Finishing*, 2011, 75, 12.
76. Anonymous, Army Approves Hex-Chrome-free Coating, *Products Finishing*, 2008, 72, 12.
77. T. Pennington, PPG Industries, AkzoNobel Launch New Aerospace Coating Products, *Products Finishing (Cincinnati)*, 2012, 76, 32-33.
78. T. Pennington, Aerospace Drives More Calls for Non-Chrome Passivate Finishes, *Products Finishing*, 2012, 76, 16-21.
79. L. Roberts and A. Galanis, Eliminating hexavalent chrome, *Industrial Paint and Powder*, 2006, 82, 13-16.
80. E. Eichinger, Osborne, J.H., Hexavalent chromium elimination: an aerospace industry progress report, *Metal Finishing (USA)*, 1997, 95, 36-41.
81. J. H. Osborne, presented in part at the Surfair, Biarritz, 5-6 June 2008.
82. A. S. Hamdy, I. Doench and H. Möhwald, Intelligent self-healing corrosion resistant vanadia coating for AA2024, *Thin Solid Films*, 2011, 520, 1668-1678.
83. A. E. Hughes, J. D. Gorman, T. G. Harvey, A. Galassi and G. McAdam, Development of permanganate-based coatings on aluminum alloy 2024-T3, *Corrosion*, 2006, 62, 773-780.
84. S. A. Kulinich, A. S. Akhtar, P. C. Wong, K. C. Wong and K. A. R. Mitchell, Growth of permanganate conversion coating on 2024-Al alloy, *Thin Solid Films*, 2007, 515, 8386-8392.
85. G. Yoganandan, J. N. Balaraju and V. K. W. Grips, The surface and electrochemical analysis of permanganate based conversion coating on alclad and unclad 2024 alloy, *Applied Surface Science*, 2012, 258, 8880-8888.

86. R. G. Buchheit, Bode, M.D., Stoner, G.E., Corrosion-Resistant, Chromate free Talc Coatings for Aluminum, *Corrosion*, 1994, 50, 205-214.
87. C. A. Drewien, Eatough, M.O., Tallant, D.R., Hills, C.R., Buchheit, R.G., Lithium-aluminum-carbonate-hydroxide hydrate coatings on aluminum: Composition, structure and processing bath chemistry, *Journal of material research*, 1996, 11, 1507-1513.
88. *R. G. Buchheit and G. E. Stoner,* US5266356-A; US35576-E, 1993.
89. M. R. S. Castro, J. C. Nogueira, G. P. Thim and M. A. S. Oliveira, Adhesion and corrosion studies of a lithium based conversion coating film on the 2024 aluminum alloy, *Thin Solid Films*, 2004, 457, 307-312.
90. C. M. Rangel and M. A. Travassos, Li-based conversion coatings on aluminium: An electrochemical study of coating formation and growth, *Surface & coatings technology*, 2006, 200, 5823-5828.
91. C. M. Rangel and M. A. Travassos, The passivation of aluminium in lithium carbonate/bicarbonate solutions, *Corrosion Science*, 1992, 33, 327-343.
92. T. G. Harvey, Cerium-based conversion coatings on aluminium alloys: a process review, *Corrosion Engineering, Science and Technology*, 2013, 48, 248-269.
93. M. Bethencourt, F. J. Botana, J. J. Calvino, M. Marcos and M. A. Rodriguez-Chacon, Lanthanide compounds as environmentally-friendly corrosion inhibitors of aluminium alloys: A review, *Corrosion Science*, 1998, 40, 1803-1819.
94. A. J. Aldykewicz, Jr., H. S. Isaacs and A. J. Davenport, Investigation of cerium as a cathodic inhibitor for aluminum-copper alloys, *Journal of the Electrochemical Society*, 1995, 142, 3342-3350.
95. S. A. Hayes, P. Yu, T. J. O'Keefe, M. J. O'Keefe and J. O. Stoffer, The phase stability of cerium species in aqueous systems. I. E-pH diagram for the Ce-HClO4-H2O system, *Journal of the Electrochemical Society*, 2002, 149, C623-C630.
96. P. Campestrini, H. Terryn, A. Hovestad and J. H. W. de Wit, Formation of a cerium-based conversion coating on AA2024: relationship with the microstructure, *Surface & Coatings Technology*, 2004, 176, 365-381.
97. A. E. Hughes, F. H. Scholes, A. M. Glenn, D. Lau, T. H. Muster and S. G. Hardin, Factors influencing the deposition of Ce-based conversion coatings, part I: The role of Al3+ ions, *Surface & Coatings Technology*, 2009, 203, 2927-2936.
98. D. Lau, A. M. Glenn, A. E. Hughes, F. H. Scholes, T. H. Muster and S. G. Hardin, Factors influencing the deposition of Ce-based conversion coatings, Part II: The role of localised reactions, *Surface and Coatings Technology*, 2009, 203, 2937-2945.
99. M. J. O'Keefe, S. Geng and S. Joshi, Cerium-based conversion coatings as alternatives to hex chrome. Rare-earth compounds provide resistance against corrosion for aluminum alloys in military applications, *Metal Finishing*, 2007, 105, 25-28.
100. S. Geng, P. Yu, M. J. O'Keefe, W. G. Fahrenholtz and T. J. O'Keefe, Screening study of spray solution parameters for depositing cerium-based conversion coatings on Al alloy 2024-T3, *Journal of Applied Electrochemistry*, 2010, 40, 551-559.
101. T. S. Schmidt-Hansberg, P. , A Comparative Study of Innovative Aluminium Pretreatments, *ATB Metallurgie*, 2003, 43, 9-14.
102. E. Morris, presented in part at the ASETSDefense 2012: Sustainable Surface Engineering for Aerospace and Defense Workshop, San Diego, CA, August 27-30, 2012.
103. *C. Matzdorf, M. Kane, J. Green, C. A. Matzdorf, M. J. Kane, J. L. Green, A. Matzdorf, J. Kane and L. Green,* WO200255758-A; EP1404894-A; US6375726-B1.
104. H. Bhatt, A. Manavbasi and D. Rosenquist, Trivalent chromium for enhanced corrosion protection on aluminum surfaces, *Metal Finishing*, 2009, 107, 31-37.
105. C. Matzdorf, presented in part at the ASETSDefense 2012: Sustainable Surface Engineering for Aerospace and Defense Workshop, San Diego, Ca, USA, August, 27-30, 2012, 2012.
106. K. Legg, Report DoD Metal Finishing Workshop - Chromate Alternatives for Metal Treatment and Sealing, *DoD Metal Finishing Workshop - Chromate Alternatives for Metal Treatment and Sealing*, 2007, SERDP/ESTCP, Layton, Utah, USA.
107. Y. Guo and G. S. Frankel, Active Corrosion Inhibition of AA2024-T3 by Trivalent Chrome Process Treatment, *Corrosion*, 2012, 68.
108. Y. Guo and G. S. Frankel, Characterization of trivalent chromium process coating on AA2024-T3, *Surface & Coatings Technology*, 2012, 206, 3895-3902.
109. A. Iyer, W. Willis, S. Frueh, W. Nickerson, A. Fowler, J. Barnes, L. Hagos, J. Escarsega, J. La Scala and S. L. Suib, Characterization of NAVAIR Trivalent Chromium Process (TCP) coatings and solutions, *Plating and Surface Finishing*, 2010, 97, 32-41.

110. S. L. Suib, J. La Scala, W. Nickerson, A. Fowler and N. Zaki, Determination of hexavalent chromium in NAVAIR trivalent chromium process (TCP) coatings and process solutions, *Metal Finishing*, 2009, 107, 28-31,33-34.
111. F. T. Museux, R., *Journal*, 2009, 7.
112. J. H. Osborne, presented in part at the DoD Metal Finishing Workshop - Chromate Alternatives for Metal Treatment and Sealing, Layton, Utah, May 16 & 17, 2007.
113. T. B. Company, Preferred Materials and Processes, http://www.boeingsuppliers.com/environmental/chromic.html, (accessed 19 october, 2013).
114. L. Zhang, G. E. Thompson, M. Curioni and P. Skeldon, Anodizing of Aluminum in Sulfuric Acid/Boric Acid Mixed Electrolyte, *Journal of the Electrochemical Society*, 2013, 160, C179-C184.
115. M. Curioni, P. Skeldon, E. Koroleva, G. E. Thompson and J. Ferguson, Role of Tartaric Acid on the Anodizing and Corrosion Behavior of AA 2024 T3 Aluminum Alloy, *Journal of the Electrochemical Society*, 2009, 156, C147-C153.
116. M. Curioni, P. Skeldon, J. Ferguson and G. E. Thompson, Reducing the energy cost of protective anodizing, *Journal of Applied Electrochemistry*, 2011, 41, 773-785.
117. M. Curioni, P. Skeleton, G. E. Thompson and J. Ferguson, *Journal*, 2008, 38, 48-55.
118. M. Curioni, T. Gionfini, A. Vicenzo, P. Skeldon and G. E. Thompson, Optimization of anodizing cycles for enhanced performance, *Surface and Interface Analysis*, 2013, 45, 1485-1489.
119. M. Mohammadi, A. Yazdani, M. E. Bahrololoom and A. Alfantazi, Corrosion behavior of 2024 aluminum alloy anodized in presence of permanganate and phosphate ions, *Journal of Coatings Technology Research*, 2013, 10, 219-229.
120. F. Mansfeld, C. Chen, C. B. Breslin and D. Dull, Sealing of anodized aluminum alloys with rare earth metal salt solutions, *Journal of the Electrochemical Society*, 1998, 145, 2792-2798.
121. M. Garcia-Rubio, M. P. de Lara, P. Ocon, S. Diekhoff, M. Beneke, A. Lavia and I. Garcia, Effect of postreatment on the corrosion behaviour of tartaric-sulphuric anodic films, *Electrochimica Acta*, 2009, 54, 4789-4800.
122. G. Boisier, A. Lamure, N. Pebere, N. Portail and M. Villatte, Corrosion protection of AA2024 sealed anodic layers using the hydrophobic properties of carboxylic acids, *Surface & Coatings Technology*, 2009, 203, 3420-3426.
123. *K. A. Krienke, K. Y. Blohowiak and J. H. Osborne,* US5814137-A.
124. J. H. Osborne, K. Y. Blohowiak, S. R. Taylor, C. Hunter, G. Bierwagon, B. Carlson, D. Bernard and M. S. Donley, Testing and evaluation of nonchromated coating systems for aerospace applications, *Progress in Organic Coatings*, 2001, 41, 217-225.
125. K. Y. Blohowiak, J. H. Osborne and J. E. Seebergh, Development and implementation of sol-gel coatings for aerospace applications, *SAE Technical Papers*, 2009, DOI: 10.4271/2009-01-3208.
126. L. Roberts and A. Galanis, Proven non-chromated technology, *Paint & Coatings Industry*, 2003, 19, 86.
127. R. L. Twite and G. P. Bierwagen, Review of alternatives to chromate for corrosion protection of aluminum aerospace alloys, *Progress in Organic Coatings*, 1998, 33, 91-100.
128. G. S. Frankel, Mechanism of Al Alloy Corrosion and the Role of Chromate Inhibitors, *AFOSR Multidisciplinary University Research Initiative*, 2001.
129. P. Visser, Chrome free corrosion inhibiting coating technology for the protection of high strength aluminum alloys, *National Association for Surface Finishing Annual Conference and Trade Show, SUR/FIN 2013, Chicago, IL, USA*, 2013.
130. M. Iannuzzi and G. S. Frankel, Mechanisms of corrosion inhibition of AA2024-T3 by vanadates, *Corrosion Science*, 2007, 49, 2371-2391.
131. M. Iannuzzi, T. Young and G. S. Frankel, Aluminum alloy corrosion inhibition by vanadates, *Journal of the Electrochemical Society*, 2006, 153, B533-B541.
132. *J. O. Stoffer, T. J. O'Keefe, E. Morris, P. Yu, S. Hayes, J. Stoffer, T. Okeefe, S. A. Hayes, E. L. Morris and T. J. Okeefe,* WO2004065497-A2; US2004249043-A1.
133. M. O'Keefe, B. Fahrenholtz, E. Morris and R. Albers, Chicago, IL, 2013.
134. *G. Pipko,* WO9840440-A; EP988347-A.
135. *G. Pipko, A. Vitner and A. Vinter,* WO200299002-A.
136. *X. Yu, W. Zhang, T. Garosshen, P. Bhatia, M. Jaworowski, F. Lamm, X. Tang, A. Besing, M. A. Kryzman, X. Chang, J. Yu, C. Xiaoyuan, B. Amy, Z. Weilong, Y. J. Xiaomei, B. Promila, L. Foster, T. Xia and G. T. Mar,* US2004262580-A1; EP1493846-A1; CA2472562-A1; CN1576324-A; MX2004006377-A1; SG118292-A1; CN1267509-C; US7341677-B2; TW200506019-A; CA2472562-C; EP1493846-B1; ES2385981-T3.
137. *J. W. Putnam and M. Jaworowski,* EP1191073-A2.
138. *D. N. Walters and J. R. Schneider,* CN101287784-B; US2008090069-A1; US8231970-B2.

139. *P. Visser and S. A. Hayes,* WO2010112605-A1; AU2010230147-A1; KR2012007506-A; US2012025142-A1; EP2414464-A1; CN102378793-A; IN201106820-P4; EP2414464-B1; RU2011144574-A.
140. S. J. Garcia, T. A. Markley, J. M. C. Mol and A. E. Hughes, Unravelling the corrosion inhibition mechanisms of bi-functional inhibitors by EIS and SEM-EDS, *Corrosion Science*, 2013, 69, 346-358.
141. P. Visser, Y. Lui, X. Zhou, T. Hashimoto, G. Thompson, S. Lyon, L. G. J. van der Ven, A. J. M. C. Mol and H. Terryn, The corrosion protection of AA 2024-T3 aluminium alloy by leaching of lithium-containing salts from organic coatings, *Faraday Discussions*, 2015, DOI: 10.1039/C4FD00237G.
142. *S. Boocock,* WO2008118950-A2; US2009092839-A1;.
143. *D. Becker, M. Geistbeck, C. Gerlach, M. Kaune, J. Kuever, A. Rabenstein, S. Schroeder, Y. Wilke, C. Gerlach, T. Pietzker, O. Schramm, S. Schroder, J. Kuver, D. Becq, O. Skram, T. Pertztek, T. Pieztker, Y. A. Kyufer, A. Rubenstein, I. Wilke, M. Gaystbek, C. Gerlah and T. Pitstker,* WO2009094975-A1, 2009.
144. T. G. Harvey, S. G. Hardin, A. E. Hughes, T. H. Muster, P. A. White, T. A. Markley, P. A. Corrigan, J. Mardel, S. J. Garcia, J. M. C. Mol and A. M. Glenn, The effect of inhibitor structure on the corrosion of AA2024 and AA7075, *Corrosion Science*, 2011, 53, 2184-2190.
145. *J. Sinko,* US5948147-A.
146. *J. Sinko,* WO9918044-A; US6139610-A.
147. *J. Sinko,* WO200292880-A; US2002197468-A1.
148. *J. Sinko and M. W. Kendig,* WO2005003408-A2; US2005022693-A1.
149. M. Kendig and M. Hon, A hydrotalcite-like pigment containing an organic anion corrosion inhibitor, *Electrochemical and Solid State Letters*, 2005, 8, B10-B11.
150. *S. Hayes, P. J. Kinlen and P. Kinlen,* US2008216705-A1; WO2008140648-A2.
151. H. Shi, E. H. Han, S. V. Lamaka, M. L. Zheludkevich, F. Liu and M. G. S. Ferreira, Cerium cinnamate as an environmentally benign inhibitor pigment for epoxy coatings on AA 2024-T3, *Progress in Organic Coatings*, 2014, DOI: 10.1016/j.porgcoat.2014.01.003.
152. M. Van Soestbergen, V. Baukh, S. J. F. Erich, H. P. Huinink and O. C. G. Adan, Release of cerium dibutylphosphate corrosion inhibitors from highly filled epoxy coating systems, *Progress in Organic Coatings*, 2014, 77, 1562-1568.
153. D. Ho, N. Brack, J. Scully, T. Markley, M. Forsyth and B. Hinton, Cerium dibutylphosphate as a corrosion inhibitor for AA2024-T3 aluminum alloys, *Journal of the Electrochemical Society*, 2006, 153, B392-B401.
154. R. Catubig, A. E. Hughes, I. S. Cole, B. R. W. Hinton and M. Forsyth, The use of cerium and praseodymium mercaptoacetate as thiol-containing inhibitors for AA2024-T3, *Corrosion Science*, 2014, 81, 45-53.
155. R. W. Revie, *Journal*, 1023-1038.
156. M. E. Nanna and G. P. Bierwagen, Mg-rich coatings: A new paradigm for Cr-free corrosion protection of al aerospace alloys, *Jct Research*, 2004, 1, 69-80.
157. *G. P. Bierwagen, M. E. Nanna, D. Battocchi, G. Bierwagen and M. Nanna,* WO2005051551-A1; EP1689534-A1.
158. S. D. Cramer and B. S. Covino, Jr., *Journal*.
159. D. Battocchi, Richter, N., Hayes, S.Hayes, Yan, M., Tallmann, D.E., Bierwagen, G.P., D. E.Tallman and G. Bierwagen, 14-18 March 2010, 2010.
160. D. Battocchi, A. M. Simões, D. E. Tallman and G. P. Bierwagen, Electrochemical behaviour of a Mg-rich primer in the protection of Al alloys, *Corrosion Science*, 2006, 48, 1292-1306.
161. R. Brown, Protecting metal with magnesium, *Finishing Today*, 2007, 83, 40-42.
162. G. Bierwagen, R. Brown, D. Battocchi and S. Hayes, Active metal-based corrosion protective coating systems for aircraft requiring no-chromate pretreatment, *Progress in Organic Coatings*, 2010, 67, 195-208.
163. B. J. E. Merten, D. Battocchi and G. P. Bierwagen, Aluminum alloy 2024-T3 protection by magnesium-rich primer with chromate-free metal salts, *Progress in Organic Coatings*, 2015, 78, 446-454.
164. H. Xu, D. Battocchi, D. E. Tallman and G. P. Bierwagen, Use of Magnesium Alloys as Pigments in Magnesium-Rich Primers for Protecting Aluminum Alloys, *Corrosion*, 2009, 65, 318-325.
165. P. Plagemann, J. Weise and A. Zockoll, Zinc-magnesium-pigment rich coatings for corrosion protection of aluminum alloys, *Progress in Organic Coatings*, 2013, 76, 616-625.
166. K. N. Allahar, D. Battocchi, M. E. Orazem, G. P. Bierwagen and D. E. Tallman, Modeling of electrochemical impedance data of a magnesium-rich primer, *Journal of the Electrochemical Society*, 2008, 155, E143-E149.
167. S. R. White, N. R. Sottos, P. H. Geubelle, J. S. Moore, M. R. Kessler, S. R. Sriram, E. N. Brown and S. Viswanathan, Autonomic healing of polymer composites, *Nature*, 2001, 409, 794-797.
168. S. J. Garcia, H. R. Fischer and S. van der Zwaag, A critical appraisal of the potential of self healing polymeric coatings, *Progress in Organic Coatings*, 2011, 72, 211-221.

169. M. G. S. Ferreira, M. L. Zheludkevich and J. Tedim, ed. A. S. H. M. a. I. Tiginyanu, Woodhead Publishing Series, 2011, DOI: 10.1533/9780857094902.2.235, pp. 235-279.
170. S. J. Garcia, H. R. Fischer, P. A. White, J. Mardel, Y. Gonzalez-Garcia, J. M. C. Mol and A. E. Hughes, Self-healing anticorrosive organic coating based on an encapsulated water reactive silyl ester: Synthesis and proof of concept, *Progress in Organic Coatings*, 2011, 70, 142-149.
171. D. Snihirova, S. V. Lamaka and M. F. Montemor, "SMART" protective ability of water based epoxy coatings loaded with CaCO 3 microbeads impregnated with corrosion inhibitors applied on AA2024 substrates, *Electrochimica Acta*, 2012, 83, 439-447.
172. A. C. Balaskas, I. A. Kartsonakis, L. A. Tziveleka and G. C. Kordas, Improvement of anti-corrosive properties of epoxy-coated AA 2024-T3 with TiO 2 nanocontainers loaded with 8-hydroxyquinoline, *Progress in Organic Coatings*, 2012, 74, 418-426.
173. F. Maia, J. Tedim, A. D. Lisenkov, A. N. Salak, M. L. Zheludkevich and M. G. S. Ferreira, Silica nanocontainers for active corrosion protection, *Nanoscale*, 2012, 4, 1287-1298.
174. T. Stimpfling, F. Leroux and H. Hintze-Bruening, Unraveling EDTA corrosion inhibition when interleaved into Layered Double Hydroxide epoxy filler system coated onto aluminum AA 2024, *Applied Clay Science*, 2013, 83-84, 32-41.
175. E. L. Ferrer, A. P. Rollon, H. D. Mendoza, U. Lafont and S. J. Garcia, Double-doped zeolites for corrosion protection of aluminium alloys, *Microporous and Mesoporous Materials*, 2014, 188, 8-15.
176. *F. Gammel, T. Hack, D. Raps and J. Wehr,* WO2009087043-A2, 2009.
177. *C. J. A. Barbe, N. Caldeira, E. Campazzi, K. S. Finnie, L. Kong, M. Villatte, C. Barbe, N. M. Caldeira and C. H. Barbe,* WO2010146001-A1; US2012085261-A1, 2010.
178. D. E. Tallman, Y. Pae and G. P. Bierwagen, Conducting polymers and corrosion: Part 2 - Polyaniline on aluminum alloys, *Corrosion*, 2000, 56, 401-410.
179. D. E. Tallman, Y. Pae and G. P. Bierwagen, Conducting polymers and corrosion: Polyaniline on steel, *Corrosion*, 1999, 55, 779-786.
180. G. Williams and H. N. McMurray, Polyaniline inhibition of filiform corrosion on organic coated AA2024-T3, *Electrochimica Acta*, 2009, 54, 4245-4252.
181. M. Kendig, M. Hon and L. Warren, 'Smart' corrosion inhibiting coatings, *Progress in Organic Coatings*, 2003, 47, 183-189.
182. M. Kendig and P. Kinlen, Demonstration of galvanically stimulated release of a corrosion inhibitor - Basis for "smart" corrosion inhibiting materials, *Journal of the Electrochemical Society*, 2007, 154, C195-C201.
183. M. C. Yan, D. E. Tallman and G. R. Bierwagen, Role of oxygen in the galvanic interaction between polypyrrole and aluminum alloy, *Electrochimica Acta*, 2008, 54, 220-227.
184. T. Stimpfling, F. Leroux and H. Hintze-Bruening, Organo-modified layered double hydroxide in coating formulation to protect AA2024 from corrosion, *Colloids and Surfaces A: Physicochemical and Engineering Aspects*, 2014, DOI: 10.1016/j.colsurfa.2014.01.042.
185. *P. J. Kinlen,* WO2003102034-A;US2004035498-A1;, 2003.
186. *M. W. Kendig, M. Hon and L. Warren,* EP1382721-A; US2004005478-A1; EP1382721-A1; US6942899-B2; EP1382721-B1, 2004.
187. P. Zarras, N. Anderson, C. Webber, J. D. Stenger-Smith, M. Spicer and D. Buhrmaster, ELECTROACTIVE MATERIALS as Smart Corrosion-Inhibiting Coatings for the Replacement of Hexavalent Chromium, *Jct Coatingstech*, 2011, 8, 40-44.
188. M. Pawlik, presented in part at the ASETSDefense 2009: Sustainable Surface Engineering for Aerospace and Defense Workshop, Westminster, CO, USA., August 31 - September 3, 2009, 2009.
189. M. Collinet-Fressancourt, N. Nuns, S. Bellayer and M. Traisnel, Characterization by TEM and ToF-SIMS of the oxide layer formed during anaphoretic paint electrodeposition on Al-alloys, *Applied Surface Science*, 2013, 277, 186-191.
190. A. Fujimoto, PPG Introduces E-coat Primer for Aerospace Use, http://www.ppg.com/en/newsroom/news/pages/20120104a.aspx, (accessed 3 December, 2013).
191. E. Charves, *Evaluation of Powder Coatings for Application to Aircraft Component Parts*, 1980.
192. J. L. Duncan, Powder coatings as an environmentally acceptable alternate to the system of MIL-P-53022 and MIL-PRF-22750, *STAR*, 2003, 41.
193. C. Geib, presented in part at the SERDP/ESTCP Workshop – Surface Finishing and Repair Issues for Sustaining New Military Aircraft, Tempe, Arizona, USA, 26-28 February, 2008.
194. M. J. O'Keefe, W. G. Fahrenholtz and B. S. Curatolo, Multifunctional UV (MUV) curable corrosion coatings for aerospace applications, *Metal Finishing*, 2010, 108, 28-31.

195. *J. R. Deantoni and B. S. Curatolo,* US2008118659-A1.
196. N. Moreau, L. Ni, C. Croutxe-Barghorn, A. Chemtob, T. Bouder and G. Hervé, UV-cured hybrid sol-gel coatings for aeronautical and Direct-To-Metal (DTM) applications, *Polym. Paint Colour J.*, 2014, 204, 36-37.
197. L. Ni, N. Moreau, A. Chemtob and C. Croutxé-Barghorn, Organic-inorganic tandem route to polymer nanocomposites: Kinetic products versus thermodynamic products, *J Sol Gel Sci Technol*, 2012, 64, 500-509.
198. T. H. Muster, D. Lau, H. Wrubel, N. Sherman, A. E. Hughes, T. G. Harvey, T. Markley, D. L. J. Alexander, P. A. Corrigan, P. A. White, S. G. Hardin, M. A. Glenn, J. Mardel, S. J. Garcia and J. M. C. Mol, An investigation of rare earth chloride mixtures: combinatorial optimisation for AA2024-t3 corrosion inhibition, *Surface and Interface Analysis*, 42, 170-174.
199. T. A. Markley, M. Forsyth and A. E. Hughes, Corrosion protection of AA2024-T3 using rare earth diphenyl phosphates, *Electrochimica Acta*, 2007, 52, 4024-4031.
200. B. D. Chambers, S. R. Taylor and M. W. Kendig, Rapid discovery of corrosion inhibitors and synergistic combinations using high-throughput screening methods, *Corrosion*, 2005, 61, 480-489.
201. S. J. García, T. H. Muster, O. Özkanat, N. Sherman, A. E. Hughes, H. Terryn, J. H. W. de Wit and J. M. C. Mol, The influence of pH on corrosion inhibitor selection for 2024-T3 aluminium alloy assessed by high-throughput multielectrode and potentiodynamic testing, *Electrochimica Acta*, 2010, 55, 2457-2465.
202. P. A. White, A. E. Hughes, S. A. Furman, N. Sherman, P. A. Corrigan, M. A. Glenn, D. Lau, S. G. Hardin, T. G. Harvey, J. Mardel, T. H. Muster, S. J. Garcia, C. Kwakernaak and J. M. C. Mol, High-throughput channel arrays for inhibitor testing: Proof of concept for AA2024-T3, *Corrosion Science*, 2009, 51, 2279-2290.
203. P. A. White, G. B. Smith, T. G. Harvey, P. A. Corrigan, M. A. Glenn, D. Lau, S. G. Hardin, J. Mardel, T. A. Markley, T. H. Muster, N. Sherman, S. J. Garcia, J. M. C. Mol and A. E. Hughes, A new high-throughput method for corrosion testing, *Corrosion Science*, 2012, 58, 327-331.
204. T. H. Muster, A. Trinchi, T. A. Markley, D. Lau, P. Martin, A. Bradbury, A. Bendavid and S. Dligatch, A review of high throughput and combinatorial electrochemistry, *Electrochimica Acta*, 2011, 56, 9679-9699.
205. P. Visser, Novel totally chrome free corrosion inhibiting coating technology for protection of aluminium alloys, *Transactions of the Institute of Metal Finishing*, 2011, 89, 291-294.
206. P. Visser, Protection for high flyers, *European Coatings Journal*, 2010, 88-92.

Chapter 3

The Corrosion Protection of AA2024-T3 Aluminium Alloy by Leaching of Lithium-Containing Salts from Organic Coatings

Chapter 2 described the state of the art of corrosion protection of in the field of aerospace coatings. In addition, it provided an overview of chromate-free coating technologies that have been considered for the replacement of chromates in the field to date. This chapter discusses the first detailed studies and analysis of the corrosion protective layers generated from lithium-salt loaded organic coatings. The layers were characterized in terms of morphology and composition. The formation of the layer was monitored over time and based on these observations, a mechanism was proposed for the formation of these protective layers from these Li-leaching coatings.

This chapter is published as a scientific paper:
P. Visser, Y. Liu, X. Zhou, T. Hashimoto, G.E. Thompson, S.B. Lyon, L.G.J. van der Ven, A.J.M.C. Mol, H.A. Terryn, The corrosion protection of AA2024-T3 aluminium alloy by leaching of lithium-containing salts from organic coatings, Faraday Discussions, 180 (2015) 511-52

Abstract

Li-carbonate and Li-oxalate were incorporated as leachable corrosion inhibitors in model organic coatings for the protection of AA2024-T3. The coated samples were artificially damaged with a scribe. It was found that the Li-salts are able to leach from the organic coating and form a protective layer in the scribe on AA2024-T3 under neutral salt spray conditions. The present paper shows the first observation and analysis of these corrosion protective layers, generated from Li-salt loaded organic coatings. The scribed areas were examined by scanning and transmission electron microscopies before and after neutral salt spray exposure (ASTM-B117). The protective layers typically consist of three different layered regions, including a relatively dense layer near the alloy substrate, a porous middle layer and a flake-shaped outer layer, with lithium uniformly distributed throughout all three layers. Scanning electron microscopy and white light interferometry surface roughness measurements demonstrate that the formation of the layer occurs rapidly and, therefore provides an effective inhibition mechanism. Based on the observation of this work, a mechanism is proposed for the formation of these protective layers

3.1 Introduction

The development of alternative surface pretreatments and pigmented coatings to eliminate the health hazards and toxicity of soluble hexavalent chromium is being pursued for many years. Especially in the aeronautical industry, the replacement or elimination of hexavalent chromium has been and still is a major challenge.[1] High strength aluminium alloys such as AA2024-T3 and AA7075-T6 are most commonly used in aircraft design because of their favourable strength to weight ratio. However, these alloys are very susceptible to localized corrosion such as pitting and intergranular corrosion.[2-4] For decades, chromate-containing organic coatings and chromate-based conversion coatings have been used for the protection of these high strength aluminium alloys, with superior performance. The corrosion protective scheme employs chromate in many steps, including pre-cleaning,[5] conversion coating/anodizing,[6-8] and the organic coatings.[9] These chemical conversion coatings and organic coatings provide active corrosion inhibition toward the substrate and have the ability to release hexavalent chromium in the case of a local defect to provide the "self-healing" protection.[10, 11] The unique properties of hexavalent chromium make the replacement of chromate inhibitor pigments in organic coatings a difficult task.[9, 12] Numerous investigations have been performed to find promising candidates to replace chromates in organic coatings. Ideally, these compounds should have a similar performance as chromates, i.e. providing corrosion protection to the substrate and serving as a reservoir of corrosion inhibitor, which has the ability to be released from the coating when damages occur and heal the defect by the formation of a protective or passivation layer.[13, 14] This leaching of soluble chemical species is the main corrosion inhibiting strategy used in corrosion inhibiting coating technology for the protection of high strength aluminium alloys.

Over the last few years, several inhibitors have been identified as promising replacement for chromates. These include oxo-anionic, cationic, metal, metal oxide, and organic inhibitors. The oxo-anionic inhibitor salts include molybdates,[15] metavanadates,[16, 17] permanganate,[18] and phosphates,[19-21] The cationic inhibitors include rare-earth compounds[22] such as cerium[23] and praseodymium.[24] Magnesium[25] and zinc[26] metals are also found to be effective when used as pigments in organic coatings. Furthermore, several organic inhibitors have shown promising results.[27-29] Whilst many approaches have been attempted to achieve acceptable alternatives, relatively few systems have demonstrated similar effectiveness as chromate containing systems.[30] Therefore, the search for suitable alternatives for chromates is continuing.

Recently, the use of Li-salts has been proposed as a potential replacement for chromate in organic coatings.[31] In the 1990s, alkaline Li-solutions have been studied as possible replacement of the traditional chromated chemical conversion process. Li-salts, including Li-carbonate,[32-36] Li-sulphate,[32] Li-hydroxide[37] and Li-chloride[32] in aqueous alkaline environment have been shown to form a continuous polycrystalline layer on super pure

aluminium,[33, 34] AA1100,[35, 36] AA6061,[32, 35] AA2024,[35, 37] and AA7075[35] aluminium alloys. The Li-based conversion coating greatly increased the corrosion resistance of the various selected substrates by increasing the pitting potential and reducing the corrosion current density. The conversion coated super pure aluminium and AA6061 aluminium alloy passed the standard salt spray tests.[35] The protective properties provided by these Li conversion layers are suggested to originate from the formation of a Li-aluminium-hydroxide-carbonate-hydrate ($Li_2[Al_2(OH)_6]_2{\cdot}CO_3{\cdot}nH2O$) layer[35] with Li-aluminate as a pore filler.[34] Li is the only monovalent cation that is known to intercalate in aluminium hydroxide to form these layered double hydroxides.[38]

Although, Li based chemical conversion layers have been studied using electrochemical approaches and corrosion tests, limited studies have been carried out with a focus on obtaining detailed morphological information, especially cross-sectional observation of the protective layer. Further, the mechanisms of layer formation remain unclear. Additionally, no detailed investigation has focused on the use of Li-containing species as leachable corrosion inhibitor incorporated into organic coatings.

In the present study, Li-containing salts, i.e. Li-carbonate or Li-oxalate, were used as corrosion inhibitors in an organic model coating for the protection of AA2024-T3. The coatings were damaged and the scribe was examined by electron microscopic techniques, before and after exposure to the neutral salt spray corrosion test (ASTM B-117). This is the first investigation of such a protective layer that was generated on AA2024-T3, from an organic coating containing Li–salt as leachable corrosion inhibitor. Specific and careful sample preparation combined with low-voltage scanning electron microscopy (SEM) cross-sectional work and high-resolution transmission electron microscopy (TEM) and electron energy loss spectroscopy (EELS) were used to reveal morphological and compositional information of the protective layer. In addition, the formation of the layer has been studied as a function of time by white light interferometry and cross-sectional SEM. A mechanism is proposed for the formation and the protective nature of this layer, based on the observations of this study.

3.2 Experimental

3.2.1 Materials

Model formulations based on polyurethane chemistry were designed using a polyester resin (Desmophen® MPA) and an aliphatic polyisocyanate (Tolonate® HDB 75 MX) with a NCO/OH ratio of 0.75 and a pigment volume concentration (PVC) of 30% as described in Table 3.1.

Tartaric-sulphuric acid (TSA) anodized AA2024-T3 unclad sheets were used as the substrate in this study (dimensions of 70 × 70 × 0.8 mm). The AA2024-T3 substrate (2024-T3 QQ-A250/5) was purchased from Alcoa and the TSA pretreatment was performed

according to aerospace requirements (AIPI 02-01-003) at Premium AEROTEC, Bremen Germany.

3.2.2 Preparation and application of the model coating

The pigmented coatings were prepared according to the following procedure:
All components of Component A were added under stirring in a 370 ml glass jar. After addition of the final component, 400 grams of Zirconox® pearls (1.7 -2.4 mm) were added to the mixture. The pigments were dispersed to a particle size smaller than 25 μm by 20 minutes shaking on a Skandex® paint shaker. After this procedure, the mixtures were filtered to remove the pearls. The ingredients of component B were mixed separately.

Component B was added to Component A and the mixture was stirred to a homogeneous mixture. The paints were applied with a HVLP spray gun on the AA 2024 –T3 unclad TSA panels, 30 minutes after mixing. The coatings were cured at 80°C for 16 h. The measured dry film thickness was 20-25 μm.

A mechanical milling device was used to artificially damage the coating with a U-shaped scribe, before exposing the samples to the neutral salt spray test (ASTM-B117). The panels were scribed from corner to corner, leaving a 1mm wide scribe that penetrated 100-150 μm deep into the metal.

Table 3.1: Composition of model organic coatings

	Supplier	Non-inhibiting	Li-carbonate	Li-oxalate
Component A				
N-Butylacetate	Sigma Aldrich	75.0 g	75.0 g	75.0 g
Desmophen 650MPA	Covestro	47.7 g	47.7 g	47.7 g
Li-carbonate	Sigma Aldrich		23.6 g	
Li-oxalate	Sigma Aldrich			32.0 g
Magnesium oxide	Sigma Aldrich		16.4 g	16.4 g
Tioxide TR 92	Huntsman		5.9 g	5.9 g
Blanc Fixe N ($Ba(SO_4)$)	Sachtleben		15.4 g	15.4 g
Component B				
Tolonate HDB 75 MX	Vencorex	28.5 g	28.5 g	28.5 g
Dynasilan Glymo	Evonik	***5.2 g***	5.2 g	5.2 g

3.2.3 Experimental techniques

The samples were exposed to the Neutral Salt Spray (ASTM-B117) test for varying periods from 30 minutes up to 168 h. After exposure, the process was quenched by a 2 minute rinse with flowing demineralised water to remove any residual chlorides and the panels were air-dried.

Scanning Electron Microscopy (SEM)

The cross sectional observation of the oxide layers, in the scribe, was carried out by scanning electron microscopy (SEM) using a ZEISS Ultra 55 instrument with an acceleration

voltage of 0.5 kV. The composition of the oxide films was analysed by energy dispersive X-ray analysis on FEI Magellan HR FEG-SEM.

Transmission electron microscopy (TEM-EELS)

The layers were also examined by transmission electron microscopy (TEM) using a JEOL FX 2000 II instrument operated at 120 kV, with a nominal sample thickness of 15 nm, prepared by a Leica EM UC6 ultra-microtome with a diamond knife. Electron energy loss spectroscopy (EELS) was conducted on a TECNAI TF30 TEM fitted with a Gif2001 detector, operated at 300 kV Mapping images were acquired with 1024×1024 pixels, this results pixel size of 0.56×0.56 nm for the selected magnification.

White light Interferometry (WLI)

The surface roughness of the scribe was measured with WLI, using a Veeco NT1100 profileometer. The high-resolution measurements were carried out using a 20x objective and multiple measurements were stitched together to sample a 2 mm length of the scribe. The data were de-trended by removal of any planar tilt. In order to remove the low frequency spatial waves associated with scribing a high pass Fourier filter was used with a frequency cut-off of 5 mm^{-1}. Visibly corroded samples were subjected to a cleaning step (1h 1M Nitric acid) to dissolve the corrosion products and reveal the attacked morphology of the substrate.

3.3 Results and discussion

3.3.1 General morphological observations in the scribed area before and after salt spray testing

The scribed regions were examined with an optical microscope. Fig. 3.1a shows the scribe before exposure to the accelerated corrosion test. The pristine scribe is 1 mm wide and 100 μm deep into the alloy. The panels were exposed to 168 h neutral salt spray (ASTM B-117). Fig. 3.1b shows the detrimental effect of the corrosive conditions when a coating does not contain an effective corrosion inhibitor. The coating remains intact but the scribe is heavily affected and contains many areas with white corrosion products. In contrast to this, the Li-salt loaded coatings remained free of corrosion products (Fig. 3.1c-d). Both, Li carbonate and oxalate show a similar protective behaviour. These Li salts were selected for this study because of their moderate solubility compared to most other Li salts, respectively 1.3 g/100 mL for Li-carbonate and 8 g/100 mL for Li-oxalate, and ease of paint formulation.

These observations and visual comparison of the scribed areas of coated AA2024-T3 before and after salt spray testing indicates the important role of the presence of Li-containing salts as corrosion inhibitor in organic coatings, leading to a detailed investigation of the protection mechanism of the AA2024-T3 by Li-containing salts, as discussed below.

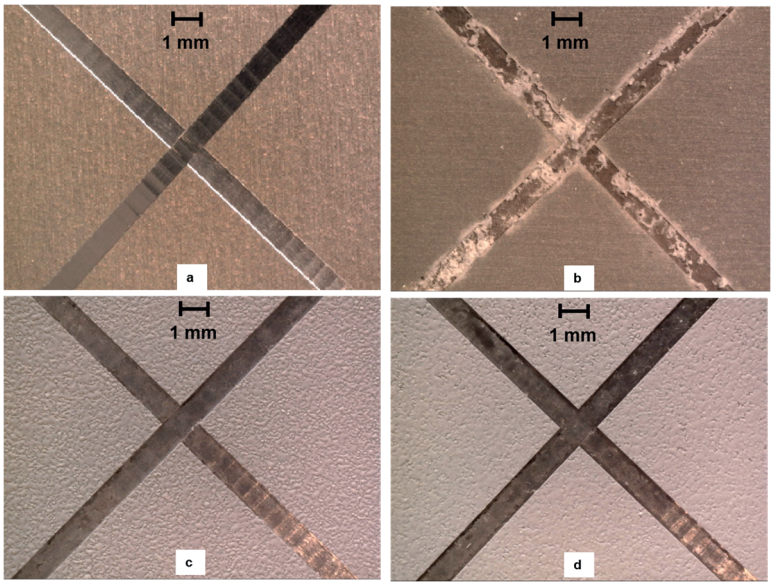

Figure 3.1 *Optical images of coated and scribed AA2024-T3 panels before and after 168 h neutral salt spray exposure (ASTM B-117) (a) unexposed (b) No inhibitor, (c) Li-carbonate, and (d) Li-oxalate.*

3.3.2 Detailed morphological observations in the scribed area before and after salt spray testing

The scribed region was examined in more detail by studying cross-sections using scanning electron microscopy. The cross-sections of the scribed area of the alloy substrate showed a "U" shape in the middle of the images, with the organic coated alloy substrate evident on both sides (Fig. 3.2a). After 168 h salt spray exposure, the scribed alloy with the non-inhibiting coating showed the presence of a large amount of corrosion products with a typical thickness about 25 µm (Fig. 3.2b). However, when Li-carbonate or Li-oxalate was incorporated as a corrosion inhibitor in the organic coating, no apparent damage is observed in the scribed area, as shown in Figs. 3.2c and 3.2d.

Non-inhibited coating

The scribed area of the non-inhibited coating has been examined after 168 h neutral salt spray exposure. The SEM cross-section clearly showed the hydrated aluminium oxide formed during salt spray exposure; Fig. 3.3a displays the full scribe with the corrosion products. Fig. 3.3b shows the cross-section of the corrosion products at higher magnification, with pores providing access to the metal surface for aggressive ions. Although the metal/oxide or hydroxide interface is relatively flat, the corrosion products are homogeneously distributed in the scribe. Fig. 3.3a indicates a relatively uniform corrosion process. However, localised corrosion, such as pitting and intergranular, was

observed as well (Fig. 3.3c). It is evident that the grain boundary of the alloy is vulnerable to corrosion attack, especially when second phase particles are present at the grain boundaries. EDX analyses revealed that the corrosion products contained mainly aluminium and oxygen, with traces of copper and magnesium present.

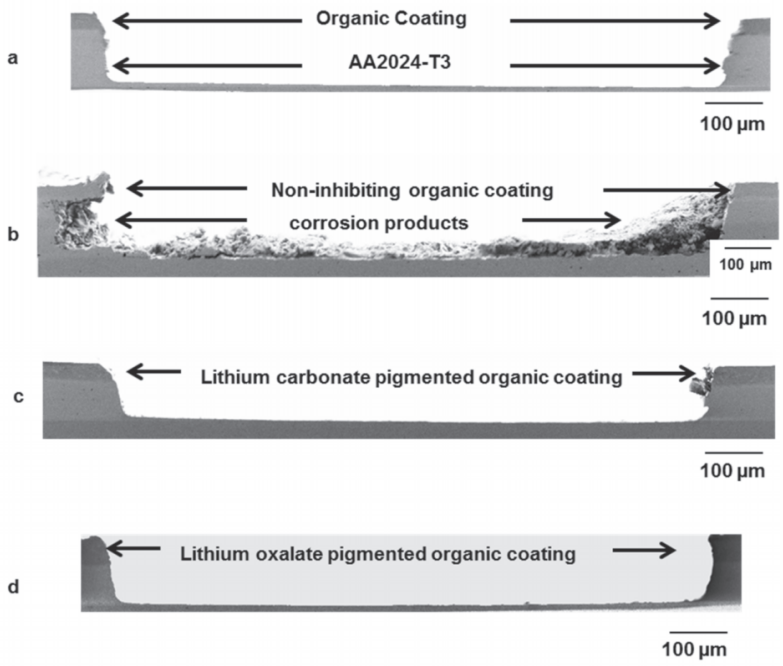

Figure 3.2 Cross-section SEM images of coated and scribed AA2024-T3 panels before and after 168 h Neutral Salt Spray exposure (ASTM B-117) (a) unexposed, (b) no inhibitor, (c) Li-carbonate, and (d) Li-oxalate

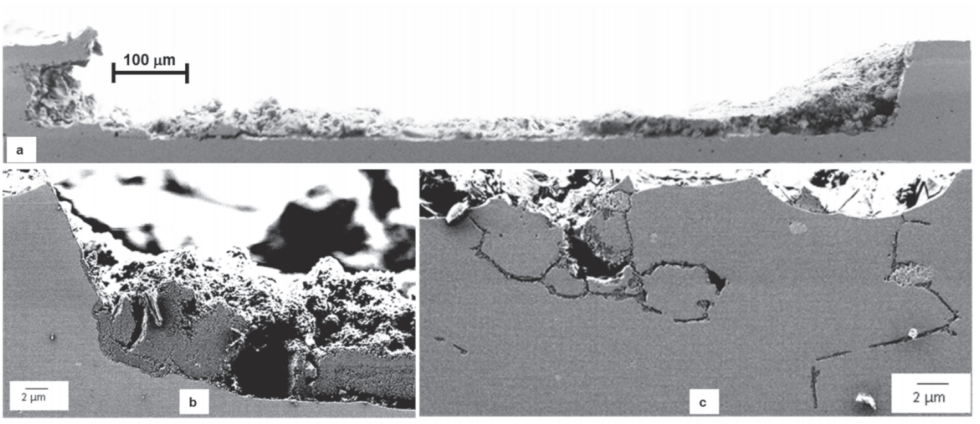

Figure 3.3 SEM crosscut images of non-inhibited coating on AA2024 T3. (a) full scribe with corrosion products, (b) detailed corrosion products, (c) intergranular corrosion

According to Foley, corrosion of aluminium commences according to a multi-step process which leads to oxide thinning and finally dissolution of the aluminium.[39] This dissolution is followed by a fast hydrolysis of the Al^{3+} ion to form $Al(OH)_3$ that transforms into $Al_2O_3{\cdot}H_2O$. Further, EDX analyses of the corrosion products indicated that the corrosion products are mainly hydrated aluminium oxide ($Al_2O_3{\cdot}H_2O$) or aluminium hydroxide ($Al(OH)_3$), with oxygen to aluminium ratios in the ranging from of 2:1 up to 4:1. This correlates with various hydrated aluminium oxides, which are common corrosion products of aluminium occurring in chloride containing solutions.[40]

Li-salt containing coatings

In contrast to the scribed area of the non-inhibited coating, the Li-salt loaded organic coatings did not show this type of corrosion and the scribed areas were without any significant amount of corrosion products after 168 h neutral salt spray exposure. For both samples, SEM investigations reveal that the substrate of the scribe is covered with a new layer.

Fig. 3.4 shows the SEM cross-sectional examination of the protective layer generated from a Li-carbonate loaded coating. A thin deposited layer, of about 0.5 to 1.5 µm thickness, developed throughout the scribed surface area (Fig. 3.4b and c). Higher magnification images reveal a typical detailed morphology of the layer formed (Fig. 3.4d). The layer comprises three distinct regions: a dense barrier region at the metal/deposited layer interface, a porous region in the middle, and a columnar outer region. This outer region can be correlated with the surface as observed with a planar view SEM image (Fig. 3.5c) Fine textures were observed on the overall surface at increased magnification (Fig. 3.5c and d).

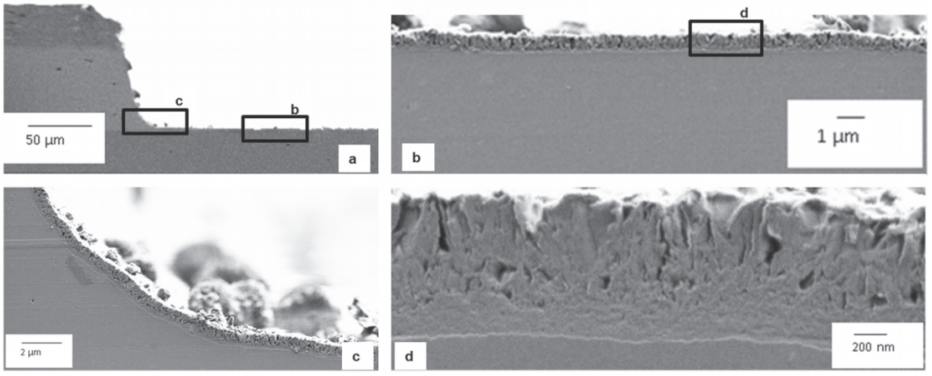

Figure 3.4 *SEM cross-cut images of protective layers generated from a Li-carbonate loaded coating after 168 h ASTM B-117 exposure (a) scribed area, (b) middle section of the scribe, (c) curved area of bottom of the scribe, (d) detailed morphology of layer (middle section of the scribe).*

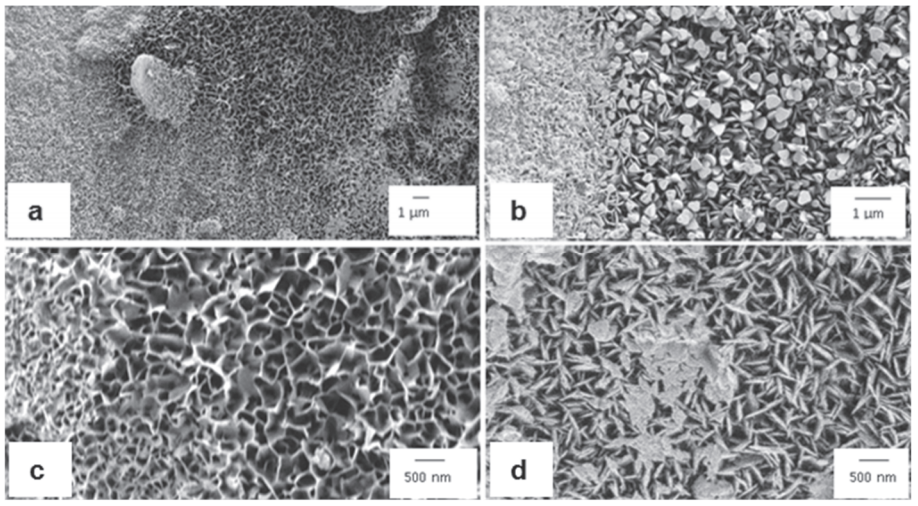

Figure 3.5 *Top view appearance of protective layer with increasing magnification after 168 h ASTM B-117 exposure. (a), (c) Li-carbonate and (b), (d) Li-oxalate.*

Both the Li-carbonate and Li-oxalate pigmented primers show this particular textures. In some regions, the texture is more significant, while in other regions the surface is still relatively flat. The textures comprised fine flakes, with some oriented almost vertical to the surface (Fig. 3.5d) while others are randomly orientated. It is unclear whether this different top-view morphology or textures is a result of the anion or different Li-ion concentrations due to the higher solubility of Li-oxalate. This study did not focus on the anion effect. However, these observations justify further studies on the effect of the anion on the formation of these protective layers.

The Li-oxalate loaded model coating demonstrates similar deposition behaviour in the scribed region after salt spray testing (Fig. 3.6.). SEM cross-sectional examination revealed the same three distinct morphologies of a dense barrier region, porous region, and columnar outer region, similar to the deposited layer of the Li-carbonate sample. Although the flakes formed are finer and denser compared with the morphologies of the film formed from the coated alloy pigmented with Li-carbonate.

The observed inhibitive effect must be a result of this layer, which was generated in-situ in the damaged area. The presence of the columnar layer at the outer region of the cross-section and the microstructure of the surface could indicate the possible formation of a lithium–aluminium-carbonate-hydroxide hydrate as reported by Drewien *et al.*[36] They generated these protective poly-crystalline layers on aluminium from saturated aluminate ($Al(OH)_4^-$) alkaline Li-solutions (pH 11.5-13) under well-controlled conditions. Besides the poly-crystalline layer, a thin very fine or poorly crystalline layer was found underneath the poly-crystalline layer. However, the performance of these layers was not sufficient for the protection of AA2024-T3. Layers with a similar morphology as found in this study, have been observed when exposing aluminium to (weak) alkaline solutions.[41, 42] The ratio of the

thickness of the inner barrier layer versus the non-barrier outer layer was found to depend on the pH of the solution. It was suggested that the layer was initially formed by initially an aluminium hydroxide gel, which aged to boehmite and pseudoboemite and later to bayerite. However, these layers did not provide long-term corrosion protection.
The results from this study suggest that Li-containing species in the organic coating provide fast and effective corrosion protection to the aluminium alloy. The layered morphology is significant different from the layers formed in the conversion process. The inhibitive properties of this layer might be derived from the presence of the dense non-porous layers near the aluminium substrate

.

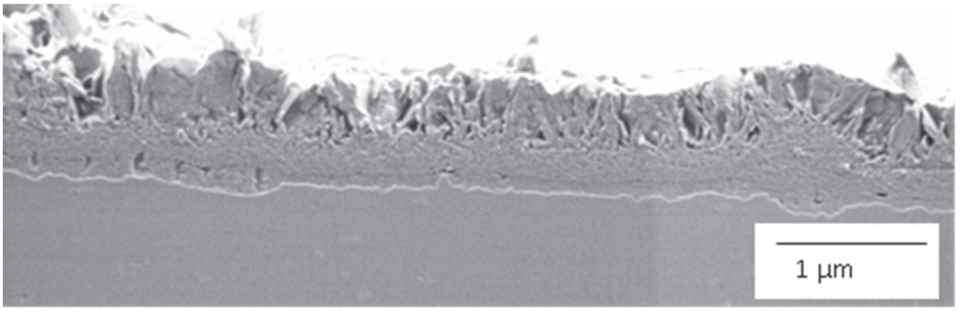

Figure 3.6 *SEM cross-sectional image of the typical morphology of the protective layer generated from a Li-oxalate loaded coating.*

3.3.3 Composition of the protective layer

The composition of the deposited layer has been analysed with transmission electron microscopy equipped with electron energy loss spectroscopy (TEM-EELS) in order to detect the Li-species in the layer. The TEM image and corresponding EELS maps of the layer generated from the Li-carbonate based coating are shown in Fig. 3.7a-d. These maps demonstrated the presence of aluminium, oxygen, and lithium throughout the deposited layer.

The bright regions in Fig. 3.7d indicate the uniform distribution of lithium throughout the entire layer. Similar results were also obtained from the scribed area of the AA2024-T3 aluminium alloy with Li-oxalate pigmented coating. The TEM images showed the presence of the barrier film on metal surface followed by fine porous and flake network regions.

The presence of lithium throughout the protective layer including the dense layer shows that Li-ions leached from the organic coating matrix into the scribe and formed a protective layer in the scribe that consists of lithium, aluminium and oxygen. Whereas the hydrated aluminium oxides of the non-inhibited sample are not able to prevent the aluminium matrix from further dissolution and pitting corrosion, these results indicate that the morphology and composition of these layers provide long-term corrosion protection.

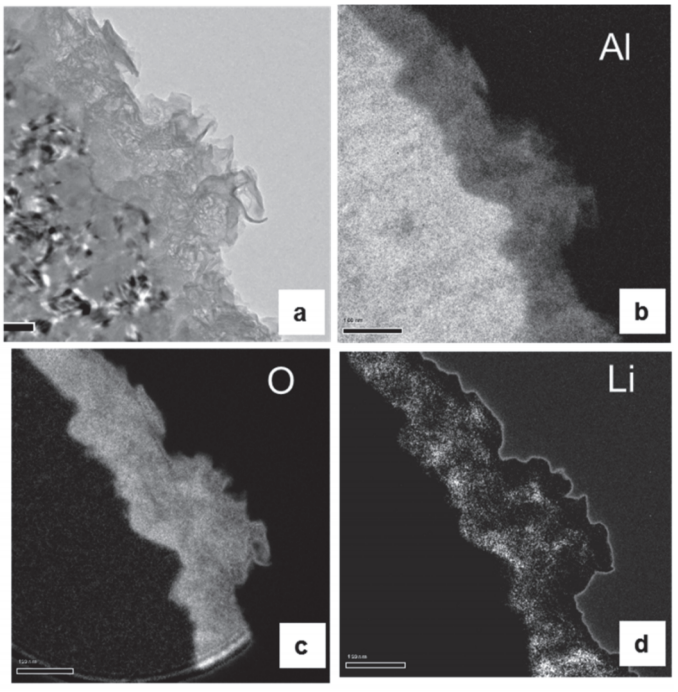

Figure 3.7 *TEM image and TEM-EELS elemental mapping of the layer generated from the Li-carbonate loaded coating (a) TEM image, (b) aluminium, (c) oxygen, and (d) lithium distribution*

3.3.4 Rate of the protective layer formation

Surface roughness development in time

White light interferometry (WLI) has been used to quantify the degree of corrosion by measuring the surface roughness (s_a) of the scribed areas after different periods of salt spray exposure. Fig. 3.8 shows the development of the surface roughness of the samples over time when exposed to the corrosive salt spray conditions. An unexposed scribe has a typical surface roughness of about 170 nm (Fig. 3.9a). The detrimental effect of the corrosive conditions on the non-inhibiting sample is evident. The surface of the scribe is severely damaged due to pitting corrosion and the dissolution of aluminium. The surface roughness of the non-inhibiting sample increased rapidly after the aluminium oxide layer had been de-stabilised and localized corrosion processes were initiated. After 24 h exposure the roughness increased up to 0.9 μm and this increased further to 1.5 μm after 168 h. In contrast to this, the surface roughness of the Li-salt containing coatings increased to 0.3-0.4 μm and remained relatively constant from then onwards. This demonstrates that slow or ineffective inhibition mechanisms result in rapid increase of the surface roughness in the scribe due to pitting corrosion and aluminium dissolution processes,[43] as illustrated for the non-inhibited sample in Fig. 3.9b.

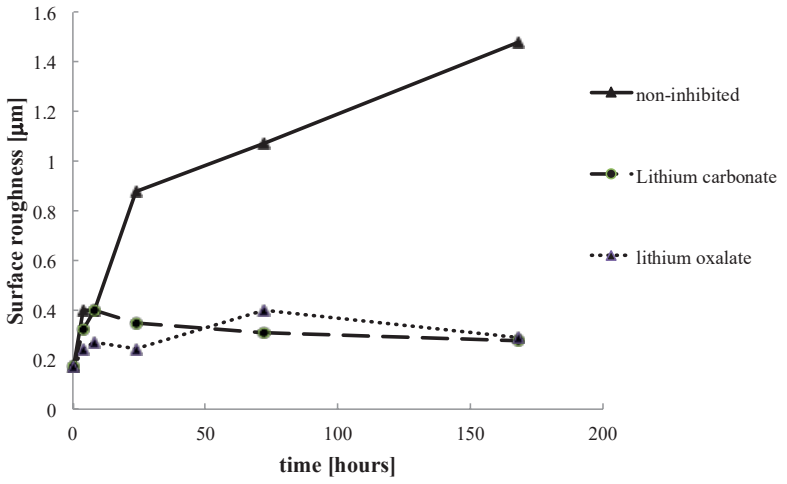

Figure 3.8 Development of the surface roughness in the scribe measured by white light interferometry after different periods of neutral salt spray exposure.

Compared to the unexposed sample, the WLI scan of non-inhibited sample visualizes the degree of damage caused by corrosion in the first 168 h. On the other hand, the Li-leaching samples show only limited pitting corrosion and a superficial attack on the surface, which is illustrated in Figs. 3.9c and 3.9d. Therefore it can be concluded that the Li-leaching coatings provide fast and effective inhibition on AA2024 –T3.

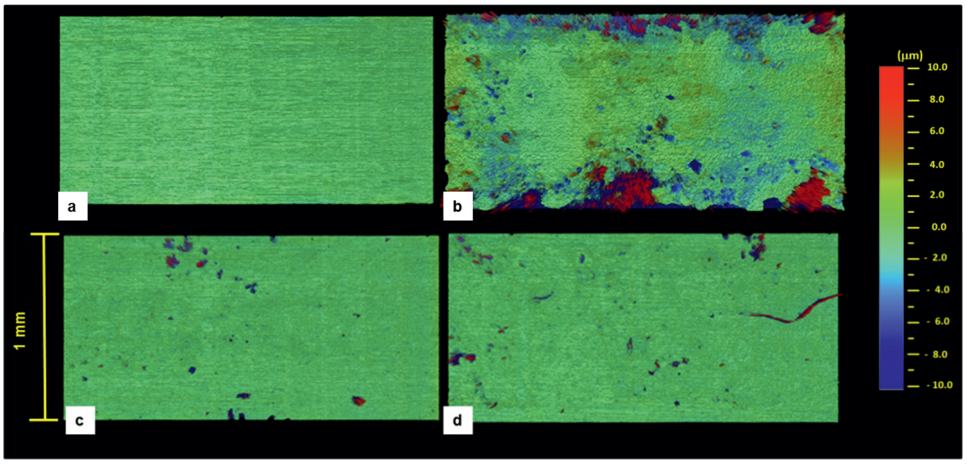

Figure 3.9 High-resolution WLI images of the scribed area before and after 168 h exposure to neutral salt spray conditions, (a) unexposed scribe, (b) non-inhibited coating, (c) Li-carbonate coating and, (d) Li-oxalate coating.

Generation of the protective layer

The WLI results indicate that the inhibition mechanism must be fast and complete within 48 h. SEM crosscuts were made after 4 and 8 h with the aim to observe the generation of the protective layer at an early stage. Fig. 3.10 and 3.11 show the formation of the protective layer after 4 and 8 h neutral salt spray exposure. After 4 h, both the Li-carbonate and Li-oxalate loaded coatings (Fig. 3.10a and 3.11a) provide a protective layer with a thickness between 200 and 400 nm in the scribe. These layers have a similar morphology and thickness as the dense layers as found underneath the porous columnar layer after 168 h exposure. After 4 and 8 h, there is some columnar material present on top of the porous layer. According to these observations, it seems that the columnar layer is formed at a later stage in the process and increases the thickness of the protective layer to 1-1.5 μm.

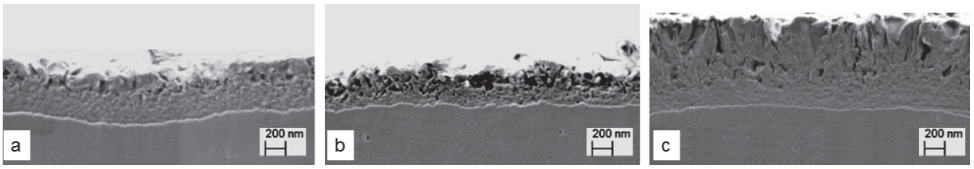

Figure 3.10 *SEM cross-cut images of the protective layer generated from the Li-carbonate loaded coating after (a) 4 h, (b) 8 h and, (c) 168 h neutral salt spray conditions.*

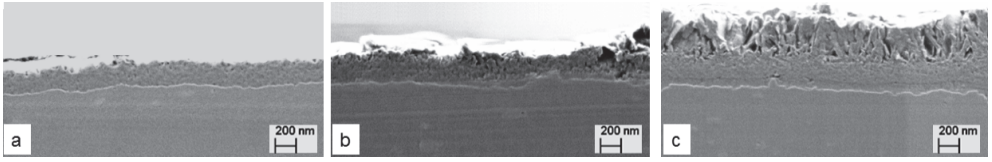

Figure 3.11 *SEM cross-cut images of the protective layer generated from the Li-oxalate loaded coating after (a) 4 h, (b) 8 h and, (c) 168 h neutral salt spray conditions.*

3.3.5 Proposed mechanism of passive film formation

Li-species have been leaching from the organic coating and a three-layered protective layer has been formed on AA2024-T3. However, the mechanism of the formation is not yet fully understood. SEM cross-sectional and TEM-EELS microscopic techniques have provided information about the protective layer in more detail. Based on this information a mechanism is proposed for the formation of such a layer.

The SEM-cross-sectional results reveal the significant different morphology for these layers compared to the poly-crystalline layers generated at high pH and saturated aluminate solutions in the chemical conversion process of Drewien *et al.*[36] This can be explained by possible concentration and pH gradients during the leaching process. The formation of the layer appears to occur via a competitive growth and dissolution process of aluminium hydroxide at the aluminium interface as suggested by Tabrizi *et al.*[41] Oxide layers with a

dual morphology were generated on aluminium, consisting of an inner barrier layer and an outer non-barrier crystalline layer, in long-term exposure to alkaline media. Similar layers were observed when aluminium was subjected to weak alkaline conditions by Hurlen and Haug.[42] The thickness of the barrier layer was decreasing with increasing pH. Considering the relatively thick dense inner layer, it can be assumed that the formation of the protective layer from these Li-leaching organic coatings occurs at weak alkaline pH. In addition to this process, the role of lithium needs to be considered.

The proposed mechanism of layer formation consists of several processes (Fig. 3.12). First, oxide thinning will occur due to chloride-ion adsorption in the oxide layer[39] when the aluminium is exposed to the sodium chloride solution of the salt spray test. At the same time, the leaching process starts and Li-salts will be released from the organic coating matrix. Both Li-carbonate and Li-oxalate have an alkaline nature in solution. In addition to this, the magnesium oxide in the coating can act as an alkaline buffer and will provide an alkaline pH in the bulk solution. Since there are no significant amounts of magnesium found in the elemental analysis, it can be assumed that magnesium is not active in the inhibition process.

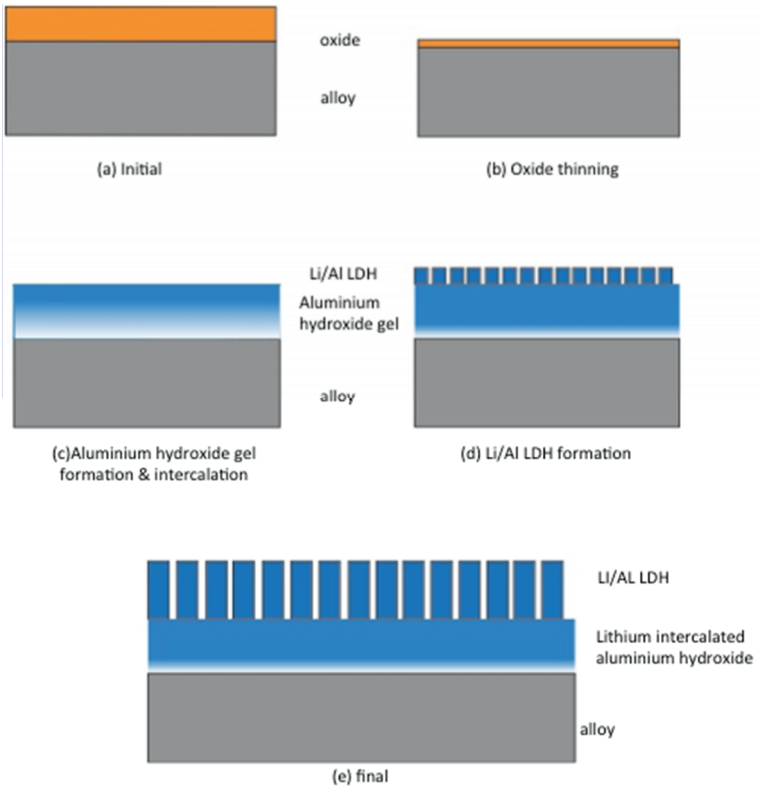

Figure 3.12 *Schematic illustration of the steps in the formation*

The second process is the destabilisation of the hydrated aluminium oxide in the alkaline chloride-containing environment. This process transfers the initial hydrated aluminium oxide into an aluminium hydroxide gel at the surface. Once the oxide layer is sufficiently thinned, the corrosion process commences via the direct attack and dissolution of the aluminium. In this alkaline chloride-containing environment, the Al^{3+} ion hydrolyses and forms amorphous $Al(OH)_3$ at the aluminium substrate interface (growth process).[40]

The third process is the dissolution reaction of the aluminium hydroxide gel at the oxide electrolyte interface. The aluminium hydroxide gel that was formed in the second process will dissolve into ionic $Al(OH)_4^-$ at the aluminium hydroxide gel / electrolyte interface (dissolution process). $Al(OH)_4^-$ is the main species present in alkaline environment.[44, 45] The equilibrium or dissolution rate depends on the pH.[46] Therefore, at high pH, the solubility of $Al(OH)_4^-$ is high and it is expected that the aluminium hydroxide gel will be thin.

The SEM results show the formation of a dense layer in the early stages of salt spray exposure. In addition, EELS data reveal the presence of lithium in the dense barrier layer. Rangel and Travassos suggest formation of Li-aluminate ($LiAlO_2$) via the AlO_2^- ion.[34] However, this seems unlikely since this dehydrated form of $Al(OH)_4^-$ does not exist in significant concentrations according to Sipos[45]. The Li-ion is known for its facile intercalation into aluminium hydroxides, such as Bayerite and Gibbsite, forming Layered double hydroxides (LDH).[47] Moreover, amorphous aluminium hydroxides are known as effective sorbents of Li-salts.[48] Therefore, it can be assumed that lithium intercalates with the aluminium hydroxide gel to generate very small grain size particles or even an amorphous structure resulting in a dense impermeable protective layer.
The fourth process is the formation of the non-barrier outer layer. It is still unclear whether this step is a precipitation reaction of or an aging process from the hydroxide gel process. It is assumed that $Al(OH)_4^-$ dissolves from the outer side of the aluminium hydroxide gel forming a Li/Al layered double hydroxide from the reaction between $Al(OH)_4^-$ and Li^+. The SEM cross-sectional results suggest that the precipitation or aging reaction occurs at a later stage in the formation of the protective layer. Process 3 and 4 (growth and dissolution) are in competition with each other. However, these processes terminate when the dense layer is thick and dense enough and does not allow any Al^{3+} of Li^+ diffusion. At this stage the inhibition process is complete.

4. Conclusions

Li-containing salts were used as leachable corrosion inhibitors in model organic coatings for the protection of AA2024-T3 aluminium alloys. These Li-salt loaded coatings demonstrated effective corrosion inhibition when exposed to corrosive conditions like neutral salt spray (ASTM B-117) for 168 h, providing clean scribes with no corrosion products. TEM-EELS and SEM cross-sectional analysis of the scribed area revealed that Li-ions were leached from the coating matrix and formed a protective layer on the 2024-T3 aluminium alloy of the scribed area, which protected the alloy from corrosion. The thickness of the layer varied, ranging from 0.5-1.5 µm. The general morphology of the protective layer salts showed three distinct regions, comprising a dense barrier layer near the metal/passive layer interface, a porous layer in the middle, and an outer columnar layer. The layer comprised aluminium, oxygen and lithium, as identified by EELS analysis and lithium was relatively uniform distributed in the layer. The poly-crystalline outer layer could be an Al/Li layered double hydroxide. The dense barrier layer is composed of lithium and aluminium hydroxide. However, it remains unclear in which form. The formation of this layer is a multistep process controlled by competitive film growth and dissolution processes.

References

1. R. L. Twite and G. P. Bierwagen, Review of alternatives to chromate for corrosion protection of aluminum aerospace alloys, *Progress in Organic Coatings*, 1998, 33, 91-100.
2. N. Birbilis and R. G. Buchheit, Electrochemical characteristics of intermetallic phases in aluminum alloys - An experimental survey and discussion, *Journal of the Electrochemical Society*, 2005, 152, B140-B151.
3. R. G. Buchheit, R. P. Grant, P. F. Hlava, B. McKenzie and G. L. Zender, Local dissolution phenomena associated with S phase (Al2CuMg) particles in aluminum alloy 2024-T3, *Journal of the Electrochemical Society*, 1997, 144, 2621-2628.
4. A. Boag, A. E. Hughes, A. M. Glenn, T. H. Muster and D. McCulloch, Corrosion of AA2024-T3 Part I: Localised corrosion of isolated IM particles, *Corrosion Science*, 2011, 53, 17-26.
5. A. E. Hughes, R. J. Taylor, K. J. H. Nelson, B. R. W. Hinton and L. Wilson, Characterisation of surface preparation of 2024 aluminium alloy for conversion coating, *Mater. Sci. Technol.*, 1996, 12, 928-936.
6. M. Kendig, S. Jeanjaquet, R. Addison and J. Waldrop, Role of hexavalent chromium in the inhibition of corrosion of aluminum alloys, *Surface and Coatings Technology*, 2001, 140, 58-66.
7. D. Chidambaram, C. R. Clayton, M. W. Kendig and G. P. Halada, Surface pretreatments of aluminum alloy AA2024-T3 and formation of chromate conversion coatings II. composition and electrochemical behavior of the chromate conversion coating, *Journal of the Electrochemical Society*, 2004, 151, B613-B620.
8. S. J. Garcia-Vergara, P. Skeldon, G. E. Thompson and H. Habazaki, A tracer investigation of chromic acid anodizing of aluminium, *Surface and Interface Analysis*, 2007, 39, 860-864.
9. J. Sinko, Challenges of chromate inhibitor pigments replacement in organic coatings, *Progress in Organic Coatings*, 2001, 42, 267-282.
10. L. Xia, E. Akiyama, G. Frankel and R. McCreery, Storage and release of soluble hexavalent chromium from chromate conversion coatings. Equilibrium aspects of CrVI concentration, *Journal of the Electrochemical Society*, 2000, 147, 2556-2562.
11. F. H. Scholes, S. A. Furman, A. E. Hughes, T. Nikpour, N. Wright, P. R. Curtis, C. M. Macrae, S. Intem and A. J. Hill, Chromate leaching from inhibited primers. Part I. Characterisation of leaching, *Progress in Organic Coatings*, 2006, 56, 23-32.
12. M. W. Kendig and R. G. Buchheit, Corrosion inhibition of aluminum and aluminum alloys by soluble chromates, chromate coatings, and chromate-free coatings, *Corrosion*, 2003, 59, 379-400.
13. H. Wang, F. Presuel and R. G. Kelly, Computational modeling of inhibitor release and transport from multifunctional organic coatings, *Electrochimica Acta*, 2004, 49, 239-255.
14. S. A. Furman, F. H. Scholes, A. E. Hughes and D. Lau, Chromate leaching from inhibited primers. Part II: Modelling of leaching, *Progress in Organic Coatings*, 2006, 56, 33-38.
15. O. Lopez-Garrity and G. S. Frankel, Corrosion Inhibition of Aluminum Alloy 2024-T3 by Sodium Molybdate, *Journal of the Electrochemical Society*, 2014, 161, C95-C106.
16. M. Iannuzzi, T. Young and G. S. Frankel, Aluminum alloy corrosion inhibition by vanadates, *Journal of the Electrochemical Society*, 2006, 153, B533-B541.
17. R. L. Cook Jr, Pigment-derived inhibitors for aluminum alloy 2024-T3, *Corrosion*, 2000, 56, 321-333.
18. A. E. Hughes, J. D. Gorman, T. G. Harvey, A. Galassi and G. McAdam, Development of permanganate-based coatings on aluminum alloy 2024-T3, *Corrosion*, 2006, 62, 773-780.
19. J. A. Hill, T. Markley, M. Forsyth, P. C. Howlett and B. R. W. Hinton, Corrosion inhibition of 7000 series aluminium alloys with cerium diphenyl phosphate, *Journal of Alloys and Compounds*, 2011, 509, 1683-1690.
20. D. Ho, N. Brack, J. Scully, T. Markley, M. Forsyth and B. Hinton, Cerium dibutylphosphate as a corrosion inhibitor for AA2024-T3 aluminum alloys, *Journal of the Electrochemical Society*, 2006, 153, B392-B401.
21. T. Stimpfling, F. Leroux and H. Hintze-Bruening, Phosphate-Based Organic Molecules Interleaved with Layered Double Hydroxide: Unraveling the Roles of Host Cations and the Guest-Inhibiting Effect in Aluminum Corrosion Protection, *European Journal of Inorganic Chemistry*, 2012, 2012, 5396-5404.
22. M. Forsyth, M. Seter, M. Y. Tan and B. Hinton, Recent developments in corrosion inhibitors based on rare earth metal compounds, *Corrosion Engineering Science and Technology*, 2014, 49, 130-135.
23. A. J. Aldykewicz, Jr., H. S. Isaacs and A. J. Davenport, Investigation of cerium as a cathodic inhibitor for aluminum-copper alloys, *Journal of the Electrochemical Society*, 1995, 142, 3342-3350.
24. M. O'Keefe, B. Fahrenholtz, E. Morris and R. Albers, Corrosion resistant polymer coatings containing rare earth compounds, *National Association for Surface Finishing Annual Conference and Trade Show, SUR/FIN, Chicago, IL, USA*, 2013.

25. M. E. Nanna and G. P. Bierwagen, Mg-rich coatings: A new paradigm for Cr-free corrosion protection of al aerospace alloys, *Jct Research*, 2004, 1, 69-80.
26. P. Plagemann, J. Weise and A. Zockoll, Zinc-magnesium-pigment rich coatings for corrosion protection of aluminum alloys, *Progress in Organic Coatings*, 2013, 76, 616-625.
27. S. V. Lamaka, M. L. Zheludkevich, K. A. Yasakau, M. F. Montemor and M. G. S. Ferreira, High effective organic corrosion inhibitors for 2024 aluminium alloy, *Electrochimica Acta*, 2007, 52, 7231-7247.
28. M. L. Zheludkevich, K. A. Yasakau, S. K. Poznyak and M. G. S. Ferreira, Triazole and thiazole derivatives as corrosion inhibitors for AA2024 aluminium alloy, *Corrosion Science*, 2005, 47, 3368-3383.
29. T. G. Harvey, S. G. Hardin, A. E. Hughes, T. H. Muster, P. A. White, T. A. Markley, P. A. Corrigan, J. Mardel, S. J. Garcia, J. M. C. Mol and A. M. Glenn, The effect of inhibitor structure on the corrosion of AA2024 and AA7075, *Corrosion Science*, 2011, 53, 2184-2190.
30. G. Bierwagen, R. Brown, D. Battocchi and S. Hayes, Active metal-based corrosion protective coating systems for aircraft requiring no-chromate pretreatment, *Progress in Organic Coatings*, 2010, 67, 195-208.
31. P. Visser and S. A. Hayes, Low-temperature-curable coating composition useful as anticorrosive primer coating for non-ferrous metal substrates, particularly aluminum or aluminum alloy, comprises film-forming resin, curing agent, and lithium salt, *patent nr. WO2010112605-A1*, 2010.
32. J. Gui and T. M. Devine, Influence of lithium on the corrosion of aluminum, *Scripta Metallurgica*, 1987, 21, 853-857.
33. C. M. Rangel and M. A. Travassos, The passivation of aluminium in lithium carbonate/bicarbonate solutions, *Corrosion Science*, 1992, 33, 327-343.
34. C. M. Rangel and M. A. Travassos, Li-based conversion coatings on aluminium: An electrochemical study of coating formation and growth, *Surface & coatings technology*, 2006, 200, 5823-5828.
35. R. G. Buchheit, Bode, M.D., Stoner, G.E., Corrosion-Resistant, Chromate free Talc Coatings for Aluminum, *Corrosion*, 1994, 50, 205-214.
36. C. A. Drewien, Eatough, M.O., Tallant, D.R., Hills, C.R., Buchheit, R.G., Lithium-aluminum-carbonate-hydroxide hydrate coatings on aluminum: Composition, structure and processing bath chemistry, *Journal of material research*, 1996, 11, 1507-1513.
37. M. R. S. Castro, J. C. Nogueira, G. P. Thim and M. A. S. Oliveira, Adhesion and corrosion studies of a lithium based conversion coating film on the 2024 aluminum alloy, *Thin Solid Films*, 2004, 457, 307-312.
38. M. Frenkel, A. Glasner and S. Sarig, Crystal modification of freshly precipitated aluminum hydroxide by lithium ion intercalation, *The Journal of Physical Chemistry*, 1980, 84, 507-510.
39. R. T. Foley, Localized Corrosion of Aluminum Alloys - a Review, *Corrosion*, 1986, 42, 277-288.
40. R. T. Foley and T. H. Nguyen, The Chemical Nature of Aluminum Corrosion: V . Energy Transfer in Aluminum Dissolution, *Journal of The Electrochemical Society*, 1982, 129, 464-467.
41. M. R. Tabrizi, S. B. Lyon, G. E. Thompson and J. M. Ferguson, The long-term corrosion of aluminium in alkaline media, *Corrosion Science*, 1991, 32, 733-742.
42. T. Hurlen and A. T. Haug, Corrosion and passive behaviour of aluminium in weakly alkaline solution, *Electrochimica Acta*, 1984, 29, 1133-1138.
43. P. Visser, Chrome free corrosion inhibiting coating technology for the protection of high strength aluminum alloys, *National Association for Surface Finishing Annual Conference and Trade Show, SUR/FIN 2013, Chicago, IL, USA*, 2013.
44. L. A. Carreiea, V. A. Maroni, J. W. Swaine Jr and R. C. Plumb, Raman and infrared spectra and structures of the aluminate ions, *The Journal of Chemical Physics*, 1966, 45, 2216-2220.
45. P. Sipos, The structure of Al(III) in strongly alkaline aluminate solutions — A review, *Journal of Molecular Liquids*, 2009, 146, 1-14.
46. C. F. Baes and R. E. Mesmer, *The hydrolysis of cations*, Wiley, 1976.
47. G. R. Williams and D. O'Hare, A kinetic study of the intercalation of lithium salts into Al(OH) 3, *J Phys Chem B*, 2006, 110, 10619-10629.
48. V. P. Isupov, Intercalation compounds of aluminum hydroxide, *Journal of Structural Chemistry*, 1999, 40, 672-685.

Chapter 4

On the Importance of Irreversibility of Corrosion Inhibitors for Active Coating Protection of AA2024-T3

Over the years, organic inhibitors have been studied extensively and demonstrated effective corrosion inhibition on AA2024-T3 aluminium alloys. However, none them performed equally to chromates nor have been authorized by the aerospace industry as a suitable alternative. The previous chapter demonstrated the active protective properties of the Li-leaching coating technology by means of a leaching mechanism. It is important to understand the corrosion inhibiting mechanism of this promising Li-leaching inhibitor technology in more detail. This chapter presents insights into the active protective mechanism of the Li-leaching inhibitor coating technology compared to the well-known organic inhibitors studied in solution and when incorporated in organic coatings. The results demonstrate the mechanistically different behaviour of the Li-leaching coating technology compared to the organic inhibitors.

This chapter is published as a scientific paper:
P. Visser, H. Terryn, J.M.C. Mol, "On the importance of irreversibility of corrosion inhibitors for active coating protection of AA2024-T3." Corrosion Science, 140 (2018) 272-285.

Abstract

Inhibitor leaching, fast, effective and irreversible passivation are essential for active protective coatings to protect aluminium alloys. This study presents the comparison of the active protective properties of lithium carbonate and two organic corrosion inhibitors, benzotriazole and 2-mercaptobenzothiazole, on aluminium alloy 2024-T3 with a special focus on the irreversibility of the inhibition. A combined approach of electrochemical measurements, optical observations, surface roughness and weight-loss measurements revealed the reversible inhibition behaviour of benzotriazole and 2-mercaptobenzothiazole on AA2024-T3. On the contrary, lithium carbonate demonstrated fast, effective and irreversible corrosion inhibition, providing the essential characteristics needed for effective active corrosion protection from coatings.

4.1 Introduction

Organic coatings loaded with corrosion inhibitors are widely used for the protection of aluminium structures.[1] The corrosion protection mechanism of these coatings is based on the release of corrosion inhibitors from the coating matrix. This active protective process, known as leaching, is initiated by the ingress of water via a defect or crack in the coating, enabling the dissolution and transport of the corrosion inhibitor to the defect to inhibit the corrosion process.[2, 3]

Aerospace aluminium alloys, such as AA2024-T3, are highly susceptible to localized corrosion in chloride-containing aqueous solutions due to the presence of copper-rich intermetallic particles in the alloy microstructure.[4-6] These intermetallic particles are known to act as active sites for the cathodic oxygen reduction reaction which enhance these localized corrosion phenomena.[7] The inhibition of the electrochemical processes at these intermetallic particles (i.e. suppressing the oxygen reduction reaction) has been an important strategy in the search for environmentally benign alternatives for the highly effective but toxic hexavalent chromium compounds.[8]

Over the years many organic compounds have been evaluated for their corrosion inhibiting activity on aluminium substrates.[9] Especially, heterocyclic compounds such as benzotriazole (BTA) and 2-mercaptobenzothiazole (2-MBT) gained interest as potential corrosion inhibitors for aerospace aluminium alloys due to their copper-complexing characteristics.[10, 11] Both corrosion inhibitors have demonstrated their ability to inhibit the oxygen reduction reaction at copper-rich cathodic intermetallic particles present in the alloys by the formation of an insoluble complex or a polymeric film via a physisorption or chemisorption mechanism providing a physical-chemical barrier for corrosive species.[12-14] These inhibitors are considered copper inhibitors but for aluminium alloys, BTA or 2-MBT have been reported as pure cathodic inhibitors covering the copper-rich intermetallic particles [12] or mixed inhibitors providing both anodic and cathodic inhibition covering the aluminium matrix as well.[13, 15] Furthermore, Harvey et al. demonstrated that both BTA and 2-MBT are able to inhibit corrosion of AA2024-T3 and AA7075-T6 aluminium alloys with inhibitor efficiencies higher than 90%.[16] Based on these inhibitive properties, BTA and 2-MBT have received significant interest of the scientific community and their active corrosion inhibiting activity has been studied widely, in solution on AA2024-T3[13, 17] or an Al/Cu galvanic-coupling model system[18, 19], in coatings[20-22] and various smart-coating approaches using nano-containers [23-28], and poly-urea micro-capsules.[29]

Since a few years, LI-salts gained interest as a potential alternative for chromates as leaching corrosion inhibitor in organic coatings and demonstrated active protective properties on AA2024-T3.[30] Li-salts demonstrated their viability as leachable corrosion inhibitor when incorporated in an industrial coating matrix in a direct comparison with a chromate inhibitor loaded coating system under industrial testing conditions.[31] It was demonstrated that LI-salts are able to leach from an organic coating matrix and create alkaline conditions that promote the formation of a protective layer on the alloy in a

coating defect and consequently inhibit corrosion effectively.[32] This layer is generated by a multistep conversion process of oxide thinning, anodic dissolution and a competitive growth and dissolution process resulting in an aluminium oxide/hydroxide layer with a three-layered morphology of dense, porous and columnar regions.[33] The corrosion protective properties of this layer can be attributed to the dense region at the aluminium/oxide interface.[34]

While the afore mentioned organic inhibitors as well as the Li-based inhibitor technology have been reported to provide significant corrosion protection to AA2024-T3, another pivotal criterion for effective active corrosion protection of these inhibitor types has not been studied in detail: the irreversibility of inhibition. Irreversibility of corrosion inhibitors can be defined as, the ability of a corrosion inhibitor to passivate the metal surface and once passivated, it retains its protective properties when the concentration of the corrosion inhibitor decreases. The irreversibility of the protective properties of a corrosion inhibitor is essential for long-term corrosion protection. Despite excellent corrosion inhibiting results with BTA at initial stage, Recloux et al. reported that the inhibitor film stability of BTA seems to be dependent on the presence of inhibitor reported that the inhibitor film stability of BTA seems to be dependent on the presence of inhibitor.[13, 15] Zheludkevich et al. observed degradation of the BTA protective layer after 50 h exposure to the inhibitor solutions.[13] These observations make it worthwhile to investigate the active protective properties and irreversibility of these well-known organic corrosion inhibitors in comparison to the new lithium carbonate (Li_2CO_3) inhibitor.

In this comparative study the active protective properties of Li_2CO_3 and the organic inhibitors BTA and 2-MBT on AA2024-T3 are investigated. The intrinsic corrosion protective properties of the inhibitors on AA2024-T3 were investigated using electrochemical impedance spectroscopy (EIS) and potentiodynamic polarization measurements. Furthermore, the corrosion inhibitors were incorporated in an organic model coating to evaluate their active corrosion protective properties by the measurement of inhibitor leaching from the coating matrix. The corrosion protective properties in a defect area of an artificially damaged coating were assessed by optical microscopy and with EIS after exposure to the neutral salt spray test. Complementary EIS, surface roughness and weight loss measurements were performed to study the reversibility and the inhibitor efficiency of the corrosion inhibitors. This combination of experimental approaches provided an enhanced insight into the mechanisms and robustness of the active corrosion inhibition provided by these corrosion inhibitors.

4.2 Experimental

4.2.1 Corrosion inhibition and inhibitor reversibility in an electrochemical cell

Materials and sample preparation

Aluminium alloy panels AA2024-T3 bare (5.0 x 7.0 cm, 0.8 mm thickness) were obtained from Arconic. Before the experiment, the panels were degreased with acetone to remove surface contaminations and abraded with Scotch-Brite™ 7447 PRO pads, rinsed with deionized water, and dried with compressed air.

The corrosion inhibitors were obtained from Sigma-Aldrich: benzotriazole (99%) (BTA), 2-mercaptobenzothiazole (2-MBT) (97%) and lithium carbonate (Li_2CO_3) (99.997%). The inhibitor solutions were prepared in an aqueous 0.05M NaCl solution with the following concentrations: no inhibitor, 5 mM BTA, 5 mM Li_2CO_3 and 1 mM 2-MBT. Throughout the manuscript these solutions will be referred to as blank solution, BTA solution, Li_2CO_3 solution and 2-MBT solution, respectively. Preliminary experiments demonstrated that 5mM was the minimum concentration needed to obtain reproducible corrosion inhibition with Li_2CO_3 and BTA. Due to the low solubility of this inhibitor in water, the concentration of the 2-MBT solution was limited to 1mM. The solubility of the inhibitors is as follows: 2-MBT, 0.1 mM/100 ml[35], BTA 1.7 mM/100 ml[36] and Li_2CO_3: 17.5 mM/100 ml[37])

4.2.2 Electrochemical assessment of corrosion inhibition and inhibitor reversibility

Electrochemical impedance spectroscopy

The aluminium panels were installed in an electrochemical cell and exposed to solutions with and without corrosion inhibitor for 24 h. After this period, EIS spectra were recorded at the open circuit potential (OCP) using a Gamry Interface 1000 computer-controlled potentiostat. A three-electrode set-up was used, consisting of the aluminium sample as the working electrode (surface area 3.14 cm^2), platinum gauze counter electrode and a saturated calomel electrode (SCE) as reference electrode in a Faraday cage. The EIS measurements were performed over a frequency range from 10^{-2} Hz to $3 \cdot 10^4$ Hz, applying a 10 mV sinusoidal amplitude and performing 10 measurements per frequency decade. All measurements were performed at least in triplicate.

Potentiodynamic polarizations

Potentiodynamic polarizations were performed after 24 h exposure to the 0.05M NaCl solutions with and without corrosion inhibitor. The samples, with a surface area of 3.14 cm^2, were polarized using a sweep rate of 1 mV/s and a sweep range of -200 to +200 mV versus the OCP. The anodic and cathodic polarizations were performed on separate samples starting from the OCP. The measurements were performed at least in triplicate for each anodic and cathodic polarization to ensure reproducibility.

Reversibility

The reversibility of the corrosion inhibitors was assessed with EIS. After the initial EIS measurement after 24 h exposure to 60 ml inhibitor solution, the inhibitor solution was removed, the electrochemical cell was 2 times gently rinsed with a 0.05 M NaCl solution to remove excess of corrosion inhibitor, and finally refilled with 60 ml 0.05M NaCl solution. The EIS spectra were recorded as described above, directly and 24 h and 5 d after the removal of the corrosion inhibitor. For data analysis the impedance spectra were fitted with Zview from Scribner Associates Inc. using the appropriate equivalent circuits.

4.2.3 Active protective properties of inhibitor loaded coatings

Preparation of the organic model coatings.

The corrosion inhibitors were incorporated into polyurethane model coatings to investigate the active protective properties. The formulations of the coatings are summarized in Table 4.1. The coatings were formulated to a total pigment volume concentration (PVC) of 30 vol%, this includes 5 vol% of corrosion inhibitor for the coatings loaded with 2-mercaptobenzothiazole (2-MBT-loaded), benzotriazole (BTA-loaded), and lithium carbonate (Li_2CO_3-loaded). The coating without corrosion inhibitor (Non-inhibited reference) contains 5 vol% of the inert barium sulphate instead of corrosion inhibitor.

Table 4.1: Composition of organic model coating

	No inhibitor	2-MBT	BTA	Li_2CO_3
Component A				
N-Butylacetate	85.0 g	85.0 g	85.0 g	85.0 g
Desmophen 650MPA	47.7 g	47.7 g	47.7 g	47.7 g
2-MBT		7.2 g		
BTA			6.8 g	
Lithium carbonate				10.5 g
Magnesium oxide	16.4 g	16.4 g	16.4 g	16.4 g
Tioxide TR 92	5.2 g	5.2 g	5.2 g	5.2 g
Blanc Fixe N ($Ba(SO_4)$)	66.0 g	43.5 g	43.5 g	43.5 g
Component B				
Tolonate HDB 75 MX	28.5 g	28.5 g	28.5 g	28.5 g
Dynasilan Glymo	5.2 g	5.2 g	5.2 g	5.2 g

Sample preparation

The coatings were prepared by mixing the raw materials as follows: component A was prepared by adding the ingredients under stirring in a 370 ml glass jar. After the addition of 400 grams Zirconox® pearls (1.7 - 2.4 mm), the pigments were dispersed to a fineness of grind less than 25 μm by shaking on a Skandex® paint shaker. After 20 min shaking, the pearls were separated from the coating. Component B was mixed separately and added to Component A just before application.

AA2024-T3 aluminium panels were anodized using tartaric sulphuric acid accordion to aerospace requirements (AIPI 02-01-003) resulting in an anodic film of 3-3.5 μm. The

coating formulations were applied on these panels with a high volume low pressure (HVLP) spray gun. After the application at 23 °C and 55 % RH, a 1 h flash-off period was applied followed by a force cure cycle of 1h at 80 °C. The dry film thickness of the coatings after drying was 20-25 μm.

Inhibitor leaching

The leaching of the corrosion inhibitors from the organic coating matrix was investigated by immersing the coated samples with a surface area of 28 cm^2 in 50 ml deionized water. Prior to the immersion, the coatings were damaged with 20 parallel cuts with a length of 5 cm until the substrate using a razor blade achieving a total scribe length of 1 meter to ensure sufficient leaching from the cut edges of the coating. Samples were taken every 10 min up to 1 h; further measurements were taken after 1.5 h, 2 h, 3 h, 4 h, and 6 h. The solutions of the exposed 2-MBT-loaded and BTA-loaded coatings were analysed with UV-VIS spectroscopy (Agilent Cary 60 UV-Vis spectrophotometer and the solutions obtained from the exposed Li_2CO_3-loaded coating were analysed with inductively coupled plasma atomic emission spectroscopy (Arcos NT ICP-AES). The samples for ICP-AES were acidified with nitric acid to a concentration of 0.1M and measured using scandium as an internal standard.

Corrosion protection in the defect area

An artificial damage was made in the samples to investigate the active protective properties of these inhibitor-loaded coatings. The artificial defect, with a surface area of 0.48 cm^2, was prepared by mechanical milling resulting in two intersecting scribes with a length of 2 cm, width of 1 mm and depth of 100-150 μm. After scribing, the coated samples were exposed to the neutral salt spray test (NSS) according to ASTM-B117 for 7 d. After exposure, the defect area was evaluated by optical microscopy and the corrosion inhibitive properties were evaluated by EIS using the same equipment and settings as described above using a 0.05 M NaCl solution. In this case, the working electrode exposed to the electrolyte was the coating with the defect area. The total surface area of the electrochemical cell was of 12.5 cm^2 and the effective electrode (i.e. the coating defect) area was 0.48 cm^2. The impedance measurements were recorded after 5 h of exposure to the 0.05 M NaCl solution.

4.2.4 Inhibitor reversibility and inhibition efficiency

AA2024-T3 samples were mechanically ground with successive grades of SiC sanding paper up to 1200 grid using water as lubricant and then polished with 1μm diamond paste. After polishing, the samples were cut into 1 cm^2 panels, ultrasonically cleaned in ethanol, dried at 40 °C and weighed with an analytical balance. The panels were immersed in 50 ml of 0.05 M NaCl solution with or without corrosion inhibitor (1 mM MBT, 5mM BTA, 5mM Li_2CO_3). One set of panels was exposed for 14 d to the corrosion inhibitor loaded solutions

and another set of panels was exposed to the inhibitor solution for 24 h, followed by immersion in a 0.05M NaCl solution without inhibitor (blank solution) for 13 d. Nitric acid is an effective desmutting agent and deoxidizer for aluminium and is a effective replacement for the toxic chromic acid desmutting method to dissolve the corrosion products from the aluminium panels.[16, 38] After exposure to the solutions, all the panels (including the unexposed sample) were cleaned by immersion in a 1M nitric acid solution for 2 h. After the cleaning procedure the panels were dried and weighed to determine the weight loss due to corrosion. The panels were visually examined with an optical microscope and the surface roughness of the sample (Sa (arithmetical mean height)) was measured with a Bruker K1 white light interferometer using a 20x objective. Sa expresses the surface roughness of an area, as an absolute value, the difference in height of each point compared to the arithmetical mean of the surface. This parameter is used to evaluate the roughness of surfaces.39, 40 For each sample a 4 x 4 mm area was measured and Vision for Profilers (version 4.2) software was used to analyse the data. All measurements were executed in duplicate. The inhibitor efficiency (IE) was determined from the weight loss measurements. First the corrosion rate (w) was calculated using equation 1[41]:

$$w = \frac{m_{before} - m_{after}}{A.t} \quad (1)$$

Where m_{before} is the mass of the sample before exposure (mg) and m_{after} is the mass of the same coupon after the exposure. A is the area of the sample (mm^2) and t is the exposure time (h). With the corrosion rate value, IE was calculated using equation 2 [41]:

$$IE = \frac{w_0 - w_{inh}}{w_0} X\ 100\ \% \quad (2)$$

In this equation, w_0 is the corrosion rate of the sample without corrosion inhibitor and w_{inh} is the corrosion rate of the sample in the presence of corrosion inhibitor in solution.

4.3 Results and Discussion

4.3.1 Corrosion inhibition in an electrochemical cell

Potentiodynamic polarization measurements

Potentiodynamic polarization measurements were performed to investigate the corrosion inhibiting effect of the corrosion inhibitors on the anodic and cathodic electrode reactions. Fig. 4.1 shows the polarization curves after 24 h exposure of the AA2024-T3 samples to the inhibitor solutions. The sample without inhibitor shows immediate pitting when polarized anodically vs. the OCP and a diffusion limited cathodic polarization curve below -0.58V_{SCE}. The polarization curves of the samples that were exposed to the inhibitor solutions for 24

h, clearly demonstrate the inhibitive nature of the corrosion inhibitors. The corrosion potential of the aluminium samples that were exposed to the BTA and 2-MBT solutions shifted to less noble potentials and the cathodic currents were suppressed by about an order of magnitude. In addition to this, the anodic currents of these samples were reduced and the pitting potential shifted to more noble values of around -0.51V_{SCE}. The corrosion potential (E_{corr}) of the sample exposed to the Li_2CO_3 solution remained at -0.54V_{SCE} and both the anodic and cathodic currents were suppressed. Table 2 summarizes the electrochemical parameters derived from the potentiodynamic polarization measurements displayed in Fig. 4.1. The corrosion current (i_{corr}) was approximated from the polarization resistance (R_{pol}) using the Stern-Geary equation. R_{pol} was obtained from the linear slope of the linear region ±20 mV vs. E_{corr}. [42, 43]

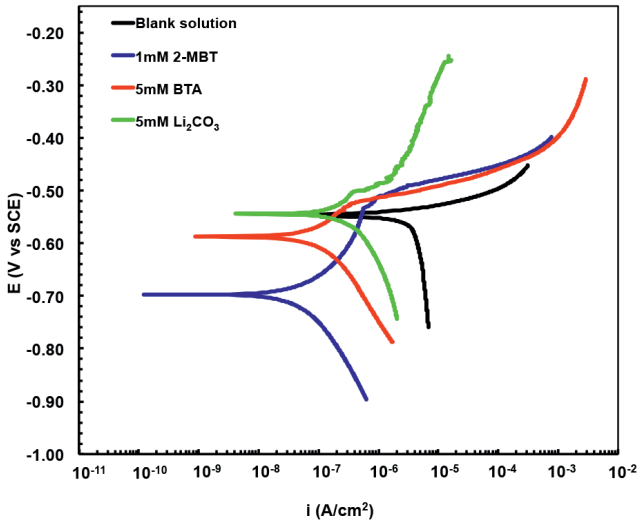

Figure. 4.1 Potentiodynamic polarization curves for AA2024-T3 aluminium alloy in 0.05 M NaCl with and without corrosion inhibitor.

From the results in Table 4.2, it can be noted that i_{corr} for the samples that were exposed to the inhibitor-loaded solutions was reduced by an order of magnitude as compared to that of the sample that was exposed to the blank solution.

Table 4.2 Electrochemical parameters obtained from the potentiodynamic polarization curves displayed in Fig. 4.1

	Ecorr (V_{SCE})	i_{corr} (A/cm^2)	R_{pol} ($k\Omega.cm^2$)	Passive range E_{pit}-E_{corr}(V)
Blank	-0.54	$3.38x10^{-6}$	3	0
1 mM 2-MBT	-0.70	$3.96x10^{-8}$	427	0.18
5mM BTA	-0.59	$7.91x10^{-8}$	215	0.07
5 mM Li_2CO_3	-0.54	$3.08x10^{-7}$	67	0.05

The 2-MBT solution provided the best corrosion protective properties on the AA2024-T3 samples with an i_{corr} of $3.96 \cdot 10^{-8}$ A/cm^2 and a R_{pol} 472 kΩ·cm^2 followed by the sample that was exposed to the BTA solution with an i_{corr} of $7.91 \cdot 10^{-8}$ A/cm^2 and a R_{pol} 215 kΩ·cm^2. The i_{corr} of the sample exposed to the Li_2CO_3 solution was $3.08 \cdot 10^{-7}$ A/cm^2 and the R_{pol} 67 kΩ·cm^2. The cathodic branches of the potentiodynamic polarization curves show the diffusion limited reduction of the dissolved oxygen. The anodic branches show the passive ranges of the samples after 24 h exposure to the corrosion inhibitor solutions. The anodic polarization curves show a shift of the pitting potential (E_{pit}) to more noble values of all samples exposed to an inhibitor solution. The sample exposed to the 2-MBT solution showed the largest anodic passive range of 180 mV compared to 70 mV for the sample in the BTA solution. The sample exposed to the Li_2CO_3 solutions showed a relative small anodic passive range of 50 mV, followed by a slight increase of the anodic current density upon further anodic polarization. This indicates some limited anodic activity or pitting corrosion around 50 mV. However, the system did not progress to full pitting corrosion over the anodic polarization range of 200 mV. The anodic current density remained below 10^{-5} A·cm^{-2}, two orders of magnitude lower than for the exposure to the organic corrosion inhibitor solutions at these potentials. This behaviour indicates that generated layer is covering the macroscopic surface area and is limiting the corrosion reactions and the breakdown potential of this layer exceeds the range of this anodic potentiodynamic polarization measurement. In general, exposure of AA2024-T3 to the tested inhibitor solutions provides improved corrosion protective properties resulting in increased R_{pol}, reduced i_{corr}, shifts in E_{corr} and the presence of passive ranges shifting E_{pit} to more noble potentials. These results imply that Li_2CO_3 and both organic corrosion inhibitors BTA and 2-MBT behave as mixed inhibitors providing anodic and cathodic inhibition as observed in earlier studies.[13, 15] Based on the electrochemical parameters from these potentiodynamic polarizations (R_{pol}, i_{corr}, E_{corr} and the passive ranges) it can be concluded that the 2-MBT solution provides the most effective inhibition on AA2024-T3 followed by the BTA and Li_2CO_3 solutions.

Electrochemical impedance measurements

Further comparative analysis of the corrosion protective properties of the inhibitor solutions was performed with EIS. Fig. 4.2 shows the Bode plots after the exposure of AA2024-T3 to the 0.05M NaCl solutions with and without corrosion inhibitor. The impedance modulus plot (Fig. 4.2a) shows that AA2024-T3 has the lowest impedance modulus value after 24 h exposure to the blank solution. The impedance modulus values increased when the alloy was exposed to the Li_2CO_3 solution. Exposure to the 2-MBT and BTA solutions resulted in an increase by more than an order of magnitude compared to the sample without inhibitor. This underlines the excellent intrinsic inhibitive properties of these organic corrosion inhibitors. The accompanying Bode phase angle plots are displayed in Fig. 4.2b.

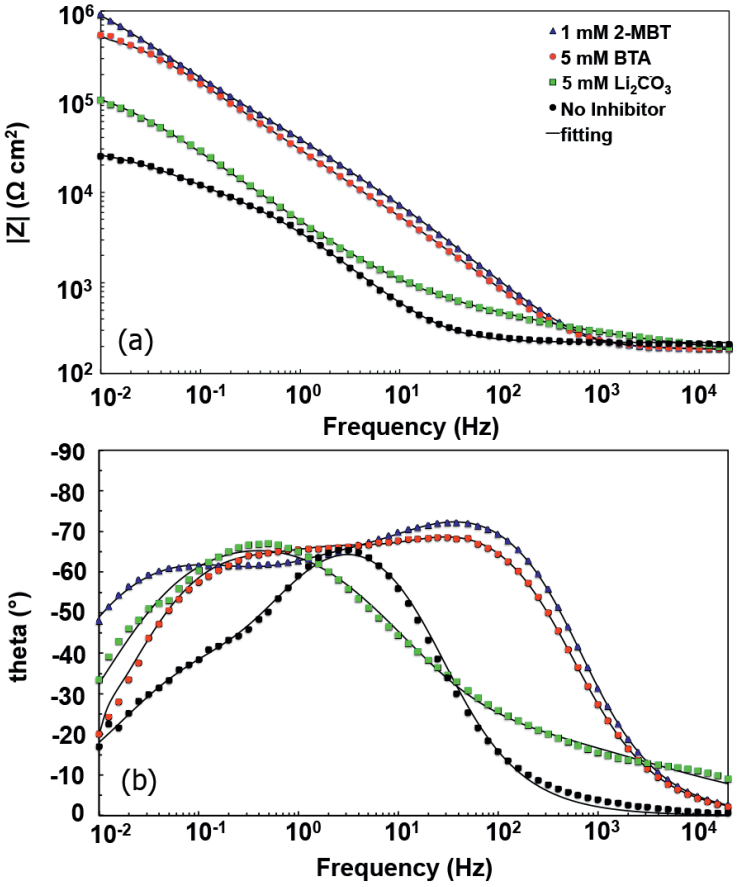

Figure 4.2 *Electrochemical impedance spectra of AA2024-T3 aluminium alloy after 24 h exposure to the 0.05 M NaCl solution with and without corrosion inhibitor. (a) impedance modulus and (b) phase angle.*

The phase angle plot of the sample exposed to the blank solution shows two time-constants, one for the oxide layer (middle frequency range 10^{1}-10^{3} Hz) and the second for the electrochemical activity at the aluminium surface (low frequency range 10^{-2}-10^{-1} Hz). The phase angle plots of the samples exposed to the BTA and 2-MBT solutions show a typical impedance spectrum of a metal in an organic inhibitor electrolyte showing three time-constants. A time-constant in the low frequency range for the electrochemical processes at the aluminium substrate and two higher frequency range time-constants related to the oxide (10^{-1}-10^{2} Hz) and organic inhibitor layer (10^{1}-10^{3} Hz) on the substrate.[13] The phase angle plot of the sample that was exposed to the Li_2CO_3 solution shows also three time-constants that can be attributed to a generated corrosion protective layer on the alloy sample. One time-constant relates to the electrochemical processes in the low frequency range and two overlapping time-constants extending over the middle frequency range (10^{-1}- 10^{3} Hz) relate to a dense and porous oxide layer.[34]

The results of these measurements have been fitted to compare corrosion protective properties of these inhibitor solutions on AA2024-T3. The fittings were performed with the equivalent circuits as shown in Fig. 4.3 derived from previous studies.[13, 34] EC1 is a two time-constant equivalent circuit model to describe a sample that is exposed to the solution without corrosion inhibitor.[13] In this model, R_{sol} is the solution resistance, and the first time-constant represents the resistance of the native aluminium oxide (R_{oxide}) and its capacitance properties (CPE_{oxide}). The second time-constant describes the electrochemical processes (corrosion) at the aluminium substrate in terms of the polarization resistance (R_{pol}) and the double layer capacitance (CPE_{dl}). Both, the organic inhibitors and Li_2CO_3 are represented by different equivalent circuits because their physical model of the corrosion protective layer is different.[34] EC2 describes the system when AA2024-T3 was exposed to the organic corrosion inhibitor solution (MBT or BTA).[13]

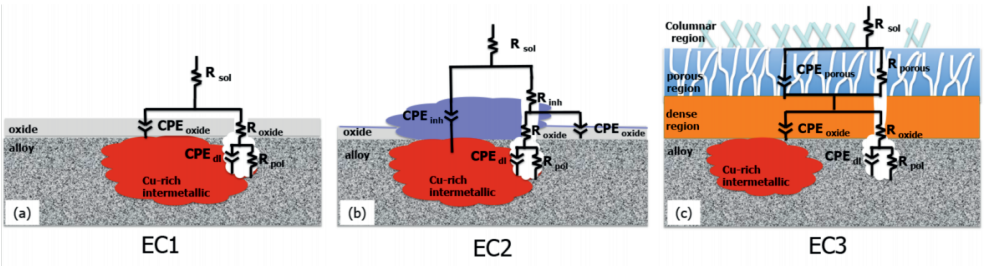

Figure 4.3 Equivalent electric circuits used to fit the EIS spectra: (a) EC1 without inhibitor; (b) EC2 with organic inhibitor; (c) EC3 with Li_2CO_3.

This EC features an additional time-constant describing the contribution of the resistance (R_{inh}) and capacitance (CPE_{inh}) of the corrosion-inhibiting layer that covers the copper-rich intermetallic particles.[13] Equivalent circuit EC3 is representative for the corrosion inhibiting layer covering the aluminium surface generated by exposing the aluminium alloy to a Li_2CO_3 solution.[34] In this system, the additional time-constant describes the contributions of the porous layer (R_{porous} and CPE_{porous}) on top of the dense oxide layer. [34] The fitted curves are displayed as solid lines in the Bode plots of Fig. 4.2. The quantitative data derived from these fittings are listed in Table 4.3. The constant phase elements (CPE) are used in these equivalent circuits to describe the elements with a non-ideal capacitive behaviour using parameter Q and n. [44]

Although the inhibitors are described in different equivalent circuits, it is possible to compare the corrosion protective properties of these systems based on the oxide resistance (R_{oxide}) and polarization resistance (R_{pol}) values. In addition, the inhibitive layer resistance (R_{inh}) can be used to compare the properties of the corrosion inhibitive layer of both organic inhibitors. Table 4.3 reveals an additional stabilizing effect on the oxide layer by 2-MBT and BTA in addition to their corrosion inhibitive action as a result of the coverage of copper-rich intermetallic particles (R_{inh}).

Table 4-3 Fitted parameters for EIS spectra of the scribed lithium oxalate loaded coating after different periods of NSS exposure.

EC1		no inhibitor	EC2		1mM 2-MBT	5mM BTA	EC 3		5 mM Lithium carbonate
R_{sol}	Ω	220	R_{sol}	Ω	184	186	R_{sol}	Ω	157
			$Q(CPE_{inh})$	Ss^ncm^{-2}	$2.80x10^{-6}$	$4.32x10^{-6}$	$Q(CPE_{porous})$	Ss^ncm^{-2}	$1.38x10^{-4}$
			n_{inh}		0.9	0.88	n_{porous}		0.45
			R_{inh}	Ωcm^2	23791	18415	R_{Porous}	Ωcm^2	505
$Q(CPE_{Oxide})$	Ss^ncm^{-2}	$4,66x10^{-5}$	$Q(CPE_{Oxide})$	Ss^ncm^{-2}	$3.09x10^{-6}$	$2.79x10^{-6}$	$Q(CPE_{Oxide})$	Ss^ncm^{-2}	$4.89x10^{-5}$
n_{oxide}		0.9	n_{oxide}		0.74	0.81	n_{oxide}		0.8
R_{oxide}	$k\Omega cm^2$	9	R_{oxide}	$k\Omega cm^2$	164	143	R_{oxide}	$k\Omega cm^2$	37
$Q(CPE_{dl})$	Ss^ncm^{-2}	$1.46x10^{-4}$	$Q(CPE_{dl})$	Ss^ncm^{-2}	$2.89x10^{-6}$	$2.91x10^{-6}$	$Q(CPE_{dl})$	Ss^ncm^{-2}	$1.58x10^{-6}$
n_{dl}		0.7	n_{dl}		0.76	0.82	n_{dl}		0.96
R_{pol}	$k\Omega cm^2$	23	R_{pol}	$k\Omega cm^2$	216	462	R_{pol}	Ωcm^2	120
χ^2		$4.29x10^{-3}$	$\chi 2$		$5.81x10^{-5}$	$7.16x10^{-4}$	$\chi 2$		$1.18x10^{-3}$

Compared to the sample that was exposed to the blank solution, R_{oxide} for the samples exposed to the 2-MBT and BTA solutions increased by a factor 15 to 19. This implies that 2-MBT and BTA have a stabilizing effect on the aluminium oxide as well, due to the adsorption of the inhibitor on the aluminium surface.
This confirms the mixed anodic/cathodic inhibiting properties of these organic corrosion inhibitors observed with the potentiodynamic polarization measurements. R_{oxide} of the sample exposed to the Li_2CO_3 solution increased with a factor 4, which is significantly lower compared to the samples exposed to the BTA and 2-MBT solutions. A similar trend can be observed for R_{pol} of these samples, with estimated values of 2.16 MΩ·cm^2, 0.46 MΩ·cm^2 and 0.12 MΩ·cm^2 for respectively the 2-MBT, BTA and Li_2CO_3 solutions. These EIS measurements and fittings show that the 2-MBT solution provides the best corrosion inhibitive properties on AA2024-T3 followed by the BTA and Li_2CO_3 solutions and confirm the findings and trends observed from the potentiodynamic polarization measurements.

4.3.2 Active protective properties in a coating

Inhibitor loaded coatings were formulated and their active protective properties were investigated in terms of leaching behaviour and the evaluation of the corrosion protective properties in an artificial defect after exposure to an accelerated corrosion test.

Leaching of the corrosion inhibitors from the organic coating

The leaching behaviour of the corrosion inhibitors from the organic model coatings is shown in Fig. 4.4. It shows the total released corrosion inhibitor as percentage of the total loading in the organic coating matrix during the first 6 h of immersion in deionized water at ambient conditions (23 °C and 55% RH). All three corrosion inhibitors show immediate leaching, but despite the equal loading in terms of volume (5% PVC) the leach rates differ significantly. The Li_2CO_3-loaded coating showed the fastest response of all inhibitors, leaching 2.5 % of the active inhibitor in the first 30 min of exposure and 3.0 % after 6 h. The 2-MBT-loaded coating showed a significantly slower leaching response compared to the Li_2CO_3-loaded coating with 0.7 % after 30 minutes and increasing to 1.5 % after 6 h followed by the BTA-loaded coating with the slowest leaching response of 0.3 and 0.5 % after 30 min and 6 h respectively.

Based on the solubility parameters, it is logical to observe such a fast leaching for the Li_2CO_3-loaded coating. However, the slow leach rate of BTA from the organic coating suggests that BTA is less mobile in the coating matrix compared to 2-MBT. All samples show a similar leaching behaviour, an initial fast release related to the direct dissolution of the inhibitor at the coating/solution interface, followed by a slower leach rate after 1 h immersion. Inhibitor leaching is a complex process of dissolution and diffusion through the coating matrix. A non-Fickian leaching behaviour is often observed and this is assumed to be related to the diffusion / mass transport of the corrosion inhibitor from deeper in the coating matrix via interconnected pathways to the coating defect.[45, 46] The leach rate is not only depending on the amount and solubility of the inhibitor, but it is also related to the

pigment distribution and connectivity (microstructure) of the coatings.[47, 48] The leach rate of the inhibitor from the coating and the irreversible reaction with the metal substrate are essential elements for effective active corrosion protection.[49] With the knowledge of the corrosion inhibiting and leaching properties of BTA, 2-MBT and Li_2CO_3, it can be assumed that these inhibitors can potentially provide active protection in a coating defect.

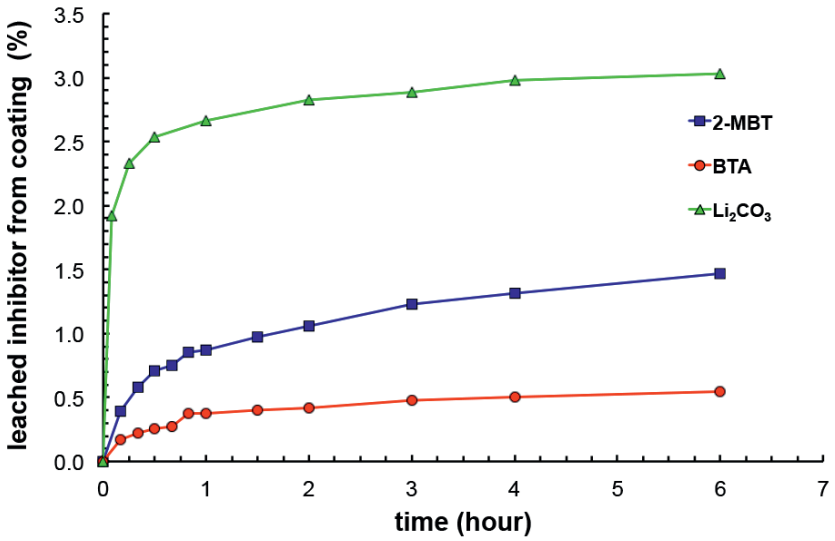

Figure 4.4 Accumulated release of corrosion inhibitor from the organic coating matrix, normalized per cm^2 model coating with a thickness of 25 µm over a 6 h time-period.

Visual evaluation of the active protective properties in a coating defect.

The coatings loaded with and without leachable corrosion inhibitor were exposed to the neutral salt spray test (NSS) according to ASTM B-117 to assess the active protective properties of a coating in an artificial defect (scribe). Fig. 4.5 shows the appearance of the defect areas of the coatings assessed with an optical microscope after 168 h exposure to the NSS test.

Despite the immediate leaching of corrosion inhibitor, as demonstrated in the previous section, the defect area of the BTA and 2-MBT loaded coatings do not show an improved corrosion protection compared to the non-inhibiting reference coating. Both samples showed darkening and white corrosion products in the defect area. In contrast to this, the defect area of the Li_2CO_3-loaded coating is free of corrosion products and retained a shiny appearance. This suggests that the LI-leaching coatings provided effective corrosion inhibition in the defect area.

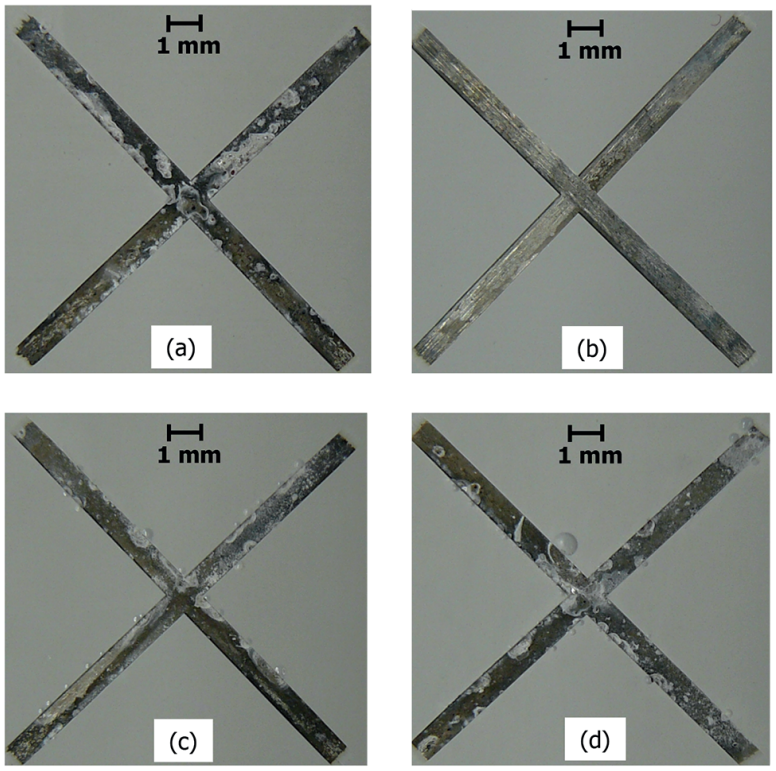

Figure 4.5 *Optical images of coated and scribed AA2024-T3 panels without and with leachable corrosion inhibitor after 168 h neutral salt spray exposure (ASTM B-117) (a) Non-inhibiting reference coating; (b) Li_2CO_3-loaded coating; (c) BTA-loaded coating, and (d) 2-MBT-loaded coating.*

Electrochemical properties of the coating defect

EIS can be used to evaluate the corrosion protective properties in a defect area as result of active protective activity of coatings.[34] Fig. 4.6 shows the EIS measurements of the defect areas acquired in a 0.05M NaCl electrolyte after 168 h NSS exposure.

The impedance modulus plot (Fig. 4.6a) reveals that the impedance of the Li_2CO_3 loaded coating is almost two to three times higher compared to the coatings loaded with BTA and MBT and the coating without corrosion inhibitor. The accompanying Bode phase angle plot (Fig. 4.6b) of the Li_2CO_3 loaded coating shows increased phase angle values and a broadened shape of the time-constant around $10^1 – 10^3$ Hz which can be associated with a protective layer in the defect area.[34] The phase angle diagrams of the coatings loaded with BTA and 2-MBT are similar to the coating without a corrosion inhibitor. From these impedance measurements it is evident that the defect area of the coating sample loaded with Li_2CO_3 as leaching corrosion inhibitor shows an improved corrosion resistance compared to the samples without corrosion inhibitor or loaded with BTA or 2-MBT. These results suggest that despite the intrinsic corrosion inhibiting properties of BTA and 2-MBT

and leaching characteristics from the organic coatings, both BTA and 2-MBT loaded coatings did not provide sufficient active corrosion protective properties to irreversibly passivate the aluminium surface in the coating defect under these conditions.

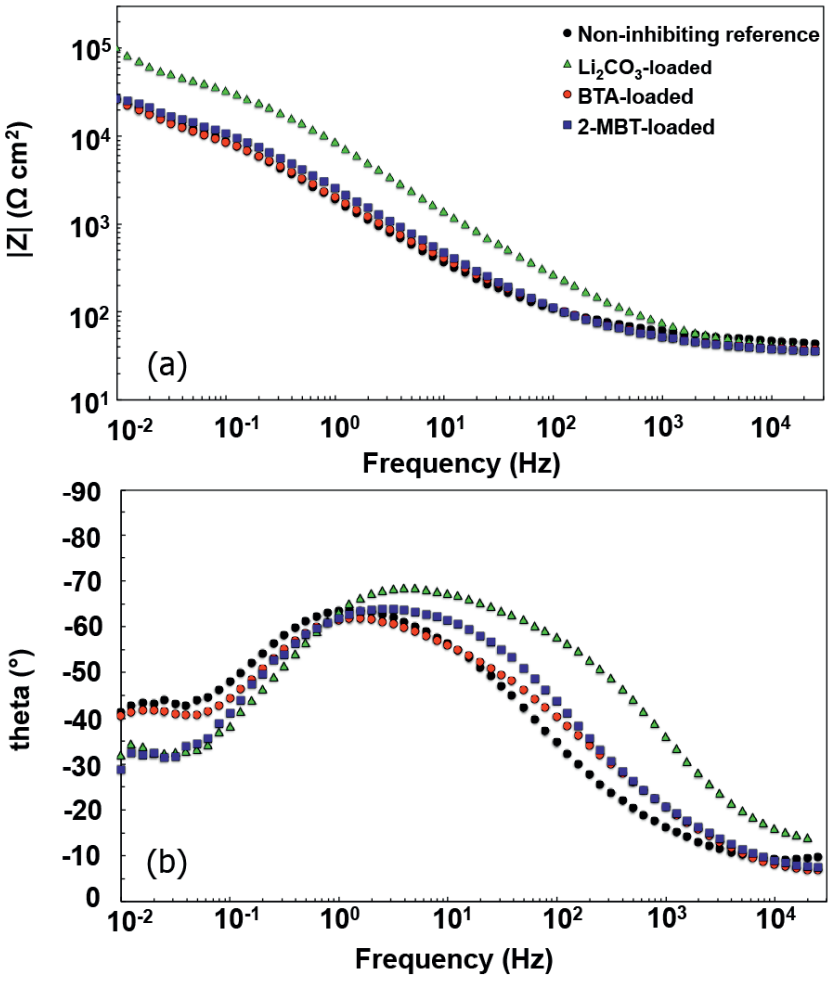

Figure 4.6 Electrochemical impedance spectra of the defect areas of coatings loaded with and without leaching corrosion inhibitor on AA2024-T3 aluminium after 168 h NSS exposure measured in a 0.05 M NaCl solution: (a) impedance modulus (b) phase angle plot.

4.3.3 Inhibitor reversibility and efficiency

In order to explain the findings of the work summarized above, the reversibility and the inhibitor efficiency of these inhibitors were investigated using EIS, surface roughness and weight-loss measurements.

Electrochemical assessment of inhibitor reversibility

The reversibility of the corrosion inhibitors on AA2024-T3 was investigated by consecutive EIS measurements in the presence and after removal of the corrosion inhibitor solutions (Fig. 4.7). The EIS spectra were recorded with the inhibitor solution present and directly after replacement of the inhibitor solution by a 0.05 M NaCl solution (blank solution) and two additional measurements, 24 h and 5 d after replacement. Fig. 4.7a shows the EIS spectra for the AA2024-T3 exposed to the blank solution at the same time intervals. Fig. 4.7b-d show the EIS spectra of the samples before and after the replacement of the inhibitor solution. When the Li_2CO_3 solution was replaced by the blank solution (Fig. 4.7b), the impedance modulus decreased slightly over the entire frequency range. In the low frequency area (10^{-2} Hz) the impedance decreased from 65 kΩ·cm^2 with the Li_2CO_3 solution present to 44 kΩ·cm^2 directly after replacement by the blank solution. However, this value increased again beyond the initial value to 93 kΩ·cm^2 after 5 d exposure to the blank solution. The Bode phase angle plot showed an initial decrease of the middle frequency time-constant (10^1-10^3 Hz) followed by the broadening and increasing phase angle values of this time-constant, indicating further development of the oxide layer and its corrosion protective properties after the replacement of the inhibitor solution. [49]

The BTA and 2-MBT solutions showed their characteristic effective corrosion inhibition on AA2024-T3 after 24 h exposure (Fig. 4.7c and d). However, the inhibitive nature of these inhibitors decreased significantly after the replacement of the inhibitor solution by the blank solution.

The impedance modulus of the sample that was exposed to the BTA solution decreased directly by an order of magnitude over the entire frequency range after the replacement of the inhibitor solution by the blank solution. The impedance modulus decreased from 320 kΩ·cm^2 to 26 kΩ·cm^2 at 10^{-2} Hz, after the replacement of the BTA solution (Fig. 4.7c). When the 2-MBT solution was replaced by the blank solution, the impedance dropped at first only in the low frequency range (10^{-2} Hz) from 820 kΩ·cm^2 to 4.0 kΩ·cm^2 (Fig. 4.7d). However, longer exposures (up to 5 d) to the blank solution resulted in a further decrease of the impedance modulus to values equal to a sample that was exposed to the blank solution for 5 d. For both organic inhibitors, BTA and 2-MBT, this phenomenon is clearly visible in the Bode phase plot as well. The characteristic broad phase angle plot, observed for the samples exposed to the BTA or 2-MBT solution, disappears after the replacement with a blank solution. Finally, the phase angle plots have a similar appearance as the sample, which was exposed to the blank solution.

These EIS measurements were fitted with the equivalent circuits (EC1, EC2 and EC3) from Fig. 4.3 in order to compare the corrosion inhibitive properties of the corrosion inhibitors before and after their replacement with a blank solution. Fig. 4.8 shows the evaluation of the oxide resistance (R_{oxide}) and the oxide capacitance (C_{oxide}) and the polarization resistance (R_{pol}) and the double layer capacitance (C_{dl}) of the AA2024-T3 samples as a function of exposure time to the inhibited and non-inhibited solutions.

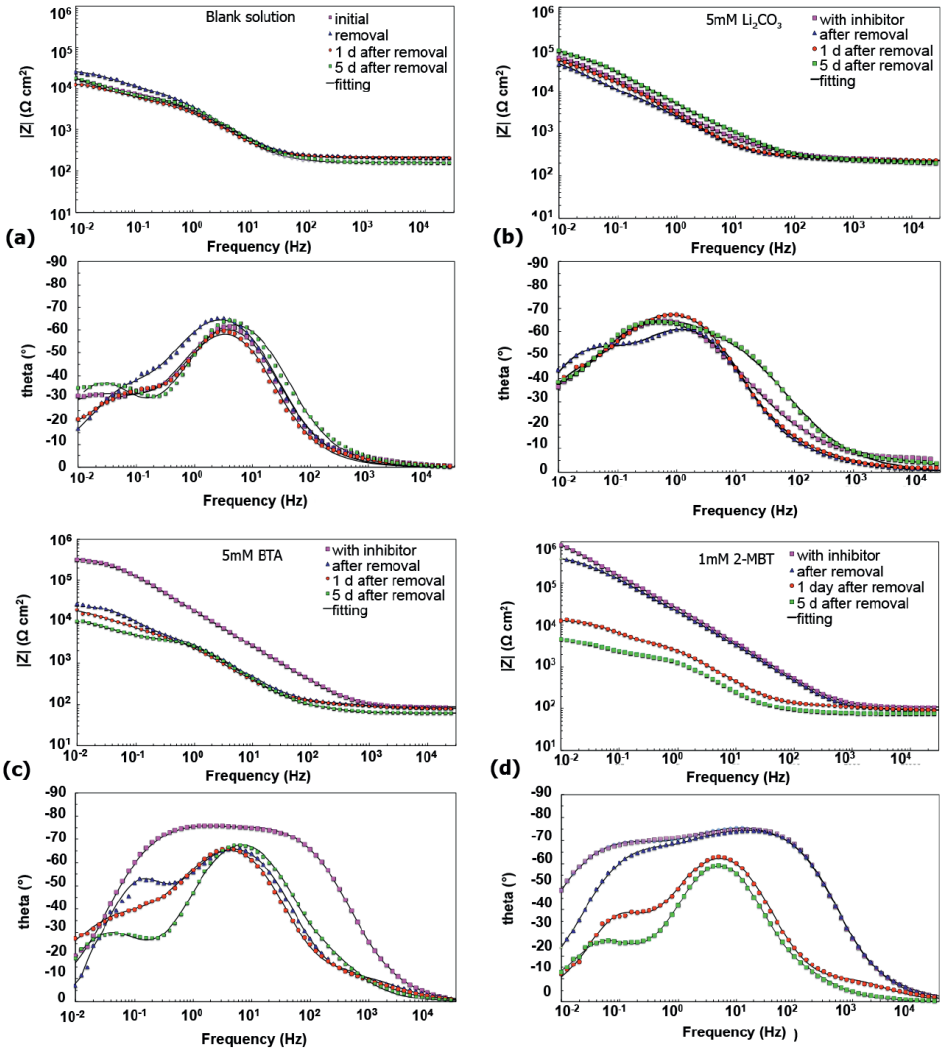

Figure 4.7 Electrochemical impedance spectra of the corrosion inhibitors measured before and after their replacement by a blank solution (0.05 M NaCl) on AA2024-T3. Impedance modulus and phase angle plot (a) blank solution; (b) Li_2CO_3; (c) BTA, and (d) 2-MBT.

The equivalent capacitance (C) values used in these graphs were calculated from CPE values (n and Q) and the resistance (R) of the respective time-constant resulting from the fitting process using the equation derived by Hirschorn et al. (Eq. 1). [50]

$$C = R^{\frac{(1-n)}{n}} \cdot Q^{\frac{1}{n}} \qquad [1]$$

Fig. 4.8a shows the evolution of the oxide resistance (R_{oxide}) as a function of exposure time. The graph shows that R_{oxide} was relatively high for the samples exposed to the 2-MBT and

BTA solutions with respective R_{oxide} values of 110 and 72 kΩ·cm^2. However, replacement of the inhibitor solution by the blank solution resulted in a decrease of R_{oxide} over time to values, around 5 kΩ·cm^2, comparable to the sample that was exposed to the blank solution. In contrast to the organic corrosion inhibitors, the samples that were exposed to the Li_2CO_3 solution exhibited an increase of the oxide resistance up to 90 kΩ·cm^2 after the removal of the corrosion inhibitor. The capacitance values of the oxide layer (C_{oxide}) are shown in Fig. 4.8b. The C_{oxide} of the alloy was very low in the presence of the BTA and 2-MBT solutions, but C_{oxide} increased directly after replacing the inhibitor solutions by the blank solution. The C_{oxide} of the sample exposed to the Li_2CO_3 solution was the highest but decreased over time. These observations are in line with the decreasing R_{oxide} of the samples that were exposed to BTA and 2-MBT and the increasing R_{oxide} values for the sample exposed to the Li_2CO_3 solution. The rate of the corrosion process at the aluminium surface can be characterized by the polarization resistance (R_{pol}).[13] Fig. 4.8b shows the development of R_{pol} before and after the removal of the inhibitor solutions. R_{pol} was relatively high for the samples when 2-MBT and BTA were present in the solution, respectively 1.1 and 0.7 MΩ·cm^2. However, the values for R_{pol} decreased significantly to 350 and 24 kΩ·cm^2 directly after the inhibitor solutions were replaced by the blank solution. The rapid decrease of R_{pol} of the sample exposed to the BTA solution confirms the stronger intrinsic inhibitive nature of 2-MBT.[13] R_{pol} of these samples decreased further upon extended exposure to values 15 Ω·cm^2, which is comparable to the sample, exposed to the blank solution after 24 and 5 d.

The inset of Fig. 4.8c shows the development of R_{pol} of the samples that were exposed to the Li_2CO_3 solution. R_{pol} was not as high (95 kΩ·cm^2) in the presence of the Li_2CO_3 solution compared to the organic corrosion inhibitors, but after replacement by the blank solution, R_{pol} increased over time to 144 kΩ·cm^2, indicating improving corrosion resistance with exposure time. The double layer capacitance (C_{dl}) displayed in Fig. 4.8d is related to the active corrosion area and hence can be linked with the corrosion activity of the samples.[13] After 24 h of exposure to the inhibitor solutions, all samples showed low double layer capacitance (Cdl) values combined with high Rpol values confirming the corrosion protective properties of these inhibitor solutions. After replacement of the inhibitor solutions by the blank solution, Cdl increased slightly for all samples. Whereas after extended exposure to the blank solution, the Cdl of the sample initially exposed to the Li_2CO_3 solution remained stable around 200 µF·cm-2, the Cdl of samples initially exposed to the 2-MBT and BTA solutions increased to respectively 1700 and 800 µF·cm-2. The increase of capacitance values (Coxide and Cdl) combined with the simultaneous decrease of the resistance values (Roxide and Rpol) are indicative for the degradation of the corrosion inhibitive properties for the samples initially exposed to the 2-MBT and BTA solutions. In contrast to this, the sample that was exposed to the Li_2CO_3 solution retained its corrosion protective properties after the removal of the Li_2CO_3 solution and even showed a further evolution of the oxide layer leading to higher Roxide and Rpol values and lower Coxide and Cdl values, thus improved corrosion protection. This increase implies that the protective layer densified after the replacement of the Li_2CO_3 by the blank solution. These results

indicate that the corrosion inhibition mechanism of 2-MBT and BTA could be reversible processes.

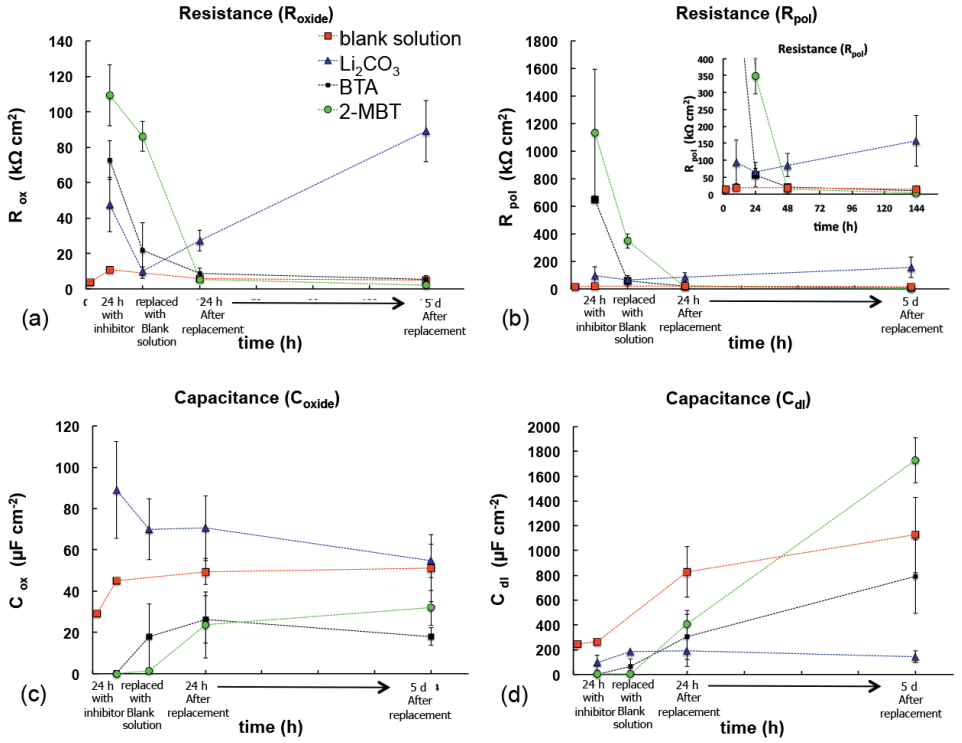

Figure 4.8 Evolution of (a) the oxide resistance (Roxide), (b) polarization resistance(Rpol), (c) oxide capacitance (Coxide), and (d) double layer capacitance (Cdl) of aluminium alloys before and after removal of the corrosion inhibitor in 0.05 M NaCl solution. The inset of (b) shows a zoomed version of the graph.

Surface roughness

AA2024-T3 is susceptible to local corrosion phenomena such as pitting corrosion.[4] This results in increased surface roughness values when the surface of the alloy is corroding. The corrosion can be observed visually, but white light interferometer (WLI) profilometry measurements can provide a quantitative link with the degree of corrosion.[51] Fig. 4.9 shows the visual appearance of polished AA2024-T3 surfaces and the respective WLI surface maps before and after exposure to a 0.05 M NaCl solution with and without corrosion inhibitor. The optical image and WLI surface map of a pristine polished surface of AA2024-T3 before exposure are shown in Fig. 4.9a. However, the effects of corrosion, severe pitting corrosion, can be observed when the sample was exposed to the blank solution for 14 d (Fig. 4.9b). This was confirmed with the WLI surface map after removal of the corrosion products. The WLI surface map shows the variation in surface height in

reference to the mean plane over the area of the sample. The mean plane is represented in green, lower areas are represented in blue shades and higher areas are displayed in red shades. The black areas are areas without information due to too deep pits or insufficient light reflection. Fig. 4.9c shows the performance when the AA2024-T3 panels were exposed for 14 d to the inhibitor solutions.

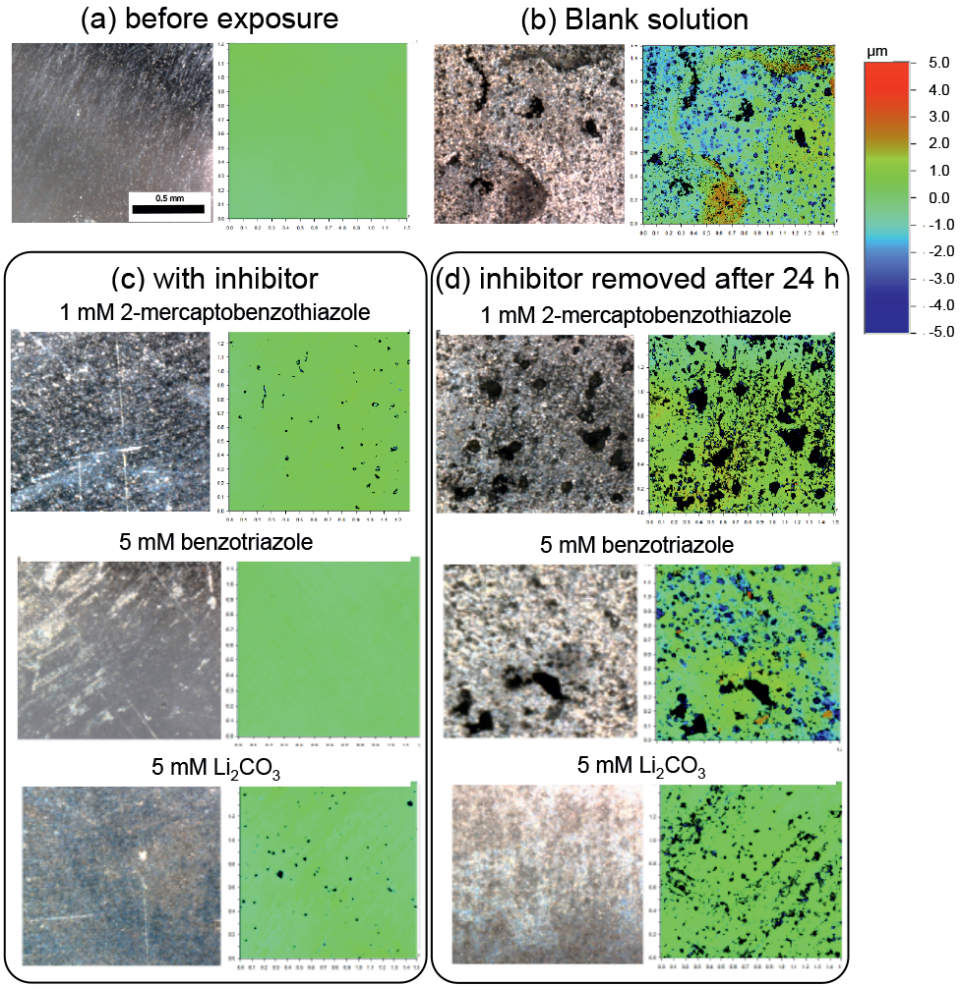

Figure 4.9 Optical images and White light interferometer surface roughness maps of polished AA2024-T3 panels before and after exposure to 0.05M NaCl solution, (a) before exposure; after (b) 14 d exposure without inhibitor; (c) 14 d exposure with corrosion inhibitor; (d) 14 d exposure but inhibitor removed after 24 h.

The optical images and WLI maps show that the aluminium surface was almost not affected after the exposure. Fig. 4.9d shows the samples that were exposed to the blank solution after an initial exposure to the inhibitor solution. In contrast to the samples with inhibitor

solution, both samples initially exposed to the BTA and 2-MBT solutions showed the effects of extensive pitting corrosion. On the other hand, the sample that was exposed to the Li_2CO_3 solution showed optically no signs of pitting corrosion and the WLI map showed only limited attack. Fig. 4.10 shows the quantitative surface roughness (S_a) results derived from the WLI measurements of the samples discussed above. The unexposed polished sample has an initial surface roughness around 80 nm, which increased due to corrosion to 670 nm after the 14 d exposure to the blank solution.

This roughness excluded the deep pits (black areas) that could not be measured. More important, Fig. 4.10 shows the large increase of surface roughness of the samples after replacing the 2-MBT and BTA solutions by the blank solution.

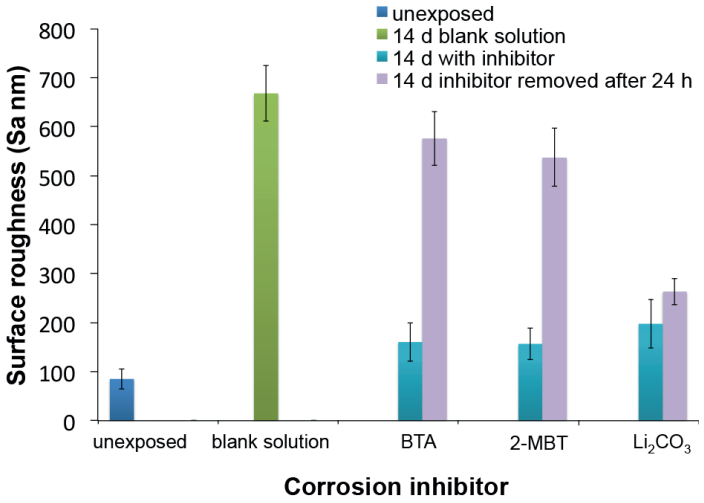

Figure 4.10 *Surface roughness (Sa) of the samples displayed in Fig. 4.9 derived from the white light interferometer surface maps*

The surface roughness increased to values from 155 nm with 2-MBT present in the solution to 540 nm after replacement of the 2-MBT solution and 160 nm with BTA present in the solution to 570 nm after replacement of the BTA solution by the blank solution.

The difference of the Li_2CO_3 exposed samples is significantly smaller, 200 nm for the sample exposed with inhibitor compared to 260 nm for the sample where Li_2CO_3 was replaced by the blank solution.

These optical observations and surface roughness measurements are in line with the EIS observations and confirm the loss of protective properties of the AA2024-T samples when the BTA and 2-MBT solutions are replaced by a blank solution resulting in severe pitting corrosion and increase of surface roughness. In contrast to this, the sample exposed to the Li_2CO_3 inhibitor solution remained protected.

Inhibitor efficiency

The inhibitor efficiency (IE) of the inhibitors on AA2024-T3 was determined with and without replacement of the inhibitor solutions by a blank solution. Fig. 4.11 shows the IE of the corrosion inhibitors on AA2024-T3.

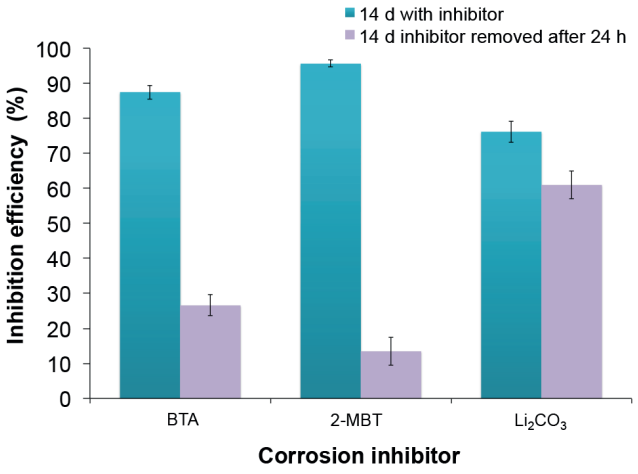

Figure 4.11 *Inhibitor efficiency of the corrosion inhibitors on AA2024-T3 after 14 d exposure to the solution with corrosion inhibitor and 14d exposure to a blank solution after removal of the corrosion inhibitor.*

Again, the excellent corrosion inhibitive nature of the BTA and 2-MBT inhibitor solutions on AA2024-T3 was demonstrated with an IE of 87% and 95% for BTA and 2-MBT, respectively. However, the IE decreased to respectively 26% and 14% when the inhibitor solution was replaced by a blank solution after 24 h. The IE of the sample in the presence of the Li_2CO_3 solution was 76% and 61% after replacement of the Li_2CO_3 solution by the blank solution. It has to be considered that the corrosion protective mechanism of Li_2CO_3 on aluminium involves dissolution of aluminium from the substrate due to anodic dissolution to generate an aluminium oxide/hydroxide layer.[33] This layer will be removed in the acidic cleaning procedure prior to the IE assessment. This results in relative lower IE values compared to the organic inhibitors. However, the results of the study still clearly demonstrate that the BTA and 2-MBT are only effective as corrosion inhibitors on AA2024-T3 when present in the solution. Moreover, it can be concluded that the IE of Li_2CO_3 is not as high as the organic inhibitors when the inhibitors are present in the solution but Li_2CO_3 out performs the organic corrosion inhibitors when the inhibitors are removed after 24 h and the exposure to corrosive conditions are continued.

4.3.4 Mechanistic difference of the inhibitors

The results of this work demonstrate that there is a significant difference in the corrosion inhibition mechanism of organic corrosion inhibitors such as BTA and 2-MBT compared to Li_2CO_3. The investigations demonstrate that the organic inhibitors were active in an electrochemical cell but showed very little active corrosion protection when incorporated as leachable corrosion inhibitor into a coating. The difference of the corrosion inhibitive mechanism of BTA and 2-MBT compared to Li_2CO_3 is schematically shown in Fig. 4.12. Organic inhibitors such as 2-MBT or BTA are very well known for their effective inhibition of AA2024-T3 aluminium alloys due to their nature to complex with the copper-rich intermetallic particles and predominantly reduce the cathodic oxygen reduction reaction. However measurements revealed that these inhibitors provide some anodic inhibition as well. This anodic inhibition can be attributed to the adsorption of the organic inhibitors to the aluminium surface.[15] Although the electrochemical and inhibitor efficiency experiments demonstrated that when the BTA and 2-MBT solutions were replaced by a blank solution the exposed AA2024-T3 showed rather low corrosion resistance. This suggests that the adsorption of these organic inhibitors on the copper-rich intermetallic particles and aluminium alloy are not permanent and that the physically adsorbed inhibitor molecules desorb when the inhibitor concentration diminishes. This would suggest that BTA and 2-MBT are intrinsically reversible corrosion inhibitors (Fig. 4.12a).

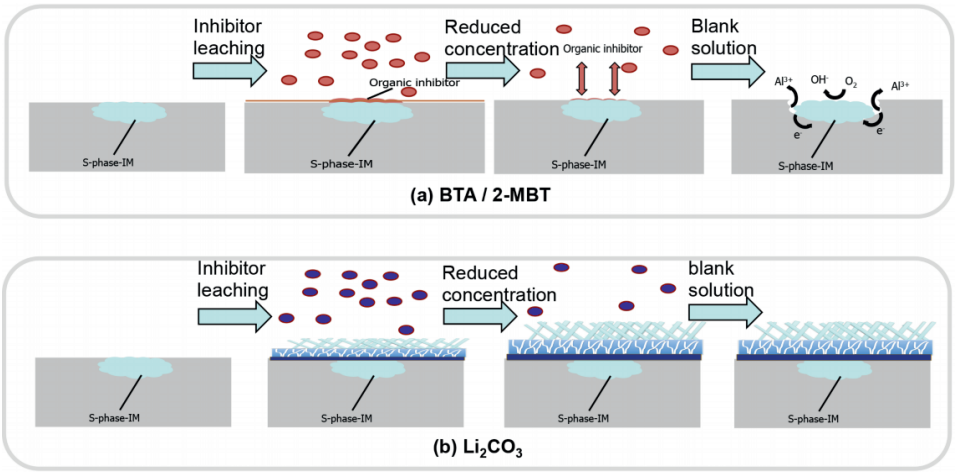

Figure 4.12 *Schematic illustration of the corrosion inhibiting mechanism of (a) organic corrosion inhibitors and (b)* Li_2CO_3 *as leachable inhibitor.*

Over the years, BTA and 2-MBT have been used in a variety of studies for (active) corrosion protection However, none of these approaches demonstrated to perform equally or better as chromates nor have been authorized as a suitable alternative in the aerospace industry.[2, 52]

Therefore, it can be postulated that these effective organic inhibitors do not meet the criteria for active corrosion protection from coatings, being: soluble and provide fast, effective, and irreversible inhibition alike chromates.[3] These results imply that organic corrosion inhibitors such as BTA and 2-MBT might not be suitable for all applications of active protective coatings and may only be used in confined spaces where the concentration of corrosion inhibitor can be maintained at a sufficient high level.

Li_2CO_3 is known for its property to passivate aluminium by the formation of a protective layer on the aluminium substrate.[53, 54] The corrosion protective properties of the samples exposed to the Li_2CO_3 solution may be not as high as the organic inhibitors but the accelerated exposure tests, electrochemical evaluations and inhibitor efficiency experiments clearly demonstrated the corrosion inhibiting effect of Li_2CO_3 on AA2024-T3. More important, the sample maintained its protective properties after the concentration of Li_2CO_3 decreased and demonstrating an irreversible nature of the protective layer that is formed on the aluminium alloy (Fig. 4.10b). Considering the criteria for corrosion inhibitors to be used in active protective coatings: soluble in water combined with fast, effective and irreversible inhibition, it can be concluded that Li_2CO_3 demonstrated all these properties. As such, this investigation demonstrates that Li_2CO_3 exhibits a unique mode of active corrosion protection that has not been demonstrated by any other environmentally friendly leaching corrosion inhibitor for the protection of high strength aluminium alloys.

4. Conclusions

This work compared the active protective properties (solubility, inhibition and reversibility) of Li_2CO_3 and the organic inhibitors, BTA and 2-MBT on AA2024-T3. In an electrochemical cell, all corrosion inhibitors demonstrated effective corrosion inhibition on AA2024-T3: 2-MBT > BTA > Li_2CO_3.

When incorporated in an organic coating, all inhibitors were able to leach from the coating. However, only the Li_2CO_3 loaded coating demonstrated effective corrosion protection in the artificial defect area exposed to the NSS accelerated corrosion test. Electrochemical analysis and inhibitor efficiency studies demonstrated that both organic corrosion inhibitors BTA and 2-MBT exhibit a reversible nature resulting in severe corrosion of the aluminium alloy when the inhibitor concentration diminishes.

Li_2CO_3 demonstrated that it is able to provide all characteristics of what is expected of corrosion inhibitors for active protective coatings: leaching, fast, effective and irreversible corrosion inhibition. The results of this study provide more insight into the unique properties of the active corrosion protective nature of the Li-leaching coating technology for the protection of aluminium alloys.

References

1. A. K. Chattopadhyay and M. K. R. Zentner, *Aerospace and Aircraft Coatings*, Federation of Societies for Coatings Technology, 1990.
2. J. Sinko, Challenges of chromate inhibitor pigments replacement in organic coatings, *Progress in Organic Coatings*, 2001, 42, 267-282.
3. M. W. Kendig and R. G. Buchheit, Corrosion inhibition of aluminum and aluminum alloys by soluble chromates, chromate coatings, and chromate-free coatings, *Corrosion*, 2003, 59, 379-400.
4. R. G. Buchheit, R. P. Grant, P. F. Hlava, B. McKenzie and G. L. Zender, Local dissolution phenomena associated with S phase (Al2CuMg) particles in aluminum alloy 2024-T3, *Journal of the Electrochemical Society*, 1997, 144, 2621-2628.
5. A. E. Hughes, Birbilis, N., Mol, J.M.C., Santiago J. Garcia, S.J., Zhou, X., Thompson, G.E. , in *Recent Trends in Processing and Degradation of Aluminium Alloys*, ed. P. Z. Ahmad, *In Tech*, 2011.
6. A. Boag, R. J. Taylor, T. H. Muster, N. Goodman, D. McCulloch, C. Ryan, B. Rout, D. Jamieson and A. E. Hughes, Stable pit formation on AA2024-T3 in a NaCl environment, *Corrosion Science*, 2010, 52, 90-103.
7. P. Leblanc and G. S. Frankel, A Study of Corrosion and Pitting Initiation of AA2024-T3 Using Atomic Force Microscopy, *Journal of The Electrochemical Society*, 2002, 149, B239-B247.
8. M. Kendig and S. Jeanjaquet Cr(VI) and Ce(III) Inhibition of Oxygen Reduction on Copper, *Journal of The Electrochemical Society*, 2002, 149, B47-B51.
9. K. Xhanari and M. Finšgar, Organic corrosion inhibitors for aluminum and its alloys in chloride and alkaline solutions: A review, *Arabian Journal of Chemistry*, 2016.
10. M. Metikos-Hukovic, R. Babic and A. Marinovic, Spectrochemical characterization of benzotriazole on copper, *Journal of the Electrochemical Society*, 1998, 145, 4045-4051.
11. M. Ohsawa and W. Suetaka, Spectro-electrochemical studies of the corrosion inhibition of copper by mercaptobenzothiazole, *Corrosion Science*, 1979, 19, 709-722.
12. G. Williams, A. J. Coleman and H. N. McMurray, Inhibition of Aluminium Alloy AA2024-T3 pitting corrosion by copper complexing compounds, *Electrochimica Acta*, 2010, 55, 5947-5958.
13. M. L. Zheludkevich, K. A. Yasakau, S. K. Poznyak and M. G. S. Ferreira, Triazole and thiazole derivatives as corrosion inhibitors for AA2024 aluminium alloy, *Corrosion Science*, 2005, 47, 3368-3383.
14. M. M. Antonijevic and M. B. Petrovic, Copper corrosion inhibitors. A review, *International Journal of Electrochemical Science*, 2008, 3, 1-28.
15. I. Recloux, F. Andreatta, M.-E. Druart, L. B. Coelho, C. Cepek, D. Cossement, L. Fedrizzi and M.-G. Olivier, Stability of benzotriazole-based films against AA2024 aluminium alloy corrosion process in neutral chloride electrolyte, *Journal of Alloys and Compounds*, 2018, 735, 2512-2522.
16. T. G. Harvey, S. G. Hardin, A. E. Hughes, T. H. Muster, P. A. White, T. A. Markley, P. A. Corrigan, J. Mardel, S. J. Garcia, J. M. C. Mol and A. M. Glenn, The effect of inhibitor structure on the corrosion of AA2024 and AA7075, *Corrosion Science*, 2011, 53, 2184-2190.
17. A. C. Balaskas, M. Curioni and G. E. Thompson, Effectiveness of 2-mercaptobenzothiazole, 8-hydroxyquinoline and benzotriazole as corrosion inhibitors on AA 2024-T3 assessed by electrochemical methods, *Surface and Interface Analysis*, 2015, 47, 1029-1039.
18. L. B. Coelho, D. Cossement and M. G. Olivier, Benzotriazole and cerium chloride as corrosion inhibitors for AA2024-T3: An EIS investigation supported by SVET and ToF-SIMS analysis, *Corrosion Science*, 2018, 130, 177-189.
19. S. Marcelin and N. Pebere, Synergistic effect between 8-hydroxyquinoline and benzotriazole for the corrosion protection of 2024 aluminium alloy: A local electrochemical impedance approach, *Corrosion Science*, 2015, 101, 66-74.
20. S. V. Lamaka, M. L. Zheludkevich, K. A. Yasakau, M. F. Montemor, P. Cecilio and M. G. S. Ferreira, TiOx self-assembled networks prepared by templating approach as nanostructured reservoirs for self-healing anticorrosion pre-treatments, *Electrochemistry Communications*, 2006, 8, 421-428.
21. A. Shanaghi and M. Kadkhodaie, Investigation of high concentration of benzotriazole on corrosion behaviour of titania-benzotriazole hybrid nanostructured coating applied on Al 7075 by the sol-gel method, *Corrosion Engineering Science and Technology*, 2017, 52, 332-342.
22. I. Recloux, Y. Gonzalez-Garcia, M. E. Druart, F. Khelifa, P. Dubois, J. M. C. Mol and M. G. Olivier, Active and passive protection of AA2024-T3 by a hybrid inhibitor doped mesoporous sol–gel and top coating system, *Surface and Coatings Technology*, 2016, 303, 352-361.

23. D. G. Shchukin, M. Zheludkevich, K. Yasakau, S. Lamaka, M. G. S. Ferreira and H. Mohwald, Layer-by-layer assembled nanocontainers for self-healing corrosion protection, *Advanced Materials*, 2006, 18, 1672-+.
24. M. Parsa, S. M. A. Hosseini, Z. Hassani and E. Jamalizadeh, Corrosion protective properties of coatings doped with inhibitors, *Anti-Corrosion Methods and Materials*, 2014, 61, 416-422.
25. M. L. Zheludkevich, D. G. Shchukin, K. A. Yasakau, H. Mohwald and M. G. S. Ferreira, Anticorrosion coatings with self-healing effect based on nanocontainers impregnated with corrosion inhibitor, *Chemistry of Materials*, 2007, 19, 402-411.
26. J. Carneiro, A. F. Caetano, A. Kuznetsova, F. Maia, A. N. Salak, J. Tedim, N. Scharnagl, M. L. Zheludkevich and M. G. S. Ferreira, Polyelectrolyte-modified layered double hydroxide nanocontainers as vehicles for combined inhibitors, *RSC Advances*, 2015, 5, 39916-39929.
27. F. Maia, J. Tedim, A. D. Lisenkov, A. N. Salak, M. L. Zheludkevich and M. G. S. Ferreira, Silica nanocontainers for active corrosion protection, *Nanoscale*, 2012, 4, 1287-1298.
28. A. C. Balaskas, T. Hashimoto, M. Curioni and G. E. Thompson, Two-shell structured PMAA@CeO2 nanocontainers loaded with 2-mercaptobenzothiazole for corrosion protection of damaged epoxy coated AA 2024-T3, *Nanoscale*, 2017, 9, 5499-5508.
29. F. Maia, K. A. Yasakau, J. Carneiro, S. Kallip, J. Tedim, T. Henriques, A. Cabral, J. Venancio, M. L. Zheludkevich and M. G. S. Ferreira, Corrosion protection of AA2024 by sol-gel coatings modified with MBT-loaded polyurea microcapsules, *Chemical Engineering Journal*, 2016, 283, 1108-1117.
30. P. Visser, Y. Liu, X. Zhou, T. Hashimoto, G. E. Thompson, S. B. Lyon, L. G. J. van der Ven, A. J. M. C. Mol and H. A. Terryn, The corrosion protection of AA2024-T3 aluminium alloy by leaching of lithium-containing salts from organic coatings, *Faraday Discussions*, 2015, 180, 511-526.
31. P. Visser, Y. Liu, H. Terryn and J. M. C. Mol, Lithium salts as leachable corrosion inhibitors and potential replacement for hexavalent chromium in organic coatings for the protection of aluminum alloys, *Journal of Coatings Technology and Research*, 2016, 13, 557-566.
32. P. Visser, A. Lutz, J. M. C. Mol and H. Terryn, Study of the formation of a protective layer in a defect from lithium-leaching organic coatings, *Progress in Organic Coatings*, 2016, 99, 80-90.
33. P. Visser, Y. Gonzalez-Garcia, J. M. C. Mol and H. Terryn, Mechanism of Passive Layer Formation on AA2024-T3 from Alkaline Lithium Carbonate Solutions in the Presence of Sodium Chloride, *Journal of The Electrochemical Society*, 2018, 165, C60-C70.
34. P. Visser, M. Meeusen, Y. Gonzalez-Garcia, H. Terryn and J. M. C. Mol, Electrochemical Evaluation of Corrosion Inhibiting Layers Formed in a Defect from Lithium-Leaching Organic Coatings, *Journal of The Electrochemical Society*, 2017, 164, C396-C406.
35. in *The MAK-Collection for Occupational Health and Safety*, Wiley-VCH Verlag GmbH & Co. KGaA, 2002, DOI: 10.1002/3527600418.mb14930kskd0029.
36. in *The MAK-Collection for Occupational Health and Safety*, Wiley-VCH Verlag GmbH & Co. KGaA, 2002, DOI: 10.1002/3527600418.mb9514kske0002.
37. D. Wright and M. C. McMills, in *Encyclopedia of Reagents for Organic Synthesis*, John Wiley & Sons, Ltd, 2001, DOI: 10.1002/047084289X.rl074.
38. U. Tiringer, J. Kovač and I. Milošev, Effects of mechanical and chemical pre-treatments on the morphology and composition of surfaces of aluminium alloys 7075-T6 and 2024-T3, *Corrosion Science*, 2017, 119, 46-59.
39. L. Deck and P. de Groot, High-speed noncontact profiler based on scanning white-light interferometry, *Appl. Opt.*, 1994, 33, 7334-7338.
40. U. C. Nwaogu, N. S. Tiedje and H. N. Hansen, A non-contact 3D method to characterize the surface roughness of castings, *Journal of Materials Processing Technology*, 2013, 213, 59-68.
41. M. Behpour, S. M. Ghoreishi, N. Mohammadi, N. Soltani and M. Salavati-Niasari, Investigation of some Schiff base compounds containing disulfide bond as HCl corrosion inhibitors for mild steel, *Corrosion Science*, 2010, 52, 4046-4057.
42. M. Stern and A. L. Geary, Electrochemical Polarization: I . A Theoretical Analysis of the Shape of Polarization Curves, *Journal of The Electrochemical Society*, 1957, 104, 56-63.
43. T. A. Zawodzinski, JES Classics, *Electrochemical Society Interface*, 2009, 59.
44. C.H. Hsu and F. Mansfeld, Concerning the conversion of the Constant Phase Element Parameter Yo into a Capacitance *Corrosion*, 2001, 57, 747.
45. T. Prosek and D. Thierry, A model for the release of chromate from organic coatings, *Progress in Organic Coatings*, 2004, 49, 209-217.

46. F. H. Scholes, S. A. Furman, A. E. Hughes, T. Nikpour, N. Wright, P. R. Curtis, C. M. Macrae, S. Intem and A. J. Hill, Chromate leaching from inhibited primers. Part I. Characterisation of leaching, *Progress in Organic Coatings*, 2006, 56, 23-32.
47. S. G. R. Emad, X. Zhou, S. B. Lyon, G. E. Thompson, Y. Liu, G. Smyth, D. Graham, D. Francis and S. R. Gibbon, Influence of volume concentration of active inhibitor on microstructure and leaching behaviour of a model primer, *Progress in Organic Coatings*, 2017, 102, 71-81.
48. A. E. Hughes, A. Trinchi, F. F. Chen, Y. S. Yang, I. S. Cole, S. Sellaiyan, J. Carr, P. D. Lee, G. E. Thompson and T. Q. Xiao, The application of multiscale quasi 4D CT to the study of SrCrO4 distributions and the development of porous networks in epoxy-based primer coatings, *Progress in Organic Coatings*, 2014, 77, 1946-1956.
49. R. Oltra and F. Peltier, Influence of mass transport on the competition between corrosion and passivation by inhibitor release after coating breakdown, *Progress in Organic Coatings*, 2016, 92, 44-53.
50. B. Hirschorn, M. E. Orazem, B. Tribollet, V. Vivier, I. Frateur and M. Musiani, Determination of effective capacitance and film thickness from constant-phase-element parameters, *Electrochimica Acta*, 2010, 55, 6218-6227.
51. P. Visser, Novel totally chrome free corrosion inhibiting coating technology for protection of aluminium alloys, *Transactions of the Institute of Metal Finishing*, 2011, 89, 291-294.
52. R. L. Twite and G. P. Bierwagen, Review of alternatives to chromate for corrosion protection of aluminum aerospace alloys, *Progress in Organic Coatings*, 1998, 33, 91-100.
53. J. Gui and T. M. Devine, Influence of lithium on the corrosion of aluminum, *Scripta Metallurgica*, 1987, 21, 853-857.
54. R. G. Buchheit, Bode, M.D., Stoner, G.E., Corrosion-Resistant, Chromate free Talc Coatings for Aluminum, *Corrosion*, 1994, 50, 205-214.

Chapter 5

Study of the Formation of a Protective Layer in a Defect from Lithium-Leaching Organic Coatings

The previous chapters discussed the corrosion inhibiting mechanism and performance of the Li-leaching coating technology. This chapter goes more in depth and provides more insight in the formation process of a protective layer in a coating defect from Li-leaching model coatings. It discusses lithium-leaching from the coating and conditions in the defect area as a result of the leaching process combined with the formation of the protective layer revealing the process of coverage and growth of the protective layer in the damaged area.

This chapter is published as a scientific paper:
P. Visser, A. Lutz, J.M.C. Mol, H. Terryn, Study of the formation of a protective layer in a defect from lithium-leaching organic coatings, Progress in Organic Coatings, 99 (2016) 80-90.

Abstract

Lithium salts were investigated as leachable corrosion inhibitor and potential replacement for hexavalent chromium in organic coatings. Coatings loaded with lithium carbonate or lithium oxalate demonstrated active corrosion inhibition by the formation of a protective layer in a damaged area. The present paper provides more insight into the formation and composition of the protective layer in a damaged area generated from the Li-salt loaded coatings when exposed to neutral salt spray testing conditions (ASTM B-117). Lithium-ion leaching from the coating matrix was demonstrated with atomic absorption spectroscopy and the pH conditions in the damaged area were determined with a scanning ion-selective electrode technique. Additionally, the formation of the protective layer was studied with microscopic and surface analytical techniques. Scanning electron micrographs and Auger electron spectroscopy depth profiles revealed the process of coverage and growth of the protective layer in the damaged area. Furthermore, X-ray photoelectron spectroscopy analysis indicated that the protective layer likely consists of a hydrated oxide in the form of a (pseudo) boehmite with lithium distributed in its matrix.

5.1 Introduction

Aluminium alloys such as AA2024 or AA7075 are high strength aluminium alloys that are extensively used in the aerospace industry. However, these alloys are susceptible to localized corrosion such as pitting corrosion and inter-granular corrosion. Especially, AA2024-T3 aluminium alloys are susceptible for pitting corrosion due to the presence of copper-rich intermetallic particles in the matrix.[1-5] The different electrochemical nature of the particles and matrix results in the formation of micro-galvanic cells within the substrate and may initiate pitting corrosion.[1-3, 6]

Corrosion control is an important aspect in the aerospace industry.[7] Therefore, active protective coatings are an essential part of the corrosion protection scheme within the aircraft design. The typical corrosion protective scheme for the protection of the aluminium alloy substrate comprises a chemical conversion coating or anodic film, corrosion inhibiting primer and in certain areas a topcoat.[8, 9] Such a scheme provides two modes of protection: barrier protection (passive) when the system is intact and inhibitor based passivation (active protection) when the coating is damaged.[10] This active protection relies on a leaching mechanism. This is a complex process where in case of a damage, the inhibitor is released from the coating and migrates to the corroding sites and passivates the substrate at the coating defect area.[11-13]

Traditionally, strontium chromate is used as leaching corrosion inhibiting pigment in coatings to protect the aluminium structures of aircraft and its exceptional corrosion protection was demonstrated in many research programs.[14, 15] Despite their unique properties and performance, these hexavalent chromium-containing inhibitors need to be replaced. They are known carcinogenic compounds and their use is expected to be restricted due to new regulations.[16, 17] Much research is conducted to find alternative inhibitors that perform equal or better compared to hexavalent chromium containing inhibitors.[18-24]

Lithium salts have become of interest as an alternative corrosion inhibitor to protect aluminium alloys after reports of passivity of aluminium in alkaline Li-salt solutions.[25, 26] Buchheit *et al.* studied Li-carbonate solutions as hexavalent chromium free chemical conversion coatings, generating a lithium aluminium carbonate hydroxide hydrate ($Li_2[Al_2(OH)_6]_2{\cdot}CO_3{\cdot}nH_2O$) coatings on aluminium alloys under alkaline conditions.[27] The composition, structure and performance were studied in relation to processing and bath chemistries.[28] Their work demonstrated that the generated hydrotalcite coatings exhibit similar protective properties as traditional conversion coatings. Rangel *et al.* used cyclic voltammetry and electrochemical impedance spectroscopy to study the protective properties of these lithium-based conversion coatings generated under these alkaline conditions.[29] From this work it was suggested that the formed layer comprised a dual structure; a porous layer and pore filler. In addition, cyclic voltammetry experiments suggested the initial formation of an aluminium hydroxide layer before the lithium incorporation.

Building on this conversion coating work, Li-salts were proposed as leaching inhibitor for coatings to protect aluminium alloys.[30] Organic coatings loaded with Li-salts provided fast and effective corrosion protection in an artificial damage when exposed to neutral salt spray conditions (ASTM B-117).[31] It was found that Li-ions were able to leach from the organic coating and generate a layer with corrosion protective properties in the scribed area. This layer comprised barrier, porous and columnar morphologies and consisted mainly of aluminium, oxygen, and lithium. A multi-step mechanism has been proposed for the formation of such a layer involving a competitive growth and dissolution process at the aluminium alloy surface.[31] This previous work described the first observations and characterization of these protective layers generated from a coating loaded with Li-salts as leaching inhibitor.

The objective of this work is to study the formation of these protective layers in a coating defect on AA2024-T3 in more detail and obtain a deeper understanding of the Li-ion leaching kinetics, the conditions in the defect area and the lateral and in-thickness formation process of the protective layer. Therefore, polyurethane model coatings were loaded with lithium-salts as leaching inhibitor. Leaching of lithium-ions from the coatings was measured with atomic absorption spectroscopy (AAS). The coated AA2024-T3 substrates were scribed. The Scanning Ion-selective Electrode Technique (SIET) was used to measure the pH in the scribed area when the defect is exposed to a corrosive environment. The samples were exposed to neutral salt spray (NSS) conditions and the formation and development of the layer was analysed with field emission scanning electron microscopy (FESEM) and surface analytical techniques. Auger spectroscopy depth profiling (AES) and X-ray photoelectron spectroscopy (XPS) were used to study the thickness and chemical composition of the protective layer as a function of formation time. Based on this information, the formation mechanism of the protective layer has been elucidated in further detail.

5.2 Experimental

5.2.1 Materials and sample preparation

Organic model coatings (Table 5.1) based on polyurethane binder chemistry containing well defined quantities of Li-carbonate and oxalate have been prepared as previously described [31]. The coatings were applied on Tartaric–Sulphuric Acid (TSA) anodized AA2024-T3 unclad sheets of 0.8 mm thickness. The AA2024-T3 substrate was purchased from Alcoa (2024-T3QQ-A250/5) and the TSA pretreatment (thickness anodic film: 3-3.5 µm) was performed according to aerospace requirements (AIPI 02-01-003) at Premium AEROTEC, Bremen Germany. The coatings were applied with a HVLP spray gun and cured at 80º C for 16 h, after 1-h flash-off at 23º C. The measured dry film thickness of the coatings was typically about 20–25 µm. A mechanical milling device was used to artificially damage the coating with a U-shaped scribe, before exposing the samples to a neutral salt spray (NSS) test

(ASTM- B117). The panels (7cm x 7cm) were scribed from corner to corner, leaving a 1 mm wide scribe that penetrated 100–150 µm deep into the metal. The samples were covered with tape on the backside and exposed to the neutral salt spray (ASTM-B117) test for varying periods from 30 minutes up to 168 h. After exposure, the process was quenched by a 2-minute rinse with flowing demineralized water to remove any residual chlorides and the panels were air-dried. Separate panels were used for each exposure period.

Table 5.1: Composition of lithium loaded model coatings

	Supplier	Lithium carbonate	Lithium oxalate
Component A			
N-Butylacetate	Sigma Aldrich	75.0 g	75.0 g
Desmophen 650MPA	Bayer Materials science	47.7 g	47.7 g
Lithium carbonate	Sigma Aldrich	23.6 g	
Lithium oxalate	Sigma Aldrich		32.0 g
Magnesium oxide	Sigma Aldrich	16.4 g	16.4 g
Tioxide TR 92	Huntsman	5.9 g	5.9 g
Blanc Fixe N ($Ba(SO_4)$)	Sachtleben	15.4 g	15.4 g
Component B			
Tolonate HDB 75 MX	Vencorex	28.5 g	28.5 g
Dynasilan Glymo	Evonik	5.2 g	5.2 g

For XPS analysis and comparison purposes, reference samples with a pseudo-boehmite and lithium based conversion coating were prepared on AA2024-T3 bare aluminium alloy panels. Before the treatment, the aluminium panels were cleaned with acetone. The hydrated aluminium oxide (pseudo-boehmite) coating was prepared by treating the panel with deionized water at 95-100º C for 1 h according to the method of Gorman *et al.*[32] The lithium based layered double hydroxide (Li-LDH) conversion coating was prepared using the conversion coating process as described by Buchheit *et al.*, by immersing a AA2024-T3 panel in a 0.1 M Li-carbonate solution (pH=11.3) for 15 minutes.[27] Following the treatments the panels were rinsed with demi water for 5 minutes and dried at the air.

5.2.2 Lithium ion leaching measurements (AAS)

The release of lithium from the coating matrix was measured by immersion of unscribed coated panels (3.5 cm x 5 cm) in 90 ml demineralized water and at each measurement interval the solution was replaced with fresh demineralized water. The Li-containing solutions were acidified with 10 ml 20% nitric acid and lithium concentrations were measured with a Varian AA 640 atomic absorption spectrophotometer. A calibration curve from 0-5 µg/L was prepared from a 1000 µg/L lithium nitrate standard solution for Merck. The concentrations of released Li-ions in $\mu g/cm^2$ were normalized to a film thickness of 25 µm and accumulated. The leaching curves were performed in triplicate.

5.2.3 Scribe condition measurements (SIET)

The pH within the scribed area was measured using the Scanning Ion-selective Electrode Technique (SIET). The measurements were performed using equipment manufactured by Applicable ElectronicsTM and controlled by ASET software (Science WaresTM). The local concentration of hydrogen ions was measured by positioning the pH sensitive glass capillary microelectrode in the scribe 50±5 µm above the surface. The glass electrodes were pulled with a micropipette puller (Sutter Instruments Company) and silanized before use. The glass-capillary was filled with pH-ionophore cocktail 1B, a tridodecylamine–based membrane of Fluka was used. The membrane possesses a linear response in the range of pH 5.5-12.0 33. Next to the scribe a small rim was made with wax and the area was filled with 1-2 ml 0.05M NaCl electrolyte. An area of 1 mm by 2 mm was scanned within the scribed area, 5 minutes after filling (initial stage) and after 5 h of exposure.

5.2.4 Surface characterization of the protective layer

Scanning Electron Microscopy

The surface morphology of the protective layer was examined using a JEOL JSM-7100F field emission scanning electron microscope (FESEM) using the lower electron detector (LED) at 5 kV and a working distance of 10 mm.

Auger electron spectroscopy

Auger Electron Spectroscopy (AES) elemental depth profiles were recorded using a PHI 650(SAM) with a LaB_6 cathode and a Cylindrical Mirror Analyzer (CMA). The base pressure in the analysis chamber was $3 \cdot 10^{-10}$Torr. Measurements were performed using a primary electron beam (energy 5 keV and 1 µA emission current) with an incident angle on the sample surface of 30° to the normal. Ion sputtering was performed with a PHI 04-303 ion gun and 3 keV Ar ions (emission current of 20 mA and Ar pressure of 10 mPa). The surface was rastered over an area of 1 mm^2. The ion beam was used at intervals of 1 minute and impinged on the sample surface at 50° to the normal. The recorded spectra were analysed with the Multipak V9.5.0.8. software.

X-ray photoelectron spectroscopy

The surface chemistry of the samples was studied with a PHI 1600/3057 X-ray Photoelectron Spectroscopy (XPS) instrument using an incident X-ray radiation (Mg $K_{\alpha 1,2}$= 1253.6 eV). The vacuum in the analysis chamber was approximately $5 \cdot 10^{-9}$ Torr. All measurements were done at an angle of 45° with respect to the sample surface. High resolution scans were recorded of the Li1s, Mg1s, Cu2p, O1s, Al2p and C1s photo peaks using a 400 µm spot diameter, a pass-energy of 23.5 eV and 00.1 eV step size. No neutralizer has been applied. The spectra obtained on the passive layers were shifted to set the C-C/C-H components of the C1s peak at a binding energy of 284.8 eV to correct for sample charging. The evaluation of the aluminium, oxygen and lithium peaks was carried

out using the PHI Multipak V9.5.0.8. software. Curve fitting was performed applying a Shirley-type background removal and mixed Gaussian (80-100%) – Lorentzian shapes according to the method of Abrahami *et al.*[34]

5.3 Results and discussion

5.3.1 Coating defect surface morphology

The corrosion inhibiting effect of the coatings loaded with Li-salts as leaching corrosion inhibitor is clearly visible after 7 d of neutral salt spray exposure as shown in Fig. 5.1. The coating without Li-salts shows an excessive amount of corrosion products (Fig. 5.1a) whereas the coatings loaded with a Li-salt have a clean and shiny scribe without corrosion products (Fig. 5.1b).

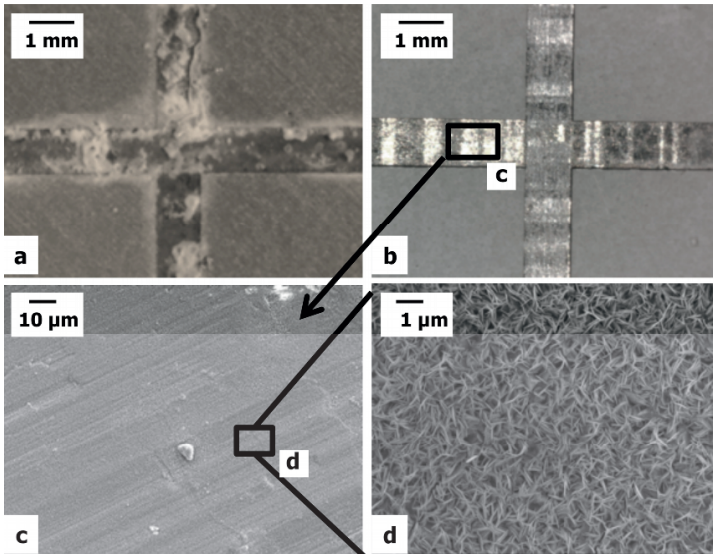

Figure 5.1 *The corrosion inhibiting effect of Li-leaching coating technology after 168 h ASTM B-117. The visual appearance of the scribe (a) without inhibitor, (b) with Li-carbonate as leachable inhibitor and scanning electron micrographs of the protective layer(c) zoomed area in scribe showing no pits and (d) characteristic surface morphology.*

It was found that the protective properties are provided by an optically transparent protective layer on the aluminium surface in the damaged area [31] . Further morphological details of the protective layer were revealed with FESEM. The protective layer was formed on the aluminium alloy without any pitting corrosion (Fig. 5.1c). Higher magnifications revealed the typical porous surface morphology of the protective layer (Fig. 5.1d). Similar porous textures comprising randomly orientated fine flakes are characteristic for hydrated aluminium oxides.[32]

5.3.2 Lithium leaching

The release of Li-ions was measured with a leaching test. Fig. 5.2 shows the results of this leaching procedure for both the Li-oxalate and Li-carbonate loaded coatings. From the graph it can be noted that the Li-oxalate loaded coating released its Li-ions significantly faster compared to the Li-carbonate loaded coating. Especially in the first 24 h the release of Li-ions from the oxalate coating is much faster but levels off after 24 h and then leaching continues at a slower rate.

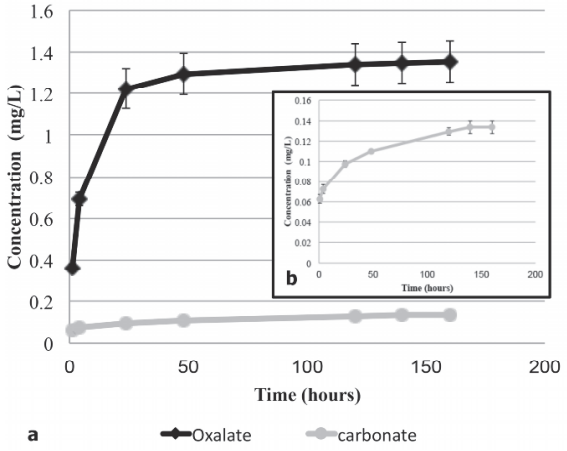

Figure 5.2 Accumulated release of lithium-ions per cm2 model coating with a thickness of 25 µm (a) Li-carbonate and oxalate from the organic model coating, (b) inset Li-carbonate for a limited concentration range.

The release of Li-carbonate is much slower but shows similar behaviour with released lithium concentrations of a factor 10 lower. After 168 h of leaching, 89% of the initial amount of Li-oxalate was released from the coating, whereas only 8% of the total amount of Li-carbonate was released. This difference can be explained due to the large difference in solubility of these Li-salts, being 1.3 g/100 ml for Li-carbonate [35] compared to 8 g/100 ml for the Li-oxalate [36]. For both cases the release starts immediately upon exposure to electrolyte. This is essential for a fast and effective corrosion protection in coating defects.

5.3.3 Coating defect alkalinity

Relevant pH changes can be expected in the scribed area due to the release of Li^+ ions, which results in the growth of a typical protective layer (Fig. 5.1d). SIET was applied to record the typical pH changes in the scribe with time. Fig. 5.3 presents a typical result of the pH scans after 5 minutes up to 5 h exposure to a 0.05 M NaCl solution. Fig. 5.3a displays the pH of the uninhibited coating after 5 minutes; it can be noted that the bulk pH is between 5 and 7 at that time whereas after 5 h of exposure the pH in the scribe increased to more alkaline values of pH 8 - 9 (Fig. 5.3d). As this coating did not contain any

leaching species, the pH change can be attributed to the corrosion process in the scribe when exposing the aluminium alloy to the 0.05M NaCl electrolyte. This is in large contrast to both coatings loaded with leaching Li-salts, which reveal a rapid change in pH when the electrolyte is added to the scribed area (Fig. 5.3b and c).

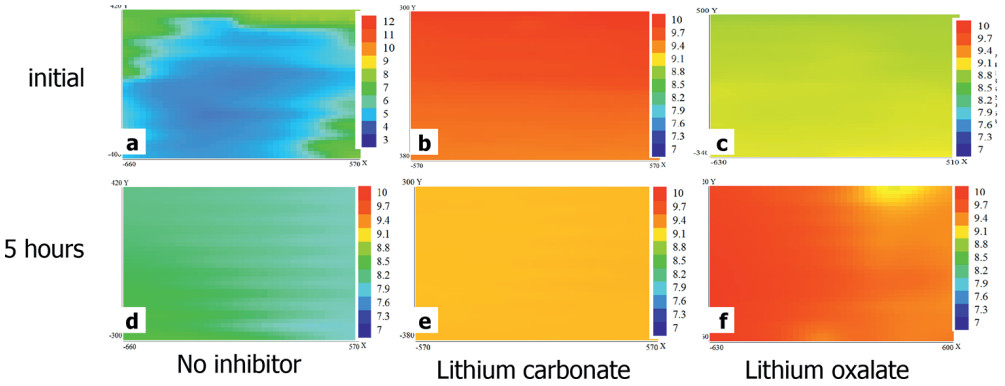

Figure 5.3 *SIET pH scans of scribed area (1mm x 2mm): initial stage after 5 minutes exposure of model coatings (a) no inhibitor, (b) Li-carbonate, (c) Li-oxalate; after 5h exposure: (d) no inhibitor, (e) Li-carbonate, (f) Li-oxalate.*

The Li-carbonate based coating shows a rapid increase to pH 9.5 after 5 minutes of exposure. The pH of Li-oxalate coating increased slower to values of pH 8.5 to 9 after 5 minutes. For both coatings, the pH in the scribe (Fig. 5.3e and f) stabilized at values between 9.4 and 9.7 after 5 h. This larger pH increase as compared to the uninhibited coating case must be caused by the leachable components from the coating. This pH increase is the result of the dissolution of the Li-salts into the electrolyte in the scribe. Li^+ ions are just as Na^+ ions indifferent and do not react with water and therefore do not affect the pH. However, the carbonate and oxalate ions are conjugated bases and therefore affect the pH. Both the carbonate (CO_3^{2-} $pK_b = 3.75$) and oxalate ($C_2O_4^{2-}$, $pK_b=9.81$) ions can recombine with a proton to form a hydrogen carbonate (HCO_3^-) or hydrogen oxalate ($HC_2O_4^-$) [36]. When the proton is obtained from water molecules (reaction 1 and 2), hydroxyl ions (OH^-) are formed which results in the alkaline pH.

$$CO_3^{2-} + H_2O \rightleftarrows HCO_3^- + OH^- \quad (1)$$

$$C_2O_4^{2-} + H_2O \rightleftarrows HC_2O_4^- + OH^- \quad (2)$$

It is important to note that the pH of 9-10 is still significantly lower compared to the Li-based conversion coatings that have been studied at pH 11-13 [28].

5.3.4 Formation of the protective layer with time

The combination of FESEM, AES depth profiles and XPS analysis were used to study the formation of the protective layer in the damaged area at the early stages of neutral salt spray exposure, i.e. until 7 d.

Evolution of the protective layer surface morphology

Fig. 5.4 shows top-view FESEM images of the surface in the scribe after different periods of NSS exposure and represents the relatively fast formation of the protective layer in the scribe. Fig. 5.4a corresponds to the aluminium after the mechanical scribing process prior to the exposure. The characteristic lines and damage of the substrate due to the scribing process can be recognized. The coated samples reveal an immediate change in the scribe, when the samples are exposed to NSS conditions. For both, the Li-carbonate and Li-oxalate loaded coatings, the surface morphology is clearly changing as the formation of a layer is observed. Figures 5.4b and f show a representative structure of the formed layer after 1 h NSS exposure. The layer generated from the Li-carbonate loaded sample shows the characteristic porous structure of a hydrated oxide [32].

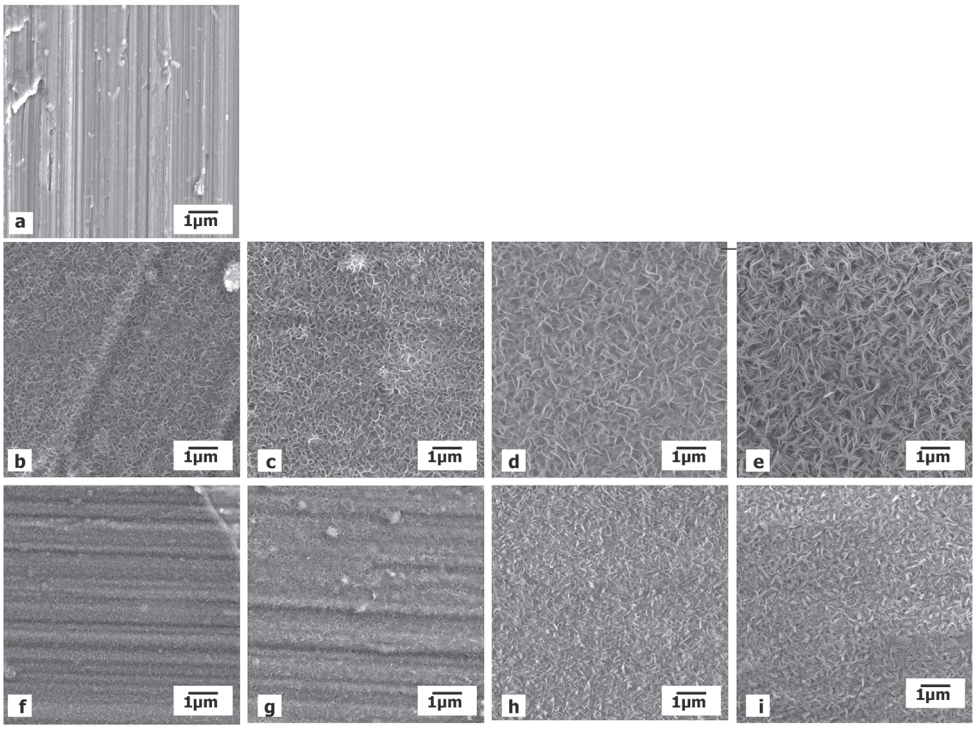

Figure 5.4 *Top-view scanning electron micrographs of the protective layer in the scribe over time: (a) scribed area prior to exposure; Li-carbonate loaded coating after (b) 1 h, (c) 8 h, (d) 48 h, and (e) 168 h; Li-oxalate loaded coating after (f) 1 h, (g) 8 h, (h) 48 h, and (i) 168 h.*

The layer formed for the Li-oxalate loaded sample appears thinner and denser. For both samples the characteristic scribe lines are still clearly visible, suggesting that the layers are still relatively thin. After 8 h of exposure a further growth of the surface layers for both inhibitor-loaded samples is clear (Figures 5.4c and g) with features of the scribe lines still visible. After 48 h of exposure (Figures 5.4d and h), the layers have thickened so much that the scribe lines cannot be distinguished anymore. However, a difference in porosity is noticed between the rather porous structures of the layer formed from the Li-carbonate loaded coating (Fig. 5.4e) as compared to the more dense layer formed from the Li-oxalate loaded coating (Fig. 5.4i) after 168 h exposure.

Fig. 5.5a and b show the fast and uniform coverage of the wall and bottom of the scribed area from the materials that leached from the coating after only 2 h NSS exposure. Fig. 5.5a displays a Li-oxalate loaded coating at the top, the vertical wall of the scribe and the horizontal bottom of the scribe, which is 150 µm deep. Fig. 5.5b shows the coating (top of image) and more detail of the vertical wall of the scribe, which is uniformly covered with the protective layer.

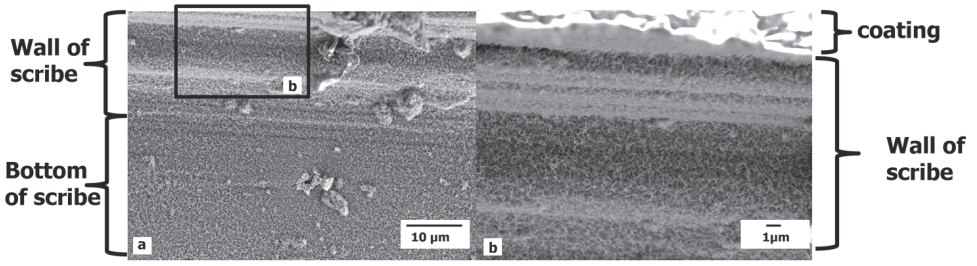

Figure 5.5 *Scanning electron micrographs of the scribe wall protective layer generated from a Li-oxalate loaded coating after 2 h NSS exposure (a) coverage of wall and bottom of scribe and (b) zoomed area at coating/ alloy interface.*

After the 168 h of exposure, a characteristic pattern of dark and light areas is observed in the scribed area (Fig. 5.6a). This effect can be attributed to areas with a different surface morphology of the protective layer (Fig. 5.6b). The more dense surface morphology appears as a darker contrast (area 1) and the more porous structure reveals a lighter contrast (area 2). The variation of the formation and resulting morphology of the protective layer at these areas can be linked with the very early stages of formation. Fig. 5.7 shows the formation of the layer in the early stages of formation from a Li-oxalate loaded coating.

Fig. 5.7a shows the pristine appearance of an unexposed scribe. After 1 h of exposure, the characteristic pattern of dark and light contrast areas becomes visible (Fig. 5.7b). Increased magnification (Fig. 5.7c) reveals that grain boundaries appear to separate the discrete areas. This image shows the intersection of three different grains, one grain covered by a layer (area 1) while the other two areas (2 and 3) are not yet covered.

Fig. 5.7d brings another example of an intersection of three grains, whereas, one grain is still bare (1), a second grain is covered (2) and the third grain displays early signs of coverage. These observations suggest that the protective layer develops differently in specific areas of the scribe and thus can lead to variation in surface morphology of the layer. In alkaline etching studies it was found that grains with a relative high stored energy display more anodic activity compared to grains with lower grain stored energy or grain orientation.[37, 38]

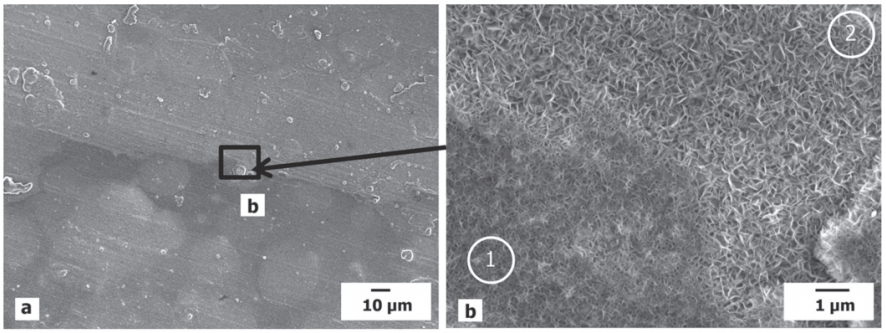

Figure 5.6 Scanning electron micrographs of the scribed area with a protective layer generated from a Li-carbonate loaded coating after 168 h neutral salt spray exposure: (a) middle of the scribed area revealing regions with light and dark appearance and (b) corresponding morphologies, region (1) dark and (2) light appearance.

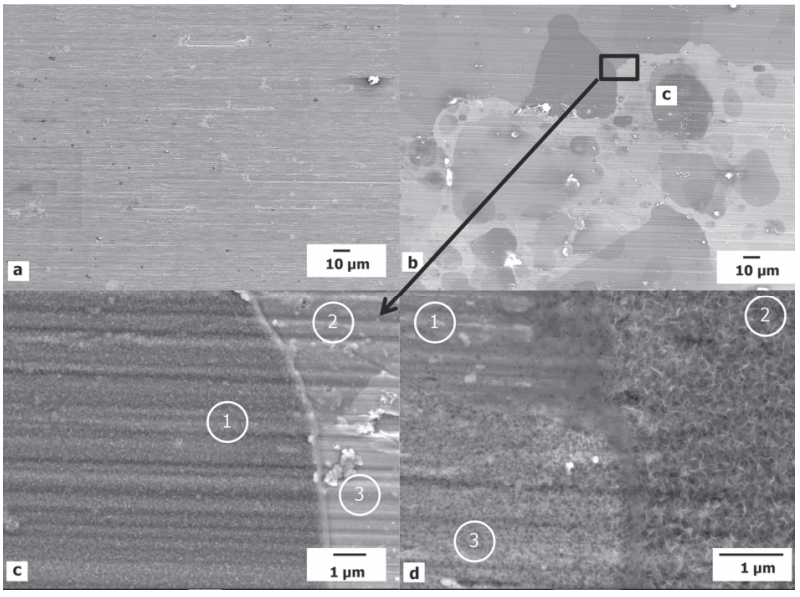

Figure 5.7 Scanning electron micrographs of the scribed area with a protective layer generated from a Li-oxalate loaded coating (a) before exposure (b) light and dark regions after 1 h exposure (c,) intersection of covered (1) and not yet covered grains (2) and (3) after 1 h and (d) a zoomed area of intersection of 3 grains, (1) not covered, (2) covered, and (3) early signs of coverage

This with the variation of local pH or local anodic and cathodic activities of different phases in the alloy matrix might lead to variations in thickness and different morphologies of the protective layer at local regions in the scribed area. This effect of different surface morphologies of the protective layer (Fig. 5.6b) was already observed in previous work.[39, 40] Morphologies local region varied from the general three-layered morphology of the protective layer. It was found that the relative thickness of these layers varied. Some areas developed a significant barrier layer with only a little columnar/petal morphology whereas other regions showed a petal-shaped morphology with almost no barrier layer. Despite these variations in morphology and thickness, electrochemical impedance spectroscopy measurements confirmed the protective nature of this layer.[40]

Thickness development during formation

Auger depth profiles were acquired to monitor the composition of the protective layer during its growth in the scribe. The KLL lines of aluminium (Al), oxygen (O), carbon (C), magnesium (Mg) and copper (Cu) were analysed. Lithium (Li) could not be resolved from the survey spectrum due to an overlap with the aluminium-oxide LVV. A typical depth profile of a protective layer formed from these Li-leaching coatings is presented in Fig. 5.8. It shows that the layer mainly comprises oxygen and aluminium and contains traces of carbon, copper and magnesium. The carbon contamination is found at the outer surface of the layer. Magnesium and copper appear with a low intensity throughout the depth profile. In contrast, the oxygen and aluminium concentrations are significant and can be directly related with the main composition of the protective layer.

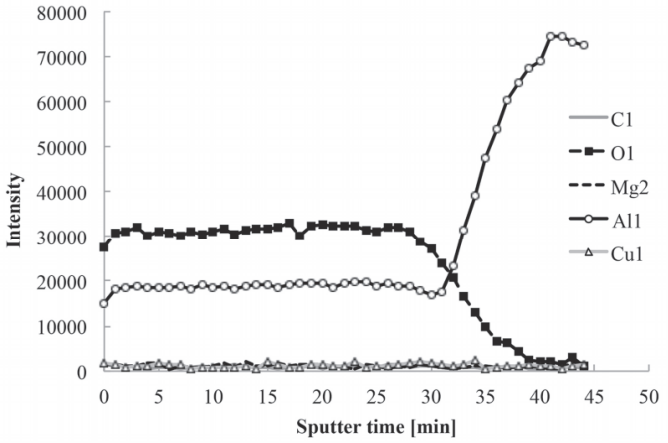

Figure 5.8 *AES depth profile of the scribe area surface layer generated from a Li-carbonate loaded coating after 48 h NSS exposure.*

A closer observation of the oxygen profile reveals three distinct regions: an increase in the initial part of the profile (representing the outer near surface region of the layer), followed by a somewhat constant concentration before a gradual decrease to zero near the aluminium metal interface. Similar aluminium and oxygen profiles suggest a constant Al/O stoichiometry and that the aluminium could be present in the form of an oxide or hydroxide. There is no evidence of the intercalation of carbonate or oxalate in the layer.

In order to get an impression of the growth of the protective layer over time, the layer thickness was determined in terms of the sputter time. The sputter time was established by fitting the Al KLL peaks to extrapolate the Al (oxide) and Al (metal) individual contributions as displayed in Fig. 5.9. The sputter time to remove coatings was established by the 50% peak-to-peak ratio as introduced by Campestrini *et al.* [41]

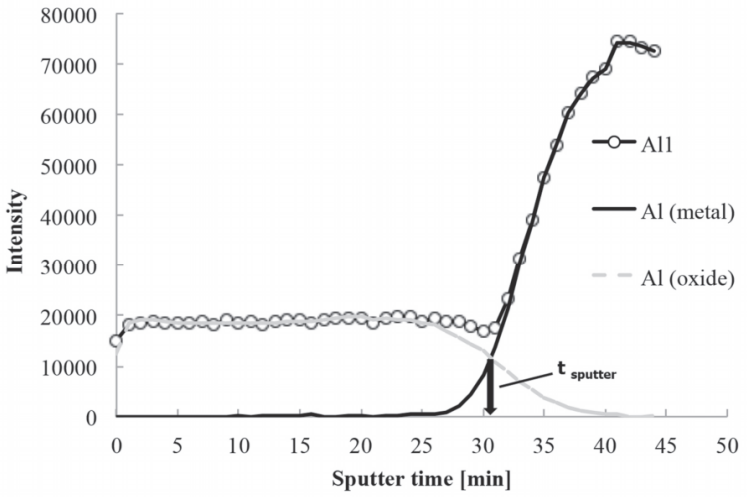

Figure 5.9 *AES depth profile fitting procedure used to establish the sputter-time.*

Fig. 5.10 (a and b) summarizes the sputter time as a function of the formation time during NSS exposure. Considering the first period of 30 h, the Li-carbonate and Li-oxalate loaded coating samples show a similar behaviour of formation (Fig. 5.10b). Two different stages can be recognized, coverage (0-10 h) and growth (10-30 h). After 48 h the sputter times are not increasing anymore indicating that the formation of the protective layer appears to be complete (Fig. 5.10 a).

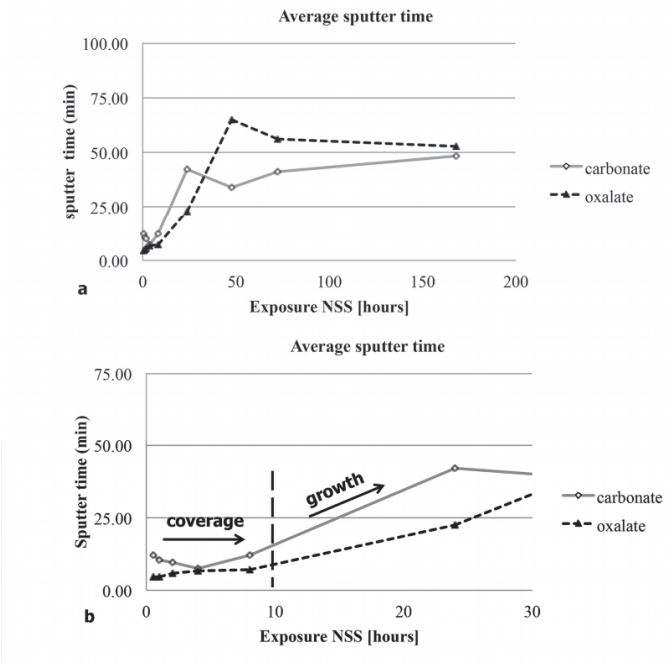

Figure 5.10 Average sputter times, derived from AES depth profiles, representing the formation of the protective layer in the scribed area over time (a) complete exposure time 168 h, and (b) First 30 h of exposure revealing the coverage and growth phase.

Layer composition during formation

The chemical composition of these films was studied additionally with XPS. These coating spectra were compared to the reference samples of a hydrated oxide, (pseudo) boehmite[32] and Li-based layered double hydroxide[27] (Li-LDH). Fig. 5.11a shows a typical survey scan of the protective layer. Again, O and Al were the main elements detected at the surface at 531 eV (O1s) and 74-74.4 eV (Al2p). High-resolution spectra of individual elements of interest are shown in Fig. 5.11b-e. Lithium could be resolved around 57.5-59 eV (Li1s) and Mg and Cu were found at 1304 eV (Mg1s) and 933 eV (Cu2p) respectively. Table 5.2 summarizes the photo peak positions and the FWHM of the O1s, Al2p (oxide), Al2p (metal) and the Li1s peaks. From the values of the Al2p (metal) it can be concluded that only a very thin natural oxide is present prior to exposure (t = 0 h). After 30 minutes NSS exposure no Al2p (metal) is observed anymore. First analysis shows that the binding energies of the O1s and Al2p are very similar throughout the formation of the protective layer. However, the FWHM's of O1s (2.5-3.1) and Al2p (1.7-2.7) change during the formation of the protective layer. Especially, the FWHM's of the O1s peak compared to the natural oxide (2.0) and the Li-LDH reference (2.0) are significantly enlarged. Broadened peaks for O1s are commonly observed and can be attributed to the hydration of the oxide [34, 42].

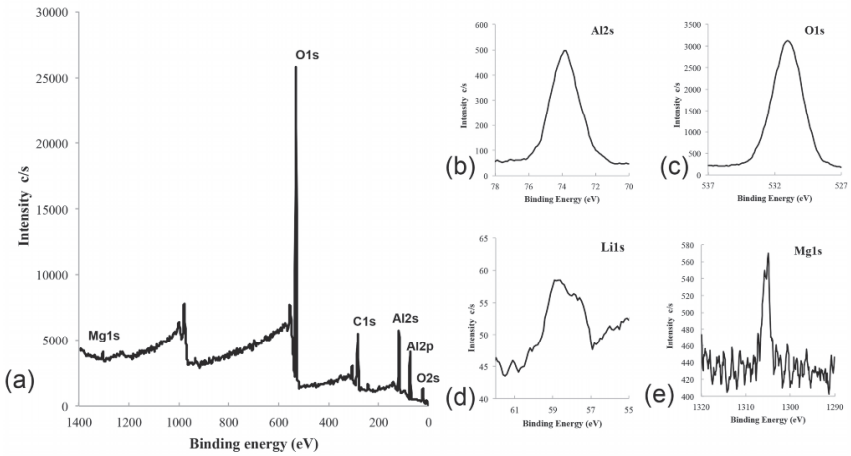

Figure 5.11 XPS (a) survey-scan and high-resolution spectra (b) Al2s, (c) O1s, (d) Li1s, and (e) Mg1s photo peaks.

Table 5.2: XPS peak positions and FWHM measured.

	O1s		Al 2p (oxide)		Al 2p(metal)	Li 1s
Exposure (time)	BE (eV)	FHWM (eV)	BE (eV)	FHWM (eV)	Be (eV)	Be (eV)
Carbonate						
0 h	531.0	2.0	74.4	1.5	71.4	-
0.5 h	531.0	2.5	74.0	2.0	-	55.6
1 h	531.0	3.1	74.5	2.7	-	55.0
2 h	531.4	2.6	74.3	2.0	-	55.9
4 h	532.2	2.6	75.3	2.0	-	56.8
8 h	531.6	2.6	74.4	2.0	-	55.2
24 h	531.0	2.7	73.8	1.7	-	54.7
48 h	531.5	3.1	74.2	2.4	-	55.9
72 h	531.8	3.5	74.5	2.4	-	-
168 h	531.0	2.5	73.9	1.7	-	54.8
Oxalate						
0 h	531.0	2.0	74.4	1.5	71.4	-
0.5 h	531.0	2.7	74.0	2.0	-	54.7
1 h	531.6	2.9	74.6	2.4	-	55.8
2 h	531.3	2.7	74.1	1.8	-	55.1
4 h	531.8	2.7	74.7	1.9	-	56.0
8 h	531.3	2.7	73.9	1.8	-	55.3
24 h	530.0	3.1	72.4	2.2	-	53.4
48 h	531.0	2.7	74.1	1.9	-	55.4
72 h	531.5	2.7	74.4	2.2	-	55.1
168 h	531.7	2.5	74.5	1.9	-	55.8
Reference						
PB	531.3	2.9	73.8	1.8	-	-
Li-LDH	531.8	2.0	74.4	1.7	-	55.4

The degree of hydration can be revealed by fitting the O1s peaks since the OH bond has a higher binding-energy compared to the O^{2-} bond (as in Al-O-Al).[34, 43] Fig. 5.12 shows examples of such fittings by a three-component deconvolution method, resolving the peaks related to OH^- and the O^{2-} and adsorbed H_2O from the O1s peak. Fig. 5.12a and b show a clear difference in hydration after the deconvolution of the O1s peak. The results of the (pseudo)boehmite reference sample are in agreement with the results of Kloprogge *et.al.*[44] (Fig. 5.12a) and shows the lower hydroxyl fraction (OH^-/O^{2-} ratio) compared to the high hydroxyl fraction of the layered double hydroxide (Li-LDH) (Fig. 5.12b). This is in agreement with the O:Al ratio of these two reference samples, respectively 2.4 and 3.7 (Table 5.3).
Fig. 5.12c and d show the high-resolution spectra of the O1s peaks of the Li-carbonate and oxalate samples after 168 h neutral salt spray exposure. Both peaks have a broadened FHWM of 2.5. The fitted curves of these figures reveal the ratio between the O^{2-} of the oxide and OH^- of the hydrated part. The FHWM of the O1s peak and the ratio of the O^{2-} and OH^- peaks are comparable to the (pseudo)boehmite reference (Fig. 5.12a). The O1s peak is significantly wider compared to the FHWM of 2.0 and hydroxyl fractions of the two exposed samples are much lower compared to the Li-LDH reference sample (Fig. 5.12b).

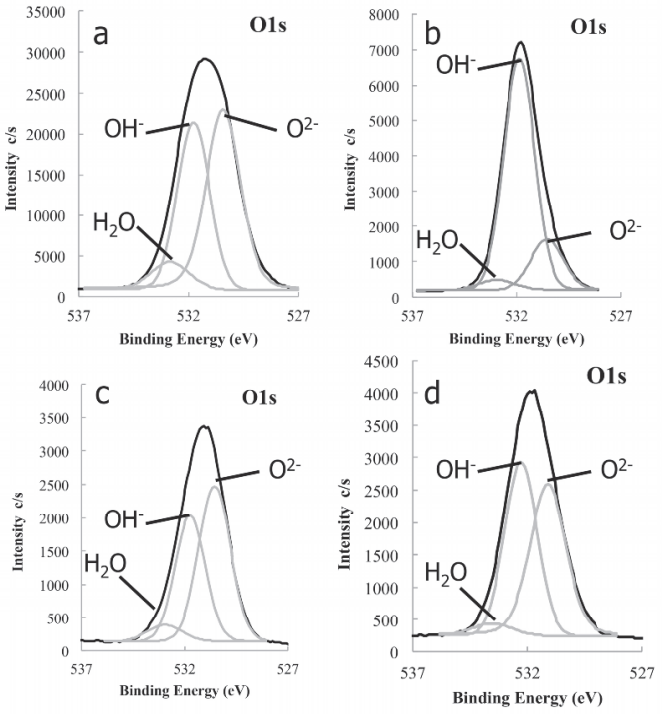

Figure 5.12 Curve fitting results of high-resolution O1s photo peaks of (a) hydrated oxide (pseudoboehmite), (b) Li-LDH, (c) surface layer in the scribe area generated from a Li-carbonate model coating and (d) from a Li-oxalate model coating, after 168 h exposure.

The elemental compositions of the protective layer from the different coatings at different stages of exposure are summarized in Table 5.3. Both samples show a maximum of 2-3 at.% lithium, at the surface of the protective layer in the defect, after 30 minutes of neutral salt spray exposure. This suggests the immediate release of lithium when the damaged area is exposed to corrosive conditions. Further exposure increases the lithium concentration to 4.5-4.8 at.% after 4 h for the Li-carbonate sample and 2 h for the Li-oxalate sample as was already revealed by the Li-leach rates (Fig. 5.2). After this maximum, the lithium concentration decreases and stabilizes at 1-2 at.%. The oxygen and aluminium concentrations remain similar during the entire formation of the layer. The O:Al ratio varied between 2.0 and 3.3. A higher O:Al ratio suggests a higher hydration of the oxide/protective layer in the scribe compared to boehmite ($Al_2O_3 \cdot H_2O$). These higher O:Al ratios could suggest the presence of pseudo-boehmite on the surface of the protective layer. [32, 45]

Table 5.3 Elemental composition of protective layer

	Atomic concentration (%)						ratio
	Li 1s	C 1s	O 1s	Mg 1S	Al 2p	Cu 2p	O/Al
Carbonate							
0.5 h	1.9	8.6	59.1	0.5	30.0	0.0	2.0
1 h	0.6	0.4	61.7	0.5	36.7	0.2	1.7
2 h	1.6	1.1	64.5	0.7	32.2	0.0	2.0
4 h	4.6	2.2	63.7	0.9	28.5	0.2	2.2
8 h	1.4	2.1	66.7	3.4	26.1	0.3	2.6
24 h	2.6	1.2	65.3	5.3	25.5	0.2	2.6
48 h	0.5	2.0	67.6	9.9	20.5	0.0	3.3
72 h	2.2	0.8	62.0	13.4	21.7	0.0	2.9
168 h	2.4	1.3	65.6	1.0	29.6	0.1	2.2
Oxalate							
0.5 h	2.8	2.2	64.0	1.1	29.6	0.2	2.2
1 h	1.9	1.3	64.0	0.7	32.0	0.1	2.0
2 h	4.8	5.1	63.7	1.2	24.7	0.5	2.6
4 h	1.9	2.8	64.2	3.2	28.0	0.0	2.3
8 h	1.5	0.6	65.9	1.1	30.7	0.2	2.2
24 h	2.8	0.3	67.8	0.8	28.3	0.0	2.4
48 h	2.4	1.9	65.8	0.1	29.7	0.1	2.2
72 h	0.4	0.7	68.2	0.9	29.6	0.2	2.3
168 h	1.2	1.8	70.5	0.8	25.6	0.1	2.8
References							
PB	-	8.0	64.5	0.2	27.2	0.1	2.4
Li-LDH	6.6	4.4	69.4	-	19.0	-	3.7

Remarkable is the high level of magnesium at the surface of the protective layer of the Li-carbonate loaded sample after prolonged exposure. It is unlikely that this large amount (9-13 at.%) of magnesium originates from the aluminium alloy matrix. Presumably, this magnesium leached from the coating matrix, since the coating contains a significant amount of magnesium oxide. Therefore, a reference experiment (not reported in this work)

was conducted using coatings containing lithium-salts but excluding magnesium oxide from the coating formulation under the same condition as this experiment. The protective layers in the damaged area, generated from coating samples without magnesium oxide, contained only 0.2-0.5 % magnesium during the same exposure to NSS conditions. This low amount can be related to the dissolution of magnesium from the alloy matrix. In addition, no significant amounts of carbon are found that could relate to the incorporation of carbonate or oxalate ions in the protective layer.

Comparing the XPS data of the protective layers versus the Li-LDH reference, we can find three main differences. The protective layer formed from these Li-leaching coatings have: 1) a significant lower amount of lithium (1-2% compared to the 6% for the Li-LDH reference), 2) a low hydroxyl fraction (Fig. 5.12 c and d versus Fig. 5.12 b (Li-LDH)) and a significantly lower O:Al ratio of the surface layer and 3) the large FWHM (2.7-3.1 compared to 2.0 for the Li-LDH). With these differences, we find argumentation to conclude that the surface of the protective layer is rather a (pseudo)boehmite with lithium distributed in the structure than a typical Li-LDH as was found for the high pH chemical conversion process used by Buchheit et al.[27, 28]

5.3.5 Mechanism of formation

The combined results demonstrate that the active corrosion protective nature of the Li-salt loaded coatings can be attributed to the formation of a protective layer in a defect as illustrated in Fig. 5.1. This layer is initiated due to the fast leaching behaviour of the Li-salts from the organic coating and the inherent generation of alkaline conditions in the damaged area.

The formation of the protective layer can be described in four stages as illustrated in Fig. 5.13. First is the stage of exposure, initiation of leaching and oxide thinning (Stage I). This is the phase when the damaged area is first exposed to the corrosive chloride-containing environment. Li-salts start to leach from the coating matrix when the aqueous electrolyte is present in the damaged area. As a result of this leaching phenomenon, the alkalinity increases to values around pH 9 to10.

Due to the presence of chlorides and an alkaline medium the natural oxide of the aluminium will be thinned.[46] The second stage represents the initial formation of the protective layer (Stage II). Anodic dissolution will be initiated due to the oxide thinning process and under these moderate alkaline conditions this results in the formation of an aluminium hydroxide gel.[47, 48] The initial growth of the aluminium hydroxide gel occurs at the walls and at the sides of the scribe progressing into the damaged area. The anodic dissolution and formation of the protective layer seems to initiate faster on specific grains due to chemical and electrochemical differences of the different grains (due to grain stored energy) at the surface of the scribe.[37, 38] The third phase represents the lateral coverage of the damaged area (Stage III) and after the coverage the fourth phase can be identified, which represents the growth in thickness direction of the protective layer (Stage IV). Both stages III and IV are driven by a growth and dissolution process, which is usually observed

for aluminium in alkaline conditions.[27, 28, 31, 49, 50] This growth and dissolution process continues until a stable state is reached and the formation of the layer is complete.

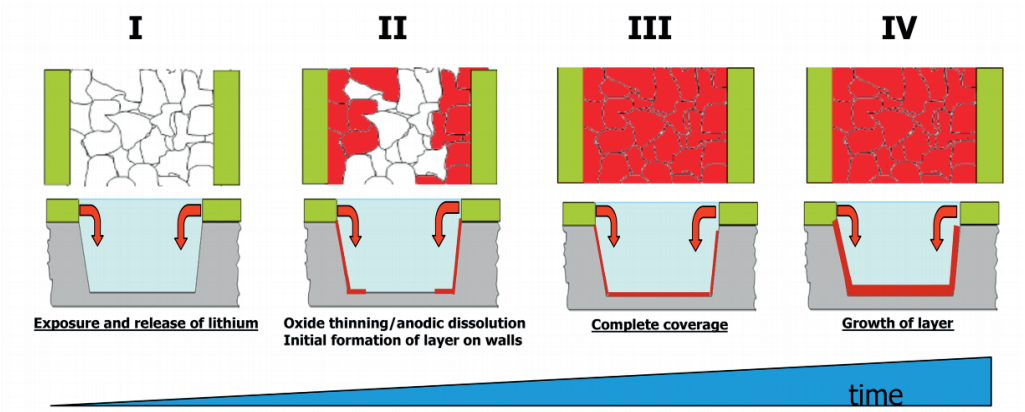

Figure 5.13 *Schematic illustration of the four stages during the formation of the protective later in the damaged area as a function of time.*

An important conclusion is that the composition of the film is identified to be more closely representative of a hydrated oxide (pseudo) boehmite and that the formation process of the protective layer is clearly different compared to the previously reported lithium-based chemical conversion process,[27] since the alkaline conditions are more moderate (pH 9-10) compared to alkaline conditions usually used to prepare Li-LDH conversion coatings (pH 11-13).[27, 51, 52] According to Alwitt, a pseudo-boehmite layer can be formed by the aging or transformation process of amorphous aluminium hydroxide in mildly alkaline conditions.[48]

5.4. Conclusions

The formation of a protective layer in a coating defect from Li-leaching organic coatings on AA-2024-T3 aluminium alloys was studied. Li-carbonate and Li-oxalate were used as leachable corrosion inhibitors for providing active corrosion protection in a coating scribe. Lithium-salt loaded model coatings demonstrated fast and effective corrosion inhibition when exposed to neutral salt spray conditions (ASTM B-117). Leaching profiles demonstrated the immediate release of lithium-ions from the coating matrix into the coating defect when exposed to corrosive conditions. Due to the lithium-ion release the pH increased to alkaline conditions between pH 9 and 10. The XPS analysis and Auger depth profiles did not show any intercalation of carbonate or oxalate ions in the protective layer. Therefore, the role of the carbonate and oxalate can be considered as a pH buffering function. The formation of the protective layer was studied with the use of microscopic and

surface analytical techniques. FESEM analysis demonstrated the fast coverage and growth of the protective layer within the coating defect. The process of growth of the protective layer has been followed by AES depth profile experiments. The formation of this protective layer can be divided in four stages: (1) exposure to environment and release of lithium-ions (II) oxide thinning and anodic dissolution initiating the formation of the protective layer, (III) coverage of the defect and finally (IV) growth of the layer. The surface of the protective layer mainly comprises aluminium and oxygen with traces of lithium and magnesium. XPS analysis suggests that the composition of the protective layer is a hydrated aluminium oxide ((pseudo)boehmite) containing 1-2 at.% lithium in its matrix rather than a Li-based layered double hydroxide (Li-LDH).

References

1. A. Boag, A. E. Hughes, A. M. Glenn, T. H. Muster and D. McCulloch, Corrosion of AA2024-T3 Part I: Localised corrosion of isolated IM particles, *Corrosion Science*, 2011, 53, 17-26.
2. A. M. Glenn, T. H. Muster, C. Luo, X. Zhou, G. E. Thompson, A. Boag and A. E. Hughes, Corrosion of AA2024-T3 Part III: Propagation, *Corrosion Science*, 2011, 53, 40-50.
3. A. E. Hughes, Birbilis, N., Mol, J.M.C., Santiago J. Garcia, S.J., Zhou, X., Thompson, G.E. , in *Recent Trends in Processing and Degradation of Aluminium Alloys*, ed. P. Z. Ahmad, *In Tech*, 2011.
4. A. Hughes, C. MacRae, N. Wilson, A. Torpy, T. Muster and A. Glenn, Sheet AA2024-T3: a new investigation of microstructure and composition, *Surface and Interface Analysis*, 2010, 42, 334-338.
5. A. Boag, A. E. Hughes, N. C. Wilson, A. Torpy, C. M. MacRae, A. M. Glenn and T. H. Muster, How complex is the microstructure of AA2024-T3?, *Corrosion Science*, 2009, 51, 1565-1568.
6. N. Birbilis and R. G. Buchheit, Electrochemical characteristics of intermetallic phases in aluminum alloys - An experimental survey and discussion, *Journal of the Electrochemical Society*, 2005, 152, B140-B151.
7. S. Benavides, *Corrosion control in the aerospace industry*, Woodhead Publishing, 2009.
8. G. Bierwagen, Next generation of aircraft coatings systems, *Journal of Coatings Technology*, 2001, 73, 45-52.
9. A. K. Chattopadhyay and M. K. R. Zentner, *Aerospace and Aircraft Coatings*, Federation of Societies for Coatings Technology, 1990.
10. G. P. Bierwagen, Reflections on corrosion control by organic coatings, *Progress in Organic Coatings*, 1996, 28, 43-48.
11. S. A. Furman, F. H. Scholes, A. E. Hughes and D. Lau, Chromate leaching from inhibited primers. Part II: Modelling of leaching, *Progress in Organic Coatings*, 2006, 56, 33-38.
12. F. H. Scholes, S. A. Furman, A. E. Hughes, T. Nikpour, N. Wright, P. R. Curtis, C. M. Macrae, S. Intem and A. J. Hill, Chromate leaching from inhibited primers. Part I. Characterisation of leaching, *Progress in Organic Coatings*, 2006, 56, 23-32.
13. S. Sellaiyan, A. E. Hughes, S. V. Smith, A. Uedono, J. Sullivan and S. Buckman, Leaching properties of chromate-containing epoxy films using radiotracers, PALS and SEM, *Progress in Organic Coatings*, 2014, 77, 257-267.
14. S. T. Pride, J. R. Scully and J. L. Hudson, Metastable pitting of aluminum and criteria for the transition to stable pit growth, *Journal of the Electrochemical Society*, 1994, 141, 3028-3040.
15. G. S. Frankel and R. L. McCreery, Inhibition of Al Alloy Corrosion by Chromates, *Electrochemical Society Interface*, 2001, 10, 34-38.
16. M. Costa and C. B. Klein, Toxicity and carcinogenicity of chromium compounds in humans, *Critical Reviews in Toxicology*, 2006, 36, 155-163.
17. P. National Toxicology, NTP 12th Report on Carcinogens, *Report on carcinogens : carcinogen profiles / U.S. Dept. of Health and Human Services, Public Health Service, National Toxicology Program*, 2011, 12, 106 - 109.
18. R. L. Twite and G. P. Bierwagen, Review of alternatives to chromate for corrosion protection of aluminum aerospace alloys, *Progress in Organic Coatings*, 1998, 33, 91-100.
19. J. Sinko, Challenges of chromate inhibitor pigments replacement in organic coatings, *Progress in Organic Coatings*, 2001, 42, 267-282.
20. M. W. Kendig and R. G. Buchheit, Corrosion inhibition of aluminum and aluminum alloys by soluble chromates, chromate coatings, and chromate-free coatings, *Corrosion*, 2003, 59, 379-400.
21. T. G. Harvey, S. G. Hardin, A. E. Hughes, T. H. Muster, P. A. White, T. A. Markley, P. A. Corrigan, J. Mardel, S. J. Garcia, J. M. C. Mol and A. M. Glenn, The effect of inhibitor structure on the corrosion of AA2024 and AA7075, *Corrosion Science*, 2011, 53, 2184-2190.
22. J. Mardel, S. J. Garcia, P. A. Corrigan, T. Markley, A. E. Hughes, T. H. Muster, D. Lau, T. G. Harvey, A. M. Glenn, P. A. White, S. G. Hardin, C. Luo, X. Zhou, G. E. Thompson and J. M. C. Mol, The characterisation and performance of Ce(dbp)3-inhibited epoxy coatings, *Progress in Organic Coatings*, 2011, 70, 91-101.
23. T. H. Muster, A. E. Hughes, S. A. Furman, T. Harvey, N. Sherman, S. Hardin, P. Corrigan, D. Lau, F. H. Scholes, P. A. White, M. Glenn, J. Mardel, S. J. Garcia and J. M. C. Mol, A rapid screening multi-electrode method for the evaluation of corrosion inhibitors, *Electrochimica Acta*, 2009, 54, 3402-3411.
24. T. H. Muster, H. Sullivan, D. Lau, D. L. J. Alexander, N. Sherman, S. J. Garcia, T. G. Harvey, T. A. Markley, A. E. Hughes, P. A. Corrigan, A. M. Glenn, P. A. White, S. G. Hardin, J. Mardel and J. M. C. Mol, A combinatorial matrix of rare earth chloride mixtures as corrosion inhibitors of AA2024-T3: Optimisation using potentiodynamic polarisation and EIS, *Electrochimica Acta*, 2012, 67, 95-103.

25. J. G. Craig, R. C. Newman, M. R. Jarrett and N. J. H. Holroyd, Local Chemistry of Stress-Corrosion Cracking in Al-Li-Cu-Mg Alloys, *J. Phys. Colloques*, 1987, 48, 825.
26. J. Gui and T. M. Devine, Influence of lithium on the corrosion of aluminum, *Scripta Metallurgica*, 1987, 21, 853-857.
27. R. G. Buchheit, Bode, M.D., Stoner, G.E., Corrosion-Resistant, Chromate free Talc Coatings for Aluminum, *Corrosion*, 1994, 50, 205-214.
28. C. A. Drewien, Eatough, M.O., Tallant, D.R., Hills, C.R., Buchheit, R.G., Lithium-aluminum-carbonate-hydroxide hydrate coatings on aluminum: Composition, structure and processing bath chemistry, *Journal of material research*, 1996, 11, 1507-1513.
29. C. M. Rangel and M. A. Travassos, Li-based conversion coatings on aluminium: An electrochemical study of coating formation and growth, *Surface & coatings technology*, 2006, 200, 5823-5828.
30. P. Visser and S. A. Hayes, Low-temperature-curable coating composition useful as anticorrosive primer coating for non-ferrous metal substrates, particularly aluminum or aluminum alloy, comprises film-forming resin, curing agent, and lithium salt, *patent nr. WO2010112605-A1*, 2010.
31. P. Visser, Y. Liu, X. Zhou, T. Hashimoto, G. E. Thompson, S. B. Lyon, L. G. J. van der Ven, A. J. M. C. Mol and H. A. Terryn, The corrosion protection of AA2024-T3 aluminium alloy by leaching of lithium-containing salts from organic coatings, *Faraday Discussions*, 2015, 180, 511-526.
32. J. D. Gorman, A. E. Hughes, D. Jamieson and P. J. K. Paterson, Oxide formation on aluminium alloys in boiling deionised water and NaCl, CeCl3 and CrCl3 solutions, *Corrosion Science*, 2003, 45, 1103-1124.
33. A. Alvarez-Pampliega, S. V. Lamaka, M. G. Taryba, M. Madani, J. De Strycker, E. Tourwé, M. G. S. Ferreira and H. Terryn, Cut-edge corrosion study on painted aluminum rich metallic coated steel by scanning vibrating electrode and micro-potentiometric techniques, *Electrochimica Acta*, 2012, 61, 107-117.
34. S. T. Abrahami, T. Hauffman, J. M. M. de Kok, J. M. C. Mol and H. Terryn, XPS Analysis of the Surface Chemistry and Interfacial Bonding of Barrier-Type Cr(VI)-Free Anodic Oxides, *The Journal of Physical Chemistry C*, 2015, 119, 19967-19975.
35. A. Seidell, *Solubilities of inorganic and organic compounds c. 2*, D. Van Nostrand Company, 1919.
36. R. C. Weast, *CRC handbook of chemistry and physics,* , CRC Press, Boca Raton :, 1st student edition edn., 1988.
37. C. Luo, X. Zhou, G. E. Thompson and A. E. Hughes, Observations of intergranular corrosion in AA2024-T351: The influence of grain stored energy, *Corrosion Science*, 2012, 61, 35-44.
38. X. Zhou, C. Luo, Y. Ma, T. Hashimoto, G. E. Thompson, A. E. Hughes and P. Skeldon, Grain-stored energy and the propagation of intergranular corrosion in AA2xxx aluminium alloys, *Surface and Interface Analysis*, 2013, 45, 1543-1547.
39. Y. Liu, P. Visser, X. Zhou, S. B. Lyon, T. Hashimoto, A. Gholinia, G. E. Thompson, G. Smyth, S. R. Gibbon, D. Graham, J. M. C. Mol and H. Terryn, An investigation of the corrosion inhibitive layers generated from lithium oxalate-containing organic coating on AA2024-T3 aluminium alloy, *Surface and Interface Analysis*, 2016, 48, 798-803.
40. Y. Liu, P. Visser, X. Zhou, S. B. Lyon, T. Hashimoto, M. Curioni, A. Gholinia, G. E. Thompson, G. Smyth, S. R. Gibbon, D. Graham, J. M. C. Mol and H. Terryn, Protective Film Formation on AA2024-T3 Aluminum Alloy by Leaching of Lithium Carbonate from an Organic Coating, *Journal of The Electrochemical Society*, 2016, 163, C45-C53.
41. P. Campestrini, G. Goeminne, H. Terryn, J. Vereecken and J. H. W. De Wit, Chromate Conversion Coating on Aluminum Alloys I. Formation Mechanism, *Journal of the Electrochemical Society*, 2004, 151, B59-B70.
42. A. Nylund and I. Olefjord, Surface analysis of oxidized aluminium. 1. Hydration of Al2O3 and decomposition of Al(OH)3 in a vacuum as studied by ESCA, *Surface and Interface Analysis*, 1994, 21, 283-289.
43. M. R. Alexander, G. E. Thompson and G. Beamson, Characterization of the oxide/hydroxide surface of aluminum using X-ray photoelectron spectroscopy: A procedure for curve fitting the O 1s core level, *Surface and Interface Analysis*, 2000, 29, 468-477.
44. J. T. Kloprogge, L. V. Duong, B. J. Wood and R. L. Frost, XPS study of the major minerals in bauxite: Gibbsite, bayerite and (pseudo-)boehmite, *Journal of Colloid and Interface Science*, 2006, 296, 572-576.
45. W. Vedder and D. A. Vermilyea, Aluminum + water reaction, *Transactions of the Faraday Society*, 1969, 65, 561-584.
46. R. T. Foley, Localized Corrosion of Aluminum Alloys - a Review, *Corrosion*, 1986, 42, 277-288.
47. R. T. Foley and T. H. Nguyen, The Chemical Nature of Aluminum Corrosion: V . Energy Transfer in Aluminum Dissolution, *Journal of The Electrochemical Society*, 1982, 129, 464-467.
48. R. S. Alwitt, The Growth of Hydrous Oxide Films on Aluminum, *Journal of The Electrochemical Society*, 1974, 121, 1322-1328.

49. L. A. Carreiea, V. A. Maroni, J. W. Swaine Jr and R. C. Plumb, Raman and infrared spectra and structures of the aluminate ions, *The Journal of Chemical Physics*, 1966, 45, 2216-2220.
50. M. R. Tabrizi, S. B. Lyon, G. E. Thompson and J. M. Ferguson, The long-term corrosion of aluminium in alkaline media, *Corrosion Science*, 1991, 32, 733-742.
51. M. Frenkel, A. Glasner and S. Sarig, Crystal modification of freshly precipitated aluminum hydroxide by lithium ion intercalation, *The Journal of Physical Chemistry*, 1980, 84, 507-510.
52. G. R. Williams and D. O'Hare, A kinetic study of the intercalation of lithium salts into Al(OH) 3, *J Phys Chem B*, 2006, 110, 10619-10629.

Chapter 6

Mechanism of Passive Layer Formation on AA2024-T3 from Alkaline Lithium Carbonate Solutions in the Presence of Sodium Chloride

The active protective properties of the lithium-leaching coating technology were demonstrated in the previous chapters. However, the mechanism of this layer formation remained unclear because it is complicated to perform these studies in-situ. This chapter presents the results of a study that followed the formation of such protective layers in an electrochemical cell under controlled conditions in order to gain enhanced insight into the formation mechanism, by mimicking the aqueous conditions in a defect area of a coated system. During the formation, the layers were analysed revealing the different stages involved in the formation mechanism of the protective layers.

This chapter is published as a scientific paper:
P.Visser, Y. Gonzalez-Garcia, J.M.C. Mol, H. Terryn, Mechanism of Passive Layer Formation on AA2024-T3 from Alkaline Lithium Carbonate Solutions in the Presence of Sodium Chloride. Journal of The Electrochemical Society 2018, 165 (2), C60-C70.

Abstract

This study focuses on the elucidation of the formation mechanism of passive layers on AA2024-T3 during the exposure to alkaline Li-carbonate solutions in the presence of sodium chloride. Under controlled conditions, in an electrochemical cell, a protective layer was generated comprising an amorphous inner layer and a crystalline outer-layer. In order to resolve the formation mechanism, the layers were characterized using surface analytical techniques to characterize the surface morphology, thickness and elemental composition of the layers at different stages of the formation process. In addition, electrochemical techniques were applied to link the electrochemical properties of the layers with the different stages of formation. The results demonstrate that the formation mechanism of these layers comprises three different stages: (I) oxide thinning, (II) anodic dissolution and film formation, followed by (III) film growth through a competitive growth-dissolution process. The passive properties of the layers are generated in the third stage through the densification of the amorphous layer. The combined results provide an enhanced insight in the formation mechanism and the development of the passive properties of these layers when Li-salts are used as leaching corrosion inhibitor for coated AA2024-T3.

6.1 Introduction

Li-salts gained interest as corrosion inhibitor after the observations of unexpected passivity of aluminium in alkaline Li-solutions by Gui and Devine.[1] Aluminium is stable in the range of pH 4 to pH 9 due to the passivity of aluminium oxide.[2] However, it is known that aluminium shows a high corrosion rate at pH values higher than 10.[3] The corrosion process under these alkaline conditions is dominated by two subsequent sub-processes leading to significant mass loss. First, there is the process of direct (anodic) dissolution of the aluminium metal and the formation of an amorphous aluminium hydroxide gel film on the aluminium substrate, and second, the process of chemical dissolution of the aluminium hydroxide gel film into the bulk solution.[4] In contrast, aluminium shows a passive behaviour by the formation of a Li-containing film when exposed to alkaline Li-salt solutions.[1, 5]

This passive behaviour was implemented by Buchheit et al. with the development of a hexavalent chromium-free chemical conversion coating from alkaline Li-carbonate solutions (pH 11-13), generating lithium aluminium carbonate hydroxide hydrate (hydrotalcite) layers on aluminium alloys.[6] They studied the composition, structure and performance of these conversion coatings in relation to processing parameters and various bath chemistries and demonstrated these hydrotalcite coatings exhibit similar corrosion protective properties as traditional conversion coatings.[7] However, application of these conversion coatings in combination with coatings did not result in an equal performance compared to hexavalent chromium-based conversion coatings.[8]

In 2010, it was discovered that Li-salts could be considered as a potential alternative for chromate-based ones as corrosion inhibitor for the protection of aluminium alloys. Visser and Hayes demonstrated the use of Li-salts as active corrosion inhibitor when incorporated as leachable inhibitor in organic coatings.[9] Further studies have shown the promising corrosion protective performance of this Li-leaching coating technology compared to chromates.[10] Initial observations and characterizations revealed that a film with a three-layered morphology was generated in a defect area.[11-13] This layer was formed under alkaline conditions around pH 10 in the presence of Li-ions, which were leached from the organic coating matrix under corrosive conditions.[14] Electrochemical characterization experiments revealed that the corrosion inhibiting properties of this layer could be attributed to a dense inner layer present at the aluminium metal/oxide interface.[15]

Recently, new examples of the corrosion protective properties of lithium on aluminium were published. Gharbi et al. observed a protective Li/Al surface film on Al-Cu-Li 2050-T3 alloy after polarization.[16] It was postulated that, Li from the substrate stabilized the generated aluminium hydroxide gel film. In addition to this, Mata et al. performed low temperature sealing of tartaric sulphuric acid anodized AA2024-T3 using Li-solutions.[17] Li-Al layered double hydroxide (LDH) structures were formed inside the pores of the anodic aluminium oxide layer by a conversion process providing improved barrier properties and improved stability of the dense oxide layer at the metal/porous oxide interface compared to the conventional hot water sealing treatments.

Our preceding studies of the Li-leaching coatings were focused on the characterization, formation, and electrochemical properties of the protective layers generated in coating defect areas when exposed to accelerated corrosion testing. However, the mechanism and the different steps of formation of such passive layers and the role of lithium under such corrosive conditions have not been studied in detail and need further elucidation.

This work aims to investigate the formation mechanism and the development of the electrochemical properties of these layers on AA2024-T3 by mimicking the aqueous conditions of a defect area in an electrochemical cell filled with a Li-carbonate-NaCl solution. Therefore, a similar layer, as observed in a coating defect when Li-salts are applied as leaching inhibitor, was generated under conversion conditions in an electrochemical cell.[11] The formation of this layer was studied using a combination of surface analytical and electrochemical techniques to gain more understanding about the formation mechanism involved and the development of the corrosion protective properties of the layer during its development under these conditions. The surface morphology was studied with scanning electron microscopy (SEM). The chemical composition and thickness of the layer was monitored with Auger electron spectroscopy (AES) depth-profiles. X-ray photoelectron spectroscopy (XPS) was applied to detect lithium in the layer. In addition, potentiodynamic polarizations and electrochemical impedance spectroscopy (EIS) were applied to study the electrochemical properties of the generated layer. The study provides an enhanced insight in the formation mechanism of these layers and links the electrochemical properties of the layers with the distinct stages of formation when AA2024-T3 is exposed to alkaline Li-carbonate-NaCl solutions.

6.2 Experimental

6.2.1. Materials and sample preparation

Unpolished samples of AA2024-T3 (5.0 x 7.0 cm, 0.8 mm thickness) were used as supplied. In order to generate an equal and reproducible starting point for all samples, the substrates were pretreated as follows. The panels were degreased with acetone to remove surface contaminations. This was followed by an immersion in a commercial alkaline cleaning solution (Ridoline 1402) for 1 minute at 55-60 °C. After a rinse in deionized water the panels were subjected to a deoxidation step in a 1 M nitric acid solution for 4 minutes at 20-25 °C, followed by a rinse in deionized water. Finally the panels were dried under ambient conditions.

Electrolyte compositions

The composition of electrolyte used in this work is based on three factors: 1) an estimated Li-concentration in a defect area when leaching from a coating, calculated from the coating thickness, Li-carbonate loading, volume of defect area and the Li-depletion depth into the coating; 2) the moderate alkaline pH as measured in a coating defect[14]; 3) the thickness

and morphology of the layer generated in a coating defect after 4 h exposure to neutral salt spray conditions (ASTM B-117).[11] Li-carbonate (Li_2CO_3) was acquired form Sigma-Aldrich and the Li_2CO_3-NaCl solution was prepared by mixing 0.01M Li_2CO_3 into a 5% NaCl solution. The pH was measured prior to each experiment in general the pH of this solution was between 10.5 and 10.7. The solution will be referred to as the Li_2CO_3-NaCl solution throughout the manuscript.

Formation of the passive layers in an electrochemical cell

The panels were placed as a working electrode in an electrochemical cell set-up (exposed area of 12.7 cm^2) using an Ag/AgCl reference electrode and a platinum gauze counter electrode. The panels were exposed to 5 ml of the Li_2CO_3-NaCl solution (pH= 10.5 – 10.6). The aluminium samples were exposed under aerated conditions from 80 s up to 4 h. During the exposure to the Li_2CO_3-NaCl solution the open circuit potential was monitored to study the formation of the passive layer and ensure the reproducibility of the process. After the specific time of exposure to the Li_2CO_3-NaCl solution, the samples were rinsed directly with copious amounts deionized water prepared with a Millipore® system to quench the formation process.

Reference samples for surface analysis

Reference samples of pseudoboehmite (PB) and Li-layered double hydroxide (Li-LDH) on AA2024-T3 aluminium alloy were prepared for comparison purposes in the X-ray photoelectron spectroscopy section. Pseudoboehmite was prepared by treating the panel with deionized water at 95–100◦ C for 1h according to the method of Gorman et al.[18] The Li-LDH reference was prepared by immersing a AA2024-T3 panel in a 0.1 M Li_2CO_3 solution (pH = 11.3) for 15 min using the conversion coating process of Buchheit et al.[6] Following the treatment, the panels were rinsed with deionized water for 5 min and dried at the air.

6.2.2 Surface analytical measurements

Scanning Electron Microscopy (SEM)

The surface morphology of the layers was examined using a JEOL JSM-7100F Field-Emission SEM (FESEM) microscope using the secondary electron detector (SEI) at a working distance of 10 mm and an acceleration voltage of 5kV. The cross-section of the layer after 4 h exposure to the Li_2CO_3-NaCl solution was examined in a ZEISS Ultra 55 microscope at a 0.5 kV acceleration voltage. The cross-sections of the aluminium panels were prepared with a Leica EM UC6 ultra-microtome equipped with a diamond knife.

Auger Electron Spectroscopy (AES)

Elemental depth profiles were acquired using a PHI 650(SAM) with a LaB_6 cathode and a Cylindrical Mirror Analyzer (CMA). The samples were analysed with a surface incident angle of 30° to the normal using a primary electron beam with an energy of 5 keV and an

emission current of 1 µA, with a base pressure of $3x10^{-10}$ Torr in the analysis chamber. A PHI 04-303 ion gun and 3 keV Ar ions (emission current of 20 mA and Ar pressure of 10 mPa) was used for ion sputtering (1 mm^2 raster). The sample surface was impinged with the ion-beam angle of 50° to the normal using 1 minute intervals. Multipak (V8.0) software was used to analyse the recorded spectra.

X-ray Photoelectron Spectroscopy (XPS)

A PHI 1600/3057 instrument was used to study the surface chemistry of the samples using an incident X-ray radiation (Mg $K_{\alpha 1,2}$= 1253.6 eV). All the measurements were performed with a take-off angle of 45° with respect to the sample surface and an analysis chamber base vacuum of about $5x10^{-9}$ Torr. High resolution scans of the Li1s, Mg1s, Cu2p, O1s, Al2p and C1s photo peaks were recorded without the use of a neutralizer from a 400 µm sample spot diameter, applying a pass-energy of 23.5 eV and 0.1 eV step size. The recorded spectra were calibrated relative to the C1s peak at a binding energy of 284.8 eV to correct for sample charging. The evaluation of the spectra was carried out using the PHI Multipak V9.5.0.8. software. Curve fitting was performed according to the method of Abrahami et al. using a Shirley-type background removal and mixed Gaussian Lorentzian shapes (80-100%). [19] The depth profile was prepared with Ar-ion sputtering using a PHI 04-303 ion gun and 3 keV A-ions (emission current of 20 mA and Ar pressure of 10 mPa). The surface was rastered over an area of 2 mm^2. The ion beam was used at intervals of 1 minute and impinged on the sample surface at 50° to the normal.

6.2.3 Electrochemical measurements

The electrochemical measurements were conducted in a conventional three-electrode cell using an Autolab PGSTAT 30 potentiostat and Nova data collection Software (version 1.10). The reference electrode was a saturated Ag/AgCl electrode, platinum gauze was utilized as counter electrode, and the aluminium sample was used as the working electrode. All measurements were conducted in a Faraday cage.

Open Circuit Potential measurements (OCP) were performed during the exposure to the Li_2CO_3-NaCl solution (exposed area 12.7 cm^2), to study the electrochemical response of the substrate during the deposition of the passive layer in-situ and as a function of time. Potentiodynamic polarizations were performed according to ASTM G57-97 using a sweep range of -200 to +200 mV versus the OCP at a sweep rate of 0.1667 mV/s on a surface area of 0.50 cm^2 after an OCP stabilization period of 2 h in a 0.05 M NaCl solution. Different samples were used for each anodic or cathodic polarization. At least two separate anodic and cathodic polarizations were performed for each sample to ensure reproducibility.

Electrochemical Impedance Spectroscopy (EIS) measurements were conducted at the OCP in the frequency range of 10^5 Hz to 10^{-2} Hz with 10 points per decade and a sinusoidal potential perturbation of ±10 mV. The exposed area of the samples was 3.14 cm^2 using 60 ml of 0.05M NaCl electrolyte. Measurements were performed after 4 h exposure to the

0.05M NaCl electrolyte on at least three samples for each stage of formation. The impedance plots were fitted with Zview from Scribner Associates Inc., using the appropriate equivalent circuits.

6.3 Results and Discussion

6.3.1 Generation of the passive layer in an electrochemical cell

The first objective of this study was to generate a similar layer as observed in a coating defect under conversion conditions in an electrochemical cell. The formation process by leaching from a coating can differ significantly from the "static" conversion process in the electrochemical cell in terms of lithium concentration gradients and the thin film formation processes. For this part of the work, an AA2024-T3 surface was exposed to the Li_2CO_3-NaCl solution for 4 h. Fig. 6.1 shows scanning electron micrographs of the surface of AA2024-T3 aluminium prior and after exposure to the Li_2CO_3-NaCl solution.

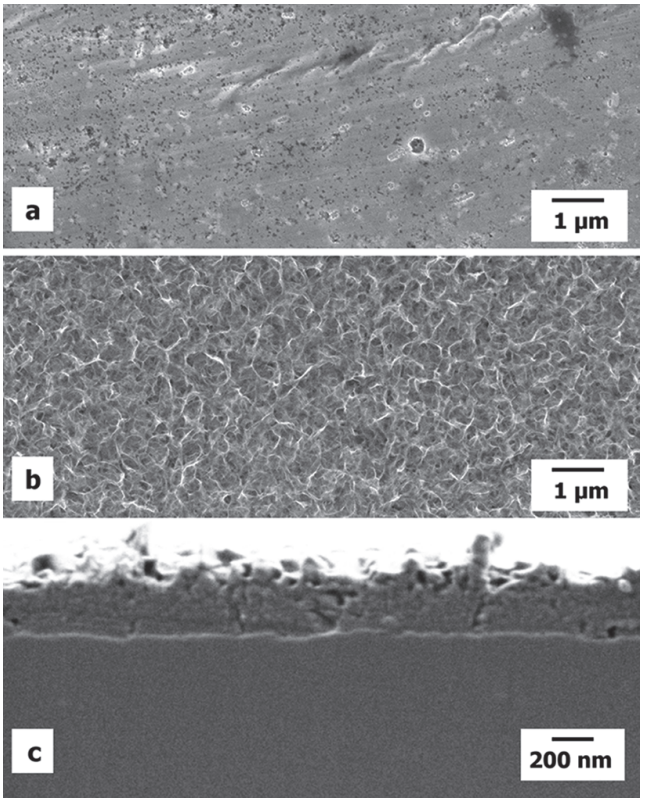

Figure 6.1 **Scanning electron micrographs of AA2024-T3 surface (a) prior to exposure; (b) after 4 h exposure; (c) cross-section of the layer after 4 h exposure to the Li2CO3-NaCl solution.**

Fig. 6.1a shows the AA2024-T3 substrate surface after alkaline cleaning and the de-oxidation steps prior to exposure and Fig. 6.1b shows the aluminium surface with the formed layer after 4 h exposure to the Li_2CO_3-NaCl solution. Fig. 6.1c shows the cross-sectional micrograph of this layer observed in Fig. 6.1b. The generated layer is about 300 to 400 nm thick and shows a dense morphology at the aluminium/ oxide (inner layer) and a porous morphology at the outer layer. The layer is similar in terms of thickness and morphology compared to the layer formed in a defect area after 4 h neutral salt spray exposure, when Li-carbonate was used as leachable corrosion inhibitor in organic coatings.[11] This demonstrates that similar layers could be generated in an electrochemical cell from Li-carbonate solutions with a moderate pH and in the presence of NaCl.

6.3.2 Open circuit potential during the formation of the layer

The 0.01M Li_2CO_3-NaCl solution was used to study the formation of the layer as a function of time using an OCP in-situ measurement to identify the different stages of the formation. Fig. 6.2 shows the OCP evolution of the AA2024-T3 aluminium alloy measured during the formation of the layer when it is exposed to the Li_2CO_3-NaCl solution for 4 h. From the OCP evolution, three stages can be identified. Stage 1 (Fig. 6.2 inset) is the initial rapid potential decrease to a minimum of -1.32 $V_{(Ag/AgCl)}$ after 60-80 s of exposure to the Li_2CO_3-NaCl solution. Stage II shows the first potential increase to a plateau of -1.20 $V_{(Ag/AgCl)}$ after 1000 s, and Stage III represents the second potential increase towards a plateau of -0.90$V_{(Ag/AgCl)}$ after 4 h. This suggests that the formation of the layer involves multiple sub-processes.

The initial drop of the potential, observed in Stage I, can be related to the activation of the aluminium by the exposure to the Li_2CO_3-NaCl solution because aluminium oxide is not stable at pH values higher than 9.[2] In addition to the alkaline conditions, chloride-ions can contribute to the thinning and dissolution of the native aluminium oxide.[20] The thinning of the oxide layer enables electron tunnelling and metal ion-migration initiating the anodic dissolution of the substrate.[21] Stage II starts after about 80 s of exposure to the Li_2CO_3-NaCl solution. At this stage, the potential starts to increase rapidly and hydrogen evolution is observed due to the water reduction reaction triggered by the cathodic over-potential. [3] This increase of potential towards the first plateau region can be attributed to the initial formation of the layer due to the anodic dissolution of substrate.[22] The first plateau can be attributed to the lateral coverage of the aluminium substrate with this layer.[22] Stage III shows the second increase of potential indicates the further growth of the layer. It is known that oxide layers grow in thickness over the general aluminium substrate as a result of the cathodic reactions at the oxide surface via electron tunnelling through the growing oxide layer or residual flaws in the layer.[23] When the thickness of the layer increases, these cathodic processes decrease and become insignificant resulting in a slow potential increase.[23] This gradual increase, observed between 2 and 4 h suggests a slow but continuous development and densification of the layer on the substrate.

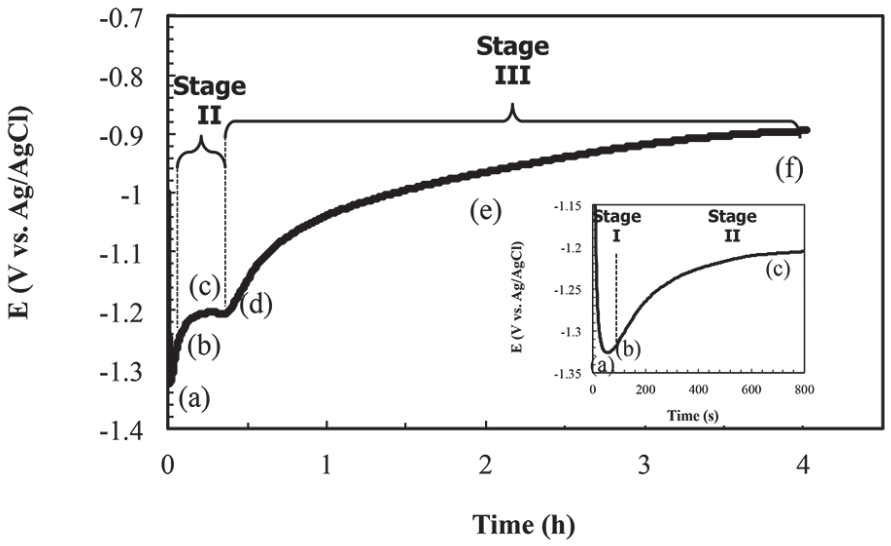

Figure 6.2 *Open circuit potential response over time of AA2024-T3 exposed to the Li_2CO_3-NaCl solution (pH=10.6): (a) 80 s; (b) 150 s; (c) 700 s; (d) 1400 s; (e) 2 h; (f) 4 h; inset: open circuit response over the first 300 s.*

6.3.3 Characterization of the layer during the formation

In order to study the composition and thickness of this formed layer as function of this OCP behavior, samples haven been taken at the specific time intervals of the formation for further characterization (Fig. 6.2): Stage I: (a) 80 s, at the OCP minimum; Stage II: (b) 150 s, during the first OCP increase, (c) 700 s, at the first plateau; Stage III: (d) 1400 s, at the second OCP increase, (e) 2 h, second plateau phase, and (f) 4 h, at the end of the process.

Evolution of the surface layer morphology during the formation

Fig. 6.3 shows top-view FESEM micrographs of the aluminium alloy surface after the selected periods of exposure to the Li_2CO_3-NaCl solution .Fig. 6.3a (80 s) shows the surface of the aluminium alloy with the thinned oxide at the minimum of the OCP (stage I). After 150 s (Fig. 6.3b), the substrate shows the aluminium with a porous morphology indicating initial anodic dissolution of aluminium from the matrix. The micrograph recorded at the OCP plateau in stage II after 700 s (Fig. 6.3c) clearly shows that the pits and porous nature of the surface observed after 150 s have been covered with small crystals. This indicates that the layer started to form on the aluminium surface. A more pronounced layer is visible after 1400 s exposure to the Li_2CO_3-NaCl solution (Fig. 6.3d). The crystals have grown and the layer appears to be thicker. Prolonged exposures to this solution of 2 and 4 h (Fig. 6.3e and 6.3f) showed the further growth of the layer and the crystals developed into a porous outer layer.

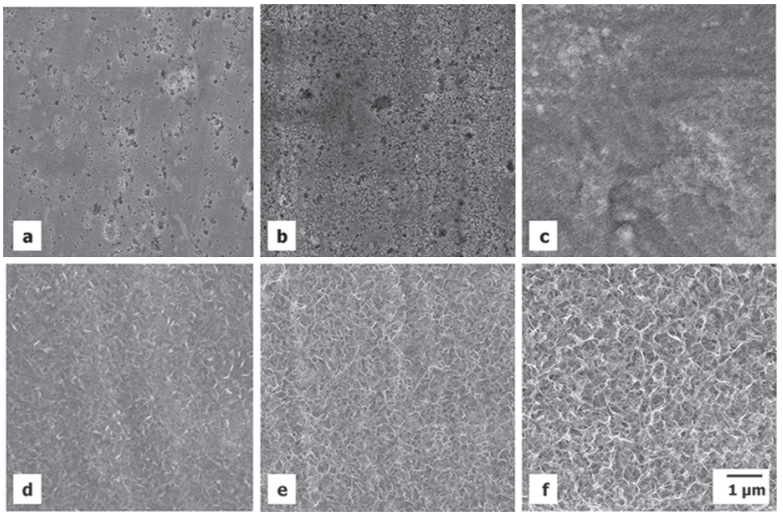

Figure 6.3 *Scanning electron micrographs of AA2024-T3 surface as function of the exposure time to the Li_2CO_3-NaCl solution: (a) 80 s; (b) 150 s; (c) 700 s; (d) 1400 s; (e) 2 h; (f) 4 h.*

Thickness development of the layer

Auger depth-profiles were recorded to follow the growth and the elemental composition of layer during the formation on the AA2024-T3 alloy. The KLL lines of oxygen (O) aluminium (Al), magnesium (Mg), copper (Cu), and carbon (C) were recorded. Lithium (Li) could not be detected due to overlap with the aluminium oxide LVV region. The Al KLL peak could be fitted to distinguish between the contribution related to the oxide ($Al_{(oxide)}$) and the substrate ($Al_{(metal)}$).[14] Fig. 6.4a-g shows the Auger depth profiles for the samples after the different periods of exposure to the Li_2CO_3-NaCl solution. The thickness of the generated layer can be related to the sputtering time needed to reach the aluminium metal/oxide interface ($t_{sputter\text{-}interface}$). This can be determined by the sputtering time corresponding to an increase of the peak-to-peak intensity of $Al_{(metal)}$ to 50% of its maximum intensity.[24] Fig. 6.4h summarizes the $t_{sputter\text{-}interface}$ in a graph demonstrating increase of the $t_{sputter\text{-}interface}$ as function of the exposure time to the Li_2CO_3-NaCl solution. From this graph, it can be noticed that $t_{sputter\text{-}interface}$ increased as a result of longer exposure to the Li_2CO_3-NaCl solution. The inset of Fig. 6.4h shows the early stages of exposure to the solution. Initially, the sample shows a shorter sputtering time compared to the pretreated sample after 80 s and up to 150 s exposure to the Li_2CO_3-NaCl solution there was no significant increase in sputtering time observed. The $t_{sputter\text{-}interface}$ increased rapidly between 150 s and 1400 s exposure to the Li_2CO_3-NaCl solution. This suggests that the initial growth of the layer occurs in this period of time. The increase of $t_{sputter\text{-}interface}$ reduced when the samples were exposed to the Li_2CO_3-NaCl solution beyond 1400 s, up to 4 h, suggesting a slower growth rate of the layer compared to the initial growth between 150 and 1400 s exposure to the solution.

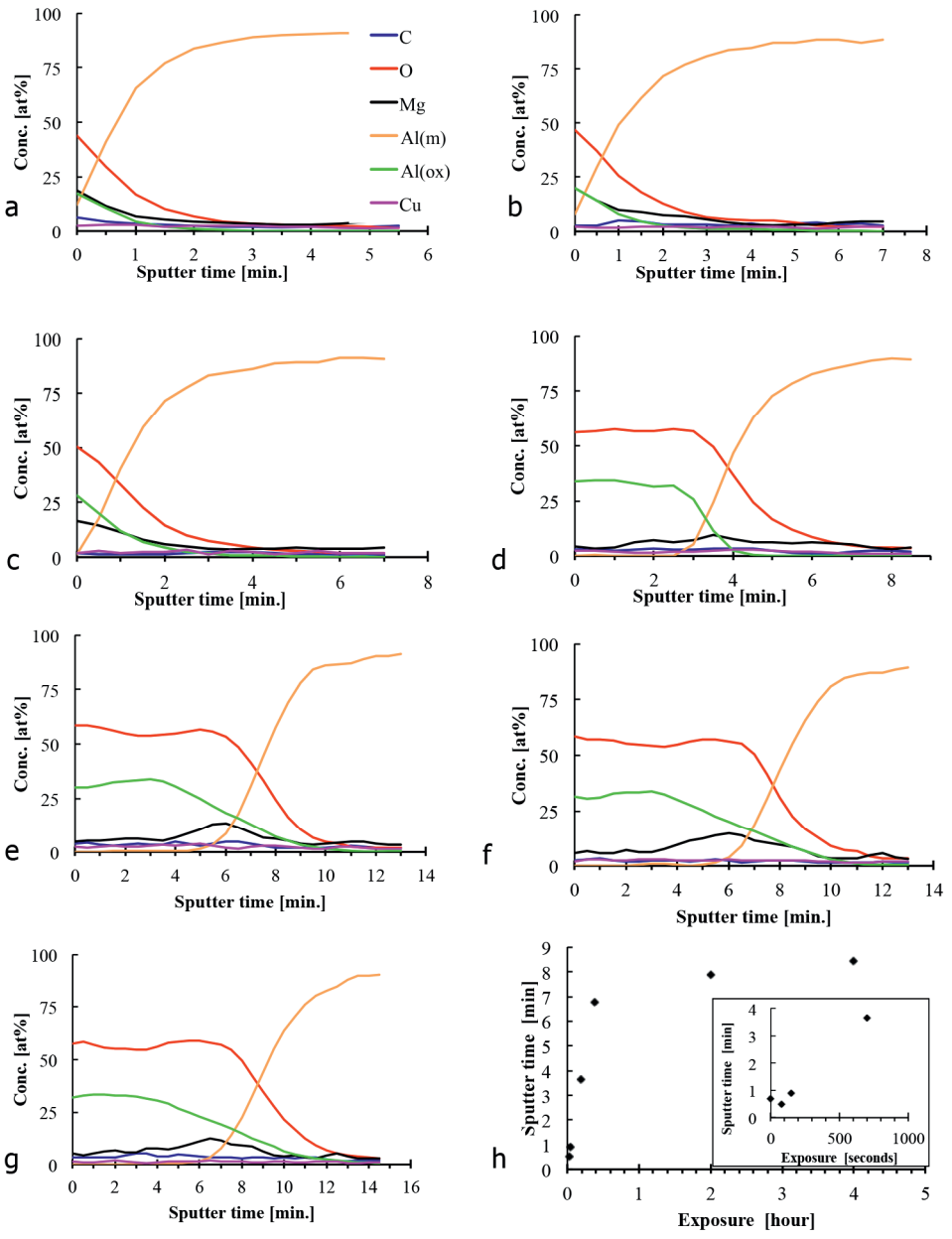

Figure 6.4 *AES depth profiles of the layers formed on AA2024-T3 after exposure to the Li_2CO_3-NaCl solution as function of time: (a) before exposure; (b) 80 s; (c) 150 s; (d) 700 s; (e) 1400 s; (f) 2 h; (g) 4 h; (h) development of sputtering time as function of time of exposure to the Li_2CO_3-NaCl solution.*

In terms of composition, the surface oxide is observed by the presence of O and $Al_{(oxide)}$. In the early stages of exposure (up to 150 s) to the Li_2CO_3-NaCl solution the outer oxide layer shows enrichment of Mg. This Mg most likely originates from the S-phase intermetallic particles in the aluminium alloy and is released into the oxide layer by anodic dissolution.[25] The sputter profiles of 700 s and beyond clearly show the presence of a layer consisting mainly of O and $Al_{(oxide)}$. Characteristic for these prolonged exposure times to the Li_2CO_3-NaCl solution is the higher levels of Mg at the Al metal/oxide interface. The presence of Mg and the low levels of Cu suggest that the substrate dissolution during the formation of the layer was limited. Furthermore, the growth rates of the layer reduced after 1400 s exposure to the Li_2CO_3-NaCl solution (Fig. 6.4f, g). In addition to this, the O/Al ratio close to the aluminium metal/oxide interface has increased compared to the O/Al ratio of the outer layer. This could indicate that the composition of the layer close to the aluminium metal/oxide interface is different compared to the outer layer.

The evolution of the sputtering times of the Auger depth-profiles is in line with the 3 phases in the OCP evolution and FESEM observations, showing the oxide thinning after 80 s (Stage I), the growth of the layer between 150 and 1400 s (Stage II) and a gradual growth upon prolonged exposure up to 4 h to the Li_2CO_3-NaCl solution (Stage III).

Elemental composition of the layer during formation

XPS was applied to study the chemical composition of the layers during the formation process. Table 6.1 shows the elemental composition and the O/Al ratio at the different stages of the formation and Table 6.2 summarizes the photo peak envelope positions of O1s, $Al2p_{(oxide)}$, $Al2p_{(metal)}$ and Li1s and the full width half-maximum (FWHM) of the peak intensities of O1s, $Al2p_{(oxide)}$. The oxide generated on AA2024-T3 after the pretreatment, consists of O and Al with traces of Mg, Cu and C. At this stage, only the oxide related aluminium $Al2p_{(oxide)}$ peak at 74 eV was observed. However, exposure for 80 s to the Li_2CO_3-NaCl solution results in the appearance of the $Al2p_{(metal)}$ peak around 71.4 eV next to the $Al2p_{(oxide)}$, this indicates that the oxide became thinner. In addition to this, the surface area showed an enrichment of Mg (8.1 at. %) and Cu (0.8 at. %) which could indicate anodic dissolution of the S-phase intermetallic particles.[25] After 700 s exposure to the Li_2CO_3-NaCl solution, Mg and Cu concentrations decreased and the $Al2p_{(metal)}$ peak disappeared. At this stage, the surface of the layer predominantly consists of Al and O with an O/Al-ratio around 3 and no lithium was detected. After 1400 s, the first significant amount of lithium (1.1 at%) was detected at the surface of the layer and the Mg and Cu concentrations decreased further. The lithium concentration of the surface layer increased to 6.0 at% after respectively 2 and 4 h. Fig. 6.5 shows the correlation between the lithium concentration at the surface of the layer and the increase of the oxide layer thickness represented by the sputtering time to the Al metal/oxide interface ($t_{sputter\text{-}interface}$) in relation the three stages of formation. This figure suggests that the lithium intercalation is related to Stage III of the layer formation.

Table 6.1: Elemental composition of the specimen surface at the different exposure times to the Li_2CO_3-NaCl solution measured by XPS.

	Atomic concentration (%)						ratio
	Li 1s	C 1s	O 1s	Mg 1s	Al 2p	Cu 2p	O/Al
initial	0.0	2.8	71.9	6.0	22.6	0.1	3.2
80s	0.0	2.2	69.9	6.9	20.8	0.4	3.4
150 s	0.0	1.7	67.3	8.1	22.6	0.8	3.0
700 s	0.0	1.3	74.6	1.8	21.8	0.4	3.4
1400 s	1.1	2.5	70.5	0.7	25.1	0.1	2.8
2 h	6.1	4.2	69.9	1.4	18.4	0.1	3.8
4 h	6.5	3.7	69.5	0.8	19.5	0.1	3.6
Reference samples							
Pseudoboehmite	-	8	64.5	0.2	27.2	0.1	2.4
Li-LDH	6.6	4.4	69.4	-	19	-	3.7

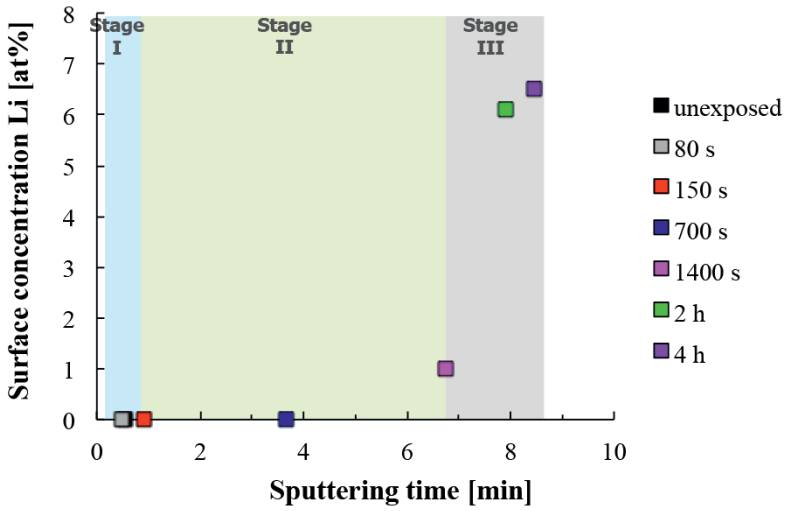

Figure 6.5 *The lithium concentration at the surface of the layer determined by XPS versus the oxide thickness indicated by AES sputtering time to the aluminium metal/oxide interface ($t_{sputter\text{-}interface}$) as a function of exposure time to the Li_2CO_3-NaCl solution, demonstrating the relation of layer growth and lithium intercalation during the three stages of formation.*

From Table 6.2 it can be noted that the FWHM of the O1s peak decreases during the formation of the layer from around 3 eV in the early stages to 1.8 eV after 4h exposure to the Li_2CO_3-NaCl solution. The FWHM of the O1s peak relates to the degree of oxide hydration because OH^- and H_2O have a higher binding energy compared to O^{2-} bond as found in Al-O-Al bonds.[19, 26] A three-component deconvolution fitting method of the O1s peak can be applied to determine the relative ratio of the contributions of O^{2-}, OH^- and H_2O in the layer.[19, 27] Fig. 6.6 shows selected O1s peaks and examples of the deconvolution

before and after the exposure to the Li_2CO_3-NaCl solution. The deconvolution results of all the samples (ratio H_2O / OH^- / O_2^-) are displayed in Table 6.2. Fig. 6.6a shows the deconvolution of the O1s peak of the oxide layer after the pretreatment but prior to exposure to the Li_2CO_3-NaCl solution. The oxide layer contains a relative small about of H_2O and the majority of the O1s peak can be attributed to OH^- and O_2^-. After the period of oxide thinning (150 s) the FWHM of the O1s peak increased slightly from 2.8 to 3.0 eV. This widening of the O1s peak can be related to the increased contribution of H_2O and O_2^- in the layer (Fig. 6.6b). The FWHM of the O1s peak decreased significantly from 3.0 to approximately 2.0 eV after 700 s exposure to the Li_2CO_3-NaCl solution. Deconvolution of the narrowed O1s peak showed decreased contributions of H_2O and O_2^- and an increased contribution of OH^- (Fig. 6.6c).

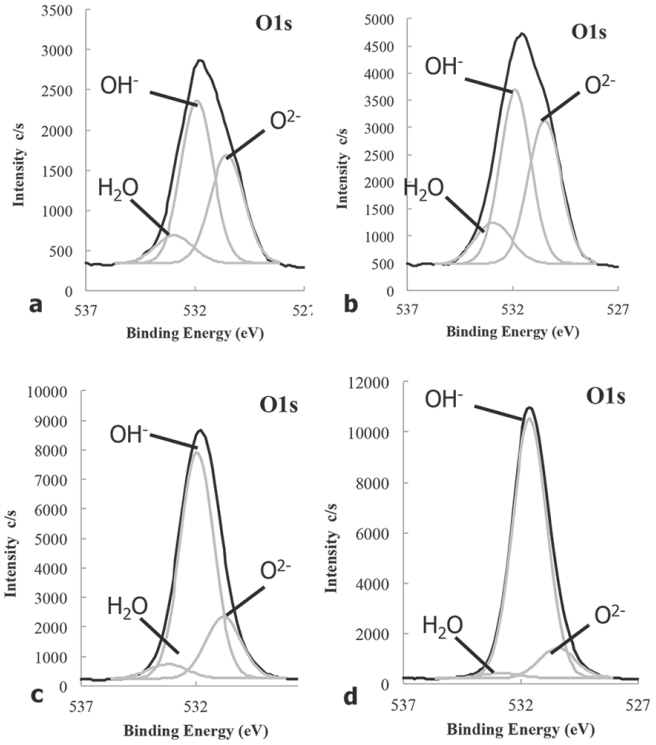

Figure.6.6 *Curve fitting results of high-resolution O1s photo peaks of (a) before; after (b) 150 s, (c) 700 s, and (d) 4 h exposure Li_2CO_3-NaCl solution.*

Extended exposure to the Li_2CO_3-NaCl solution for 4 h (Fig. 6.6d) resulted in a further narrowing of the O1s peak to 1.8 eV and fitting revealed a further increase in the contribution of OH^-. The combination of these observations with the data of the elemental composition and reference samples (Table 6.1 and 6.2), indicates that between 150 and 1400 s the surface oxide transformed into $Al(OH)_3$ during the layer growth process. After

150 s, this layer seems to be rather hydrated but the surface layer seems to crystallize upon longer exposure 700-1400 s. Prolonged exposure (2 and 4 h) to the Li_2CO_3-NaCl solution lead to a second transformation of the surface. From the comparison with the reference samples it can be concluded that surface of the layer transformed into a lithium layered double hydroxide (Li-LDH).

Table 6.2: XPS peak positions and the measured FWHM (O and Al) of the specimen surface at the different exposure times to the Li_2CO_3-NaCl solution.

	O1s		Al 2p (oxide)		Al 2p(metal)	Li 1s	Fitting O1s
Exposure (time)	BE (eV)	FHWM (eV)	BE (eV)	FHWM (eV)	BE (eV)	Be (eV)	Rel. ratio area H_2O / OH^- / O^{2-}
Initial	531.7	2.8	74	1.6	-	-	0.12/ 0.52/ 0.36
80 s	531.5	2.9	74.2	1.8	71.4	-	0.14/ 0.46/ 0.40
150 s	531.3	3	73.9	2.0	71.2	-	0.19/ 0.43/ 0.38
700 s	531.8	2.1	74.3	1.9	-	-	0.05/ 0.71/ 0.24
1400 s	531.5	2.3	74	1.7	-	54.6	0.09/ 0.64/ 0.27
2 h	531.8	1.8	74.4	1.5	-	55.5	0.01/ 0.87/ 0.12
4 h	531.6	1.8	74.1	1.4	-	55.3	0.02/ 0.85/ 0.13
Reference samples							
Pseudoboehmite	531.3	2.9	73.8	1.8	-	-	0.03/ 0.44/ 0.53
Li-LDH	531.8	2.0	74.4	1.7	-	55.4	0.02/ 0.95/ 0.03

Lithium distribution in the layer

The XPS-analysis demonstrated that the generated layer contains Li-LDH ($Li_2[Al_2(OH)_6]_2{\cdot}CO_3{\cdot}nH_2O$). Microscopic analysis of the surface of the layer showed the crystalline nature of a Li-LDH (Fig. 6.1b). However, the cross-section (Fig. 6.1c) and analysis of previous work indicate an amorphous layer below the crystalline top layer.[12] XPS-depth profiling was applied to obtain more detailed information of the elemental composition as a function of depth of the formed layer with a special focus on the lithium concentration. Fig. 6.7a shows the XPS-depth profile of a generated layer after 4 h exposure to the Li_2CO_3-NaCl solution. Fig. 6.7b shows the profile for the low concentration elements (Li, C, Cu and Mg). From the profiles it is apparent that the highest concentration of lithium is located at the outer surface of the generated layer. The concentration of lithium decreased rapidly after the first sputtering cycles. After 5 minutes sputtering the concentration of lithium decreased below 1.0 at% and could not be detected anymore. The sputter profile also shows carbon (C) enrichment of around 2.8 at% at the outer surface of the layer. Upon sputtering, the concentration of the carbon decreased at a similar rate as the lithium concentration. Therefore, this carbon, observed at 289eV, can be attributed to the carbon of the carbonate of Li-LDH. The rest of the layer consists of oxygen (O) and aluminium (Al) and traces of copper (Cu) and magnesium (Mg). Fig. 6.7b shows as well the enriched Mg concentration at the metal/oxide interface possibly due to anodic dissolution of S-phase intermetallic particles that are present in the alloy.[25] Under these alkaline conditions Mg will precipitate as $Mg(OH)_2$. In addition only traces of Cu dissolved from the alloy. This

indicates that there was only limited substrate dissolution during the formation of the layer. These results suggest that only the outer part of the layer is a Li-LDH and the inner layer an aluminium oxide/hydroxide.

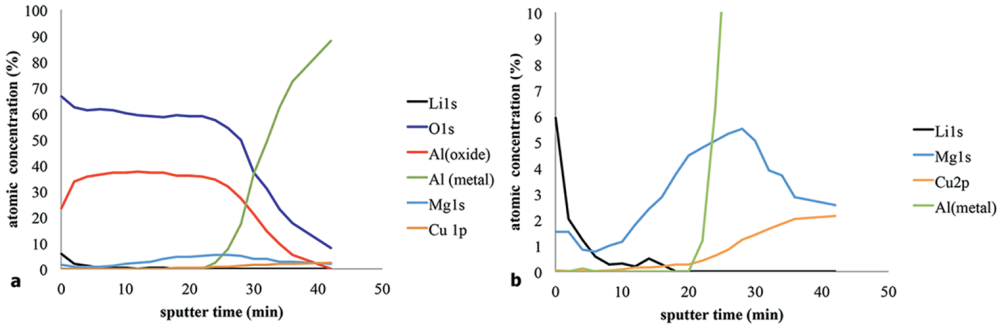

Figure 6.7 *XPS depth-profile of the passive layer formed after 4h exposure to the Li_2CO_3-NaCl solution: (a) complete profile; (b) low concentration elements.*

6.3.4 Mechanism of formation

The results of this investigation show that the mechanism of the formation of these layers involves multiple stages. Fig. 6.8 shows a schematic illustration of these formation stages related to the OCP evolution. First, there is the activation phase (stage I). Aluminium oxide is stable in the pH range from 4 to 9 [28], but the oxide is weakened by adsorption of chloride ions and the alkaline nature (pH 10.5) of the solution of the Li-solution. [20, 29]

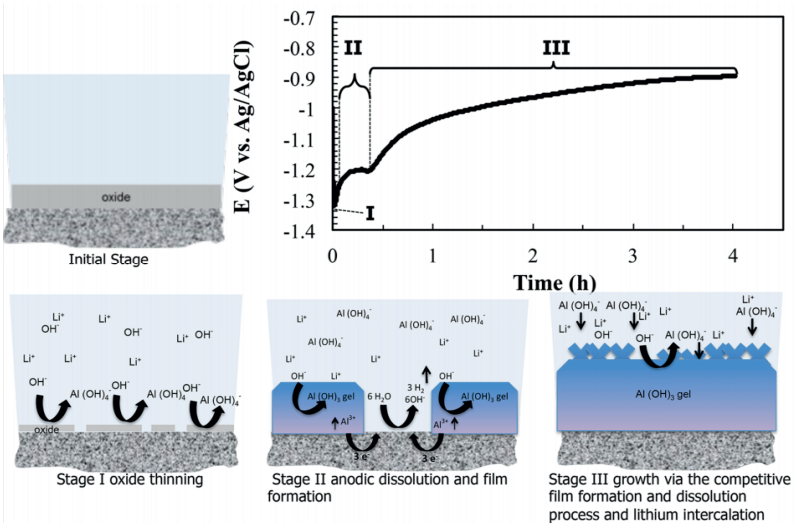

Figure 6.8 *Schematic representation of the formation of the passive layer in relation to the development of the open circuit potential.*

The oxide will be thinned due to the dissolution reaction of the oxide in the alkaline solution (Eq.1).

$$Al_2O_3 + 2OH^- + 3H_2O \rightleftharpoons 2Al(OH)_4^- \quad [1]$$

When the oxide is sufficiently thinned, the OCP reaches its minimum value and stage II initiates with the direct (anodic) dissolution of aluminium (Eq. 2). This dissolution results in the formation of an aluminium hydroxide gel layer at the aluminium metal surface (Eq. 3) because aluminium ions are not stable under alkaline conditions. [4, 30]

$$Al + 3e^- \rightleftharpoons Al^{3+} \quad [2]$$
$$Al^{3+} + 3OH^- \rightleftharpoons Al(OH)_3 \quad [3]$$

Under these alkaline conditions, the aluminium hydroxide layer will be chemically dissolved at the aluminium hydroxide/solution interface (Eq. 4). [3, 4]

$$Al(OH)_3 + OH^- \rightleftharpoons Al(OH)_4^- \quad [4]$$

The rate of dissolution depends on the pH of the environment.[31] Moderate pH values lead to thicker aluminium hydroxide gel layers due to lower dissolution rate compared to the case of high pH conditions. The dissolution of the aluminium hydroxide layer will consequently trigger further anodic dissolution of the aluminium metal resulting in a competitive growth/dissolution reaction. The direct aluminium dissolution is accompanied by hydrogen evolution due to the water reduction reaction (Eq. 5).[4]

$$2e- + 2H_2O \rightleftharpoons H_2 + 2OH^- \quad [5]$$

During stage II, the open circuit potential increases with time. This can be attributed to the growth of the aluminium hydroxide gel film as observed in the Auger depth profiles recorded after 150 and 1400s exposure to the Li_2CO_3-NaCl solution. The direct dissolution of Al and the growth of the hydroxide layer are suppressed when the layer becomes thicker during stage II. This relation of OCP development and layer growth of aluminium under alkaline conditions has been observed and described earlier by Burstein et al. [32] and Zang et al. [33] From the surface analysis it seems that lithium does not play an active role in this initial process because no detectable amounts of lithium were observed in the layer during these stages of formation. A slower growth process (Stage III) follows the fast process in Stages I and II.

This third stage is characterized by the competitive growth and dissolution process and intercalation of lithium into the outer layer. Lithium is known for its facile intercalation with aluminium hydroxides to form a layered double hydroxide under alkaline conditions.[34] Li-ions react with the $Al(OH)_4^-$ and the carbonate-ion to form a lithium aluminium hydroxide

carbonate hydrate or layered double hydroxide ($Li_2[Al_2(OH)_6]_2.CO_3.nH_2O$ (Li-LDH)). Prolonged exposure under these conditions resulted in the further growth of the film, thus an increase of the OCP. The competitive growth/dissolution process will proceed until the layer becomes of considerable thickness, limiting the diffusion of OH^- and Al^{3+} ions through the layer or when the pH drops to lower values (<pH 9). From this process it can be postulated that the Li-Al LDH is a side-product at the outer layer resulting from the aging process of the aluminium hydroxide gel under these alkaline conditions in the presence of lithium. These observations show the three stages involved in the mechanism of formation of a protective layer on AA2024-T3 and provide more insight on the active protective inhibition mechanism of the Li-leaching coating technology.[14]

6.3.5 Corrosion protective properties during formation of the oxide layer

Potentiodynamic polarization measurements

Potentiodynamic polarization measurements were performed in a 0.05M NaCl solution after the same time intervals of exposure to the Li_2CO_3-NaCl solution as studied in the section above (Fig. 6.9). The polarizations were performed from -0.2 V to 0.2 V vs. the open circuit potential. The cathodic branch of the unexposed sample shows a diffusion–limited behavior from potentials lower than 0.54 $V_{(Ag/AgCl)}$. On the other hand the anodic branch of this sample shows no passive region but immediate pitting under potentiodynamic polarization. Exposure to the Li_2CO_3-NaCl solution up to 150 s resulted in an increase of the cathodic current density while the behavior of the anodic polarization remained similar.

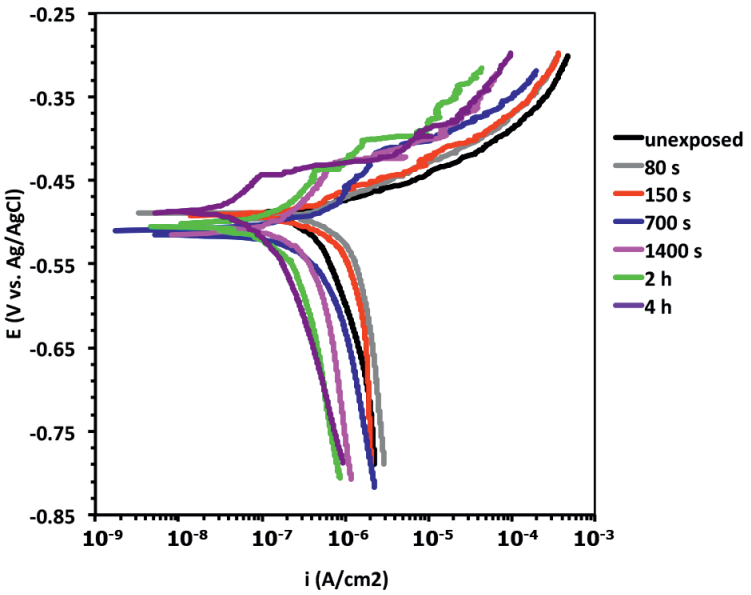

Figure 6.9 *Potentiodynamic polarization curves of the passive layers in 0.05M NaCl solution as a function of time after exposure to Li_2CO_3-NaCl solution.*

Exposure to the Li_2CO_3-NaCl solution longer than 700 s resulted in the decrease of the cathodic current density by an order of magnitude. At the same time, the anodic polarization curves show a decrease in the anodic current density and the pitting potential is shifted to more noble potentials. From the graph it can be noted that i_{corr} decreases over time with the decrease of i_{anodic} and $i_{cathodic}$ while the corrosion potential (E_{corr}) remains similar over time. Table 6.3 lists the corrosion potential (E_{corr}), the corrosion current densities (i_{corr}), the polarization resistance (R_{pol}) and the pitting potential (E_{pit}) of the samples displayed in Fig. 6.9. R_{pol} was calculated from the linear slope of the linear region ±20 mV from E_{corr} (Eq. 6). Using this value, i_{corr} was calculated with the Stern-Geary equation (Eq. 7).[35, 36]

$$\boldsymbol{R_P = \frac{\Delta E}{\Delta i}\Big|_{E=E_{corr}}} \qquad [6]$$

In this equation, R_p is the polarization resistance (Ω cm^2) , ΔE is change in potential (V) and Δi is change in current (A / cm^2).

$$\boldsymbol{i_{corr} = \frac{b_a|b_c|}{(b_a+|b_c|)2.3R_{pol}}} \qquad [7]$$

The Stern–Geary equation (Eq. 2) relates the corrosion current to R_p using the anodic (b_a) and cathodic (b_c) Tafel-slopes. From Table 6.3 is can be noted that R_{pol} increased as a result of exposure to the Li_2CO_3-NaCl solution from 25 kΩ cm^2, at the initial stage, to around 330 kΩ cm^2 after 4 h and simultaneously the corrosion current density (i_{corr}) decreased over time. This behavior can be attributed to the formation of the passive layer on the anodic and cathodic areas of the aluminium substrate.

Table 6.3: Electrochemical parameters obtained from the potentiodynamic polarization curves displayed in Fig. 6.9

	E_{corr} ($V_{(Ag/AgCl)}$)	i_{corr} (A/cm^2)	R_{pol} ($k\Omega.cm^2$)	E_{pit} ($V_{(Ag/AgCl)}$)
initial	-0.50	$6.6x10^{-07}$	24.4	-0.49
80s	-0.50	$5.7x10^{-07}$	29.8	-0.49
150 s	-0.49	$3.1x10^{-07}$	38.8	-0.49
700 s	-0.51	$2.1x10^{-07}$	53.2	-0.43
1400 s	-0.51	$1.9x10^{-07}$	95.8	-0.44
2 h	-0.51	$1.5x10^{-07}$	135.0	-0.45
4 h	-0.48	$7.3x10^{-08}$	332.0	-0.44

EIS Measurements

The electrochemical properties of the layers formed in the Li_2CO_3-NaCl solution were measured by EIS, in a 0.05 M NaCl solution as a function of the exposure time to the Li_2CO_3-NaCl solution, in order to link the electrochemical properties with the different stages of formation of the layer. Fig. 6.10a shows the development of the Bode impedance modulus as a function of exposure time to the Li_2CO_3-NaCl solution.

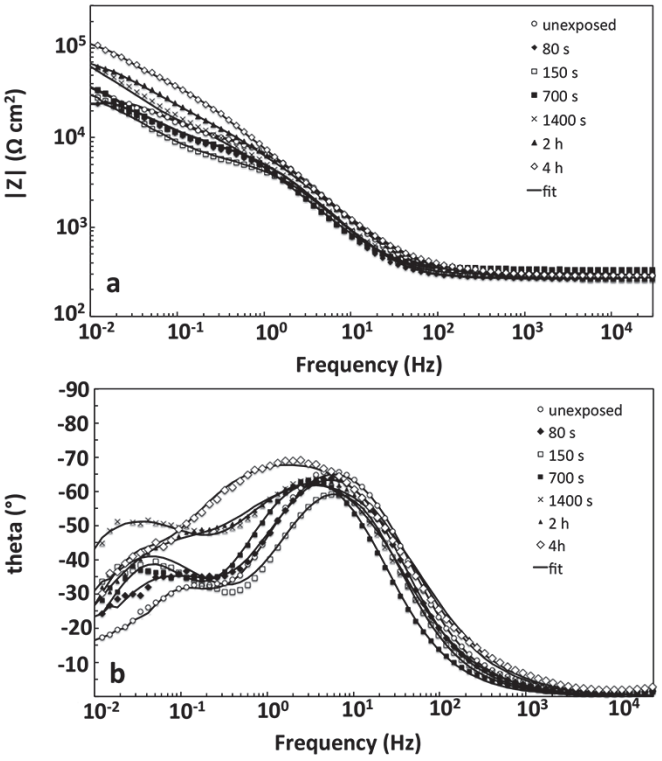

Figure 6.10 *Electrochemical impedance spectra of the AA2024-T3 aluminium alloy in 0.05M NaCl solution before and after exposure to the Li_2CO_3-NaCl solution (a) impedance modulus and (b) phase angle as a function of exposure time to Li_2CO_3-NaCl solution.*

Compared to the sample prior to exposure (unexposed), the impedance modulus dropped during the first phase until 150 s exposure to the Li_2CO_3-NaCl solution. Following this initial period, the impedance modulus values in the low frequency range (10^{-1} – 10^{-2} Hz) started to increase. After 1400s exposure to the Li_2CO_3-NaCl solution the impedance modulus showed increasing values in both the lower and middle frequency range and reached the highest values after 4 h exposure to the Li_2CO_3-NaCl solution. When considering the Bode phase angle plots (Fig. 6.10b) in general two time-constants can be distinguished, one at the middle frequency range of 10 Hz and one in the low frequency range of 10^{-1} to 10^{-2} Hz. The first time-constant can be attributed to the (oxide) layer and the latter to the

electrochemical activity at the aluminium substrate.[37] During the oxide thinning stage (Stage I), 80 and 150 s of exposure to Li_2CO_3-NaCl solution, it can be noticed that the peak of the phase angle related to the time-constant in the middle frequency range initially decreases and becomes narrower. The shift in the phase angle is associated with the magnitude and dispersion in the time constant related to the oxide. After 700 s exposure to the Li_2CO_3-NaCl solution, the phase angle plot in the middle frequency starts to broaden. This broadening together with the increase of the impedance modulus in the middle frequency indicates the formation of a layer on the surface of the alloy[38]. This is in agreement with FESEM and Auger results discussed in the previous section.

Based on the physical properties of the layer as observed in the cross-section in Fig. 6.4, a two time-constant equivalent circuit model (Fig. 6.11) was selected to fit the EIS measurements and quantitatively describe the electrochemical properties of the layer at the different stages of the formation.[39, 40]

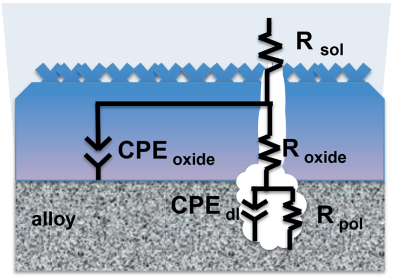

Figure 6.11 *Equivalent electric circuit used to fit EIS spectra for the formed layer from the Li_2CO_3-NaCl solution.*

In this model, R_{sol} is the resistance of the electrolyte. The first time-constant represents the resistance (R_{oxide}) and the capacitance properties (CPE_{oxide}) of the layer that is formed. The second time-constant describes the electrochemical processes (corrosion) at the aluminium substrate in terms of the polarization resistance (R_{pol}) and the double layer capacitance (CPE_{dl}). Constant phase elements (CPE) are used to describe the frequency dependence of elements with a non-ideal capacitive behavior using parameter Q and n.[41] The equivalent capacitance (C) of the respective time-constant was calculated from the resulting R, Q and n values for further comparison and analysis using the equation derived by Hirschorn et al. (Eq. 8). [42]

$$\boldsymbol{C = R^{\frac{(1-n)}{n}} \cdot Q^{\frac{1}{n}}} \qquad [8]$$

The fitted curves are displayed in Fig. 6.10 and the resistance and capacitance values after the different stages of formation was calculated from at least three measurements. The evolution and scatter of the resistance and capacitance of the oxide/hydroxide layer and the metal/oxide interface as a function of time is shown in Fig. 6.12.

Fig. 6.12a shows the initial drop of R_{oxide} from 16 to 5 kΩ cm^2 after 80 and 150 s exposure to the Li_2CO_3-NaCl solution followed by a gradual increase over time to a value of about 40 kΩ cm^2 after 4 h exposure to the Li_2CO_3-NaCl solution. On the other hand, the capacitance (C_{oxide}) increased initially from 12 to 42 µF cm^{-2} after 80 to 150 s and decreases over time when the layer develops over prolonged exposure to the Li_2CO_3-NaCl solution (Fig. 6.12b). This behavior of R_{oxide} and C_{oxide} aligns with the process of oxide thinning and consequently the formation of the layer. The corrosion activity at the aluminium metal/oxide interface was characterized by the polarization resistance (R_{pol}) and the double layer capacitance (C_{dl}). The evolution of R_{pol} (Fig. 6.12c) and that of C_{dl} (Fig. 6.12d) shows a similar behavior of initial decrease of resistance and increasing capacitance followed by increased polarization resistance and decreasing double layer capacitance indicating the formation of a passive layer on the aluminium substrate.

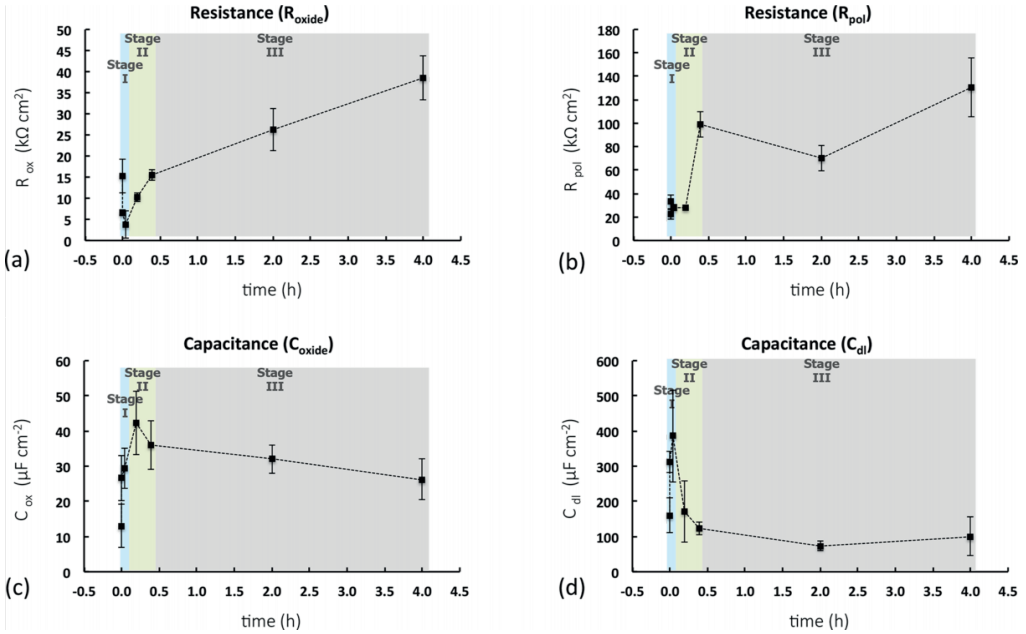

Figure 6.12 *The evolution of the (a) oxide resistance (R_{oxide}), (b) polarization resistance (R_{pol}), (c) oxide capacitance (C_{oxide}), and (d) double layer capacitance (C_{dl}) of the passive layers formed on AA2024-T3 from a Li_2CO_3-NaCl solution in relation to the three stages of formation.*

6.3.6 Mechanism of formation and the relation with the electrochemical properties

The development of electrochemical properties of the layer can be related to the three stages of formation as identified earlier in this paper. Stage I, the oxide-thinning phase, is characterized by a fast decrease of the oxide resistance (R_{oxide}) and low polarization resistance values (R_{pol}). Stage II, represents the first indication of the formation of a passive layer. After 700 s exposure to the Li_2CO_3-NaCl solution, R_{oxide} increased by a factor 2 and

the potentiodynamic polarization measurements showed decreasing values for the anodic and cathodic current densities and the i_{corr} decreased as well. Stage III is related to the growth and dissolution process of the layer due to the longer exposure to the Li_2CO_3-NaCl solution (1400 s up to 4 h). During this stage the corrosion protective properties of the layer started to increase significantly. At this stage the potentiodynamic polarizations show decreasing values of corrosion current (i_{corr}) and anodic and cathodic current densities. Furthermore, a shift of the pitting potential to more anodic values is observed. This together with the increasing resistance and decreasing capacitance values observed in the EIS measurements demonstrate that the corrosion protective properties of the layer are developing in stage III of the mechanism. At this point the layer is not growing as fast in thickness but the increase in the oxide resistance and decrease of the oxide capacitance suggest that the layer gains improved passive properties due to a densification process of the amorphous inner layer at the aluminium surface. These observations show that the layer provides fast and effective corrosion inhibition once the surface of the aluminium is covered. These results are in agreement with the observations when Li-salts are used as leachable corrosion inhibitor in organic coatings.[15]

6.4 Conclusions

This work studied the formation mechanism of passive layers on AA2024-T3 from moderate alkaline Li-carbonate solutions in the presence of sodium chloride. A similar layer, as observed in a coating defect when Li-salts are applied as leaching inhibitor, could be generated under conversion conditions in an electrochemical cell. The generated layer consists of an amorphous inner-layer and a crystalline outer-layer. The formation mechanism involves three stages:

- Stage I: Oxide thinning
- Stage II: anodic dissolution and film formation
- Stage III: growth through competitive film formation and dissolution process.

Surface analysis revealed the fast formation of an aluminium hydroxide layer in stage II. During stage III, the layer grows further and the outer aluminium hydroxide layer transforms into a lithium layered double hydroxide (Li-LDH).

Electrochemical characterization confirmed the three phases involved in the formation of the layer and demonstrated that the corrosion protective properties passive properties of the layer can be attributed to the development of the compact inner layer at the aluminium metal/oxide interface during stage III. The results of this study provide an enhanced view and understanding of the active corrosion inhibiting mechanism of organic coatings with Li-salts as leachable inhibitor for the protection of aluminium alloys.

References

1. J. Gui and T. M. Devine, Influence of lithium on the corrosion of aluminum, *Scripta Metallurgica*, 1987, 21, 853-857.
2. E. Deltombe and M. Pourbaix, The Electrochemical Behavior of Aluminum—Potential pH Diagram of the System Al-H2O at 25 C, *Corrosion*, 1958, 14, 16-20.
3. M. R. Tabrizi, S. B. Lyon, G. E. Thompson and J. M. Ferguson, The long-term corrosion of aluminium in alkaline media, *Corrosion Science*, 1991, 32, 733-742.
4. S.-I. Pyun and S.-M. Moon, Corrosion mechanism of pure aluminium in aqueous alkaline solution, *Journal of Solid State Electrochemistry*, 2000, 4, 267-272.
5. J. G. Craig, R. C. Newman, M. R. Jarrett and N. J. H. Holroyd, Local Chemistry of Stress-Corrosion Cracking in Al-Li-Cu-Mg Alloys, *J. Phys. Colloques*, 1987, 48, 825.
6. R. G. Buchheit, Bode, M.D., Stoner, G.E., Corrosion-Resistant, Chromate free Talc Coatings for Aluminum, *Corrosion*, 1994, 50, 205-214.
7. C. A. Drewien, Eatough, M.O., Tallant, D.R., Hills, C.R., Buchheit, R.G., Lithium-aluminum-carbonate-hydroxide hydrate coatings on aluminum: Composition, structure and processing bath chemistry, *Journal of material research*, 1996, 11, 1507-1513.
8. M. R. S. Castro, J. C. Nogueira, G. P. Thim and M. A. S. Oliveira, Adhesion and corrosion studies of a lithium based conversion coating film on the 2024 aluminum alloy, *Thin Solid Films*, 2004, 457, 307-312.
9. P. Visser and S. A. Hayes, Anti-corrosive coating composition, *Patent WO2010112605-A1*, 2010.
10. P. Visser, Y. Liu, H. Terryn and J. M. C. Mol, Lithium salts as leachable corrosion inhibitors and potential replacement for hexavalent chromium in organic coatings for the protection of aluminum alloys, *Journal of Coatings Technology and Research*, 2016, 13, 557-566.
11. P. Visser, Y. Liu, X. Zhou, T. Hashimoto, G. E. Thompson, S. B. Lyon, L. G. J. van der Ven, A. J. M. C. Mol and H. A. Terryn, The corrosion protection of AA2024-T3 aluminium alloy by leaching of lithium-containing salts from organic coatings, *Faraday Discussions*, 2015, 180, 511-526.
12. Y. Liu, P. Visser, X. Zhou, S. B. Lyon, T. Hashimoto, M. Curioni, A. Gholinia, G. E. Thompson, G. Smyth, S. R. Gibbon, D. Graham, J. M. C. Mol and H. Terryn, Protective Film Formation on AA2024-T3 Aluminum Alloy by Leaching of Lithium Carbonate from an Organic Coating, *Journal of The Electrochemical Society*, 2016, 163, C45-C53.
13. Y. Liu, P. Visser, X. Zhou, S. B. Lyon, T. Hashimoto, A. Gholinia, G. E. Thompson, G. Smyth, S. R. Gibbon, D. Graham, J. M. C. Mol and H. Terryn, An investigation of the corrosion inhibitive layers generated from lithium oxalate-containing organic coating on AA2024-T3 aluminium alloy, *Surface and Interface Analysis*, 2016, 48, 798-803.
14. P. Visser, A. Lutz, J. M. C. Mol and H. Terryn, Study of the formation of a protective layer in a defect from lithium-leaching organic coatings, *Progress in Organic Coatings*, 2016, 99, 80-90.
15. P. Visser, M. Meeusen, Y. Gonzalez-Garcia, H. Terryn and J. M. C. Mol, Electrochemical Evaluation of Corrosion Inhibiting Layers Formed in a Defect from Lithium-Leaching Organic Coatings, *Journal of The Electrochemical Society*, 2017, 164, C396-C406.
16. O. Gharbi, N. Birbilis and K. Ogle, Li reactivity during the surface pretreatment of Al-Li alloy AA2050-T3, *Electrochimica Acta*, 2017, 243, 207-219.
17. D. Mata, M. Serdechnova, M. Mohedano, C. L. Mendis, S. V. Lamaka, J. Tedim, T. Hack, S. Nixon and M. L. Zheludkevich, Hierarchically organized Li-Al-LDH nano-flakes: a low-temperature approach to seal porous anodic oxide on aluminum alloys, *RSC Advances*, 2017, 7, 35357-35367.
18. J. D. Gorman, A. E. Hughes, D. Jamieson and P. J. K. Paterson, Oxide formation on aluminium alloys in boiling deionised water and NaCl, CeCl3 and CrCl3 solutions, *Corrosion Science*, 2003, 45, 1103-1124.
19. S. T. Abrahami, T. Hauffman, J. M. M. de Kok, J. M. C. Mol and H. Terryn, XPS Analysis of the Surface Chemistry and Interfacial Bonding of Barrier-Type Cr(VI)-Free Anodic Oxides, *The Journal of Physical Chemistry C*, 2015, 119, 19967-19975.
20. R. T. Foley, Localized Corrosion of Aluminum Alloys - a Review, *Corrosion*, 1986, 42, 277-288.
21. K. Shimizu, G. M. Brown, K. Kobayashi, G. E. Thompson and G. C. Wood, The role of electron-tunneling in the development of chemical conversion coatings on high-purity aluminum, *Corrosion Science*, 1993, 34, 1853-1857.

22. F. Andreatta, A. Turco, I. de Graeve, H. Terryn, J. H. W. de Wit and L. Fedrizzi, SKPFM and SEM study of the deposition mechanism of Zr/Ti based pre-treatment on AA6016 aluminum alloy, *Surface and Coatings Technology*, 2007, 201, 7668-7685.
23. G. M. Brown, K. Shimizu, K. Kobayashi, G. E. Thompson and G. C. Wood, Further evidence for the presence of residual flaws in a thin oxide layer covering high purity aluminium, *Corrosion Science*, 1993, 34, 2099-2104.
24. P. Campestrini, G. Goeminne, H. Terryn, J. Vereecken and J. H. W. De Wit, Chromate Conversion Coating on Aluminum Alloys I. Formation Mechanism, *Journal of the Electrochemical Society*, 2004, 151, B59-B70.
25. R. G. Buchheit, R. P. Grant, P. F. Hlava, B. McKenzie and G. L. Zender, Local dissolution phenomena associated with S phase (Al2CuMg) particles in aluminum alloy 2024-T3, *Journal of the Electrochemical Society*, 1997, 144, 2621-2628.
26. M. R. Alexander, G. Beamson, P. Bailey, T. C. Q. Noakes, P. Skeldon and G. E. Thompson, The distribution of hydroxyl ions at the surface of anodic alumina, *Surface and Interface Analysis*, 2003, 35, 649-657.
27. A. Nylund and I. Olefjord, Surface analysis of oxidized aluminium. 1. Hydration of Al2O3 and decomposition of Al(OH)3 in a vacuum as studied by ESCA, *Surface and Interface Analysis*, 1994, 21, 283-289.
28. P. A. Schweitzer, *Corrosion and Corrosion Protection Handbook*, M. Dekker, 1989.
29. Z. Szklarska-Smialowska, Pitting corrosion of aluminum, *Corrosion Science*, 1999, 41, 1743-1767.
30. R. T. Foley and T. H. Nguyen, The Chemical Nature of Aluminum Corrosion: V . Energy Transfer in Aluminum Dissolution, *Journal of The Electrochemical Society*, 1982, 129, 464-467.
31. T. Hurlen and A. T. Haug, Corrosion and passive behaviour of aluminium in weakly alkaline solution, *Electrochimica Acta*, 1984, 29, 1133-1138.
32. G. T. Burstein and R. J. Cinderey, Evolution of the corrosion potential of repassivating aluminium surfaces, *Corrosion Science*, 1992, 33, 475-492.
33. J. Zhang, M. Klasky and B. C. Letellier, The aluminum chemistry and corrosion in alkaline solutions, *Journal of Nuclear Materials*, 2009, 384, 175-189.
34. G. R. Williams and D. O'Hare, A kinetic study of the intercalation of lithium salts into Al(OH) 3, *J Phys Chem B*, 2006, 110, 10619-10629.
35. M. Stern and A. L. Geary, Electrochemical Polarization: I . A Theoretical Analysis of the Shape of Polarization Curves, *Journal of The Electrochemical Society*, 1957, 104, 56-63.
36. T. A. Zawodzinski, JES Classics, *Electrochemical Society Interface*, 2009, 59.
37. J. Tedim, M. L. Zheludkevich, A. C. Bastos, A. N. Salak, A. D. Lisenkov and M. G. S. Ferreira, Influence of preparation conditions of Layered Double Hydroxide conversion films on corrosion protection, *Electrochimica Acta*, 2014, 117, 164-171.
38. B. Van der Linden, H. Terryn and J. Vereecken, Investigation of anodic aluminium oxide layers by electrochemical impedance spectroscopy, *Journal of Applied Electrochemistry*, 1990, 20, 798-803.
39. G. Yoganandan, J. N. Balaraju and V. K. W. Grips, The surface and electrochemical analysis of permanganate based conversion coating on alclad and unclad 2024 alloy, *Applied Surface Science*, 2012, 258, 8880-8888.
40. J. T. Qi, T. Hashimoto, J. R. Walton, X. Zhou, P. Skeldon and G. E. Thompson, Trivalent chromium conversion coating formation on aluminium, *Surface & Coatings Technology*, 2015, 280, 317-329.
41. C.H. Hsu and F. Mansfeld, Concerning the conversion of the Constant Phase Element Parameter Yo into a Capacitance *Corrosion*, 2001, 57, 747.
42. B. Hirschorn, M. E. Orazem, B. Tribollet, V. Vivier, I. Frateur and M. Musiani, Determination of effective capacitance and film thickness from constant-phase-element parameters, *Electrochimica Acta*, 2010, 55, 6218-6227.

Chapter 7

Electrochemical Evaluation of Corrosion Inhibiting Layers Formed in a Defect from Lithium-Leaching Organic Coatings

Whereas, the previous chapters focused on the mechanistic aspects of the formation of protective layers from the lithium-leaching coating technology, this chapter discusses the study of the development of the corrosion protective properties of the layer during the formation in the defect. The study combines a range of techniques to follow the growth of the protective layer and its protective nature as a function of time. The study provides a link between the electrochemical behavior and the physical model of the protective layer and demonstrated the non-reversible corrosion protective properties of these layers generated from lithium-leaching coating technology.

This chapter is published as a scientific paper:
P. Visser, M. Meeusen, Y. Gonzalez-Garcia, H. Terryn and J.M.C. Mol, Electrochemical evaluation of corrosion inhibiting layers formed in a defect from lithium-leaching organic coatings, Journal of The Electrochemical Society, 2017, 164, C396-C40

Abstract

This work presents the electrochemical evaluation of protective layers generated in a coating defect from Li-leaching organic coatings on AA2024-T3 aluminium alloys as a function of neutral salt spray exposure time. Electrochemical impedance spectroscopy was used to study the electrochemical properties on a macroscopic scale. An electrochemical model allowed to quantitatively link the electrochemical behavior with the physical model of the layer in the damaged area as studied by scanning electron microscopy. Local potentiodynamic polarization curves obtained from micro-cell measurements showed an increase of the passive range in the defect area due to the formation of a robust protective layer. Scanning vibrating electrode technique measurements confirmed the non-reversible long-term corrosion protection of these generated layers in the coating defect.

7.1 Introduction

In 2010, Li-salts were introduced as possible alternative to chromates as leachable corrosion inhibitor from organic coatings by Visser and Hayes.[1] It was found that organic coatings loaded with Li-salts demonstrated effective corrosion inhibition in a defect under neutral salt spray (NSS) conditions. Further investigations revealed that under NSS corrosive conditions Li-salts leached from the organic coating into an artificial defect and increased the pH in the defect to values between 9 and 10.[2] Under these alkaline conditions a hydrated aluminium oxide layer is formed in the defect area with a final thickness of 0.5-1.5 µm after 168 h NSS exposure. The protective layer has a typical physical morphology consisting of a dense barrier layer at the aluminium interface, a porous middle layer and a columnar outer layer.[3] NSS testing according to aerospace standards demonstrated that this protective layer provides long-term corrosion protection comparable with chromate based inhibitor technology.[4] X-ray photoelectron spectroscopy (XPS) indicated that the formed layers have the characteristics of a hydrated aluminium oxide like (pseudo)boehmite.[2]

Protective aluminium oxide/hydroxide layers have been of interest since the late 1950s. It was reported at that time that the native aluminium oxide film is hydrated to form pseudoboehmite and boehmite upon immersion in water at elevated temperatures.[5] Alwit and Kudo[6, 7] studied the formation of these pseudoboehmite layers at 50-100°C and prepared TEM cross-sections demonstrating a duplex structure with a dense inner layer and a porous outer layer. Buchheit et al.[8] studied protective layers prepared by a chemical conversion process from alkaline Li-salt solutions and demonstrated good corrosion protection on several aluminium alloys. Such conversion coatings showed clearly a two-layer morphology comprising a thin amorphous inner layer and an outer crystalized hydrotalcite layer.[9] Din et al. generated boehmite layers with a similar duplex morphology with the accelerated oxide film growth method, using steam.[10] In their work, they demonstrated that these layers provide corrosion protection on AA6060 alloys by electrochemical analysis and standard corrosion testing such as acid assisted salt spray and filiform corrosion resistance. Potentiodynamic polarization measurements showed a reduction in anodic and cathodic activity and the pitting potential shifted to more noble values.[11]

While our previous studies focused on the structure, morphology, and formation of the protective hydrated aluminium oxide layer in a defect, the development of the electrochemical response of these layers over time has not yet been studied.[2, 4, 12, 13] Therefore, the aim of this work is to study the development of the electrochemical characteristics and to link these with the physical properties of the protective layer during and after its formation in an artificial coating defect on AA2024-T3, using field emission scanning electron microscopy (FESEM) and (local) electrochemical techniques. To this aim, artificially damaged lithium-leaching organic model coatings applied on AA2024-T3 aluminium alloys were exposed to a neutral salt spray corrosion test (ASTM B-117). Cross-

sectional analysis of the defect area using FESEM showed the thickness evolution and morphological formation of the protective layer over time. The evolution of the electrochemical response of the layer in the defect area was studied as a function of time using a combination of (local) electrochemical techniques. Electrochemical impedance spectroscopy (EIS) was used for the quantification of the electrochemical characteristics of the hydrated aluminium oxide in the coating defect on a macroscopic scale. Local potentiodynamic polarization measurements in an electrochemical micro-cell arrangement were performed to determine the passive range and breakdown potential of the generated layers in the defect area on a microscopic scale. Scanning vibrating electrode technique (SVET) measurements were performed to investigate the electrochemical stability of the formed layer after NSS exposure. This dedicated combination of electrochemical techniques provides pivotal information on the electrochemical and physical development of the layer in a coating defect aimed to develop our insights into the corrosion protective properties of these lithium-leaching organic coatings.

7.2. Experimental

7.2.1 Materials and sample preparation

Polyurethane model coatings with a composition as listed in Table 7.1 were used for this work. The lithium-salt loaded coatings have a total pigment volume concentration (PVC) of 30 vol %, comprising 15 vol % inorganic pigments and fillers and 15 vol % Li-salt respectively. Analytical grade Li-carbonate and Li-oxalate purchased from Sigma Aldrich were used as lithium-leaching compounds for active inhibition.

Table 7.1: Composition of uninhibited reference and the lithium-leaching organic model coatings.

	Non-inhibiting	Lithium carbonate	Lithium oxalate
Component A			
N-Butylacetate	75.0 g	75.0 g	75.0 g
Desmophen 650MPA	47.7 g	47.7 g	47.7 g
Lithium carbonate		23.6 g	
Lithium oxalate			32.0 g
Magnesium oxide		16.4 g	16.4 g
Tioxide TR 92		5.9 g	5.9 g
Blanc Fixe N ($Ba(SO_4)$)		15.4 g	15.4 g
Component B			
Tolonate HDB 75 MX	28.5 g	28.5 g	28.5 g
Dynasilan Glymo	5.2 g	5.2 g	5.2 g

The pigmented organic coatings were prepared according to the following procedure. The raw materials of Component A were added sequentially while stirring into a 370 ml glass jar. Subsequently, 400 grams Zirconox® pearls (1.7 -2.4 mm) were added to the mixture for grinding and dispersion of the pigments. The samples were shaken for 20 minutes on a

Skandex® paint shaker to achieve a fineness of grind less than 25 μm. After shaking the pearls were separated from the coating. Component B was added separately, and the paint was stirred to a homogeneous mixture.

AA2024-T3 bare aluminium alloy (Alcoa) was anodized in tartaric-sulfuric acid (TSA) according to aerospace requirements (AIPI 02-01-003). The model coatings were applied with a high volume low pressure (HVLP) spray gun at ambient conditions (23°C and 55 % RH). After the application and a 1 h flash-off period, the coated panels were cured at 80°C for 16 h. The dry film thickness of the coatings after drying was 20-25 μm.

An artificial damage was made on the coated panels with a mechanical milling device leaving a U-shaped scribe of 1 mm wide and 100-150 μm deep. After scribing, the samples were exposed to the neutral salt spray test (ASTM-B117) for varying periods of time, from 2 h up to 168 h. Before each sample analysis, the corrosion process was quenched and any residual chlorides were removed by rinsing the panels with flowing deionized water for 2 min and air-drying.

7.2.2 Surface analytical measurements

Scanning electron microscopy

Cross-sectional observations of the scribed region were carried out using a JEOL JSM-7100F field emission SEM using the backscatter electron detector (BED-C) at 5 kV and a working distance of 3 mm. The samples were sectioned using a diamond saw and consecutively ion milled using a Hitachi IM4000 ion milling system at 6kV Ar-ion acceleration, a 3 times-per-minute sample rotation speed and a swing angle of +/- 30º.

7.2.3. Electrochemical measurements

Electrochemical impedance spectroscopy

The electrochemical behaviour of coated AA2024-T3 samples in the presence of a coating defect was studied with EIS before and after different periods of neutral salt spray (NSS) exposure. EIS measurements were performed at OCP using a Gamry Interface 1000 computer-controlled potentiostat over a frequency range from 10^{-2} Hz to $3 \cdot 10^{4}$ Hz, 7 points per decade and a sinusoidal amplitude of 10 mV, using a three-electrode set-up in a Faraday cage, equipped with a saturated calomel electrode (SCE) as the reference electrode, platinum wire as the counter electrode and a scribed panel as the working electrode using a 0.05 M NaCl electrolyte. The area exposed to the electrolyte was 12.5 cm^2, the effective bare electrode (i.e. the coating defect) area was 0.48 cm^2 and the volume of electrolyte was 60 cm^3. Measurements were recorded after 4 to 8 h exposure to the 0.05M NaCl electrolyte on at least three samples for each exposure condition. The impedance plots were fitted using different equivalent circuits with Zview from Scribner Associates Inc.

Electrochemical micro-cell technique

The micro-cell technique was used for local potentiodynamic polarization measurements. The polarizations were performed using the equipment set-up as developed by Suter and Böhni[14]. A micro-capillary with an internal diameter of about 100 µm was selected to perform the measurements in the (scribed) defect area. This capillary diameter corresponds to an exposed sample area of about $7.85 \cdot 10^{-5}$ cm^2. The capillary was pulled with a Sutter Instruments micro-pipette puller followed by grinding and polishing it to the required size. Before use, a deformable hydrophobic silicone gasket was prepared at the end of the micro-capillary tip. The set-up of the cell comprised a three-electrode configuration: the sample scribe area as working electrode; a Pt-counter-electrode and an Ag/AgCl 3M KCl reference electrode. The measurements were controlled by a high resolution Jaissle IMP83 PCT-BC potentiostat. The anodic potentiodynamic scans were performed at a scan rate of 1 mVs^{-1}, starting -50 mV from the open circuit potential (OCP) and 5-10 minutes after the micro-capillary was positioned on the surface in the scribe. All experiments were performed in 0.05 M NaCl aqueous solution. For each exposure time at least 3 measurements were taken to ensure reproducibility.

Scanning Vibrating Electrode Technique (SVET)

The electrochemical stability of the protective layer in the coating defect area has been investigated using a SVET instrument from Applicable Electronics Inc. controlled with ASET software from ScienceWares Inc. Current density maps were recorded by scanning the Pt-Ir vibrating micro-electrode over a defect in the coating. A defect, penetrating the coating into the AA2024-T3 substrate (1.3 mm diameter and about 150 µm deep), was made with a flat-bottom drilling bit using a Gravograph engraving machine. The lithium-leaching coatings with the defect were exposed to 168 h NSS exposure. Following the exposure the samples were immersed in the 0.05 M NaCl electrolyte and SVET current density maps were recorded up to 14 d immersion. The SVET probe was located at 100 µm from the coating around the defect and as a result the tip-defect bottom distance is 200-250 µm. The dimensions of the SVET maps were around 1700 × 1700 µm using 41x41 points per map.

7.3. Results and discussion

7.3.1 Visual and microscopic coating defect analysis as a function of NSS exposure time

In the aerospace industry, the active protective properties of coatings are tested by means of neutral salt spray (NSS) exposure according to ASTM B-117.[15] Prior to exposure, an artificial defect is made through the coating into the metal and the degree of corrosion is assessed after various periods of exposure. Fig. 7.1a-d shows the rapid formation of

corrosion products in such a defect when exposed to corrosive conditions as a function of time in case a coating has no inhibitive capabilities for protection of AA2024-T3 bare aluminium alloy. The first signs of corrosion are evident after only 2 h of exposure (Fig. 7.1a) illustrating the intrinsic high corrosion susceptibility of the AA2024-T3 alloy. The corrosion continues with time and results in a large amount of voluminous corrosion products in the scribe after 48 and 168 h of exposure (Fig. 7.1c and d). In contrast to the coating without corrosion inhibitor, both model coating formulations, loaded with Li-carbonate (Fig. 7.1e-h) and Li-oxalate (Fig. 7.1i-l) as leachable corrosion inhibitor, showed no corrosion products in the scribed area after 168 h of NSS exposure. This demonstrates the effective active protective properties of these lithium-based inhibitor loaded coatings.

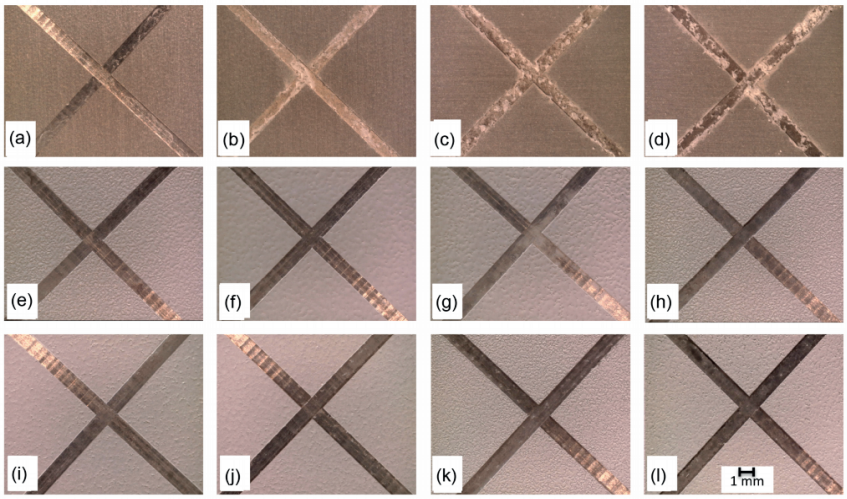

Figure 7.1 *Top view of scribe area after neutral salt spray exposure: non-inhibited coating after (a) 2 h, (b) 8 h, (c) 48 h, and (d) 168 h; Li-carbonate loaded coating after (e) 2 h, (f) 8 h, (g) 48 h, and (h) 168 h; Li-oxalate loaded coating after (i) 2 h, (j) 8 h, (k) 48 h, and (l) 168 h.*

Fig. 7.2 shows micrographs of cross-sections of defect areas before and after NSS exposure. Fig. 7.2a shows the general overview of the cross-sectional edge region of the defect prior to exposure. Fig. 7.2b shows the typical surface of the unexposed scribe bottom. Fig. 7.2c shows the cross-sectional edge region of the defect in case lithium-leaching coatings are applied and exposed to NSS after 168 h of exposure. The cross-sectional micrographs of a coating defect of a Li-oxalate loaded coating covered samples confirm the absence of corrosion and reveal the protective layer that was formed throughout the scribed area. Fig. 7.2d shows the typical morphology of the hydrated aluminium oxide layer that is formed from this Li-oxalate loaded coating covered sample under these corrosive conditions[3]. The layer covers the entire surface of the damaged alloy. This characteristic layer is formed rapidly from the lithium-leaching coating technology and protects the damaged area effectively.

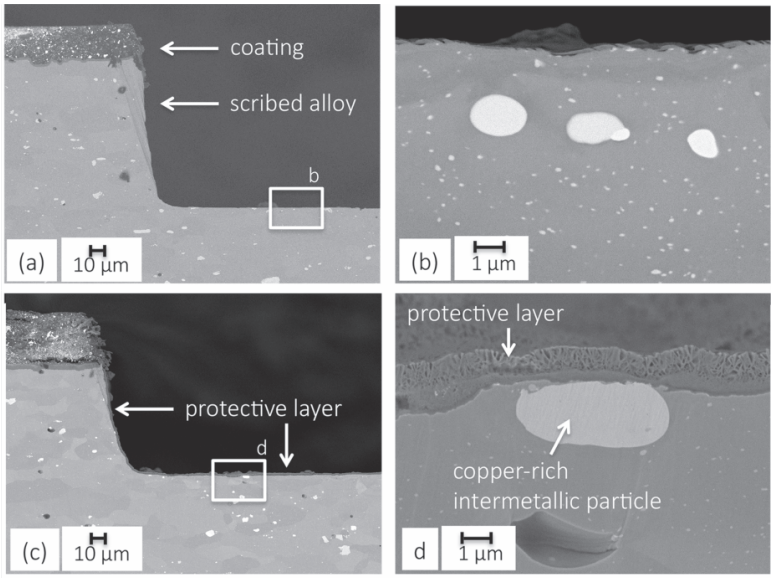

Figure 7.2 Microscopic cross-sectional view of the coating scribe area: (a) edge region of the defect and (b) defect bottom region before NSS exposure; (c) edge region of the defect and (d) defect bottom region after 168 h NSS exposure for the Li-oxalate loaded coating covered sample.

7.3.2 Protective layer formation as a function of NSS exposure time

To study the formation and the characteristics of the protective layer in the defect area over time, ion-milled cross-sections of Li-carbonate and Li-oxalate loaded coatings were analyzed after 2, 8, 48, and 168 h of NSS exposure. Fig. 7.3 shows cross-sectional micrographs of the protective layer during its formation over this period of time.

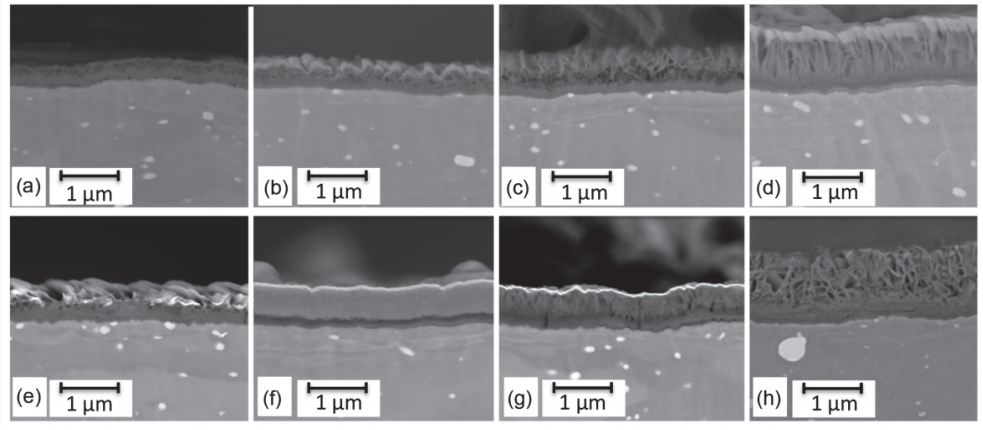

Figure 7.3 Cross-sectional scanning electron micrographs of the protective layer in the scribe: Li-carbonate loaded coating after (a) 2, (b) 8, (c) 48, and (d) 168 h of NSS exposure; Li-oxalate loaded coating after (e) 2, (f) 8, (g) 48, and (h) 168 h of NSS exposure.

The micrographs show that after 2 h NSS exposure a layer of 0.3 to 0.5 µm has been formed on the aluminium surface of the scribe. (Fig. 7.3 a,e). The layer has a dense morphology at the aluminium metal/oxide interface of ~ 0.1 µm and a more porous morphology at the outer surface. As result of longer exposure, the layer develops in thickness and morphology on the outer side. After 8 to 48 h of exposure, the layer thickness varies between 0.6-0.8 µm and both the Li-carbonate and Li-oxalate loaded samples shows the development of a columnar structure at the outer surface and maintaining a dense layer at the aluminium interface (~0.1 µm) (Fig. 7.3b and 7.3f, 8 h; Fig. 7.3c and 7.3g, 48 h). After 168 h the protective layers have grown to a thickness of about 1.0-1.2 µm and show the characteristic morphology of a dense inner layer (~0.1 µm), a porous middle layer and a columnar outer layer as observed in our previous studies.[4] It is important to notice that the thickness of the dense inner layer remains similar, ~0.1 µm, for both lithium-leaching coatings for the full exposure time of 168 h. Fig. 7.4 shows the quantitative development of the thickness of the layer derived from the micrographs of the cross-sections.

It can be noted that after 2 and 8 h NSS exposure, the thickness of the layers from the Li-oxalate loaded coating are thicker compared to the layers generated from the Li-carbonate loaded coatings. This can be explained by the lower initial pH in the defect area of the Li-oxalate coatings as observed by local pH measurements in previous work.[2] The development of the aluminium hydroxide gel layer is a result of the competitive film formation process of chemical dissolution at aluminium hydroxide gel/solution interface and film growth at the metal/ aluminium hydroxide gel interface. This in line with the results of Hurlen and Haug, who observed that thickness of the layer is related to the pH of the solution. A higher pH accelerates the chemical dissolution at the aluminium hydroxide gel/solution interface resulting in thinner layers.[16, 17]

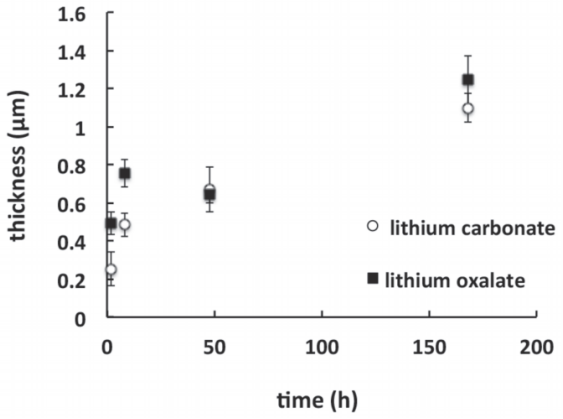

Figure 7.4 Measured thickness of the protective layers from Li-carbonate and Li-oxalate loaded coatings after different periods of NSS exposure.

The results confirm the previously proposed multistep-process to comprise basically 4 steps[2]: oxide thinning, anodic dissolution, formation of an aluminium hydroxide gel layer, and finally the aging of this gel into a hydrated aluminium oxide.[17, 18] The cross-sections revealed the formation of the protective aluminium hydroxide gel on the alloy in the early stages, followed by the ageing process resulting in the characteristic three-layered morphology of the protective layer with a dense layer at the aluminium interface, a porous transition layer in the middle and a columnar morphology at the top.

7.3.3 Corrosion protective properties as a function of NSS exposure time

EIS measurements

The electrochemical characteristics of the layers formed in a defect from coatings with and without lithium-leaching compounds were measured by EIS. Fig. 7.5 shows the Bode plots of the coatings with and without lithium-leaching compounds after 168 h NSS exposure. A non-exposed reference sample was measured to show the initial state of the scribe (damaged area) representing the alloy with a native oxide. After exposure to the corrosive NSS conditions, the Bode plots of the impedance modulus (Fig. 7.5a) of both lithium-leaching coatings show an increase of impedance values in the middle frequency (10^1-10^3 Hz) and low frequency (10^{-1}-10^{-2} Hz) ranges compared to the unexposed sample and the sample without inhibitor. This increase of the impedance modulus in the middle frequency range can be associated with the formation of an (oxide) layer in the damaged area[19]. The increase of the impedance modulus at low frequencies by approximately one order of magnitude can be associated with the increased corrosion resistance of the layers generated from the lithium-leaching coatings.[20] The accompanying phase angle plots of these measurements are shown in Fig. 7.5b. In case of the unexposed scribe the phase angle diagram shows clearly two time-constants, one at 10^1 Hz for the thin oxide layer and one at 10^{-1} Hz related to the electrochemical activity at the aluminium interface in the coating defect, which are characteristic for the native oxide on aluminium.[21] After NSS exposure, the Bode phase angle diagram of the coating without inhibitor shows still two time-constants. However, the time-constant at the middle frequency shifted to a lower frequency and the second time-constant at the low frequency increased slightly. This behavior can be explained due to the formation of corrosion products in the defect area. The Bode phase angle plots for both lithium-leaching coatings show a broadening of the phase angle around 10^1 – 10^3 Hz as a result of the generated layer in the defect area. It can be noted that this phase angle peak has an asymmetric shape and shows a shoulder in the higher frequency area around 10^2 to 10^3 Hz. This asymmetry suggests that there are possibly two overlapping time-constants in this frequency range. The phase angle of the time-constant observed at the low frequency range (10^{-1} Hz) has increased. This increase of the phase angle in the low frequency range can be associated with an improved corrosion protection.

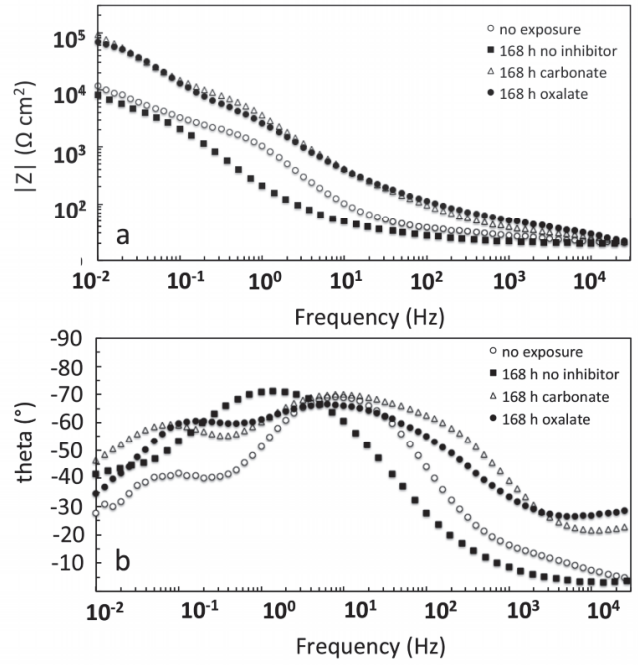

Figure 7.5 Electrochemical impedance spectra of the defect areas of coatings with and without Li-salts on AA2024 aluminium alloy before and after 168h NSS exposure measured in a 0.05M NaCl solution: (a) impedance modulus (b) phase angle plot.

Fig. 7.6 shows the Bode plots representing the behavior of the impedance of the samples with and without lithium-leaching coatings before and after the various exposure times in the NSS. The coating without inhibitor (Fig. 7.6a and d) shows a decrease of the impedance in the mid frequency range and the time-constant shifts to lower frequencies over time. This phenomenon can be explained by the dissolution of the native oxide. When analyzing the Bode impedance modulus plots of the lithium-leaching coatings (Fig. 7.6b and c) it can be noticed that impedance modulus values increase almost instantaneously for both samples due to the NSS exposure. After only 2 h NSS exposure, the impedance modulus values have increased significantly in the middle and low frequency range and increased further as a result of longer exposure times. After 168 h the impedance modulus reaches a maximum. Compared to the sample with the native oxide, the impedance modulus of the hydrated aluminium oxide layer increased by about one order of magnitude in the low frequency range and increased a half order of magnitude in the middle frequency range. The Li-carbonate and Li-oxalate coatings show similar protective behavior independent of the anion used. The Bode phase angle plots of the lithium-leaching coatings are shown in Fig. 7.6d and e. It can be noted that the phase angle of the respective time-constants increased and broadened as a result of the NSS exposure time. Overall, this indicates that the electrochemical characteristics can be linked with the formation of the protective layer as observed in the FESEM cross sections (Fig. 7.3)

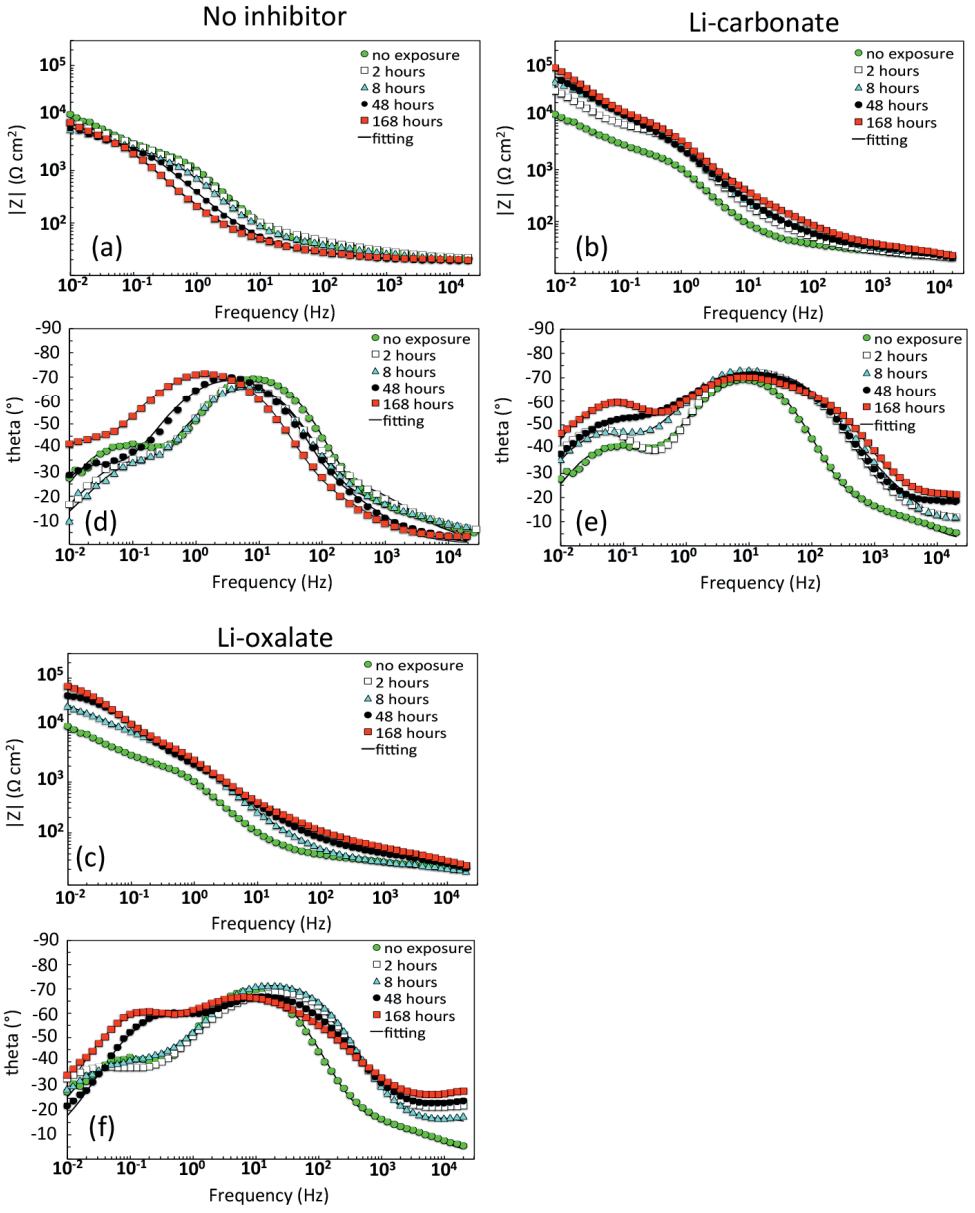

Figure 7.6 Electrochemical impedance spectra of the defect areas of Li-salt loaded coatings on AA2024-T3 aluminium alloy before and after NSS exposure for 2 h up to 168 h: coating with no inhibitor (a) impedance modulus (d) phase angle plot; Li-carbonate loaded coating (b) impedance modulus (e) phase angle plot; Li-oxalate loaded coating (c) impedance modulus (f) phase angle plot.

The EIS spectra of these measurements were fitted with equivalent circuits (ECs) to quantitatively describe the electrochemical properties of the generated layers in the defect during the formation.[22] Fig. 7.7 shows the two equivalent circuit models used to fit the data from the EIS measurements. EC1 is a two time-constant circuit, was used to describe the commonly used physical model of a damaged coating with direct exposed aluminium. This model represents the defect of a damaged coating prior to exposure or when no protective layer is formed (coating without inhibitor) after NSS exposure. In this model R_{sol} represents the resistance of the electrolyte; R_{oxide} is the resistance of the (native) oxide layer and the CPE_{oxide} is the constant phase element (CPE) describing the capacitance of the oxide layer using parameters Q_{oxide} and n_{oxide}, the electrochemical processes at the aluminium interface are represented by R_{pol} and CPE_{dl}. R_{pol} is the polarization resistance and CPE_{dl} is accounting for the double layer capacitance.

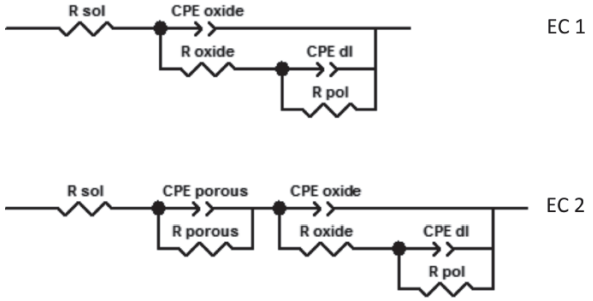

Figure 7.7 Equivalent electric circuits used to fit EIS spectra for coating defect areas: (a) EC1 for unexposed scribe and coating without inhibitor (b) EC2 for the lithium-based inhibitor generated protective layers.

CPE's are commonly used to describe the frequency dependence of elements with a non-ideal capacitive behavior.[23] In this work, CPE is used to account for the dispersive behavior of the time-constants due to the non-uniformity of the layers generated in the defect.[2, 12]
An equivalent circuit model (EC2) with three time-constants was used for the fitting of the EIS spectra of the lithium-leaching samples. The physical morphology of the protective hydrated aluminium oxide layer observed in the defect by FESEM and represented by the Bode phase angle plots (Fig. 7.6e and f) indicate that a three time-constant equivalent circuit model (EC2) is more appropriate compared to the two time-constant model (EC1). The metal/oxide layer interface and dense barrier layer are represented by two clearly defined time-constants at the low ($5 \cdot 10^{-2}$ - 10^{-1} Hz) and middle (10^{1} - 10^{3} Hz) frequency range respectively. The third time-constant of EC2 describes the contribution of the shoulder of phase angle peak at the higher frequencies (10^{2} - 10^{3} Hz) related to the porous middle layer. EC2 can be interpreted as: R_{sol} for the solution resistance, R_{porous} and CPE_{porous} describe the contribution of the porous middle layer, R_{oxide} and CPE_{oxide} represent the dense inner layer, and CPE_{dl} and R_{pol} describe the double layer capacitance and polarization resistance at the metal/oxide interface. The fitted curves are displayed as solid lines in the Bode plots of Fig. 7.6. The numerical values of the fittings from these spectra are listed in Table 7.2, 7.3 and 7.4.

The results for the coating without inhibitor (Table 7.2) showed an initial decrease of R_{oxide} followed by a gradual increase. This behavior could indicate the process of oxide thinning followed by the precipitation of the corrosion products in the defect area.

Table 7.2: Fitted parameters for EIS spectra of the scribed coating without inhibitor after different periods of NSS exposure.

		T=0	T=2 h	T= 8 h	T=48 h	T= 168 h
EC		1	1	1	1	1
R_{sol}	Ω	27	28	24	20	21
Q (CPE_{Oxide})	Ss^ncm^{-2}	$1.16x10^{-4}$	$1.33\ x10^{-4}$	$1.80x10^{-4}$	$2.38x10^{-4}$	$3.50\ x10^{-4}$
n_{oxide}		0.87	0.82	0.78	0.83	0.82
R_{oxide}	Ωcm^2	3846	3799	3990	4506	9931
Q (CPE_{dl})	Ss^ncm^{-2}	$4.30x10^{-4}$	$1.0\ x10^{-3}$	$1.15x10^{-3}$	$1.69\ x10^{-3}$	$2.10\ x10^{-3}$
n_{dl}		0.85	0.90	0.92	0.89	0.95
R_{pol}	Ωcm^2	9683	3820	6954	6591	11609
χ^2		$3.5\ x10^{-3}$	$6.0\ x10^{-3}$	$5.1\ x10^{-3}$	$4,5\ x10^{-3}$	$5.7\ x10^{-3}$

Table 7.3 and 7.4 show the fitting results of the lithium-leaching coatings. The most important observation from these data is the significant increase of R_{oxide} and R_{pol} over time for both coatings related to the generation of a dense oxide layer at the aluminium interface. R_{oxide} increases by a factor 7 and 10 for the Li-carbonate and Li-oxalate loaded coatings respectively. In addition, the polarization resistance increased by a factor 20 for the Li-carbonate loaded coating and a factor 10 for the Li-oxalate loaded coating compared to the native oxide and the coating without inhibitor.

Further analysis and comparison, the equivalent capacitance of the different elements in the equivalent circuit was calculated using the CPE parameters (Q and n) and the resistance corresponding to each time-constant using the equation:

$$C = R^{\frac{(1-n)}{n}} Q^{\frac{1}{n}} \quad (1)$$

This is equation is applicable to a normal time-constant distribution through a surface layer according to Hirschorn et al.[24] The resistance and capacitance of the dense oxide layer (R_{oxide} and C_{oxide}) and the metal/oxide interface (R_{pol} and C_{dl})) was calculated from at least 3 replicate measurements. Fig. 7.8 shows the evolution and scatter of the resistance and capacitance of the oxide layer and the metal/oxide interface as a function of NSS exposure time. Fig. 7.8a shows that resistance of the oxide (R_{oxide}) increased over time due to the formation of the dense layer from the lithium-leaching coatings. Whereas the defect area has a R_{oxide} of about 3.7 kΩ cm^2 before NSS exposure, the resistance almost tripled after only 2 h NSS exposure. Over prolonged exposure, R_{oxide} shows a gradual increase to values

of 25-30 kΩ cm^2 after 168 h (Fig. 7.8a). At the same time, the capacitance of the formed dense layer (C_{oxide}) is reduced by a factor 5 lower after 2 h NSS exposure compared the native oxide and remains stable over time around 20-30 µF/cm^2 (Fig. 7.8c). This behavior can be related to the rapid formation of the dense layer on the substrate and a gradual further densification and reducing porosity increasing the oxide resistance while maintaining its thickness as reflected by the FESEM cross-sectional analysis in Fig. 7.3.

Table 7.3: Fitted parameters for EIS spectra of the scribed Li-carbonate loaded coating after different periods of NSS exposure.

		T=0	T=2 h	T= 8 h	T=48 h	T= 168 h
EC		1	2	2	2	2
R_{sol}	Ω	26	19	21	15	15
$Q(CPE_{porous})$	Ss^ncm^{-2}	-	1.30×10^{-4}	1.95×10^{-4}	1.42×10^{-5}	1.35×10^{-5}
n_{porous}		-	0.69	0.67	0.76	0.75
R_{Porous}	Ωcm^2	-	13	18	15	17
$Q(CPE_{Oxide})$	Ss^ncm^{-2}	1.06×10^{-4}	3.40×10^{-5}	2.89×10^{-5}	3.47×10^{-5}	2.82×10^{-5}
n_{oxide}		0.84	0.87	0.86	0.84	0.81
R_{oxide}	Ωcm^2	3788	9153	17009	17562	29636
$Q(CPE_{dl})$	Ss^ncm^{-2}	4.80×10^{-4}	1.76×10^{-4}	8.18×10^{-5}	5.21×10^{-5}	3.30×10^{-5}
n_{dl}		0.85	0.88	0.76	0.73	0.86
R_{pol}	Ωcm^2	12515	62248	105030	129400	237430
χ^2		3.9×10^{-3}	9.4×10^{-4}	1.1×10^{-3}	1.73×10^{-4}	7.8×10^{-4}

Table 7.4: Fitted parameters for EIS spectra of the scribed Li-oxalate loaded coating after different periods of NSS exposure.

		T=0	T=2 h	T= 8 h	T=48 h	T= 168 h
EC		1	2	2	2	2
R_{sol}	Ω	26	15	15	13	13
$Q(CPE_{porous})$	Ss^ncm^{-2}	-	9.31×10^{-6}	9.98×10^{-6}	1.97×10^{-5}	1.74×10^{-5}
n_{porous}		-	0.76	0.82	0.7	0.7
R_{Porous}	Ωcm^2	-	23	12	24	34
$Q(CPE_{Oxide})$	Ss^ncm^{-2}	1.06×10^{-4}	2.11×10^{-5}	3.55×10^{-5}	3.98×10^{-5}	4.22×10^{-5}
n_{oxide}		0.84	0.83	0.86	0.8	0.77
R_{oxide}	Ωcm^2	3788	10775	8160	9942	37847
$Q(CPE_{dl})$	Ss^ncm^{-2}	4.80×10^{-4}	1.54×10^{-4}	1.31×10^{-4}	2.71×10^{-5}	2.03×10^{-5}
n_{dl}		0.85	0.72	0.7	0.82	0.97
R_{pol}	Ωcm^2	12515	58012	42597	50748	96352
χ^2		7.1×10^{-3}	1.56×10^{-4}	2.7×10^{-4}	5.2×10^{-4}	7.4×10^{-4}

The resistance of the oxide (R_{oxide}) of the coating without inhibitor remains at a level of 5 to 9 kΩ cm^2. In addition, the oxide capacitance of the coating without inhibitor is increasing rapidly indicating degradation of the oxide layer (inset Fig. 7.8c). The corrosion activity at the substrate can be characterized by the time-constant consisting of the polarization resistance (R_{pol}) and the double layer capacitance (C_{dl}). Fig. 7.8b and d show the evolution of the R_{pol} and C_{dl} during the formation of the protective layer in the defect. Compared to the defect prior to NSS exposure, both lithium-leaching coatings show increasing polarization resistance (Fig. 7.8b) and decreasing double layer capacitance (Fig. 7.8d) over time indicating improved corrosion protective properties of the formed layer on the aluminium in the defect area. For the coatings without inhibitor the polarization resistance (R_{pol}) remained around the initial level and the double layer capacitance (C_{dl}) increased to very large values (inset Fig. 7.8d), indicating the presence of the corrosion process. The observed trend of increasing resistances and decreasing capacitances of the lithium-leaching coatings is consistent with the formation and densification of the protective layer in the defect area. The observed effect corresponds with the trend of increasing layer thickness over time in Fig. 7.4.

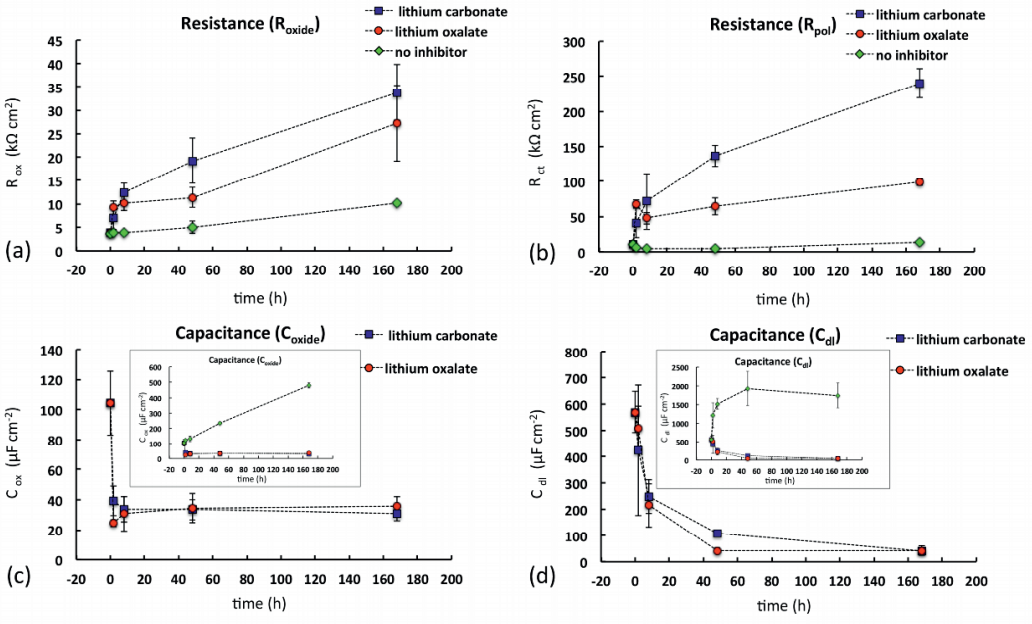

Figure 7.8 Evolution of (a) the dense layer resistance (R_{oxide}), (b) polarization resistance (R_{pol}) of coatings with and without Li-salts, (c) dense layer capacitance (C_{oxide}), and (d) double layer capacitance (C_{dl}) of scribed lithium-leaching coatings during NSS exposure. The insets of (c) and (d) show the evolution of C_{oxide} and C_{dl} in the defect of coatings without inhibitor compared to the Li-leaching coatings.

The inhibition efficiency (IE) of the generated layers in the defect was calculated from the impedance data at the various intervals using the following equation[25, 26]:

$$\mathrm{IE}\ (\%) = \frac{R_{\mathrm{pol\ (lithium)}} - R_{\mathrm{pol\ (no\ inhibitor)}}}{R_{\mathrm{pol\ (lithium)}}} \times 100\% \qquad (2)$$

where $R_{pol(lithium)}$ represents the polarization resistance of the protective layer generated from a lithium-leaching coating and $R_{pol(no\ inhibitor)}$ represents the polarization resistance in the defect from a coating without inhibitor after the same NSS exposure time.

The inhibiting efficiency of the layers generated in a defect area from Li-leaching coatings are shown in Fig. 7.9. The inhibition efficiency of the Li-carbonate loaded coating demonstrates an inhibiting efficiency of around 80% after only 2 h which develops further up to 95% after 48 h and remains at a similar level upon longer exposure. The inhibition efficiency of the protective layer from the Li-oxalate loaded coating develops faster in the first hours, this can be related to the faster layer thickness development of these Li-oxalate loaded coatings in Fig. 7.4.

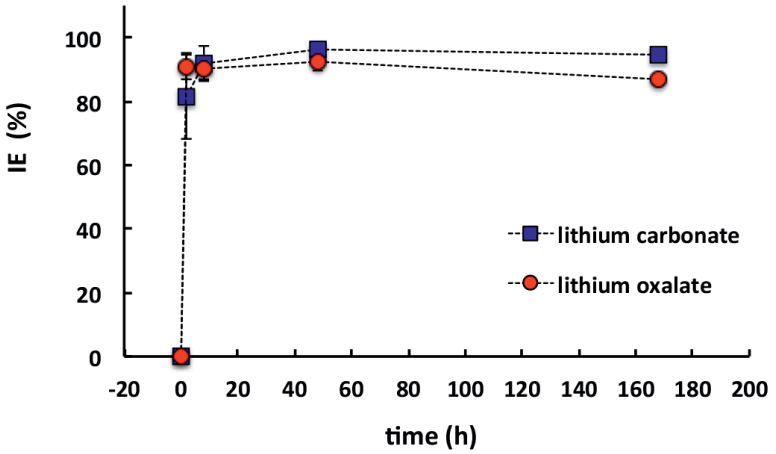

Figure 7.9 Evolution of inhibition efficiency in the defect area of the Li-leaching coatings during NSS exposure.

The development of the inhibition efficiency confirms the fast and effective inhibition provided by protective layers generated in the defect area. Fig. 7.10 shows the schematic equivalent circuit that can be related with the physical morphology of the corrosion protective layer in the defect. Considering the physical morphology of the protective layers and the quantitative EIS results, it can be concluded that the improved corrosion protective properties of the formed layer can be attributed to the rapid formation of the dense and compact layer at the aluminium interface. The impedance part related from the porous part plays only a minor role in the overall corrosion resistance.

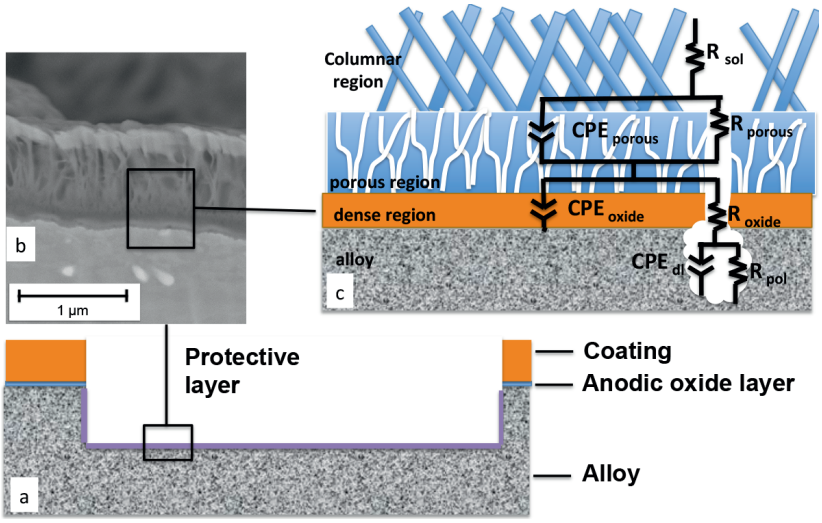

Figure 7.10 Schematic representation of the fitted equivalent circuit based on the physical properties of the protective layer generated in the defect from lithium-leaching organic coatings (a) the defect area with protective layer, (b) the physical coating morphology and (c) schematic representation of EC in protective layer.

Electrochemical micro-cell measurements

Whereas EIS measurements provide averaged information on the electrochemical response of the protective layer in the coating defect over a large area, complementary information on a local scale was obtained using the electrochemical micro-cell technique. This technique provides the opportunity to perform potentiodynamic polarization measurements on the formed layer on a local area in the defect, using a micro-capillary. The micro-cell technique was used to correlate the local passivity (breakdown potential) of the protective layer with the morphology of the layer as observed with the SEM. Fig. 7.11 shows the anodic polarization curves of the protective layer generated in the scribe of the lithium-leaching coatings after different periods of neutral salt spray exposure. Cathodic polarization measurements were not considered since their interpretation can be misleading.[27] The silicone gasket at the end of the micro-capillary is permeable to oxygen This enables the diffusion of oxygen through the gasket, and may increase the oxygen reduction reaction and mask any diffusion control. Fig. 7.11a and b show that the polarization curve of the unexposed samples show that the native oxide has a breakdown potential of about + 0.15 V from the OCP. In contrast to this, the lithium-leaching coatings show a large passivity region with a shift of the breakdown potential to significantly more positive values. In Fig. 7.11a, the Li-carbonate loaded coating shows a shift of the breakdown potential to values from +0.9 up to +1.6 V. These values are already achieved after 2 h exposure and fluctuate over time. The same behavior is observed for the Li-oxalate loaded coatings (Fig. 7.11b). For this system the anodic passive range even exceeds +2.5 V from the OCP after 168 h exposure.

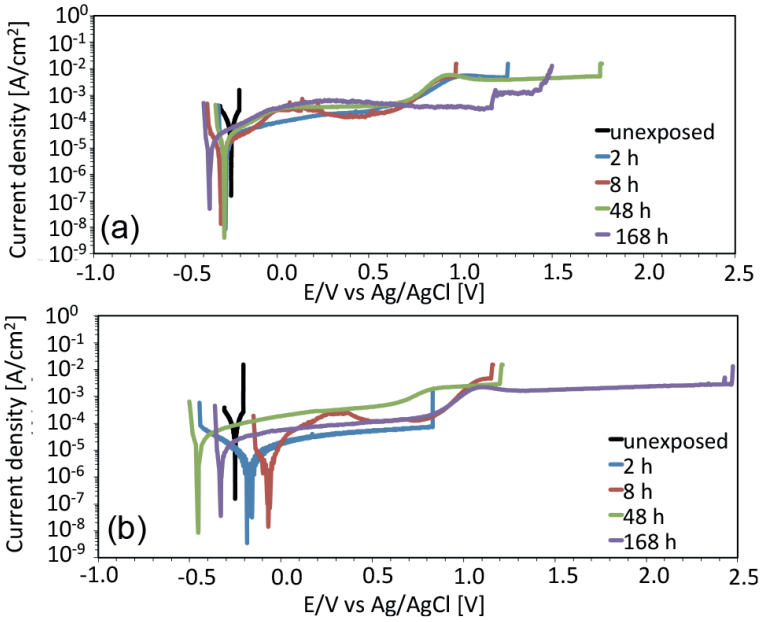

Figure 7.11 Potentiodynamic polarization curves in 0.05 M NaCl, solution acquired with the electrochemical micro-cell (approx. diameter 100 µm) in the defect area after NSS exposure for (a) Li-carbonate loaded coatings and (b) Li-oxalate loaded coatings.

Table 7.5 lists the average corrosion and breakdown potentials for the lithium-loaded coatings systems before and after exposure. It can be noted that there is some scatter for the corrosion potential and breakdown potential. This scatter in electrochemical behavior measured with the local micro-cell technique can be related to the heterogeneous nature of both the aluminium alloy and the oxide layer as also observed by others in previous works[12, 28]. For both lithium-leaching coatings, the polarization curves of the neutral salt spray exposed samples exhibit a large passive behavior compared to the unexposed scribe. However, in the case of the Li-oxalate loaded coatings, a more gradual increase in the average breakdown potential is observed, ranging from +0.4 V after 2 h exposure, and increasing to +0.9, +1.3 and +2.3 V versus OCP after 8, 48 and 168 h, respectively. This can indicate that the protective nature of the layer develops more gradually compared to the Li-carbonate loaded coating.

From these micro-cell measurements, we can conclude that the protective layers are formed quickly and they have a good stability and polarization resistance as shown by the passive anodic behavior and the increased breakdown potential. These results correspond rather well with the FESEM and EIS results, previously discussed. A similar passive behavior was observed by Din et al.[11] who prepared corrosion protective layers with a similar structure on aluminium alloys by the steam assisted oxide growth method.

Table 7.5: Micro-cell data of lithium-leaching coatings after different periods of NSS exposure.

Lithium carbonate				
	Ecorr/V Ag/AgCl (3M KCl)		Ebreak/V Ag/AgCl (3M KCl)	
	Average	St. dev.	Average	St. dev.
t=0	-0.47	0.04	-0.32	0.04
t =2 h	-0.27	0.03	1.49	0.3
t= 8 h	-0.26	0.06	0.9	0.06
t= 48 h	-0.3	0.02	1.6	0.23
t= 7 d	-0.32	0.05	1.1	0.46
lithium oxalate				
	Ecorr/V Ag/AgCl (3M KCl)		Ebreak/V Ag/AgCl (3M KCl)	
	Average	St. dev.	Average	St. dev.
t=0	-0.47	0.04	-0.32	0.04
t =2 h	-0.27	0.03	1.49	0.3
t= 8 h	-0.26	0.06	0.9	0.06
t= 48 h	-0.3	0.02	1.6	0.23
t= 7 d	-0.32	0.05	1.1	0.46

7.3.4 Stability of the protective layer as a function of NSS exposure time

It is essential that the generated protective layer has an irreversible nature and provides long term corrosion protection once formed. The Scanning Vibrating Electrode Technique (SVET) has been used to investigate the long-term resistance to electrochemical degradation of the generated protective layer in the defect. The SVET enables to monitor in situ the distribution and magnitude of local ionic currents over an electrochemically active surface with µm-scale resolution within a mm-sized sample area. Fig. 7.12 shows the SVET maps and the corresponding optical images of the defects of the three systems: unexposed coating without inhibitor and the lithium-leaching coatings after 168 h of exposure to NSS conditions. A sequence of SVET maps was obtained for each system at different immersion times in NaCl solution.

Fig. 7.12a shows SVET maps corresponding to the unexposed coating without inhibitor. After initiation of the immersion, the map shows low current density values below 10 µA·cm^2 and no clear evidences of corrosion activity. Optical image of the sample showed a pristine surface. After 24 h, local activity is observed in the SVET map. A localized anodic region was detected with maximum current density values of about 50 µA·cm^2. Cathodic regions were observed next and close to the anodic area, with maximum current density values of around -50 µA·cm^2. This activity is also confirmed by the optical image of the sample that showed indications of corrosion in the defect. After 7 d, SVET measurements were not possible due to the presence of voluminous corrosion products in the defect area. In the case of the lithium-leaching coatings, both, the Li-carbonate (Fig. 7.12b) as well as the Li-oxalate (Fig. 7.12c) systems showed SVET maps with very low anodic and cathodic current densities (less than 10 µA·cm^2) up to 14 d exposure to the electrolyte.

Furthermore, no corrosion products or pits are being formed in the defect area over time. In addition to the fast and effective formation of the protective layer in the defect, these SVET results demonstrate the irreversible nature of the corrosion resistance provided the hydrated aluminium oxide layer which is essential to ensure long-term corrosion protection.

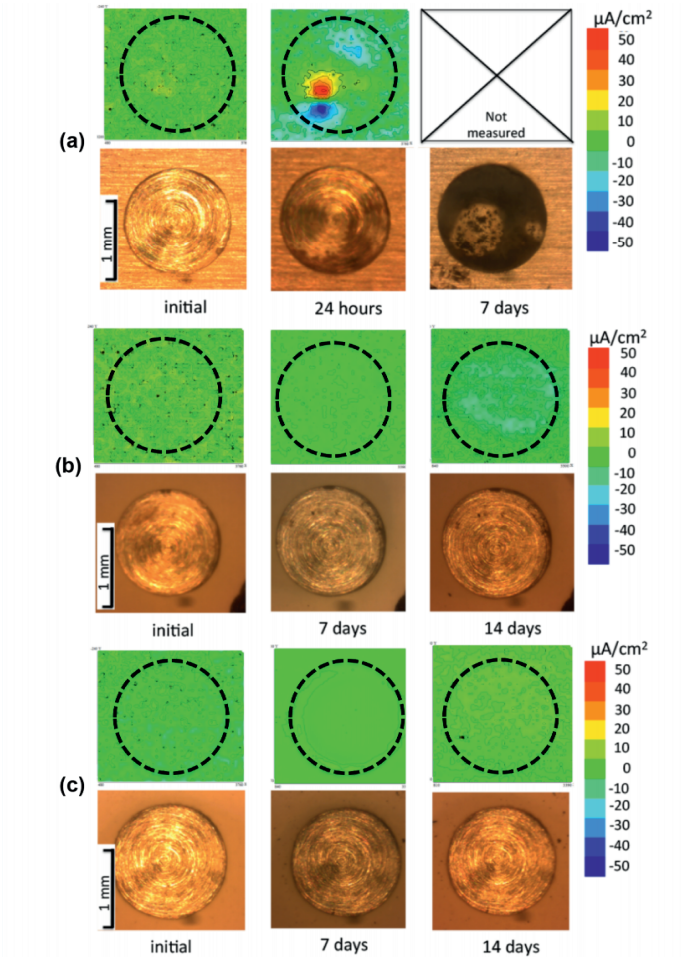

Figure 7.12 SVET maps to study the stability of the protective layers in a defect area immersed in 0.05M NaCl solution as a function of time: (a) uninhibited reference coating, (b) Li-carbonate coating after 168h NSS exposure, (c) Li-oxalate coating after 168h NSS exposure.

7.3.5 Corrosion inhibition mechanism with lithium-leaching coatings

The results demonstrate that the corrosion inhibiting mechanism of these lithium-leaching coatings is fundamentally different compared to previously studied corrosion inhibitors. Corrosion inhibitors such as vanadates, cerium compounds, and organic inhibitors are known to inhibit by precipitation on the heterogeneous surface microstructure of AA2024-

T3, hence preventing high microgalvanic activity.[29-33] The inhibition mechanism of the lithium-leaching coatings differentiates itself from other inhibitor technologies by the spontaneous conversion of the surface of a damaged area with a relatively thick and stable hydrated aluminium oxide layer.

Although thicker and different in nature, the behavior of these protective layers is comparable to an anodic oxide layer or layers generated by chemically assisted hydrothermal sealing.[22, 34] Oxides generated by these treatments also cover the entire aluminium interface with a duplex layer consisting of a dense inner barrier layer and porous outer layer but these are generally prepared in well-controlled solutions and need a considerable amount of energy.[19, 35] There is no clear difference between the protective properties of the layers generated from the two different lithium-salts. Although, electrochemical and microscopy results indicate that the layers generated from the Li-oxalate loaded coatings are forming faster compared to the Li-carbonate loaded coating. However, there is not a significance difference in corrosion protection between the layers generated from both salts. These results combined with the previous results on the morphology of the layer, leaching behavior and pH development provide more understanding about the processes during development and characteristics of the protective properties of these layers generated in the defect from lithium-leaching organic coatings.[2, 3] It must be noted that, due to the nature of the NSS exposure test, these experiments did not provide exact information about the lithium concentration needed to obtain this degree of corrosion protection. More research is needed to investigate the role of lithium in this corrosion inhibiting mechanism in more detail.

7.4. Conclusions

The electrochemical characteristics of the corrosion protective layers generated in a coating defect from lithium-leaching coatings on AA2024-T3 aluminium alloys when exposed to neutral salt spray conditions over time were studied. The electrochemical properties were linked with the physical properties of the protective properties using microscopy and (local) electrochemical techniques. Effective corrosion inhibition from these lithium-leaching coatings was observed after NSS exposure. Cross-sectional microscopic analysis revealed the fast and effective growth of protective layers in thickness and morphology covering the entire damaged area. The complementary results obtained from (local) electrochemical techniques demonstrate the development of the corrosion resistant properties due to the generation of a protective layer in the defect area and this layer exhibits an irreversible long-term resistance to corrosive conditions. The corrosion protective properties of this layer can be attributed to the dense inner layer of the protective layer. There were no significant differences in corrosion protection observed between Li-carbonate and Li-oxalate salts. The results of this study confirm the fast and effective active protective nature of these lithium-leaching coatings.

References

1. P. Visser and S. A. Hayes, Low-temperature-curable coating composition useful as anticorrosive primer coating for non-ferrous metal substrates, particularly aluminum or aluminum alloy, comprises film-forming resin, curing agent, and lithium salt, *patent nr. WO2010112605-A1*, 2010.
2. P. Visser, A. Lutz, J. M. C. Mol and H. Terryn, Study of the formation of a protective layer in a defect from lithium-leaching organic coatings, *Progress in Organic Coatings*, 2016, 99, 80-90.
3. P. Visser, Y. Liu, X. Zhou, T. Hashimoto, G. E. Thompson, S. B. Lyon, L. G. J. van der Ven, A. J. M. C. Mol and H. A. Terryn, The corrosion protection of AA2024-T3 aluminium alloy by leaching of lithium-containing salts from organic coatings, *Faraday Discussions*, 2015, 180, 511-526.
4. P. Visser, Y. Liu, H. Terryn and J. M. C. Mol, Lithium salts as leachable corrosion inhibitors and potential replacement for hexavalent chromium in organic coatings for the protection of aluminum alloys, *Journal of Coatings Technology and Research*, 2016, 13, 557-566.
5. R. K. Hart, The formation of films on aluminium immersed in water, *Transactions of the Faraday Society*, 1957, 53, 1020-1027.
6. T. Kudo and R. S. Alwitt, Cross-sections of hydrous and composite aluminum oxide films, *Electrochimica Acta*, 1978, 23, 341-345.
7. R. S. Alwitt, The Growth of Hydrous Oxide Films on Aluminum, *Journal of the Electrochemical Society*, 1974, 121, 1322-1328.
8. R. G. Buchheit, Bode, M.D., Stoner, G.E., Corrosion-Resistant, Chromate free Talc Coatings for Aluminum, *Corrosion*, 1994, 50, 205-214.
9. C. A. Drewien, Eatough, M.O., Tallant, D.R., Hills, C.R., Buchheit, R.G., Lithium-aluminum-carbonate-hydroxide hydrate coatings on aluminum: Composition, structure and processing bath chemistry, *Journal of material research*, 1996, 11, 1507-1513.
10. R. U. Din, V. C. Gudla, M. S. Jellesen and R. Ambat, Accelerated growth of oxide film on aluminium alloys under steam: Part I: Effects of alloy chemistry and steam vapour pressure on microstructure, *Surface and Coatings Technology*, 2015, 276, 77-88.
11. R. U. Din, K. Bordo, M. S. Jellesen and R. Ambat, Accelerated growth of oxide film on aluminium alloys under steam: Part II: Effects of alloy chemistry and steam vapour pressure on corrosion and adhesion performance, *Surface and Coatings Technology*, 2015, 276, 106-115.
12. Y. Liu, P. Visser, X. Zhou, S. B. Lyon, T. Hashimoto, M. Curioni, A. Gholinia, G. E. Thompson, G. Smyth, S. R. Gibbon, D. Graham, J. M. C. Mol and H. Terryn, Protective Film Formation on AA2024-T3 Aluminum Alloy by Leaching of Lithium Carbonate from an Organic Coating, *Journal of The Electrochemical Society*, 2016, 163, C45-C53.
13. Y. Liu, P. Visser, X. Zhou, S. B. Lyon, T. Hashimoto, A. Gholinia, G. E. Thompson, G. Smyth, S. R. Gibbon, D. Graham, J. M. C. Mol and H. Terryn, An investigation of the corrosion inhibitive layers generated from lithium oxalate-containing organic coating on AA2024-T3 aluminium alloy, *Surface and Interface Analysis*, 2016, 48, 798-803.
14. T. Suter and H. Böhni, A new microelectrochemical method to study pit initiation on stainless steels, *Electrochimica Acta*, 1997, 42, 3275-3280.
15. P. Visser , H. A. Terryn and J. M. Mol, in *Active Protective Coatings, New-Generation Coatings for Metals*, eds. A. E. Hughes, J. M. Mol, M. L. Zheludkevich and R. G. Buchheit, Springer, Netherlands, 1 edn., 2016, vol. 233, ch. 12, pp. 315-372.
16. T. Hurlen and A. T. Haug, Corrosion and passive behaviour of aluminium in weakly alkaline solution, *Electrochimica Acta*, 1984, 29, 1133-1138.
17. M. R. Tabrizi, S. B. Lyon, G. E. Thompson and J. M. Ferguson, The long-term corrosion of aluminium in alkaline media, *Corrosion Science*, 1991, 32, 733-742.
18. R. T. Foley and T. H. Nguyen, The Chemical Nature of Aluminum Corrosion: V . Energy Transfer in Aluminum Dissolution, *Journal of The Electrochemical Society*, 1982, 129, 464-467.
19. B. Van der Linden, H. Terryn and J. Vereecken, Investigation of anodic aluminium oxide layers by electrochemical impedance spectroscopy, *Journal of Applied Electrochemistry*, 1990, 20, 798-803.
20. J. Tedim, M. L. Zheludkevich, A. C. Bastos, A. N. Salak, A. D. Lisenkov and M. G. S. Ferreira, Influence of preparation conditions of Layered Double Hydroxide conversion films on corrosion protection, *Electrochimica Acta*, 2014, 117, 164-171.

21. M. L. Zheludkevich, K. A. Yasakau, S. K. Poznyak and M. G. S. Ferreira, Triazole and thiazole derivatives as corrosion inhibitors for AA2024 aluminium alloy, *Corrosion Science*, 2005, 47, 3368-3383.
22. B. Kuznetsov, M. Serdechnova, J. Tedim, M. Starykevich, S. Kallip, M. P. Oliveira, T. Hack, S. Nixon, M. G. S. Ferreira and M. L. Zheludkevich, Sealing of tartaric sulfuric (TSA) anodized AA2024 with nanostructured LDH layers, *Rsc Advances*, 2016, 6, 13942-13952.
23. C.H. Hsu and F. Mansfeld, Concerning the conversion of the Constant Phase Element Parameter Yo into a Capacitance *Corrosion*, 2001, 57, 747.
24. B. Hirschorn, M. E. Orazem, B. Tribollet, V. Vivier, I. Frateur and M. Musiani, Determination of effective capacitance and film thickness from constant-phase-element parameters, *Electrochimica Acta*, 2010, 55, 6218-6227.
25. A. A. Al-Amiery, F. A. Binti Kassim, A. A. H. Kadhum and A. B. Mohamad, Synthesis and characterization of a novel eco-friendly corrosion inhibition for mild steel in 1M hydrochloric acid, *Scientific Reports*, 2016, 6, 19890.
26. S. Martinez and M. Metikos-Hukovic, A nonlinear kinetic model introduced for the corrosion inhibitive properties of some organic inhibitors, *Journal of Applied Electrochemistry*, 2003, 33, 1137-1142.
27. R. Oltra, B. Vuillemin, F. Thebault and F. Rechou, Effect of the surrounding aeration on microcapillary electrochemical cell experiments, *Electrochemistry Communications*, 2008, 10, 848-850.
28. F. Andreatta, M. E. Druart, A. Lanzutti, M. Lekka, D. Cossement, M. G. Olivier and L. Fedrizzi, Localized corrosion inhibition by cerium species on clad AA2024 aluminium alloy investigated by means of electrochemical micro-cell, *Corrosion Science*, 2012, 65, 376-386.
29. M. Iannuzzi, T. Young and G. S. Frankel, Aluminum alloy corrosion inhibition by vanadates, *Journal of the Electrochemical Society*, 2006, 153, B533-B541.
30. K. D. Ralston, S. Chrisanti, T. L. Young and R. G. Buchheit, Corrosion inhibition of aluminum alloy 2024-T3 by aqueous vanadium species, *Journal of the Electrochemical Society*, 2008, 155, C350-C359.
31. B. R. W. Hinton, Corrosion inhibition with rare earth metal salts, *Journal of Alloys and Compounds*, 1992, 180, 15-25.
32. T. G. Harvey, S. G. Hardin, A. E. Hughes, T. H. Muster, P. A. White, T. A. Markley, P. A. Corrigan, J. Mardel, S. J. Garcia, J. M. C. Mol and A. M. Glenn, The effect of inhibitor structure on the corrosion of AA2024 and AA7075, *Corrosion Science*, 2011, 53, 2184-2190.
33. G. Williams, A. J. Coleman and H. N. McMurray, Inhibition of Aluminium Alloy AA2024-T3 pitting corrosion by copper complexing compounds, *Electrochimica Acta*, 2010, 55, 5947-5958.
34. S. J. Garcia-Vergara, P. Skeldon, G. E. Thompson and H. Habazaki, A tracer investigation of chromic acid anodizing of aluminium, *Surface and Interface Analysis*, 2007, 39, 860-864.
35. J. D. Gorman, A. E. Hughes, D. Jamieson and P. J. K. Paterson, Oxide formation on aluminium alloys in boiling deionised water and NaCl, CeCl3 and CrCl3 solutions, *Corrosion Science*, 2003, 45, 1103-1124.

Chapter 8

The Chemical Throwing Power of Lithium-Based Inhibitors from Organic Coatings on AA2024-T3

The efficacy and reach of leachable corrosion inhibitors depends on their leach rate and can be influenced by parameters such as inhibitor solubility, concentration in the coating, and water flux in the coating. The work presented in the previous chapters demonstrated the fast and effective protection of the lithium-leaching technology in coating defects. This chapter discusses the active protective performance of the lithium-leaching coating technology using systems with a high and low loading of lithium-salts in artificial defects with increasing width. The chemical throwing power of the lithium-leaching coating technology was linked with properties such as leach rate, corrosion inhibition, lithium spread in the defect areas and composition of the protective layer.

This chapter published as a scientific paper:

P. Visser, K. Marcoen, G.F. Trindade, M.L. Abel, J.F. Watts, T. Hauffman, J.M.C. Mol, H. Terryn, The chemical throwing power of lithium-based inhibitors from organic coatings on AA2024-T3, *Corrosion Science*, 150 (2019) 194-206.

Abstract

Chemical throwing power, being the distance over which an inhibitor is able to protect a defect effectively, is an important parameter for active protective coatings. This study investigates the chemical throwing power of lithium-based leachable corrosion inhibitors exhibiting different leaching kinetics, from coatings at different inhibitor loading concentrations. The results demonstrate that Li-salt loaded coatings provide corrosion protection of defect areas up to a width of 6 mm. Time-of-flight secondary ion mass spectrometry (ToF-SIMS) was used to detect the lateral spread of Li in the defect areas and provide the chemical speciation of corrosion protective layers in the defect areas.

8.1 Introduction

Traditionally, active protective coatings have typically two functionalities. Firstly, the coating provides barrier properties and secondly, active corrosion protection can be achieved by the ability to release corrosion inhibitors from the coating matrix into in a defect area in case the coating is damaged. Leaching of the inhibitor is the complex process where condensed moisture diffuses into the coating matrix and triggers the dissolution of the corrosion inhibitor and facilitates the transport of the corrosion inhibitive species from the coating matrix to the exposed substrate.[1] The release kinetics and the capacity of the reservoir of corrosion inhibitor in the coating are essential parameters to consider for such active protective systems.[2, 3] The inhibitor release kinetics are affected by the solubility of the corrosion inhibitor, the loading in the coating, and the microstructure of the coating matrix.[4] Several studies have been performed on the leaching behaviour of chromate inhibitors, which have been the industry standard for an effective active corrosion protection for many decades. [5-10] In these studies it was found that the inhibitor release does not occur via diffusion through the resin of the coating itself and is not controlled by a Fickian diffusion process either.[5, 6] Instead, the inhibitor is released due to the direct dissolution of clusters of inhibitors, which are in contact with the electrolyte at the surface of the coating or at the defect area.[8] After this initial fast inhibitor release, the process continues via diffusion through a fractional network of voids and inter-connected pathways deeper in the coating matrix left after the prior dissolution of the corrosion inhibitor, resulting in a slower inhibitor release over time.[8, 9] This knowledge has been modelled to further understand the mechanism of inhibitor transport in coatings.[6, 7]

Another important parameter is the distance over which the coating is able to protect a defect effectively, known as the "throwing power".[11, 12] The ability of a coating to provide corrosion protection of a defect by the release of inhibitors can be classified as the "chemical" throwing power, this process involves a concentration gradient-driven random transport from inhibitor-rich regions (coating) to unprotected sites (defect).[13] Scully and Presuel-Moreno studied the phenomenon of chemical throwing power in addition with the galvanic throwing power using an Al-Co-Ce metallic coating over AA2024-T351 under thin electrolyte films representative of atmospheric conditions and demonstrated the effect of defect size, showing that the larger the scratch size, the more difficult it is to transport sufficient inhibitor to the centre-line of the defect and suppress corrosion.[12, 14] In addition to the galvanic protection mechanism, the conditions for the chemical throwing power under which Al-Co-Ce coatings released and transported Ce^{3+} ions to a defect on AA2024-T351 was investigated. One of the key criteria to obtain effective inhibition by was the ability to achieve a critical inhibitor concentration in the defect within a few hours. It was demonstrated that that such Al-Co-Ce coatings could be tailored to optimize coating functionality by a combination of galvanic and chemical inhibition properties.

The concept of chemical throwing power can also be projected on the concept of active corrosion protection from coatings with an organic matrix. Fig. 8.1 shows the concept of

chemical throwing power as the lateral spread of a corrosion protective layer in a defect as a result of the release of corrosion inhibiting species from a coating matrix through leaching. Inhibitor leaching is triggered by water ingress through the top-surface and the cut-edge of the coating to provide active protection in the defect area. In addition to parameters such as inhibitor leach-rate and permeability of the coating matrix are key criteria to obtain the critical inhibitor concentration. In addition to this, the irreversibility or stability of the developed passive layer in the defect is an other important aspect to obtain effective active corrosion protection.[13, 15]

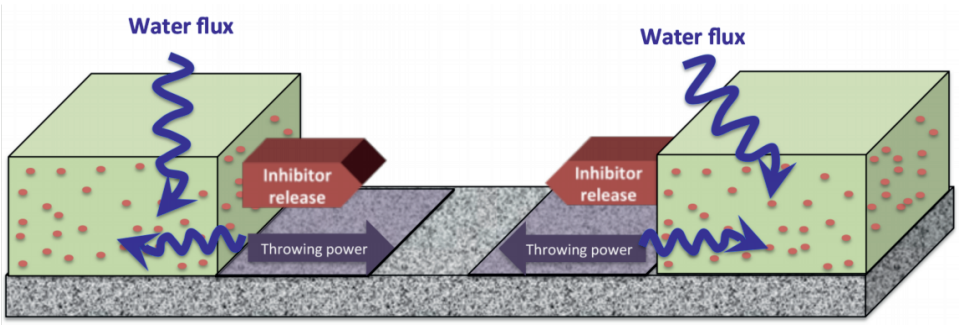

Figure 8.1 *The concept of chemical throwing power by active corrosion protective coatings*

In 2010, Li-salts were introduced as leachable corrosion inhibitor in active protective coatings for the protection of aluminium alloys.[16] Several studies have demonstrated that Li-leaching coatings provide fast, effective and irreversible corrosion protection in a coating defect and the technology is regarded as a promising environmentally friendly alternative to the toxic chromates.[17-19]. The active protective properties of these coatings are obtained by the leaching of Li-salts from the organic coating matrix, this release of the Li-salts provides favourable alkaline conditions in the defect area which facilitates the formation of a protective aluminium oxide/hydroxide layer in the defect area.[20, 21] The protective layer comprises mainly aluminium, oxygen and lithium and electrochemical studies revealed that the corrosion protective properties of the layer could be linked to the dense layer at the aluminium substrate.[20, 22] Further investigations showed that the protective layer in the defects featured different surface morphologies which indicates possible different compositions as a consequence of different Li concentrations and pH during the formation of the layer. [23, 24] Marcoen et al. used the high sensitivity towards Li and the high lateral resolution of time-of-flight secondary ion mass spectrometry (ToF-SIMS) to investigate the Li-spread in a 1 mm wide defect area and unravelled the surface composition of the protective layers.[25] It was found that the Li-spread in a 1 mm wide defect area was relatively fast and the entire defect area was covered with Li-based species within 15 minutes of exposure in the neutral salt spray test (NSS). Short exposures to these corrosive conditions induced the formation of a Li-containing pseudoboehmite (Li-PB) and longer

exposure times resulted in higher Li-concentrations in the defect area and the formation of a Li-based layered double hydroxide (Li-LDH) covering the entire surface area. However, the chemical throwing power of Li-salts as corrosion inhibitor by leaching from organic coatings has not been studied yet.

This paper presents the study of the chemical throwing power of Li-salts, i.e. lithium carbonate and lithium oxalate, when incorporated into organic coatings as leachable corrosion inhibitor. Firstly, the leaching characteristics and the corrosion protective properties of organic coatings with high and low loadings of Li-salts were investigated. Then, the chemical throwing power was assessed by exposing these coatings with increasing defect widths up to 6 mm to neutral salt spray conditions for 7 days. The corrosion protective performance of the systems was assessed optically and by using profilometry. In addition, ToF-SIMS was used to investigate the lateral Li-spread and the surface composition of the protective layer in the defect areas. This study provides a further understanding of the active corrosion protective properties, the surface composition of the protective layer in the defect area and demonstrates the "chemical" throwing power of the Li-salt based inhibitor leaching technology, a feature that has not been demonstrated for any other chromate-free inhibitor leaching coating technology.

8.2. Experimental

8.2.1 Materials and sample preparation

Inhibitor loaded coatings

Polyurethane model coatings with a total pigment volume concentration (PVC) of 30% and respective loadings of 15 and 2.5% PVC Li-salt as leachable corrosion inhibitor were used in this study. The composition of the model coatings is listed in Table 1. Analytical grade lithium carbonate and lithium oxalate were acquired from Sigma-Aldrich.

Table 8.1: Composition of the Li-salt loaded organic model coatings

leachable inhibitor		lithium carbonate		lithium oxalate	
loading (PVC %)		15%	2.50%	15%	2.50%
Component A					
N-Butylacetate	Sigma Aldrich	85.0 g	85.0 g	85.0 g	85.0 g
Desmophen 650MPA	Covestro	47.7 g	47.7 g	47.7 g	47.7 g
Lithium carbonate	Sigma Aldrich	23.6 g	3.6 g	-	-
Lithium oxalate	Sigma Aldrich	-	-	23.2 g	3.6 g
Magnesium oxide	Sigma Aldrich	16.4 g	16.4 g	16.4 g	16.4 g
Tioxide TR 92	Huntsman	5.2 g	5.2 g	5.2 g	5.2 g
Blanc Fixe N ($Ba(SO_4)$)	Sachtleben	15.4 g	58.1 g	15.4 g	58.1 g
Component B					
Tolonate HDB 75 MX	Vencorex	28.5 g	28.5 g	28.5 g	28.5 g
Dynasilan Glymo	Evonik	5.2 g	5.2 g	5.2 g	5.2 g

Preparation of the organic model coatings

The Li-leaching model coatings were prepared in a similar way as described in previous papers.[20, 21] Component A was prepared by the sequential addition of the raw materials to a 370 ml glass jar. After mixing the materials to a homogeneous mixture, 400 grams of Zirconox pearls® (1.7-2.4 mm) were added and the samples were shaken on a Skandex® paint shaker to grind and disperse the pigments to a grind fineness less than 25 µm. After this shaking procedure, the pearls were separated from the paint and Component B was added. The paint was then stirred for 5 minutes to a homogeneous mixture.

Sample preparation

Sheet material of AA2024-T3 aluminium alloy with a thickness of 0.8 mm was anodized according aerospace requirements (AIPI 02-01-003) in tartaric sulphuric acid (TSA) to obtain an anodic film with a thickness of 3-3.5 µm. The model coatings were applied using a high-volume low-pressure (HVLP) spray gun at 23°C and 55% relative humidity. After the application, all coatings were cured with a forced cure cycle of 16 h at 80°C after a 1 h flash-off period. All coatings had a dry film layer thickness of 20-25 µm.

Inhibitor leaching

Two coated panels of 7 x 2 cm were immersed in a plastic test tube (total sample area 28 cm^2) with 50 ml demineralized water to study the leaching behaviour of the coatings with different loading concentrations of corrosion inhibitor. After 4 h, 24 h, 72 h, 120 h and 192 h immersion the entire solution with the leached inhibitor was removed and replaced by fresh demineralized water. The removed solutions were acidified with nitric acid to a concentration of 0.1M and analysed with inductively coupled plasma atomic emission spectroscopy (Arcos NT ICP-AES) using scandium as an internal standard. On order to compare the different coatings, the accumulated release of Li in mM/L in the water was normalized to a dry film thickness of 25 µm/cm^2. All measurements for the leaching curves were executed in triplicate.

Corrosion protection in the defect area

In order to assess the active protective properties of these coatings, an artificial defect consisting of two intersecting scribes with a width of 1 mm, a length of 2 cm and a depth of 100-150 µm was made in the coatings by mechanical milling. The damaged coatings were exposed to the neutral salt spray test (NSS) according to ASTM-B117 for 168 h. After the exposure the scribes were studied using microscopy techniques.

Inhibitor throwing power

Coated panels with four parallel defects with varying widths (0.5 mm, 1.5 mm, 3mm and 6 mm) were prepared using a Gravograph® mechanical engraving machine as shown in Fig. 8.2. The panels were placed in the NSS cabinets at an angle of 20 degrees with a vertical

positioning of the defects to assess the lateral chemical throwing power of these active corrosion inhibiting coating systems.
After 168 h NSS exposure, the scribed panels were examined with an optical microscope and the surface roughness (Sa) of the defect areas was measured with a Bruker K1 white light interferometer using a 20 X objective. The Sa value expresses the surface roughness of an area, as an absolute value, the difference in height of each point compared to the arithmetical mean of the surface. All data was analysed with the Vision for Profilers (version 4.2) software.

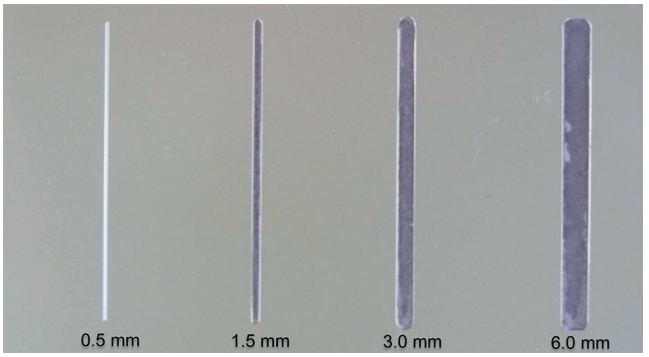

Figure 8.2 Example of a coated panel with vertical scribes ranging from 0.5 mm to 6 mm in width used to assess the chemical throwing power.

Reference samples

Reference samples were prepared for the compositional analysis of the deposites generated within the protective layer in the defect area.[25] Aluminium panels, AA2024-T3 (0.8 mm thickness), were cleaned with acetone (> 99.9%, SASOL Chemie Gmbh & Co. KG) and scribed (1 mm) as described above. Pseudoboehmite (PB) and Li-containing pseudoboehmite (Li-PB) reference samples were prepared according to the method of Gorman et al. by immersing the scribed panels in (i) demineralized water or (ii) a 0.02 M LiCl (BioXtra, ≥99.0%, Sigma–Aldrich) solution in demineralized water at 95-100°C for 1 hour to obtain PB or Li-PB respectively.[26] In addition, a Li-based layered double hydroxide (Li-LDH) reference coating was obtained by the immersion of a scribed AA2024-T3 panel in a 0.1 M Li-carbonate solution for 15 min according to the method of Buchheit et al.[27]. Following the treatment, the panels were rinsed with copious amounts of demineralized water and dried at the air. All ToF–SIMS measurements were performed in the scribed areas.

8.2.2 Surface analytical methods

Optical and scanning electron microscopy (SEM)

The defect areas were examined by optical and scanning electron microscopy techniques. The optical microscope was used to visualize the effects of the corrosive conditions in the

defect areas of the coatings. A JEOL JSM-7100F field emission scanning electron microscope was used to study the surface and cross-section morphology of the corrosion inhibiting layers in the defect areas. The surface morphology investigations were performed with the secondary electron detector (SEI) using an acceleration voltage of 5 kV at a working distance of 10 mm. The cross-sectional analysis of the defect areas were performed with a backscatter electron detector (BED-C) at 5 kV and a working distance of 3 mm. Prior to the analysis of the cross-sections, the samples were sectioned with a diamond saw and the defect area was prepared with a Hitachi IM4000 ion milling system using 6kV Ar-ion acceleration, a rotation speed of 3 rpm and a swing angle of +/- 30°.

Time-of-Flight Secondary Ion Mass Spectrometry (ToF-SIMS)

In order to study the Li-spread in the defect areas, ToF-SIMS measurements were performed on a TOF.SIMS 5 system (ION-TOF GmbH, Münster, Germany). Positive ion mass spectra were acquired over a mass range of 1–800amu using a 30keV Bi^+_3 primary-ion beam operated in the high current bunched mode for high mass resolution (m/Δm approximately 8000 at 29amu ($^{29}Si^+$)). A lateral resolution of 3 µm was achieved in the high current bunched mode and the pulsed ion beam target current was approximately 0.37pA. A list of fragments of known composition (CH^+_3 , $C_2H_3O^+$, $LiOH^+$, $AlOH^+$ and Al^+_2) was used to calibrate the mass spectra. The accuracy of a mass assignment (Δ in ppm) was calculated by dividing the absolute difference between the experimental (M_{ex}) and theoretical (M_r) mass of a fragment by the experimental mass, as shown below:

$$\Delta = \frac{|M_{ex} - M_r|}{M_r} \cdot 10^6 \qquad (1)$$

The images of the large scribe areas after NSS exposure and the images of PB, Li-PB and Li-LDH reference samples were obtained by rastering the scribe area in patches of 400 µm × 400 µm. The analysis time of each patch was 60 s, using a pixel density of 250 pixels/mm. Based on a compositional analysis of Marcoen et al.[25], a characteristic peak list was created for the reference materials and subsequently applied to spectra obtained by large area imaging of NSS exposed scribes.

Compositional analysis using a multivariate analysis method (MVA)

Since every pixel of the ToF-SIMS image contains a complete mass spectrum, large area ToF-SIMS imaging provides large amounts of data. Multivariate analysis (MVA) is an efficient tool for ToF-SIMS data analysis.[28] Especially, in this work the main reason to use MVA is that the compounds of interest will share most of the secondary ions thus making them unambiguously distinguishable only via MVA methods A peak list containing, characteristic for the reference materials, was first created using the *SurfaceLab* software (IONTOF GmbH) and data cuboids containing the maps of the areas of all selected peaks were then exported as binary .BIF6 files for each large area surface analysed.. The .BIF6

files were loaded into the *simsMVA* MATLAB app (http://mvatools.com) using the stitch function to perform matrix augmentation and create a single matrix containing all (stitched) patches and the reference images enabling the entire dataset to be processed as a single matrix.[29] The insertion of rows containing measurements of well-known reference materials has proven to be effective and more details of the methodology can be found elsewhere.[25, 28, 30]

Prior to MVA, two pre-processing steps were performed: normalisation of all map intensities by total counts per pixel and Poisson scaling of the peak intensities according to a method proposed in the literature[31]. Non-negative matrix factorisation (NMF) was then applied to the resulting dataset. NMF is a non-supervised machine learning method that seeks to reduce the dimensionality of a dataset down to a few "pure compounds".[30, 32] This method enables the interpretation and visualization of the surface chemistry because it provides data that can be directly assigned to fingerprint mass-spectra of "pure" compounds and their distribution maps.[30] The algorithm used to achieve non-negative factorisation of all datasets presented in this paper is the one created by Lee and Seung[33], based on multiplicative update rules and applied by Trindade et. al.[30]

8.3. Results and Discussion

8.3.1. Leaching behaviour of the coatings

Leaching profiles were obtained for the Li-salt loaded coatings with 15 and 2.5% PVC Li-salt. Fig. 8.3 shows the accumulative inhibitor release for the coatings in mM/L during 200 h leaching. The inset of Fig. 8.3 shows the expanded graph for the samples with a lower Li release from the coating.

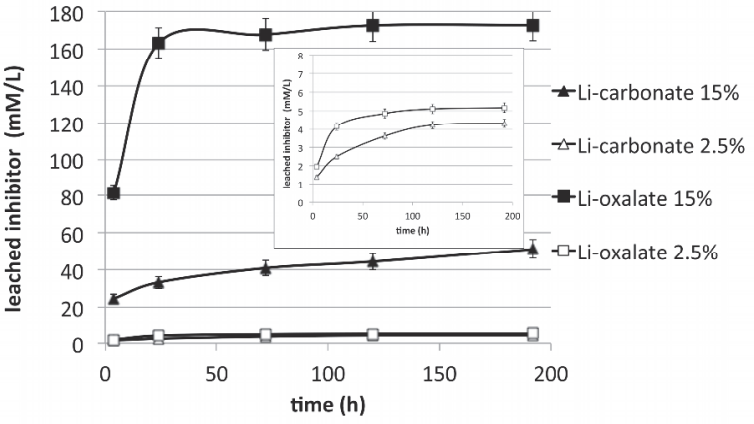

Figure 8.3 *Accumulated release of corrosion inhibitor from coatings containing high (15% PVC) and low (2.5% PVC) loadings of Li-salt, normalized per cm2 model coating with a thickness of 25 µm over a 192 h exposure time period.*

From the graphs it can be noted that both Li-salt loaded coatings with 15% PVC inhibitor leach significantly faster compared to the coatings loaded with only 2.5% PVC inhibitor. The 15% PVC Li-oxalate sample in particular leaches faster at higher concentrations of Li compared to the sample with 15% PVC Li-carbonate. These differences and of magnitude are in line with the solubility of these corrosion inhibitors being 1.3 g/100ml for Li-carbonate[34] and 8.0 g/100 ml for Li-oxalate[35].

The inhibitor release of corrosion inhibitors from an organic coatings depends on the PVC and the quantity and solubility of the corrosion inhibitor in the coating [4]. Since all coatings in this study were formulated to a total PVC of 30%, the leaching curves demonstrate that the dissolution of Li from these coatings depends on the solubility of the Li-salt and the loading of the Li-salt in the coating.

8.3.2 Active protective properties from the coating

Optical and electron microscopy assessment of the defect area

To assess the active protective properties, the Li-loaded coatings were artificially damaged and exposed to the NSS test for 168h. Fig. 8.4 shows the optical images (I) of the defect area, the top-view (II) and cross-sectional (III) scanning electron micrographs of the surface of the substrate in the defect area of the different coatings. The analysis with the optical microscope (Fig. 8.4$_{(I)}$) showed that all coatings provide effective corrosion protection because no voluminous white corrosion products, typical for aluminium corrosion, were observed in the defect areas after the NSS exposure.[20] The highly loaded samples with 15% PVC Li-salts showed almost pristine scribes with no corrosion products. The lower loaded (2.5% PVC) samples showed some darkening but no corrosion products were observed in the defect area. The formation of the protective layer in the defect area involves a surface corrosion process whereas aluminium is anodically dissolved from the alloy matrix and forms the aluminium hydroxide layer at the aluminium surface in the defect area. The formation of such a protective layer can cause some discoloration (darkening) to the defect area. This darkening is observed in different gradations in the defect area since the optical appearance of the resulting layer in a defect area is a complex matter which is influenced by multiple factors such as scattering due to surface etching[36], the optical properties of the formed species[37], the thickness of the layer[38], and the local dissolution of other alloying elements such as magnesium which deposit at the alloy /oxide interface.[39]

The SEM micrographs of Fig. 8.4$_{(II)}$ show that a protective layer was formed in the defect areas of the Li–salt loaded coatings independently of the loading level of the Li-salt in the coating. The surface morphology of the layers generated from the 15% PVC samples is similar for both the Li-carbonate and Li-oxalate samples showing a polycrystalline surface morphology representative for hydrated oxides such as layered double hydroxides.[27] The layers generated by active inhibition from the coatings with 2.5% PVC Li-salts have a slightly different surface morphology compared to the 15% PVC samples.

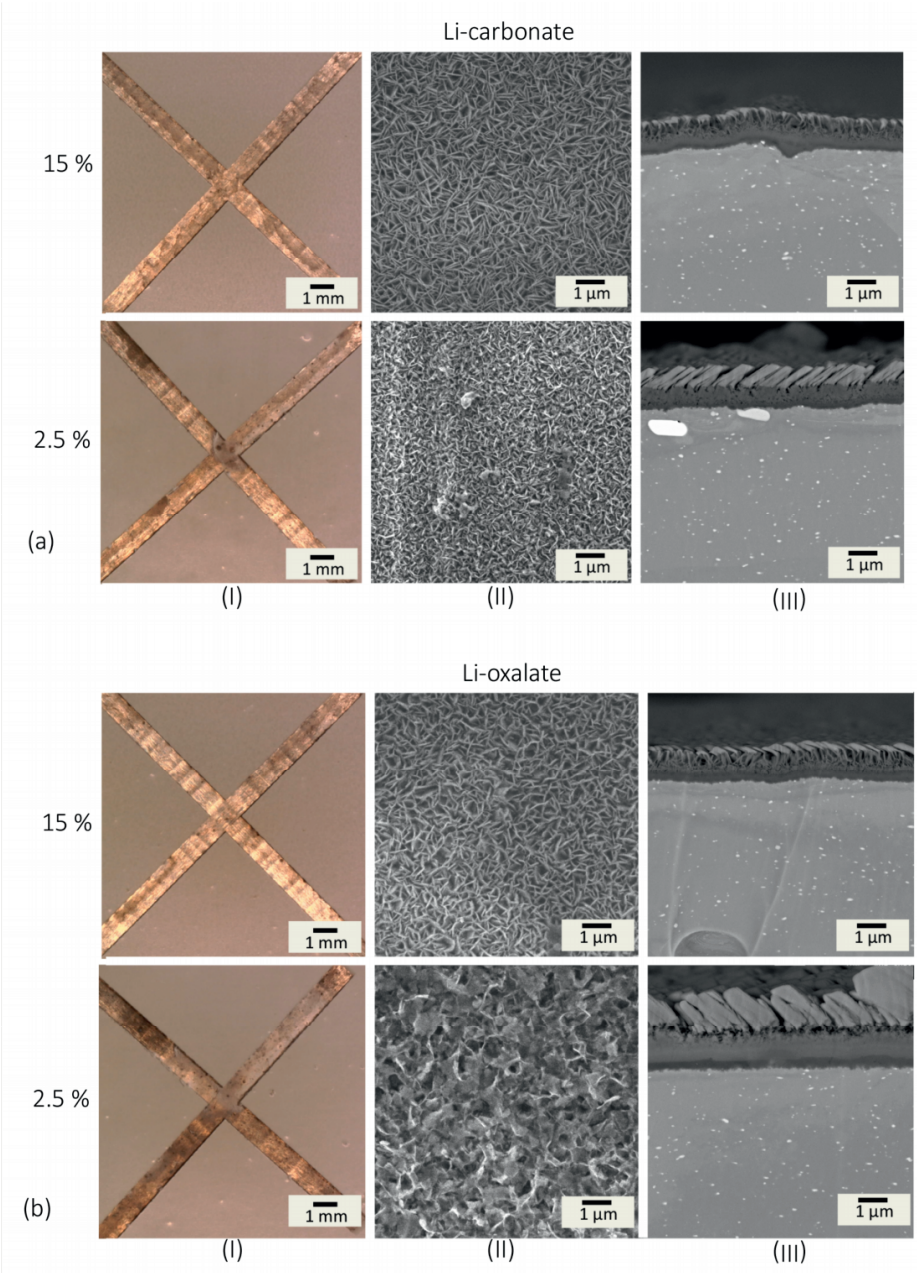

Figure 8.4 Optical and scanning electron microscopy analysis of the defect areas of Li-leaching coatings after 168h NSS exposure: (a) Li-carbonate loaded coating (15 and 2.5 % PVC) and (b) Li-oxalate loaded coating (15 and 2.5 % PVC). (I) Optical microscope image of the defect area; scanning electron micrograph of (II) the defect area in planar view; (III) cross-sectional view of the defect area.

Whereas the Li-carbonate sample (Fig. 8.4a$_{(2.5\%\ (II))}$) featured a finer structure compared to the 15% loaded sample, the Li-oxalate sample showed a more porous surface morphology (Fig. 8.4b$_{(2.5\%\ (II))}$). However the cross-sectional analysis (Fig. 8.4$_{(III)}$) revealed that the thickness of the generated protective layers was approximately 1.0 to 1.5 µm for all samples and featured a similar morphology typical for Li-leaching coatings with a dense inner layer and a porous outer layer.[20]

8.3.3 Corrosion inhibition of large defect areas

Optical analysis of large defect areas after NSS

The corrosion inhibiting reach (throwing power) of these coatings was assessed by exposing panels with increasing scribe widths from 0.5 mm up to 6 mm (Fig. 8.5) with a vertical orientation in the NSS for 168 h. Fig.5 shows the partial scribe areas after the NSS exposure. Fig. 8.5a shows the detrimental corrosion effects in the defect areas on AA2024-T3 when a coating has no corrosion inhibitor, All scribes are severely affected by corrosion in this case. In addition to several pits, large amounts of voluminous white corrosion products can be observed. The images in Fig. 8.5b show the effect of the coatings loaded with 15% and 2.5% PVC Li-carbonate. Both coatings with high and low loading show effective corrosion inhibition in the defect areas up to 3 mm. The 6 mm scribe is even protected by the 15% PVC Li-carbonate sample, whereas the sample with 2.5% PVC Li-carbonate shows some darkening and some white corrosion products on the left hand side of the defect which indicates that locally the active corrosion protection was not sufficient. A similar behaviour is observed for the Li-oxalate based coatings in Fig. 8.5c. Both coatings loaded with 15% and 2.5% PVC Li-oxalate show almost well protected scribes without signs of corrosion products in the scribes up to 3 mm wide. Like the Li-carbonate loaded samples, the difference in throwing power can be observed in the scribe with a width of 6 mm. Whereas the 15% PVC Li-oxalate loaded coating shows complete passivation of the area without the presence of white corrosion products, the 6 mm scribe of the 2.5% PVC Li-oxalate shows several pits and some white corrosion products. These results show that it is possible to protect large defect areas (up to 6 mm) with the Li-leaching technology. Local and superficial dealloying has been observed as part of the formation of the protective layer in the defect area after 168 h NSS exposure. This phenomenon of limited local attack can be observed by the presence of several small black pits in the defect area which have not lead to significant active pitting corrosion as observed in Fig. 8.5a . Hence, from the results in Fig. 8.5 it can be concluded that Li-leaching coatings are able to protect large defect areas. Even the coating with only 2.5% lithium salts and slow litium release kinetics are are able to provide effective corrosion inhibition. These observations underline the active protective nature of Li-leaching coatings.

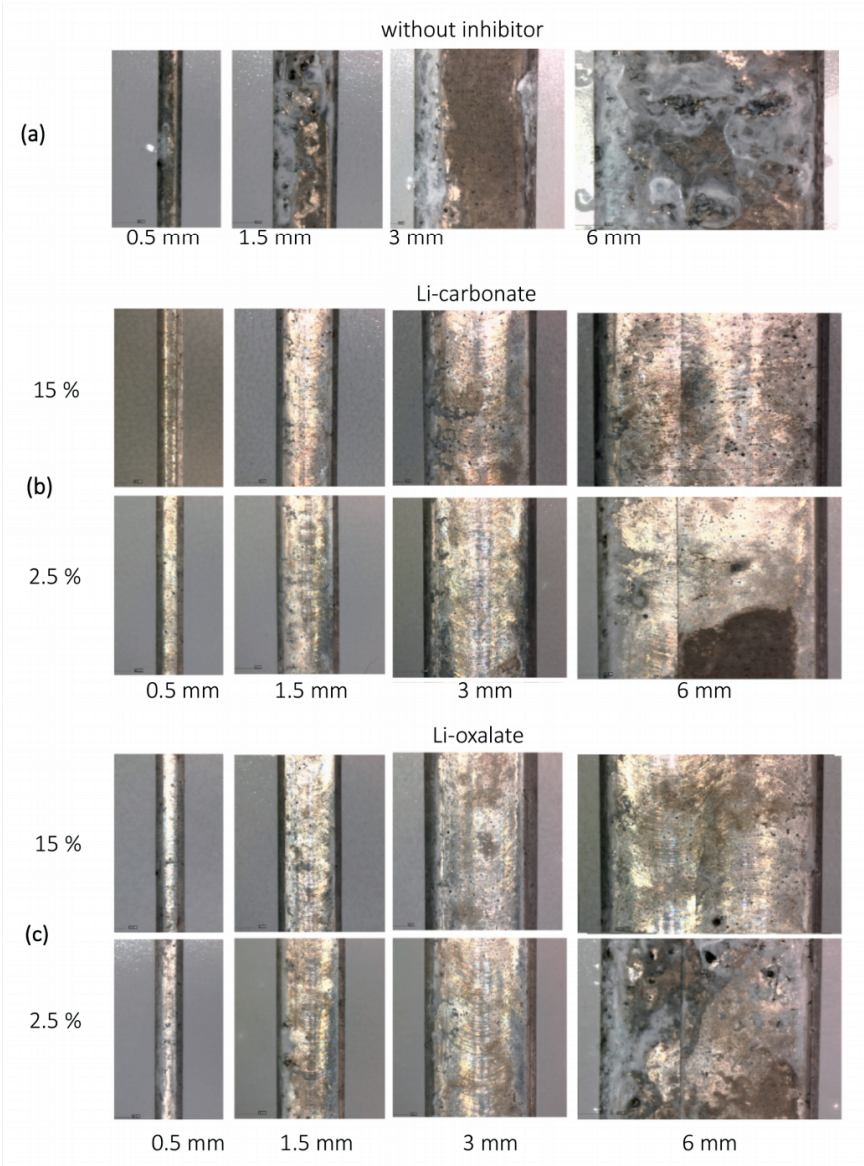

Figure 8.5 *Optical images of the defect areas with different scribe widths (0.5 mm, 1.5 mm, 3.0 mm and 6.0 mm) after 168 h NSS exposure of coatings loaded with (a) no active corrosion inhibitor; (b) Li-carbonate (15 and 2.5 % PVC); (c) Li-oxalate (12 and 2.5 % PVC).*

Surface roughness in the defect area

White light interferometer (WLI) profilometry was used to measure the surface roughness (Sa) in the defect areas to obtain absolute values for the degree of corrosion in the defect areas as a result of local corrosion phenomena such as pitting corrosion.[40] Fig. 8.6a shows a

graph with the surface roughness values of the different scribes before and after 168 h exposure to NSS. This graph shows the effect of the active protective nature of the Li-salts when used as leachable corrosion inhibitors. The graph confirms the damaging effect in the defect area when the coating does not provide active corrosion protection. The Sa increases with increasing scribe width from 0.5 µm before exposure to values of 2.5 to 3.5 µm in scribes of 3 mm and 6 mm due to the effects of general and local corrosion processes in the defect area after exposure. The surface roughness of the Li-leaching coatings increases only slightly compared to the unexposed samples. Fig. 8.6b shows the WLI surface roughness maps of the 3 mm scribes highly loaded coatings before and after 168 h NSS exposure.

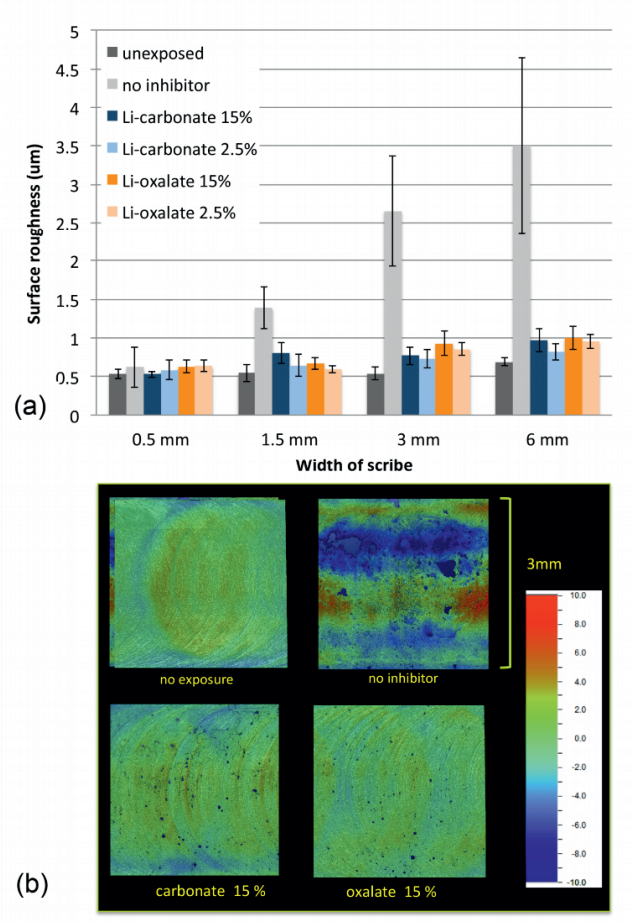

Figure 8.6 Surface roughness (Sa) of (a) the defect areas displayed in Fig. 8.5 acquired by WLI measurements; (b) typical WLI surface maps of the 3 mm wide scribes prior to exposure as well as for coatings without inhibitor and coatings with a high loading of Li-carbonate and Li-oxalate.

The uninhibited sample shows large areas that were affected by (pitting) corrosion. The 3 mm scribes of the 15 % PVC Li-leaching coatings have a smooth surface with only a few very small pits. These results confirm the efficient active protective properties of Li-salts when used as leachable corrosion inhibitors in organic coatings.

Scanning electron microscopy analysis of wide scribes

Fig. 8.7 displays the SEM micrographs of the widest scribes of the Li-leaching coatings with the best inhibition performance focussing on (I) the top view appearance of the scribe, (II) the morphology of the protective layer, and (III) the cross-sectional analysis. The 6 mm scribe was investigated for the samples with 15% PVC Li-salt (Fig. 8.7a and 7c) and the 3 mm scribe was selected for the samples with 2.5% PVC Li-salt (Fig. 8.7b and 8.7d). The top view analysis in Fig. 8.7(I) of the scribes showed no signs of pitting corrosion for all the samples investigated.

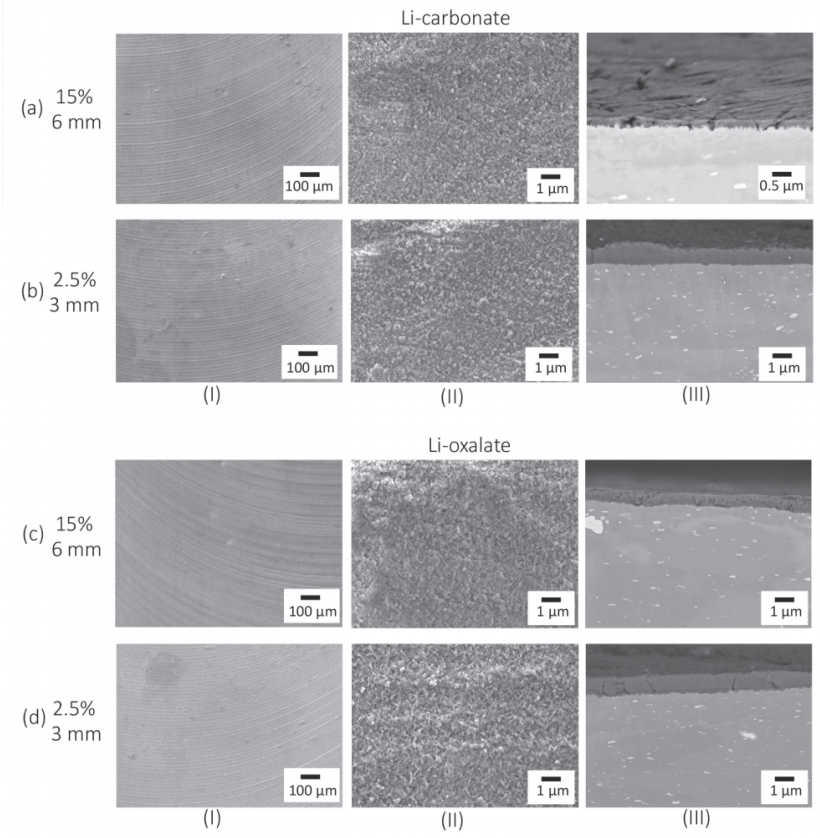

Figure 8.7 *Scanning electron micrographs of the defect areas of the Li-leaching coatings after 168h NSS exposure: Li-carbonate loaded coating (a) 15% PVC, 6 mm wide defect area; (b) 2.5% PVC, 3 mm wide defect area; Li-oxalate loaded coating (c) 15% PVC, 6 mm wide defect area; (d) 2.5% PVC, 3 mm wide defect area. (I) Planar view of the defect area; (II) top view of the protective layer; (III) cross-sectional view of the protective layer in the defect area.*

The fast effective inhibition of the Li-leaching coatings preserved the machining patterns resulting from the scribing process. At higher magnification the protective layer was revealed (Fig. 8.7(II)) showing a very different surface morphology for all samples compared to observations in the 1mm scribes as shown in Fig. 8.4. None of the samples shows the characteristic polycrystalline morphology. The cross-sectional analysis (Fig. 8.7(III)) revealed that all scribes were covered with a protective layer. The Li-carbonate samples showed a thin protective layer of 240 – 280 nm in the 6 mm scribe of the 15% PVC sample (Fig. 8.7a(III)) and a layer with an approximate thickness of 1.0 µm in the 3mm scribe of the 2.5% PVC Li-carbonate sample (Fig. 8.7b(III)). The Li-oxalate loaded samples showed slightly thicker layers of 1.0 µm and 1.2 µm for the 15% PVC and 2.5 % PVC samples respectively(Fig..8. 7c and 8.7d(III)).

8.3.4. Li-spread and compositional analysis using time-of-flight secondary ion mass spectrometry

Li is a difficult element to detect with regular surface analytical techniques, due to its low atomic number. In this work, the surface composition of the protective layer formed in a defect on AA2024-T3 from Li-leaching was studied using time-of-flight secondary ion mass spectrometry (ToF-SIMS). It was aimed to analyse the layer's surface composition(s) and the distribution of lithium in the defect area. ToF-SIMS has a large sensitivity towards lithium and it has demonstrated its ability to identify the chemical speciation of inorganic compounds.[41] ToF-SIMS provides compositional data of the very surface of the protective layers, but in combination with the high lateral resolution of the technique, the lateral spread of the lithium based species within defect areas after NSS exposure could be imaged. Characteristic ion-fragment assignments were made and a multivariate analysis method non-negative matrix factorisation (NMF)) was applied to identify the various species present at the surface of the protective layer.

Non-negative matrix factorization (NMF) method

Previous ToF-SIMS work made it possible to observe the lateral Li-distribution in the defect area and to identify and determine relative concentrations of two chemical compositions (Li-PB and Li-LDH) present at the surface of the protective layer in 1 mm defect areas.[25] In this work, the NMF methodology was extended to identify and map the distribution of three chemical compositions at the surface of the protective layers generated in the defect area: PB, Li-PB and Li-LDH. Fig. 8.8a-g shows the different steps involved in this procedure. (Fig. 8.8a) An optical image of the defect area to be analysed is shown. (Fig. 8.8b) Large area ToF-SIMS images (total ion maps are shown) are obtained for the defect area and for three reference materials (PB, Li-PB and Li-LDH). Each pixel contains a full mass spectrum. (Fig. 8.8c) Nineteen fragments of interest, characteristic for the reference materials were selected based on a compositional ToF-SIMS analysis.[25] Each fragment has its own map, as

shown for $^{6}Li^{+}$, Li_2OH^{+} and $AlO_2H_2^{+}$.[25] (Fig. 8.8d) All data cubes from the maps of defect area for the three compounds of interest and three reference compounds were stitched into a single data set. Given that three different reference materials were included in the dataset, the entire dataset was processed with NMF into three pure compounds according to the method of Trindade et. al.[30] (Fig. 8.8e) The resulting NMF output provides, on one hand the fingerprint spectra of the three reference materials and on the other hand, the normalized NMF intensities of the pure compound were plotted per pixel in an overlay map in the defect. (Fig. 8.8f) In order to determine the percentage of surface coverage for each compound, each pixel was assigned to a single compound, based on thresholds applied to the NMF intensities. Each compound is mapped separately for the defect area. (Fig. 8.8g) Based on the total amount of pixels, these normalized NMF intensities can be converted into a compositional ratio of the pure compounds present at the surface of the protective layer in the defect area.

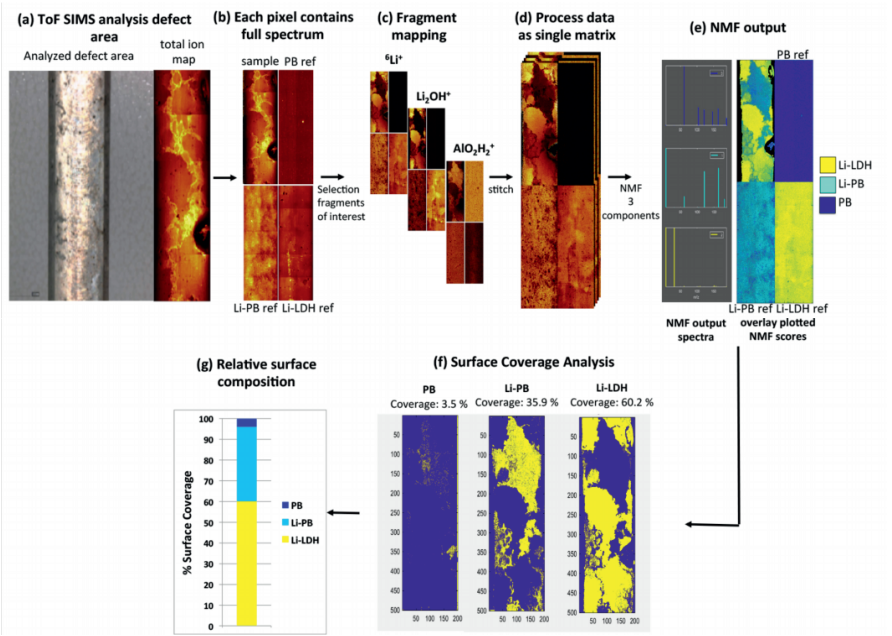

Figure 8.8 Schematic description of the NMF process used for the compositional study of the corrosion protective layer in the defect area formed by the Li-leaching coatings

Lithium spread and composition in a defect area over time

ToF-SIMS analysis of the surface composition in the defect area, as described above was applied on samples of the 15 % PVC Li-carbonate loaded coating to study the Li-spread and the surface composition of the protective layer in the 1 mm wide scribe as a function of NSS exposure time (Fig. 8.9). The minor isotope $^{6}Li^{+}$ was used to visualise the distribution of Li ions within the defect area, as the high ionisation cross section of Li means that the $^{7}Li^{+}$ fragment was too intense and saturated the detector (Relative abundances: $^{7}Li^{+}$ = 92.5%

and $^{6}Li^{+}$ = 7.5%).[25] Fig. 8.9a shows the $^{6}Li^{+}$ maps as function of the NSS exposure time. These maps reveal the fast Li-spread in the defect due to the leaching of the Li-carbonate from the coating. From the surface maps it can be noted that the defect area is already completely covered with Li-compounds after only after 15 min of NSS exposure. Furthermore, the images show the Li-spread initiating at the edges of the defect area and interacting with specific areas in the defect area.

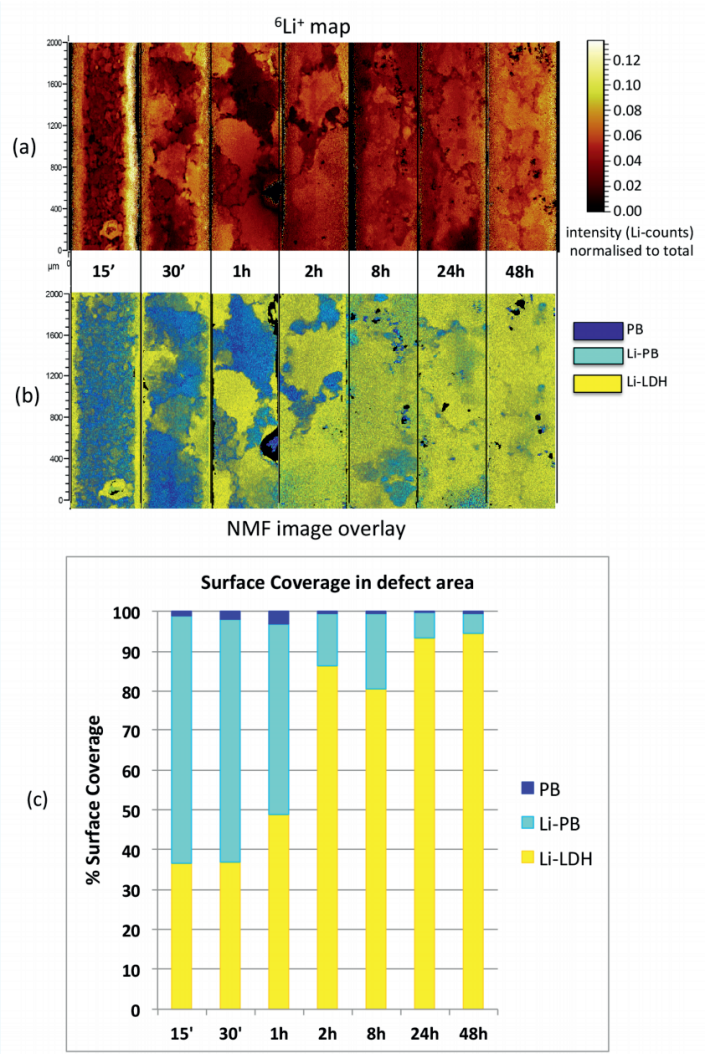

Figure 8.9 *Li-spread and compositional analysis during the formation of a corrosion protective layer in a 1 mm wide defect area from a 15% PVC Li-carbonate loaded coating as a function NSS exposure time: (a) 6Li+ maps; (b) Overlay images of normalised NMF intensities; (c) Relative surface composition of the corrosion protective layer in the defect area for PB, Li-PB and Li-LDH after 15 min up to 48 h NSS exposure.*

The different Li concentrations observed in the $^{6}Li^{+}$ map can indicate the presence of different surface compositions in the defect area. It can be noted that over longer exposure time Li spreads out further. After 2 h NSS exposure the entire scribe was covered with a homogeneous concentration of Li. Further Li-enrichment is visible after 48 h exposure. The NMF procedure was used to reveal evolution of the surface composition of the generated layer in the defect areas after different NSS exposure times. The complete data set was factorised by NMF using the data of the three reference samples. Fig. 8.9b shows the NMF overlay maps of the respective ToF-SIMS $^{6}Li^{+}$ maps of Fig. 8.9a, representing the normalized NMF intensities of PB, Li-PB, and Li-LDH as a function of exposure time. These maps show the fast lateral spread of the Li-based compounds in the defect. After only 15 minutes NSS exposure, the entire defect area was basically covered with two Li based compounds, Li-PB and Li-LDH. The Li-PB layer was generated almost instantly throughout the coating defect whereas Li-LDH was formed along the edges of the defect area. Initially, Li-LDH was generated only at selective areas in the defect area (1-2h) but longer NSS exposure resulted in the lateral spread of Li-LDH throughout the entire defect area. Fig. 8.9c shows the NMF intensities of PB, Li-PB, and Li-LDH detected in the defect area as a function of NSS exposure time. After only 15 min NSS, 37% of the relative surface coverage could be attributed to Li-LDH. This value increased to 94% Li-LDH surface coverage after 48 h NSS exposure.

These results revealed the very fast action of Li-salts in the coating defect when released from the coating matrix and show that two main compounds are involved in the formation of the protective layer in the defect area. Initially, the leaching of Li-ions into the defect area results in a Li-PB layer throughout the defect area. Further leaching of Li-carbonate in the defect area due to extended exposure to the NSS conditions provide conditions that contribute to the formation of a Li-LDH throughout the defect area. Under these conditions, only small amounts, if indeed any, PB were detected.

Li-spread and compositional analysis in large coating defects

The previous section demonstrated that the 15% PVC Li-carbonate loaded coating was able to cover the entire 1 mm defect area fast and effectively with a Li-LDH layer demonstrating a sufficient degree of chemical throwing power for the 15% PVC Li-carbonate sample under these conditions. The same ToF-SIMS methodology was applied on the coated panels with increasing scribe widths, which were optically assessed earlier in this work to determine the lateral chemical throwing power of the coatings with high and low Li-salt loadings after 7d NSS exposure. Fig 10 shows the Li^{+} distribution maps (top rows) of a section of the scribes including the normalized total Li^{+} counts per mm^{2} and the corresponding NMF image overlays (bottom rows). The ToF-SIMS analysis was performed in each defect area with the exclusion of the areas close to the sides of the scribe to avoid artefacts due to edge effects of the scribe. The Li^{+} distribution maps show that Li is detected throughout all scribes, even up to 6mm scribe widths after the 7 d NSS exposure. This demonstrates that all coatings with a fast leach rate (15% PVC Li-salts) and a relatively low leach rate (2.5 %

PVC Li-salts) were able to generate conditions in the defect areas that enabled the formation of a protective layer on the aluminium alloy. The highest concentrations of Li^+ (counts/mm^2) were detected in scribes of the coatings with the 15% PVC Li-salt loaded coatings (Fig 10a and 10c). and Li^+ concentrations decreased with increasing scribe widths. Higher concentrations of Li^+ were detected in the scribes of the Li-oxalate loaded coatings compared to the Li-carbonate coatings. This is in line with the faster leach rate of the Li-oxalate loaded coatings. The concentrations of Li^+ distributed in the defect areas of the 2.5% PVC loaded samples were clearly lower than the 15% PVC loaded samples. However, the defect areas up to 6 mm were still covered with Li-containing compounds. This demonstrates the mobility, reactivity and the chemical throwing power of the lithium-ions, even at low concentrations.

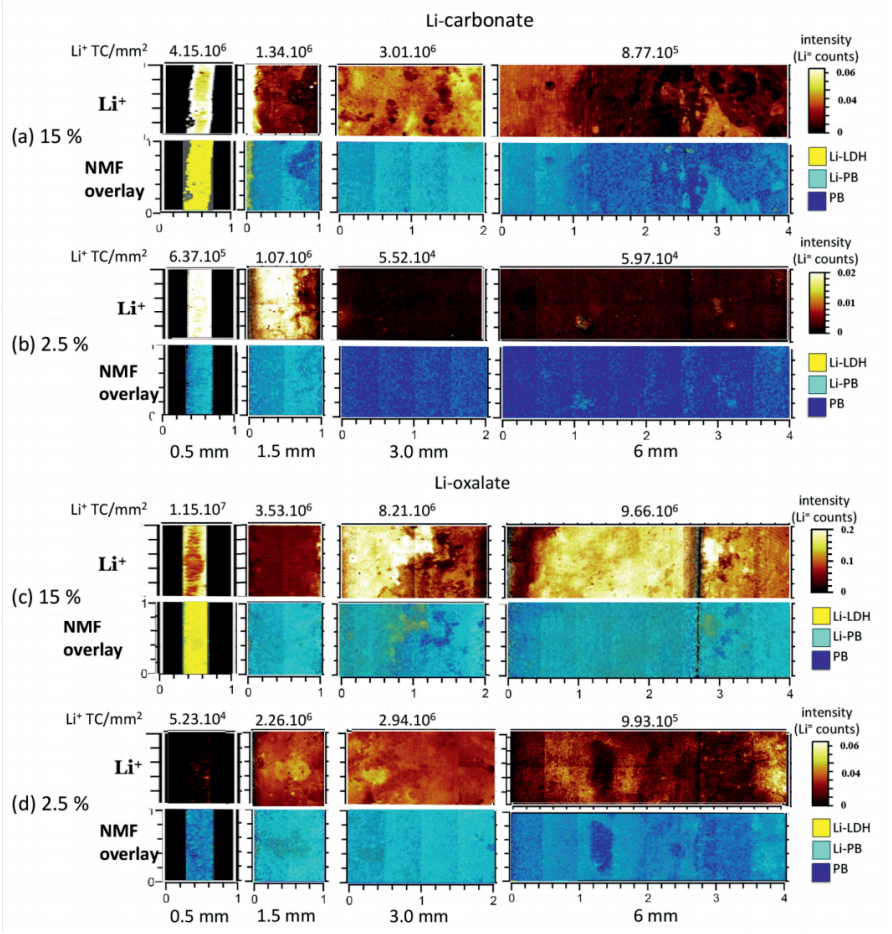

Figure 8.10 Lithium spread (top row) and normalized Li+ counts with the corresponding NMF image overlay images (bottom row) of the corrosion protective layers generated in the defect areas (0.5 mm, 1,5mm, 3.0 mm and 6.0 mm width) from the Li-carbonate loaded coating (a) 15% PVC; (b) 2.5% and the Li-oxalate loaded coating (c)15% PVC; (d) 2.5 % PVC after 168 h NSS exposure.

The NMF procedure was applied on these samples to generate compositional maps of the surface chemistry and to distinguish a relative quantification of pure compounds in the defect areas using three reference samples (PB, Li-PB, and Li-LDH). The bottom rows of each figure in Fig. 8.10 show the NMF overlay images showing the distribution of the three compounds in the analysed defect areas. The NMF overlay images of Fig. 8.10a show that the surface of the 0.5 mm defect of the 15 % PVC Li-carbonate is fully covered with Li-LDH. However, it can be observed that the surface composition of the wider defect areas can be attributed to Li-PB and that Li-LDH is not detected. Fig. 8.10b shows the uniform distribution of Li^+ in the defect areas of the 2.5 % PVC Li-carbonate coatings. The NMF overlay maps of these defect areas reveal that little or no Li-LDH was formed in these defect areas but these defect areas where covered with a protective layer composed of a mixture of Li-PB and PB. A similar behaviour was observed for the Li-oxalate coatings in Fig 10c and 10d. The NMF analysis showed that the relative surface composition of the protective layer in the 0.5 mm defect of 15% PVC Li-oxalate coating (Fig. 8.10c) comprises mainly Li-LDH, whereas the surface composition of protective layers in the wider scribes contain primarily Li-PB with some local areas of Li-LDH. The protective layers in all defect areas of the 2.5% PVC Li-oxalate coated samples comprise mainly Li-PB.

Fig. 8.11 summarizes the relative surface composition intensities of the 3 pure compounds detected at the surface of the protective layer in the defect derived from the NMF procedure applied on the samples with increasing defect widths.

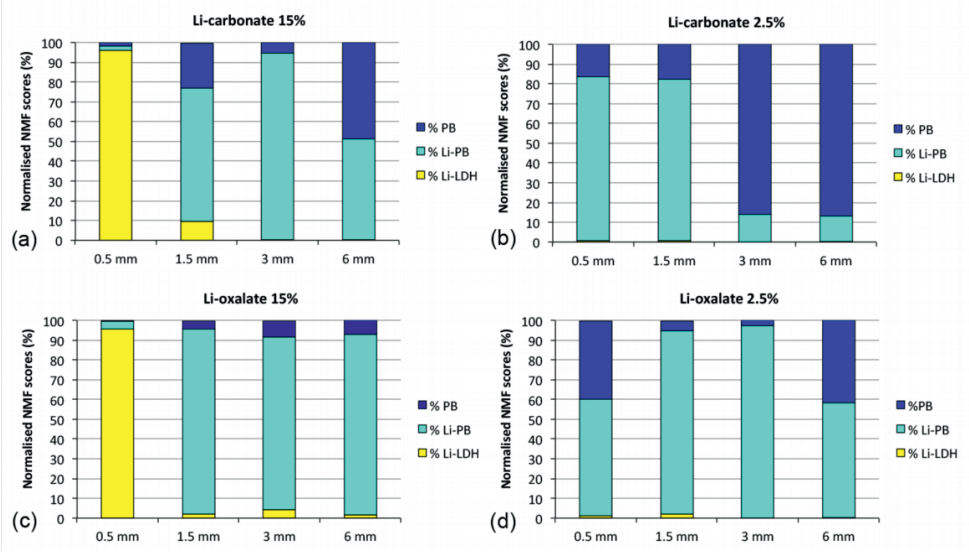

Figure 8.11 Relative surface composition of the corrosion protective layer in the defect areas (Li-LDH vs. Li-PB) obtained from the NMF image overlay data displayed in Fig. 8.10: Li-carbonate loaded coating (a) 15% PVC; (b) 2.5% PVC and Li-oxalate loaded coating (c) 15% PVC and (d) 2.5% PVC.

For the 15% PVC Li-carbonate loaded coating (Fig. 8.11a) it can be observed that the occurrence of Li-LDH decreases rapidly when the defects become wider. The coverage with Li-LDH drops from 95% in a 0.5 to 1 mm scribe to values below 10% when the defects becomes 1.5 mm or wider. Instead of Li-LDH, Li-PB becomes the most abundant species. A similar trend is observed for the 15% PVC Li-oxalate samples in Fig. 8.11c. Li-PB is also the most abundant species found at the surface of the protective layer throughout the defect areas of the 2.5% PVC Li-salt coatings (Fig. 8.11b and 8.11d). Only in the wider scribes of the 2.5% PVC Li-carbonate the levels of Li are lower at the surface of the protective layer and the majority of the species in the defect area can be related to PB. In summary, the graphs of Fig. 8.10 and 11 imply that the surface composition of the protective layer in the defect areas depends on the inhibitor release rate and loading of the coating and the size of the defect. The occurrence of Li-LDH seems to be related to systems with fast leaching and high Li-loading (15% PVC Li-salts) and relatively small defect widths (0.5 mm). These parameters will result in high Li concentrations and alkaline conditions which are favourable for the formation Li-LDH.[27]

A surprising and novel observation from this work is that the main surface compound of protective layers generated in the wider scribes and slower leaching systems can be identified as Li-PB. For the 2.5% PVC Li-carbonate coatings the contribution of PB in surface layer increases with scribe width. The combination of these observations with the knowledge that the defect areas were effectively protected, leads to the conclusion that Li-LDH is not the key corrosion inhibiting species needed for effective corrosion inhibition but in essence appears to be a side-product which is generated when high levels of Li carbonate and oxalate are present in the defect area.

8.3.5. Chemical throwing power of Li-leaching coatings

The approach in this study confirmed the important aspects that are considered as essential for effective active corrosion protection from organic coatings. In order to have a sufficient chemical throwing power, coatings must be able to leach sufficient amounts of corrosion inhibitor to achieve a critical inhibitor concentration in the defect area in a short time to obtain a fast and irreversible corrosion inhibition[12, 15] However, it is known that the larger the defect size is, the more difficult it is to obtain these critical concentrations of corrosion inhibitor in the defect to prevent corrosion. [14]

In the work discussed above, Li-leaching coatings were investigated varying inhibitor loading, inhibitor solubility and defect size to obtain more insight in the throwing power characteristics of this novel chromate-free active protective coating technology. These factors contribute to the inhibitor accumulation in the defect area and the efficacy of the Li-based coating technology. The results of the investigation showed that the investigated Li-leaching coatings have a chemical throwing power of 3 to 6 mm and the ability to cover and protect these wide defect areas effectively. The ToF-SIMS analysis of the defects areas revealed that Li is distributed throughout the defect areas and three different compounds

(Li-LDH, Li-PB, and PB) were found. The ratio of these compounds seems to be related to the dissolution of the corrosion inhibitor from the coating matrix (i.e. loading in the coating and solubility of the Li-salts). The work indicates that Li-LDH is a side-product in the generation of these protective layers due to fast release of the Li-salts leading to high Li concentrations and high pH values in small defect areas.

With these results, it is possible to discuss the proposed formation mechanism of these protective layers from lithium leaching coatings in more detail (Fig. 8.12).[21, 39] Considering the possible event of a coating defect, the aluminium alloy AA2024-T3 will be exposed to environmental conditions and a thin layer of electrolyte will be formed in the defect.

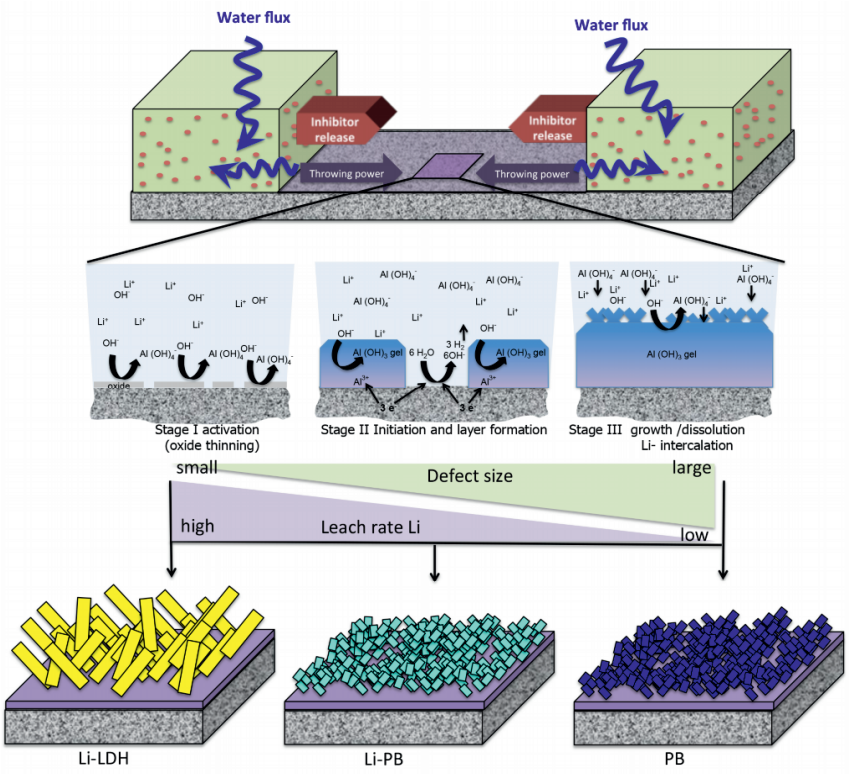

Figure 8.12 Schematic illustration of the mechanism and the relation between the surface composition of the protective layer in the defect related to the Li leach rate and the size of the coating defect

This moisture will trigger the dissolution and diffusion of the Li-salt from the organic coating matrix into the defect area initiating Stage I of the formation mechanism. Due to the alkalinity of the Li-salts, the conditions in the defect area will become alkaline (pH 9-10) and the presence of chlorides in the electrolyte the natural oxide of the aluminium alloy will be thinned.[21, 42] This oxide thinning will enable the initial formation of the protective layer (Stage II) via direct anodic dissolution of aluminium, resulting in the formation of

aluminium hydroxide gel on the aluminium substrate under these moderate alkaline conditions.[43, 44] When the film of aluminium hydroxide gel covers the surface, the layer will develop by a growth and dissolution process until a stable state is reached. This growth and dissolution process (Stage III) is characteristic for aluminium in alkaline conditions.[20, 27, 45-47] Stages I and II are known to be fast processes and the growth-rate in stage III is limited by diffusion of species across the dense inner oxide.[44, 48] This oxide growth process may be accelerated by the presence of chloride ions which are thought to be able to facilitate the hydration and dissolution process of amorphous oxide.

This aluminium corrosion process results in a surface-covering layer on the aluminium alloy with a dense morphology at the inner layer near the aluminium alloy / (hydr)oxide interface and a porous morphology at the outer region of the protective layer. From the results obtained in this work, it became apparent that three different compounds can be identified at the outer region of the protective layer: (i)Li-LDH: in the case of high Li concentrations and small defect areas; (ii)Li-PB: in the case of moderate Li concentrations and wider defect areas and (iii)PB: in the case low Li concentrations and wide defect areas. It is known that Li-LDH can be formed when there is sufficient $Al(OH)_4^-$, Li^+, CO_3^- or OH^- in solution at pH values higher than 10.[27] On the other hand, it is known that amorphous aluminium hydroxide transforms into pseudo-boehmite by an aging process in mildly alkaline conditions.[44] The results from this research indicate that Li-LDH is not the primary corrosion inhibiting species in the defect area from these Li-leaching coatings and that the relative Li^+ concentration in the defect area determines whether Li-LDH is formed or not.

Li-PB was the most prominent surface species detected in most of the defect areas. It is known that ions (e.g Cerium)[26] can be incorporated in pseudoboehmite layers promoting oxide growth.[26] The results show that most of the defect areas are protected by PB layers with high and low amounts of Li depending on the leach rate and width of the defect area. This combined with the Li distribution in the defect areas strongly suggests that Li is involved in the stabilization of the aluminium hydroxide layer in the defect area. However, additional studies are needed to explain the chemical stabilization mechanism of the aluminium hydroxide layer by Li. In addition this work, demonstrated the chemical throwing power properties of lithium-leaching coatings and has shown that only small amounts or low concentrations of Li are needed to provide active corrosion protection in large defect areas. The efficacy of the corrosion protection seems to be limited by the amount of Li that can be released from the coating into the defect area and the ability to reach the critical concentration and conditions for effective corrosion inhibition. The insights obtained in this work provide an enhanced view on the active corrosion inhibiting properties and the mechanism of Li-leaching coatings for the protection of aluminium alloys

8.4. Conclusions

This work studied the chemical throwing power of Li-leaching coatings and the compositional analysis of the protective layers in the coating defects. Organic coatings were formulated with different Li-salts as corrosion inhibitors and different loadings to obtain different leaching behaviours to evaluate the distance (throwing power) these leaching Li-inhibitors are able to protect coating defects with increasing widths.
It was demonstrated that Li-inhibitors were able to protect coating defects with a width up to 6 mm from coatings with different leaching behaviours by the formation of a protective layer in the defect area.

ToF-SIMS was used to map the distribution and relative concentration of lithium in the defect areas. An NMF analysis of the ToF-SIMS datasets was applied to link the Li distribution in the defect areas with the compositional characterisation of the surface of the protective layer. It was found that Li-PB is the main surface compound encountered and Li-LDH is a side-product, which is generated in small defect areas and at fast Li-leaching rates.

This study provides a further understanding of the active corrosion protective properties, the surface composition in the defect and demonstrates the chemical throwing power of the Li-leaching technology, a feature that has not been demonstrated for any other chromate-free inhibitor leaching coating technology.

References

1. I. M. Zin, R. L. Howard, S. J. Badger, J. D. Scantlebury and S. B. Lyon, The mode of action of chromate inhibitor in epoxy primer on galvanized steel, *Progress in Organic Coatings*, 1998, 33, 203-210.
2. M. A. Jakab and J. R. Scully, On-demand release of corrosion-inhibiting ions from amorphous Al–Co–Ce alloys, *Nature Materials*, 2005, 4, 667.
3. P. Klomjit and R. G. Buchheit, Characterization of inhibitor storage and release from commercial primers, *Progress in Organic Coatings*, 2018, 114, 68-77.
4. S. G. R. Emad, X. Zhou, S. B. Lyon, G. E. Thompson, Y. Liu, G. Smyth, D. Graham, D. Francis and S. R. Gibbon, Influence of volume concentration of active inhibitor on microstructure and leaching behaviour of a model primer, *Progress in Organic Coatings*, 2017, 102, 71-81.
5. F. H. Scholes, S. A. Furman, A. E. Hughes, T. Nikpour, N. Wright, P. R. Curtis, C. M. Macrae, S. Intem and A. J. Hill, Chromate leaching from inhibited primers. Part I. Characterisation of leaching, *Progress in Organic Coatings*, 2006, 56, 23-32.
6. S. A. Furman, F. H. Scholes, A. E. Hughes and D. Lau, Chromate leaching from inhibited primers. Part II: Modelling of leaching, *Progress in Organic Coatings*, 2006, 56, 33-38.
7. T. Prosek and D. Thierry, A model for the release of chromate from organic coatings, *Progress in Organic Coatings*, 2004, 49, 209-217.
8. A. E. Hughes, A. Trinchi, F. F. Chen, Y. S. Yang, I. S. Cole, S. Sellaiyan, J. Carr, P. D. Lee, G. E. Thompson and T. Q. Xiao, The application of multiscale quasi 4D CT to the study of SrCrO4 distributions and the development of porous networks in epoxy-based primer coatings, *Progress in Organic Coatings*, 2014, 77, 1946-1956.
9. S. Sellaiyan, A. E. Hughes, S. V. Smith, A. Uedono, J. Sullivan and S. Buckman, Leaching properties of chromate-containing epoxy films using radiotracers, PALS and SEM, *Progress in Organic Coatings*, 2014, 77, 257-267.
10. M. W. Kendig and R. G. Buchheit, Corrosion inhibition of aluminum and aluminum alloys by soluble chromates, chromate coatings, and chromate-free coatings, *Corrosion*, 2003, 59, 379-400.
11. B. Kannan, C. F. Glover, H. N. McMurray, G. Williams and J. R. Scully, Performance of a Magnesium-Rich Primer on Pretreated AA2024-T351 in Full Immersion: a Galvanic Throwing Power Investigation Using a Scanning Vibrating Electrode Technique, *Journal of The Electrochemical Society*, 2018, 165, C27-C41.
12. J. R. Scully, F. Presuel-Moreno, M. Goldman, R. G. Kelly and N. Tailleart, User-Selectable Barrier, Sacrificial Anode, and Active Corrosion Inhibiting Properties of Al-Co-Ce Alloys for Coating Applications, *Corrosion*, 2008, 64, 210-229.
13. J. R. Scully, N. Tailleart and F. Presuel-Moreno, in *Rare Earth-Based Corrosion Inhibitors*, Woodhead Publishing, 2014, pp. 267-290.
14. F. J. Presuel-Moreno, H. Wang, M. A. Jakab, R. G. Kelly and J. R. Scully, Computational modeling of active corrosion inhibitor release from an Al-Co-Ce metallic coating - Protection of exposed AA2024-T3, *Journal of the Electrochemical Society*, 2006, 153, B486-B498.
15. P. Visser, H. Terryn and J. M. C. Mol, On the importance of irreversibility of corrosion inhibitors for active coating protection of AA2024-T3, *Corrosion Science*, 2018, 140, 272-285.
16. P. Visser and S. A. Hayes, Low-temperature-curable coating composition useful as anticorrosive primer coating for non-ferrous metal substrates, particularly aluminum or aluminum alloy, comprises film-forming resin, curing agent, and lithium salt, *patent nr. WO2010112605-A1*, 2010.
17. O. Gharbi, S. Thomas, C. Smith and N. Birbilis, Chromate replacement: what does the future hold?, *npj Materials Degradation*, 2018, 2, 12.
18. P. Visser, Y. Liu, H. Terryn and J. M. C. Mol, Lithium salts as leachable corrosion inhibitors and potential replacement for hexavalent chromium in organic coatings for the protection of aluminum alloys, *Journal of Coatings Technology and Research*, 2016, 13, 557-566.
19. P. Visser, H. Terryn and J. M. C. Mol, On the importance of irreversibility of corrosion inhibitors for active coating protection of AA2024-T3, *Corrosion Science*, 140 (2018) 272-285.
20. P. Visser, Y. Liu, X. Zhou, T. Hashimoto, G. E. Thompson, S. B. Lyon, L. G. J. van der Ven, A. J. M. C. Mol and H. A. Terryn, The corrosion protection of AA2024-T3 aluminium alloy by leaching of lithium-containing salts from organic coatings, *Faraday Discussions*, 2015, 180, 511-526.
21. P. Visser, A. Lutz, J. M. C. Mol and H. Terryn, Study of the formation of a protective layer in a defect from lithium-leaching organic coatings, *Progress in Organic Coatings*, 2016, 99, 80-90.

22. P. Visser, M. Meeusen, Y. Gonzalez-Garcia, H. Terryn and J. M. C. Mol, Electrochemical Evaluation of Corrosion Inhibiting Layers Formed in a Defect from Lithium-Leaching Organic Coatings, *Journal of The Electrochemical Society*, 2017, 164, C396-C406.
23. Y. Liu, P. Visser, X. Zhou, S. B. Lyon, T. Hashimoto, M. Curioni, A. Gholinia, G. E. Thompson, G. Smyth, S. R. Gibbon, D. Graham, J. M. C. Mol and H. Terryn, Protective Film Formation on AA2024-T3 Aluminum Alloy by Leaching of Lithium Carbonate from an Organic Coating, *Journal of The Electrochemical Society*, 2016, 163, C45-C53.
24. Y. Liu, P. Visser, X. Zhou, S. B. Lyon, T. Hashimoto, A. Gholinia, G. E. Thompson, G. Smyth, S. R. Gibbon, D. Graham, J. M. C. Mol and H. Terryn, An investigation of the corrosion inhibitive layers generated from lithium oxalate-containing organic coating on AA2024-T3 aluminium alloy, *Surface and Interface Analysis*, 2016, 48, 798-803.
25. K. Marcoen, P. Visser, G. F. Trindade, M. L. Abel, J. F. Watts, J. M. C. Mol, H. Terryn and T. Hauffman, Compositional study of a corrosion protective layer formed by leachable lithium salts in a coating defect on AA2024-T3 aluminium alloys, *Progress in Organic Coatings*, 2018, 119, 65-75.
26. J. D. Gorman, A. E. Hughes, D. Jamieson and P. J. K. Paterson, Oxide formation on aluminium alloys in boiling deionised water and NaCl, CeCl3 and CrCl3 solutions, *Corrosion Science*, 2003, 45, 1103-1124.
27. R. G. Buchheit, Bode, M.D., Stoner, G.E., Corrosion-Resistant, Chromate free Talc Coatings for Aluminum, *Corrosion*, 1994, 50, 205-214.
28. G. F. Trindade, J. Bañuls-Ciscar, C. K. Ezeh, M. L. Abel and J. F. Watts, Characterisation of wood growth regions by multivariate analysis of ToF-SIMS data, *Surface and Interface Analysis*, 2016, 48, 584-588.
29. G. F. Trindade, M.-L. Abel and J. F. Watts, simsMVA: A tool for multivariate analysis of ToF-SIMS datasets, *Chemometrics and Intelligent Laboratory Systems*, 2018, 182, 180-187.
30. G. F. Trindade, M.-L. Abel, C. Lowe, R. Tshulu and J. F. Watts, A Time-of-Flight Secondary Ion Mass Spectrometry/Multivariate Analysis (ToF-SIMS/MVA) Approach To Identify Phase Segregation in Blends of Incompatible but Extremely Similar Resins, *Analytical Chemistry*, 2018, 90, 3936-3941.
31. M. R. Keenan and P. G. Kotula, Accounting for Poisson noise in the multivariate analysis of ToF-SIMS spectrum images, *Surface and Interface Analysis*, 2004, 36, 203-212.
32. G. F. Trindade, M.-L. Abel and J. F. Watts, Non-negative matrix factorisation of large mass spectrometry datasets, *Chemometrics and Intelligent Laboratory Systems*, 2017, 163, 76-85.
33. D. D. Lee and H. S. Seung, Learning the parts of objects by non-negative matrix factorization, *Nature*, 1999, 401, 788.
34. A. Seidell, *Solubilities of inorganic and organic compounds c. 2*, D. Van Nostrand Company, 1919.
35. R. C. Weast, *CRC handbook of chemistry and physics, ,* CRC Press, Boca Raton :, 1st student edition edn., 1988.
36. H. Terryn, J. Vereecken and G. E. Thompson, The electrograining of aluminium in hydrochloric acid—II. Formation of ETCH products, *Corrosion Science*, 1991, 32, 1173-1188.
37. S. Van Gils, C. A. Melendres and H. Terryn, Quantitative chemical composition of thin films with infrared spectroscopic ellipsometry: application to hydrated oxide films on aluminium, *Surface and Interface Analysis*, 2003, 35, 387-394.
38. S. Van Gils, P. Mast, E. Stijns and H. Terryn, Colour properties of barrier anodic oxide films on aluminium and titanium studied with total reflectance and spectroscopic ellipsometry, *Surface and Coatings Technology*, 2004, 185, 303-310.
39. P. Visser, Y. Gonzalez-Garcia, J. M. C. Mol and H. Terryn, Mechanism of Passive Layer Formation on AA2024-T3 from Alkaline Lithium Carbonate Solutions in the Presence of Sodium Chloride, *Journal of The Electrochemical Society*, 2018, 165, C60-C70.
40. P. Visser, Novel totally chrome free corrosion inhibiting coating technology for protection of aluminium alloys, *Transactions of the Institute of Metal Finishing*, 2011, 89, 291-294.
41. L. Van Vaeck, in *ToF-SIMS : material analysis by mass spectrometry*, ed. J. C. Vickerman, Chichester : IM,, 2nd edn., 2013, pp. p. 125-150
42. R. T. Foley, Localized Corrosion of Aluminum Alloys - a Review, *Corrosion*, 1986, 42, 277-288.
43. R. T. Foley and T. H. Nguyen, The Chemical Nature of Aluminum Corrosion: V . Energy Transfer in Aluminum Dissolution, *Journal of The Electrochemical Society*, 1982, 129, 464-467.
44. R. S. Alwitt, The Growth of Hydrous Oxide Films on Aluminum, *Journal of The Electrochemical Society*, 1974, 121, 1322-1328.
45. L. A. Carreiea, V. A. Maroni, J. W. Swaine Jr and R. C. Plumb, Raman and infrared spectra and structures of the aluminate ions, *The Journal of Chemical Physics*, 1966, 45, 2216-2220.

46. M. R. Tabrizi, S. B. Lyon, G. E. Thompson and J. M. Ferguson, The long-term corrosion of aluminium in alkaline media, *Corrosion Science*, 1991, 32, 733-742.
47. C. A. Drewien, Eatough, M.O., Tallant, D.R., Hills, C.R., Buchheit, R.G., Lithium-aluminum-carbonate-hydroxide hydrate coatings on aluminum: Composition, structure and processing bath chemistry, *Journal of material research*, 1996, 11, 1507-1513.
48. W. Vedder and D. A. Vermilyea, Aluminum + water reaction, *Transactions of the Faraday Society*, 1969, 65, 561-584.

Chapter 9

Active Corrosion Protection of Various Aluminium Alloys by Lithium-Leaching Coatings

The work in this thesis focused on high strength aluminium alloy AA2024-T3. This aluminium alloy is most commonly studied to evaluate the performance of new chromate-free coating technologies because it is one of the most used aerospace alloys and is very susceptible to localized corrosion. However, there are many more types of aluminium alloys, each with a specific metallurgy and electrochemical activity. This chapter discusses the active protective properties of the lithium-leaching coating technology on other alloys than AA2024-T3.

This chapter is published as a scientific paper:
P. Visser, H. Terryn, J.M.C. Mol, "Active corrosion protection of various aluminium alloys by lithium- leaching coatings." Surface and Interface Analysis. (2019) 1–12. https://doi. org/10.1002/sia.6638

Abstract

This study presents the active protective properties of Li-leaching coatings for a range of aluminium alloys. Coatings with and without lithium carbonate as leachable inhibitor were applied on the aluminium alloys, artificially damaged and exposed to the neutral salt spray. A combined approach of scanning electron microscopy and electrochemical measurements revealed that the lithium carbonate leaching coating provided effective corrosion inhibition on AA2024, AA7075, AA5083 and AA6014 by the formation of a protective layer in the defect area and preventing local corrosion processes despite the different intrinsic electrochemical activity of the alloys.

9.1 Introduction

The corrosion resistance of aluminium alloys depends on the heterogeneous microstructure from the alloying additions and heat-treatments. The nature, concentration and distribution of second-phase intermetallic particles is a dominant factor controlling localized corrosion mechanisms and kinetics as the electrochemical characteristics of the particles may differ from those of the surrounding matrix, which can make the alloy susceptible to localized corrosion. [1, 2] Intermetallic particles with a more noble potential relative to the alloy matrix can facilitate cathodic reactions and initiate localized corrosion in the surrounding alloy.[3] On the other hand, intermetallic particles can have a more anodic potential compared to the alloy matrix which can result in anodic activity (including dealloying) of the intermetallic particle when exposed to a corrosive environment.[4]

Prior to this work, lithium (Li) salts gained interest as corrosion inhibitor for aluminium alloys after Gui and Devine demonstrated the passivation of AA6061-T6 in alkaline Li-carbonate solutions.[5] Based on this observation, Buchheit et al. continued and formulated an approach for a chemical conversion coating for aluminium alloys based on alkaline Li-carbonate solutions.[6] It was found that the corrosion inhibiting performance of these conversion layers depended on the type of aluminium alloy. In general the performance of the layers followed the intrinsic corrosion resistance of the aluminium alloys: AA1100>AA6061-T6>AA7075-T6>AA2024-T3.[6]

Recent studies have demonstrated that lithium-leaching coatings provide fast and effective corrosion protection on the high strength aluminium alloy AA2024-T3 and is regarded as a promising environmental friendly alternative for chromate based coatings for active corrosion protection.[7, 8] It was demonstrated that when exposed to neutral salt spray conditions, Li-salts were able to leach from the organic coating matrix to form a corrosion protective layer on the exposed aluminium alloy in an artificial coating defect.[9, 10] The formation of the layer involves a multi-step mechanism of oxide thinning, anodic dissolution, and a competitive growth-dissolution process.[11] Further characterization revealed that the protective layer comprises mainly aluminium, oxygen and lithium and features a three-layered structure of a columnar outer layer, a porous middle layer and a dense layer near the aluminium substrate. [9] Electrochemical analysis demonstrated that the corrosion protective properties could be attributed to the dense inner layer.[12]

All recent studies with lithium-salts as leachable corrosion inhibitor were performed on AA2024-T3 and no other substrates were evaluated as yet. This study presents the first investigation of the active corrosion protective properties of lithium-leaching coatings on other alloys than AA2024-T3 under neutral salt spray (ASTM B-117) conditions. A set of industrially relevant alloys with different local electrochemical activities was selected. The relative order of corrosion susceptibility of these alloys increases from AA6014-T4 > AA5083-H111 > AA2024-T3 > AA7075-T6.[13] Organic coatings with and without Li-carbonate as leachable inhibitor were applied on the aluminium alloys and the samples were damaged with an artificial scribe and exposed to the neutral salt spray corrosion test (ASTM B-117).

After the exposure the samples were examined with an optical microscope and a detailed investigation of the defect area was performed using scanning electron microscopy (SEM). Furthermore, the corrosion protective properties of the layers in the defect area were investigated using electrochemical impedance spectroscopy (EIS). The combination of these techniques provides a new insight into the corrosion protective properties of lithium-leaching coatings for these intrinsically different aluminium alloys.

9.2 Experimental

9.2.1 Materials and sample preparation

Aluminium alloys were acquired from various sources (Table 9.1).

Table 9.1: Alloys used in this study and their intended application areas[14]

Alloy	Temper	Thickness	Supplier	Application area
2024	T3	0.8 mm	Arconic	aerospace
5083	H111	1.0 mm	Thyssen-Krupp	automotive/marine
6014	T4	1.0 mm	Chemetall	automotive
7075	T6	0.8 mm	Thyssen-Krupp	aerospace/automotive

The composition of the alloys and their major alloying elements (highlighted) are summarized in Table 9.2.[15]

Table 9.2: Chemical composition of the aluminium alloys[15]

Alloy	Si	Fe	Cu	Mn	Mg	Cr	Zn	Ti	Others	Al
2024-T3	0.5	0.5	3.8-4.9	0.3-0.9	1.2-1.8	0.1	0.25	0.15	0.15	rest
7075-T6	0.4	0.5	1.2-2.0	0.3	2.1-2.9	0.18-0.28	5.1-6.1	0.2	0.15	rest
5083-H111	0.4	0.4	0.1	0.4-1.0	4.0-4.9	0.05-0.25	0.25	0.15	0.15	rest
6014-T4	0.3-0.6	0.35	0.25	0.05-0.2	0.4-0.8	0.2	0.1	0.1	0.15	rest

Prior to the coating application, the panels were degreased with acetone to remove surface contaminations and abraded with Scotch-Brite™ 7447 PRO pads, and finally cleaned again with acetone.

9.2.2 Preparation of the organic model coatings

Epoxy-amine based model coatings were formulated, loaded with and without Li-carbonate as a leaching corrosion inhibitor. The formulations of the epoxy coatings are summarized in Table 9.3. The coating with Li-carbonate as leaching corrosion inhibitor contains 8 vol % pigment volume concentration (PVC) of Li-carbonate. Both coatings (with and without Li-carbonate) were formulated to a total PVC of 30 vol % using pigments and extenders.

The epoxy coatings were prepared according to the following procedure: the ingredients of component A were added under stirring into a 370 ml glass jar. The pigments were dispersed to a fineness of grind less than 25 μm by shaking, on a Skandex® paint shaker,

using 400 grams Zirconox® pearls (1.7-2.4 mm) as a grinding medium. The pearls were separated from the mixture after the dispersion phase. Component B was prepared separately and added to Component A prior to the application.

The coating formulations were spray applied on the abraded and cleaned alloys using a high volume low pressure (HVLP) spray gun. All samples were applied at ambient conditions at 23 °C and 55 % RH. After a 1 h flash-off period, the samples were cured in an oven (1 h at 80 °C). The dry film thickness of the coatings was 28 ± 3 μm for all samples.

Table 9.3: Composition of organic model coatings

	Supplier	Without inhibitor	Li-carbonate
Component A			
Methyl isobutyl ketone	Brenntag	12.9 g	12.9 g
Epikote 828	Momentive	20.8 g	20.8 g
Lithium carbonate	Sigma Aldrich	-	6.9 g
Magnesium oxide	Sigma Aldrich	11.8 g	11.8 g
Tioxide TR 92	Huntsman	12.0 g	12.0 g
Blanc Fixe N ($Ba(SO_4)$)	Sachtleben	28.0 g	13.0 g
Component B			
Xylene	Brenntag	6.0 g	6.0 g
Ancamine 2500	Evonik	14.5 g	14.5 g
Dynasilan Glymo	Evonik	2.0 g	2.0 g

9.2.3. Referencing of the samples

In this paper, the alloys that were coated with the Li-carbonate loaded coating will be referenced as AAXXXXW (e.g. AA2024W) and the samples that were coated with the coating without Li-carbonate will be referenced as AAXXXXWO (e.g. AA7075WO)

9.2.4. Active corrosion protection in the defect area

The coatings were artificially damaged in order to assess the active protective properties of the Li-leaching coating. On a sample panel of 7 x7 cm, two intersecting scribes penetrating through the coating and 100-150 μm into the alloy with a width of 1 mm and a length of 2 cm were prepared by mechanical milling resulting in a defect with a surface area of 0.48 cm^2. The damaged samples were exposed to the neutral salt spray test (NSS) according to ASTM-B117 for 168 h. After the exposure, the defect areas were assessed for their appearance using optical microscopy. In addition, further assessments of the defect areas were performed using scanning electron microscopy and electrochemical impedance spectroscopy.

9.2.5 Scanning electron microscopy (SEM)

A JEOL JSM-7100F field emission SEM was used to investigate the defect areas. The surface morphology of the defect areas was examined in planar view with a lower electron detector (LED) at 5kV and a working distance of 10 mm. Cross-sections of the defect areas were prepared by polishing using a Hitachi IM4000 ion milling system at 6kV Ar-ion

acceleration, applying a 3 times-per-minute sample rotation speed and a swing angle of +/- 30º. These cross-sections were examined using the backscatter electron detector (BED-C) at 5 kV and a working distance of 4 mm.

9.2.5 Electrochemical assessment of the defect area

All electrochemical measurements were executed with a Gamry Interface 1000 computer-controlled potentiostat using an electrochemical cell with a three-electrode set-up in a Faraday cage. The three-electrode set-up consisted of a saturated calomel electrode (SCE) as reference electrode, the coating defect area as the working electrode, and a graphite counter electrode. The electrochemical cell had a total surface area of 12.5 cm^2 and the effective electrode (i.e. the coating defect) area was 0.48 cm^2.

Potentiodynamic polarisations were performed in a 3.5 % NaCl solution to obtain comparative information related to the electrochemical activity in terms of kinetics of anodic and cathodic reactions in the defect areas of the different aluminium alloys. In order to assess the electrochemical behaviour in the defect area of the different alloys under potentiodynamic polarisation conditions, the aluminium panels were masked with a polyester tape and mechanically milled as described above for the coatings. The open circuit potential (OCP) was measured for 10 min prior to polarisation to establish an approximately stable potential. It was found that 10 minutes was sufficient time for the OCP to stabilize in the defect area to obtain reproducible potentiodynamic polarisation measurements. The samples were polarised using a sweep rate of 0.5 mV/s and a sweep range of -300 and +300 mV versus the OCP. Separate samples were used for anodic and cathodic potentiodynamic polarisations starting from the OCP. In order to assess reproducibility, all tests were performed in triplicate for each anodic and cathodic polarisation. The polarisation curves were used to approximate the corrosion current density (i_{corr}) of the alloys from the linear slope of the linear region ±20 mV vs. E_{corr} using the Stern-Geary equation. [16, 17]

Electrochemical impedance spectroscopy (EIS) was applied to assess the corrosion activity and inhibition in the defect area with a surface area of 0.48 cm^2 before and after exposure to the neutral salt spray test. The EIS measurements were performed at the open circuit potential (OCP) in a 0.05 M NaCl solution as electrolyte over a frequency range from 10^{-2} Hz to $2 \cdot 10^4$ Hz, applying a 10 mV sinusoidal amplitude and recording 10 measurements per frequency decade. The impedance spectra were fitted with Zview from Scribner Associates Inc. using the appropriate equivalent circuits for further data analysis. The values resulting from the fitting were scaled to a surface area of 1 cm^2.

9.3 Results and Discussion

9.3.1 Optical observations of the scribed defect areas after NSS exposure

The defect areas of the coated alloys were examined with an optical microscope after 168 h exposure to NSS. The optical images, displayed in Fig. 9.1, show the effects of the corrosive conditions in the scribed areas after exposure to the NSS of the coated alloys with and without Li-carbonate as leaching inhibitor. The detrimental effects of these corrosive conditions are observed on the samples coated with the coating without an inhibitor. Especially the samples of AA2024WO and AA7075WO (Fig. 9.1$a_{(wo)}$ and 9.1$b_{(wo)}$) show a darkened scribe with a significant amount of voluminous corrosion products and extensive corrosion creeping under the coating from the defect area. Apart from some darkening of the scribed area, the other alloys, AA5083WO, and AA6014WO (Fig. 9.1$c_{(wo)}$ and 9.1$d_{(wo)}$) do not show severe signs of corrosion nor extensive corrosion underneath the coatings. The corrosion inhibiting effect of the coatings loaded with Li-carbonate as leachable corrosion inhibitor on the different alloys can clearly be observed from the corresponding images (Fig. 9.1$a_{(w)}$-9.1$d_{(w)}$). All alloys coated with the lithium-loaded coatings show almost pristine scribes without corrosion products and no corrosion creep under the coating.

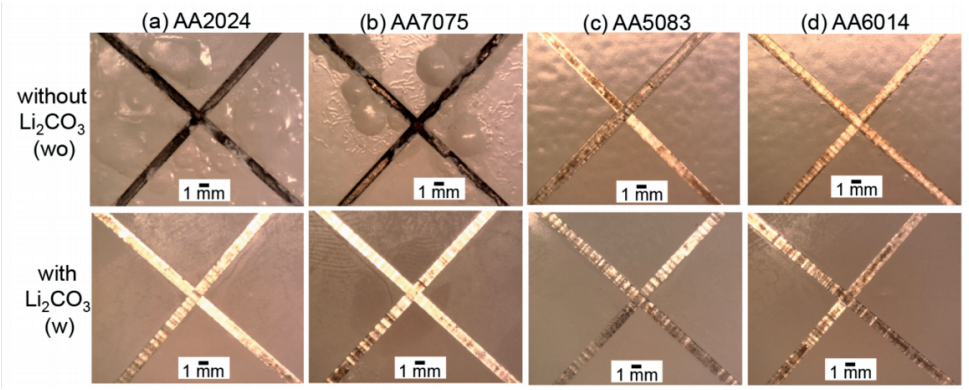

Figure 9.1 Optical images of the coated and scribed panels of the different aluminium alloys after 168 h neutral salt spray exposure (ASTM B-117):(a) AA2024-T3, (b) AA7075-T6, (c) AA5083-H111, and (d) AA6014-T4 (WO) coating without and (W) with Li-carbonate.

9.3.2 Detailed morphological observations in the scribed defect area after NSS exposure

The defect areas were examined in more detail using SEM. Fig. 9.2 shows top-view SEM micrographs of the scribed area of the samples discussed in the previous section. This figure shows the large amount of corrosion products in the scribed areas of AA2024WO and AA7075WO (Fig. 9.2a_{wo} and 9.2b_{wo}) after the NSS exposure when the coating did not contain Li-carbonate as leachable corrosion inhibitor. The corresponding images of these alloys (Fig. 9.2a_{w} and 9.2b_{w}) show the corrosion inhibiting effect on these alloys of the Li-

carbonate loaded coatings, clearly revealing scribes without any signs of corrosion in the defect area. The micrographs of the other alloys (AA5083 and AA6014) show no significant differences between the samples with and without Li-carbonate. It can be observed that all scribes are covered with a layer but no severe corrosion was observed at this magnification. Fig. 9.3 shows a more detailed overview of the surface morphologies of a representative area of each of the scribes at higher magnification.

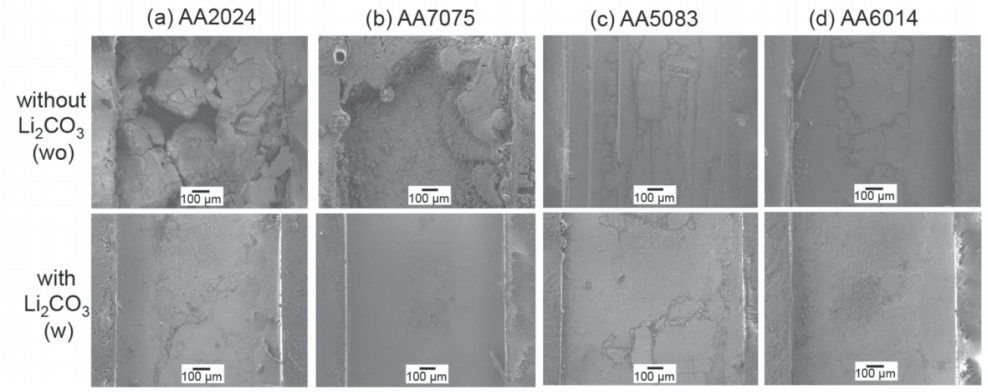

Figure 9.2 SEM micrographs of the top-view appearance of the scribes of the samples after 168 h neutral salt spray exposure (ASTM B-117)(a) AA2024-T3,(b) AA7075-T6, (c) AA5083-H111, and (d) AA6014-T4, (WO) coating without and (W) with Li-carbonate.

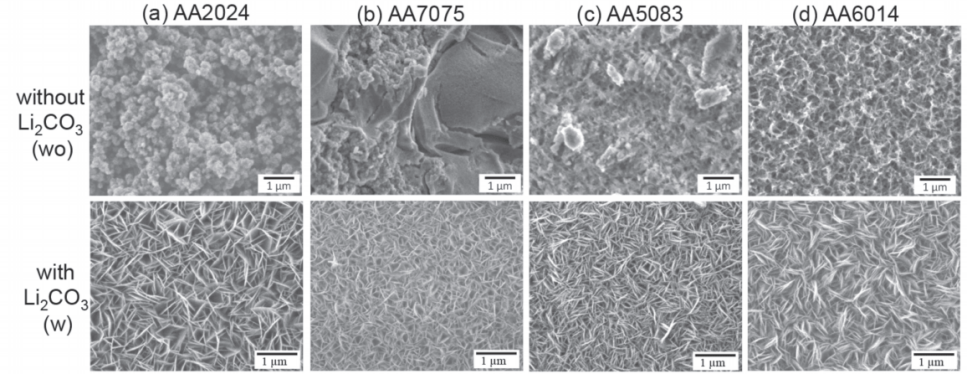

Figure 9.3 SEM micrographs of the top-view morphology of the layer in the scribe after 168 h neutral salt spray exposure (ASTM B-117)(a) AA2024-T3,(b) AA7075-T6, (c) AA5083-H111, and (d) AA6014-T4, (WO) coating without and (W) with Li-carbonate.

It shows a clear difference in the surface morphology of the layers in the defect areas of the samples without Li-carbonate (Fig. $9.3a_{wo}$- $9.3d_{wo}$) compared to the samples with the Li-carbonate loaded coating (Fig. $9.3a_{w}$- $9.3d_{w}$). Fig. $9.3a_{wo}$ and $9.3b_{wo}$ show the voluminous

corrosion products present in the scribes of AA2024WO and AA7075WO. The scribe of AA5083WO did not show a lot of corrosion products with the optical and initial SEM assessment of the scribed area, but the magnified micrograph Fig. 9.3c_{wo} shows a layer of dense corrosion products.
Fig. 9.3d_{wo} reveals that the scribe of AA6014WO is covered with a layer with the morphology of a hydrated aluminium oxide, which can indicate that the substrate is affected by corrosion

In contrast to these samples, all the scribes of the alloy samples coated with the Li-carbonate loaded coatings were covered by a layer with a polycrystalline morphology, featuring intersecting plate-like crystals that is commonly observed for layered double hydroxide compounds generated on aluminium[6, 18, 19] and is typical for the protective layer generated from the Li-leaching coating technology.[9, 20] The size of the crystals varies per alloy but it is evident that the formation of these layers is a result from the active protective nature of the Li-leaching coatings.

9.3.3. Cross-sectional analysis of the defect areas after NSS exposure

Ion-milled cross-sections of the defect areas were prepared to study these layers and the effects of the NSS exposure on the different alloys in more detail using SEM. Fig. 9.4 shows the cross-sectional micrographs of the defect areas of the alloys after 168 h NSS exposure. Fig. 9.4a_{wo} shows the cross-section of the corroded surface of the scribe of the AA2024WO sample. The layer of corrosion products is about 6 µm thick and has been formed due to the detrimental effects of the corrosive environment during the NSS exposure. The alloy surface is severely attacked. In contrast to this, a layer with a thickness of 2 µm is formed on the AA2024W sample (Fig. 9.4a_w).

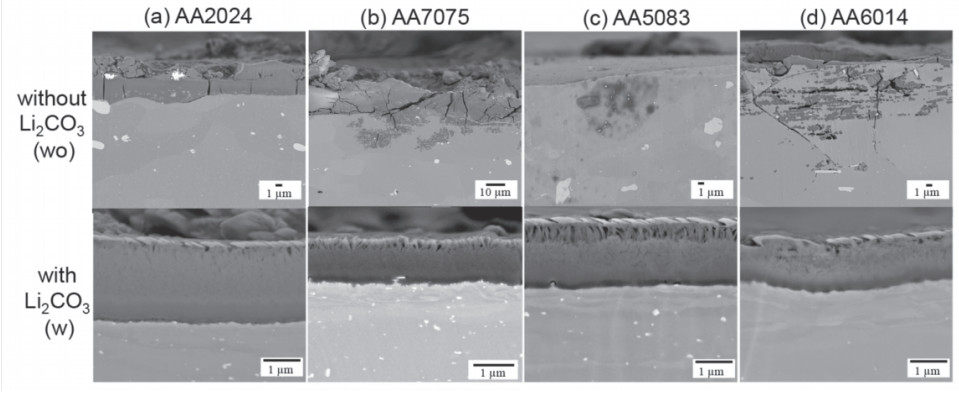

Figure 9.4 *Cross-sectional scanning electron micrographs of the scribes of the different alloys after 168 h NSS exposure (ASTM B-117): (a) AA2024-T3,(b) AA7075-T6, (c) AA5083-H111, and (d) AA6014-T4 (WO) coating without and (W) with Li-carbonate.*

The layer has the characteristic three-layered morphology, featuring a dense inner layer, a porous middle layer and a columnar outer layer as observed in previous work on AA2024-T3 and no signs of (local) corrosion phenomena were observed.[9]
The defect area of the AA7075WO sample (Fig. 9.4b_{wo}) shows severe corrosion into the substrate besides a layer of voluminous corrosion products, with a thickness of more than 10 µm. Similar to AA2024W, a layer with the three-layered morphology, with an approximate thickness of 1.0 µm, was formed on the aluminium substrate in the defect of the AA7075W sample (Fig. 9.4b_{w}). The cross-sectional analysis of the defect area of the sample AA5083WO (Fig. 9.4c_{wo}) shows no significant amounts of corrosion products after 168h NSS exposure. A thin oxide layer is present on the aluminium surface in the defect and the alloy seems to be locally affected by corrosion of specific grains at the surface of the scribe, possibly due to local anodic dissolution of magnesium. However, such local corrosion attacks were not observed in the defect areas of the AA5083W sample Similar to AA2024W and AA7075W, a protective layer with a typical three-layered morphology with a total thickness of 1.5-2 µm was formed in the defect area after the NSS exposure (Fig. 9.4c_{w}). A similar protective layer was formed in the defect area of the sample of the AA6014W sample after 168 h NSS exposure (Fig. 9.4d_{w}) Whereas optically, the defect of the AA6014WO sample looked optically still free of corrosion, the cross-sectional analysis revealed (intergranular) corrosion of the substrate (Fig. 9.4dwo). These observations show that a layer is formed in the defect areas of all alloys when a Li-leaching coating was used independent from the alloy composition. Despite some slight differences in contrast and thickness, in general the layers feature the similar characteristic morphology of a dense inner layer, a porous middle layer and columnar outer layer known for protective layers generated from Li-leaching coatings Furthermore, the results confirm that AA5083-H111 and AA6014-T4 are less sensitive to corrosion compared to the 2XXX and 7XXX series of alloys.[21]

9.3.4. Corrosion protective properties the layers in the defect areas of the different alloys

Electrochemical activity of the defect areas prior to exposure

Potentiodynamic polarisation measurements were performed on the taped panels with a scribed defect area to determine the difference of the electrochemical activity in the defect areas of the different alloys. Fig. 9.5 shows the potentiodynamic polarisation curves recorded for each of the alloys. When polarised anodically, AA6014-T4 and AA5083-H111 show a passive range and a distinct pitting potential (E_{pit}) whereas, the high strength aluminium alloys (AA2024-T3 and AA7075-T6) show their typical active character.[22, 23] Furthermore, the alloys show different cathodic reaction kinetics. The values of corrosion potential (E_{corr}), pitting potential (E_{pit}) and the corrosion current density (i_{corr}) were derived from the potentiodynamic polarisation curves and summarized in Table 9.4.

The high-strength aluminium alloys, AA2024-T3 and AA7075-T6, have a more noble E_{corr} compared to AA6014-T4 and AA5083-H111. In addition it can be observed that the

cathodic branches of these alloys have higher current density values indicating faster cathodic reaction kinetics. The magnitude of this E_{corr} shift and increased cathodic reaction kinetics is related to the copper content in the alloy.[13] The low copper alloys (AA6014-T4 and AA5083-H111) show a reproducible and similar E_{pit} but differ slightly in E_{corr} and cathodic reaction kinetics (AA6014-T4 < AA5083-H111). For AA7075-T6 with a copper content of (1.2-2 wt.%), the E_{corr} shifts 68 mV to the more noble potentials and higher cathodic reaction kinetics. AA2024-T3 shows an even larger shift to more noble potential (289 mV) due to the higher copper content (3.8-4.9 Wt.% Cu) also here an increase in the cathodic reaction kinetics is observed. All together this leads to significant higher corrosion current density values compared to the low copper alloys. Considering these observations and the i_{corr} values of 5.0 and 4.4 µA/cm^2 for respectively AA7075-T6 and AA2024-T3 compared to the i_{corr} values of 1.5 and 1.4 µA/cm^2 for AA5083-H111

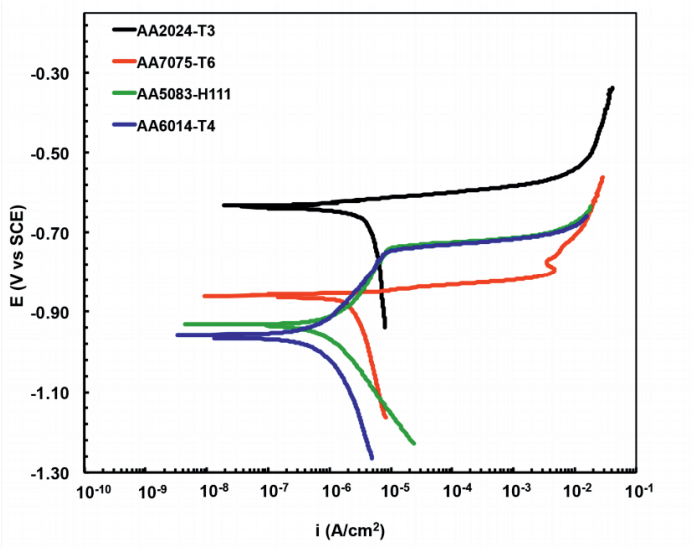

Figure 9.5 Potentiodynamic polarisation curves of the damaged areas of aluminium alloys in 3.5% NaCl solution.

Table 9.4: Electrochemical parameters obtained from the potentiodynamic polarisation curves of the different alloys displayed in Fig. 9.5

	E_{corr} (V_{SCE})	i_{corr} (µA/cm^2)	Passive range E_{pit}-E_{corr}(V)
2024-T3	-0.638±0.01	4.4± 1.7	0
7075-T6	-0.859±0.01	5.0± 0.2	0
5083-H111	-0.927±0.01	1.5± 0.1	0.2±0.01
6014-T4	-0.957±0.02	1.4± 0.0	0.23±0.02

The high-strength aluminium alloys, AA2024-T3 and AA7075-T6, have a nobler E_{corr} compared to AA6014-T4 and AA5083-H111. In addition it can be observed that the cathodic branches of these alloys have higher current density values indicating faster

cathodic reaction kinetics. The magnitude of this E_{corr} shift and increased cathodic reaction kinetics is related to the copper content in the alloy.[13] The low copper alloys (AA6014-T4 and AA5083-H111) show a reproducible and similar E_{pit} but differ slightly in E_{corr} and cathodic reaction kinetics (AA6014-T4 < AA5083-H111). For AA7075-T6 with a copper content of (1.2-2 wt.%), the E_{corr} shifts 68 mV to the more noble potentials and higher cathodic reaction kinetics. AA2024-T3 shows an even larger shift to more noble potential (289 mV) due to the higher copper content (3.8-4.9 Wt. % Cu) also here an increase in the cathodic reaction kinetics is observed.

All together this leads to significant higher corrosion current density values compared to the low copper alloys. Considering these observations and the i_{corr} values of 5.0 and 4.4 μA/cm^2 for respectively AA7075-T6 and AA2024-T3 compared to the i_{corr} values of 1.5 and 1.4 μA/cm^2 for AA5083-H111 and AA6014-T4 the defect areas of the aluminium alloys can be ordered based on increasing electrochemical activity or corrosion sensitivity: AA6014-T4 < AA5083 < < AA2024-T3 < AA7075-T6.

EIS measurements

EIS was used to measure the electrochemical characteristics of the layers formed in the defects of the different alloys from the coatings with and without Li-carbonate. Fig. 9.6 shows the recorded EIS spectra of the coated alloys before and after the 168 h NSS exposure. The figure shows the Bode plots of the impedance modulus and the accompanying phase angle plots of the measurements for each alloy. Each graph shows a measurement of an unexposed sample to demonstrate the initial stage of the defect area with the native aluminium oxide and the measurements of the samples with and without Li-carbonate after 168 h NSS exposure. Fig. 9.6a shows the typical response of the impedance modulus (top) and phase angle (bottom) of a AA2024-T3 coated with and without Li-carbonate as leaching inhibitor.[12] The impedance modulus (Fig. 9.6a$_{top}$) of the sample with the Li-carbonate loaded coating increased in the middle (10^1-10^3 Hz) and low frequency (10^{-1}-10^{-2} Hz) ranges compared to the samples without Li-carbonate and the unexposed sample. This increase of the impedance modulus can be attributed to the formation of an oxide layer and the increased corrosion resistance of such layers in the defect area.[24, 25]

Fig. 9.6a$_{bottom}$ shows the phase angle diagrams of the respective AA2024-T3 samples. The phase angle plot of the unexposed sample shows two time-constants, one at 10^1 Hz associated with the native oxide layer and one time-constant around $2{\cdot}10^{-2}$Hz for the electrochemical activity at the aluminium substrate in the coating defect.[26] Compared to the unexposed sample and the sample without Li-carbonate, the phase angle plot of the sample with the Li-carbonate loaded coating showed a broadening of the time-constant related with formation the oxide layer and increases phase angle values at the lower frequency range which indicates improved corrosion resistance. This behaviour is characteristic for the Li-leaching coating technology on AA2024-T3.[12, 20]

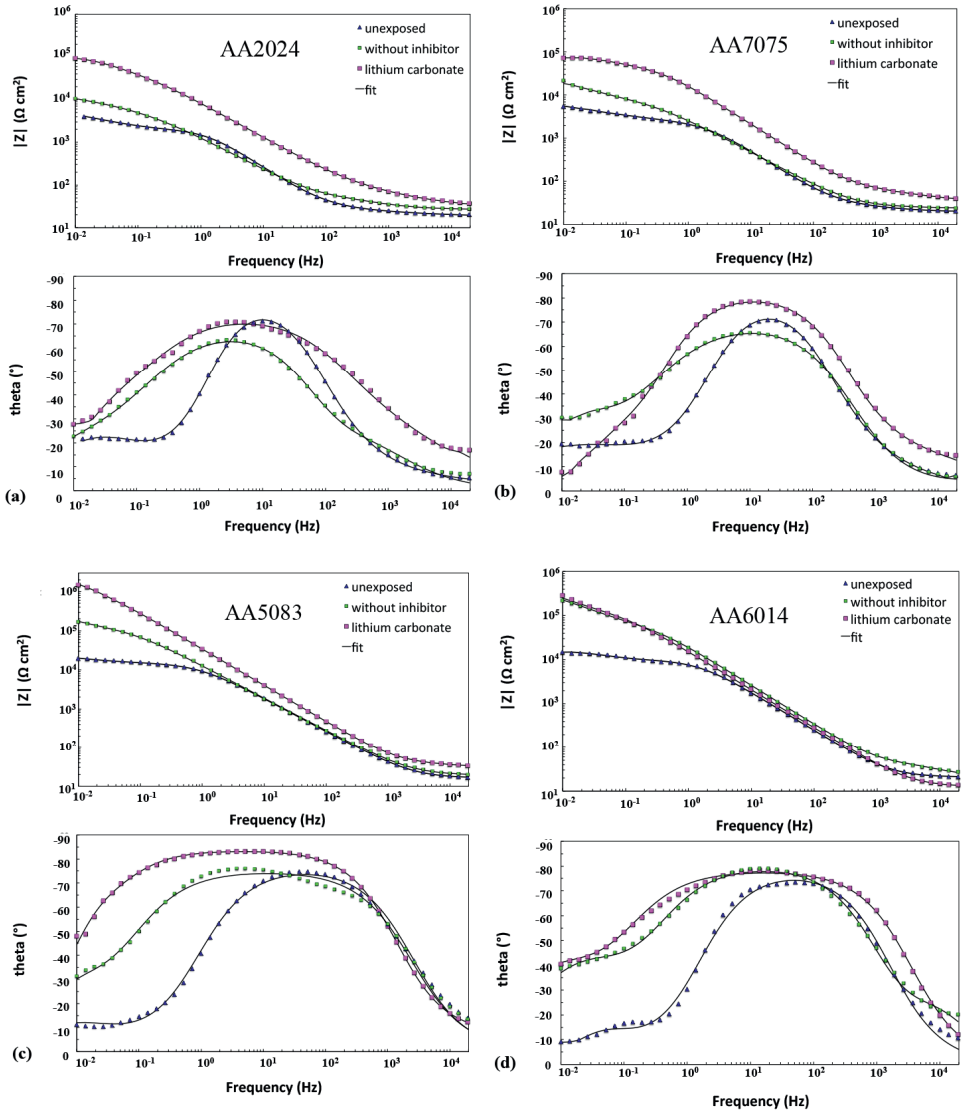

Figure 9.6 Electrochemical impedance spectra of the coated aluminium alloys with a defect area in 0.05 M NaCl solution before and after 168 h NSS. (a) AA2024; (b) AA7075; (c) AA5083; and (d) AA6014 showing impedance modulus (top) and phase angle plots (bottom).

A similar behaviour was observed for the samples with the Li-carbonate loaded coatings on the AA7075W (Fig. 9.6b) and the AA5083W (Fig. 9.6c) after 168 h NSS exposure. Therefore, it can be stated that the generated layers in the defects of these alloys provide enhanced corrosion protective properties. The sample with the Li-carbonate loaded coating on AA6014 showed a slightly different behaviour (Fig. 9.6d). Whereas, the cross-section

revealed the formation of a protective layer in the defect of the AA6014 aluminium alloy, the impedance modulus in the middle frequency range does not increase significantly for the AA6014W sample. However, the low frequency impedance increased about 10 times for both the samples AA6014WO and AA6014W compared to the unexposed sample. While initially the differences in the Bode magnitude plot are relatively small, it is clear from the cross-sectional analysis that the layer generated in the defect area of AA6014W provided additional corrosion protection compared to the sample AA6014WO.

Electrochemical properties of the protective layers.

Three physical models (Fig. 9.7) were defined with their respective equivalent circuit (EC) to fit the measurements and quantitatively describe the electrochemical properties of the layers present in the defect areas after the NSS exposure. . The selection of the relevant equivalent circuits used for the fitting of the different samples was based on the physical morphology observed by the cross-sectional analysis of the defect area. EC1 is a model with two time-constants used to describe the effect in a defect area of a damaged coating representing the aluminium substrate with a thin or native oxide layer.

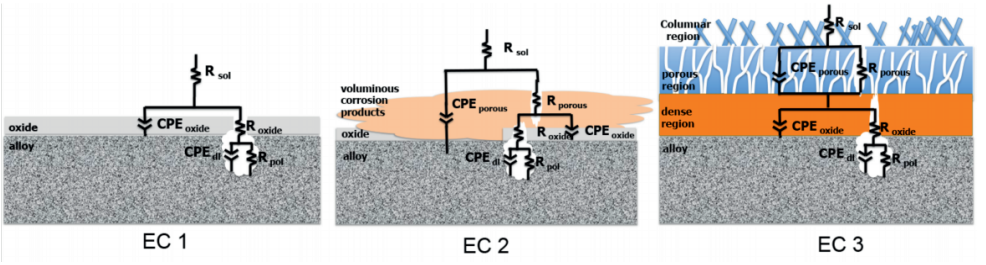

Figure 9.7 *Equivalent electric circuits used to fit the EIS spectra: (EC1) unexposed defect areas and defect areas with few or no corrosion products;(EC2) defect areas with voluminous porous corrosion products; (EC3) defect areas with protective layer generated from the Li-carbonate loaded coatings.*

In this EC, R_{SOl} is the electrolyte resistance; R_{oxide} is the resistance of the (native) oxide layer and the CPE_{oxide} is the constant phase element (CPE_{dl}) describing the capacitance of the oxide layer using parameters Q_{oxide} and n_{oxide}. R_{pol} and CPE_{dl} describe the electrochemical processes at the aluminium substrate in the second time-constant, which represent the polarisation resistance and the double layer capacitance. The CPEs are used in these ECs to describe the frequency dependence of elements with a non-ideal capacitive behaviour and because of the non-uniformity of the generated layers in the defect.[27, 28] EC 2 describes the physical model with an additional time-constant to account for the voluminous porous corrosion products (CPE_{porous} and R_{porous}) in the defect, on top of the oxide layer and EC3 is the model that is used to describe the three-layered morphology of the protective layer that is generated from the Li-carbonate loaded coating.[12] The three time-constants of EC3 are represented by: R_{sol} for the electrolyte resistance, CPE_{porous} and R_{porous} and describe the contribution of the porous middle layer which is usually very minor, the dense inner layer at the aluminium substrate is represented by R_{oxide} and CPE_{oxide} , and the double layer

capacitance and polarisation resistance at the metal/oxide interface are described by CPE_{dl} and R_{pol}. The fitted curves are displayed as solid lines in the Bode plots of Fig. 9.6. The numerical values of the fittings from these spectra are listed in Table 9.5.

Table 9.5: Fitted parameters of the EIS spectra of the scribed coatings on the different alumium alloys

AA2024-T3				
		Unexposed	Without inhibitor	Lithium-leaching
EC		1	2	3
R_{sol}	Ω	24	24	28
$Q(CPE_{porous})$	Ss^ncm^{-2}	-	1.14×10^{-3}	1.95×10^{-5}
n_{porous}		-	0.45	0.5
R_{Porous}	Ωcm^2	-	31	57
$Q(CPE_{Oxide})$	Ss^ncm^{-2}	8.67×10^{-5}	1.72×10^{-4}	2.85×10^{-5}
n_{oxide}		0.9	0.80	0.88
R_{oxide}	Ωcm^2	2192	6875	60493
$Q_{(CPE_{dl})}$	Ss^ncm^{-2}	2.03×10^{-3}	6.92×10^{-4}	1.31×10^{-4}
n_{dl}		0.77	0.74	0.7
R_{pol}	Ωcm^2	4201	7574	62693
χ^2		2.5×10^{-4}	2.8×10^{-4}	1.1×10^{-3}

AA7075-T6				
		unexposed	Without inhibitor	Lithium-leaching
EC		1	2	3
R_{sol}	Ω	24	18	29
$Q(CPE_{porous})$	Ss^ncm^{-2}	-	1.50×10^{-4}	1.77×10^{-4}
n_{porous}		-	0.50	0.51
R_{Porous}	Ωcm^2	-	8	45
$Q(CPE_{Oxide})$	Ss^ncm^{-2}	$4{,}84 \times 10^{-5}$	7.91×10^{-5}	1.05×10^{-5}
n_{oxide}		0.89	0.79	0.92
R_{oxide}	Ωcm^2	2654	9021	49841
$Q_{(CPE_{dl})}$	Ss^ncm^{-2}	1.03×10^{-3}	3.19×10^{-4}	7.74×10^{-5}
n_{dl}		0.6	0.75	0.83
R_{pol}	Ωcm^2	6144	15948	29750
χ^2		1.8×10^{-3}	1.5×10^{-4}	5.0×10^{-4}

AA5083				
		unexposed	Without inhibitor	Lithium-leaching
EC		1	1	3
R_{sol}	Ω	17	19	26
$Q(CPE_{porous})$	Ss^ncm^{-2}	-	-	2.73×10^{-4}
n_{porous}		-	-	0.5
R_{Porous}	Ωcm^2	-	-	18
$Q(CPE_{Oxide})$	Ss^ncm^{-2}	1.51×10^{-5}	1.67×10^{-5}	5.11×10^{-6}
n_{oxide}		0.86	0.83	0.93
R_{oxide}	Ωcm^2	15000	156190	500000
$Q_{(CPE_{dl})}$	Ss^ncm^{-2}	6.90×10^{-4}	9.04×10^{-5}	9.02×10^{-7}
n_{dl}		0.69	0.82	0.89
R_{pol}	Ωcm^2	9863	160170	1690200
χ^2		2.03×10^{-3}	3.29×10^{-3}	6.7×10^{-4}

AA6014				
		unexposed	Without inhibitor	Lithium-leaching
EC		1	2	3
R_{sol}	Ω	21	22	13
$Q(CPE_{porous})$	Ss^ncm^{-2}	-	2.46×10^{-5}	2.2×10^{-4}
n_{porous}		-	0.69	0.81
R_{Porous}	Ωcm^2	-	21	35
$Q(CPE_{Oxide})$	Ss^ncm^{-2}	1.40×10^{-5}	9.36×10^{-6}	1.27×10^{-5}
n_{oxide}		0.88	0.88	0.88
R_{oxide}	Ωcm^2	10174	77722	146490
$Q_{(CPE_{dl})}$	Ss^ncm^{-2}	6.18×10^{-4}	2.63×10^{-5}	3.59×10^{-5}
n_{dl}		0.88	0.71	0.76
R_{pol}	Ωcm^2	5780	431000	474670
χ^2		3.46×10^{-3}	8.25×10^{-4}	3.01×10^{-3}

In order to compare the electrochemical properties of the defect areas, the equivalent capacitance of the oxide layer (C_{oxide}) and double layer (C_{dl}) in the different EC's was calculated using the respective CPE parameters (Q and n) and the resistance corresponding to each time-constant of the measurements summarized in Table 5 using the equation of to Hirschorn et al.[29]:

$$C = R^{\frac{(1-n)}{n}} Q^{\frac{1}{n}} \quad (1)$$

The results in Table 9.5 also show that there is a small contribution of the porous regions of the layers in the defects after 168 h NSS exposure. The values of Q(CPE_{porous}) and R_{porous} mentioned in table 5 represent the contribution of two different porous materials. In case of the coatings without lithium, this parameter represents the contribution of the voluminous corrosion products (EC2) and for the samples with lithium it represents the contribution of the porous region in the protective layer. (EC3) The n values of $Q_{(CPE\ porous)}$ are around 0.5. This indicates that the contribution of the porous element does not behave as an ideal capacitor. These low N (CPE) values suggest a diffusion process or a porous electrode [30] It is known that the protective layer in the defect area is not uniform and capacitive values may vary throughout the layer. The relative contribution of the porous element of the layer is small and may seem insignificant compared to the parameters of the dense oxide layer. However, the physiochemical model used for the electrochemical analysis can be justified by the micrographs of the protective layers and the contribution of the porous layer cannot be ignored for the fitting of the equivalent circuit. [12]

Fig. 9.8 shows the trends of the resistance and capacitance values of the oxide layer (R_{oxide} and C_{oxide}) and the metal/oxide interface (R_{pol} and C_{dl}) in the defects of different coated alloys before and after exposure to the NSS test. Fig. 9.8a shows the corrosion inhibiting effect of the protective layer generated in the defect area on AA2024W after the NSS exposure. From the graph it can be observed that both the resistance values (R_{oxide} and R_{pol}) of the sample AA2024W are 8 to 10 times higher compared to the sample AA2024WO or the unexposed sample. For the same sample, the capacitance values dropped to 32 µF/cm^2 and 320 µF/cm^2 for respectively C_{oxide} and C_{dl} which is in good agreement with previous findings.[12] These increased resistances and decreased capacitances are consistent with the presence of a corrosion protective layer in the defect area.

Besides the optical and microscopy analysis, the EIS measurements demonstrate the weak corrosion resistance in the defect area of the sample AA2024WO. The R_{oxide} and R_{pol} remained low around 7 kΩ.cm^2 and the capacitance values increased to 180 µF/cm^2 and 1240 µF/cm^2 indicating the occurrence of corrosion. A similar behaviour as the AA2024 alloy is observed for the AA7075 and AA5083 alloys in Fig. 9.8b and 9.8c. Both alloys show the increase resistances and strongly reduced capacitance values for the samples coated with the Li-carbonate loaded coating. These results clearly demonstrate that the layer in the defect area generated from the Li-carbonate loaded coating provides effective

corrosion inhibition on AA7075 and AA5083 as well. Aluminium alloy AA6014 (Fig. 9.8d) exhibits a different behaviour compared to the other alloys.

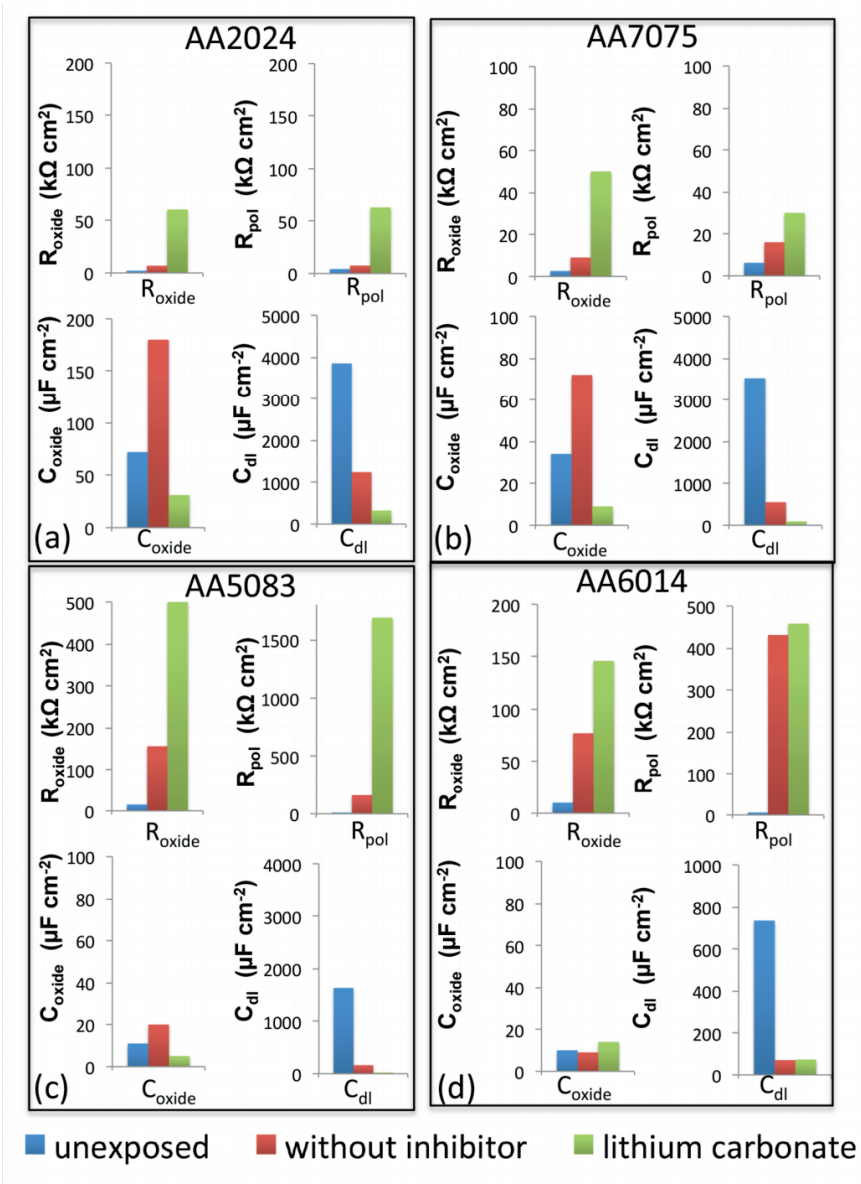

Figure 9.8 Comparison of the electrochemical parameters, oxide resistance (Roxide), polarisation resistance (Rpol), oxide capacitance (Coxide), and double layer capacitance (Cdl) in the defect areas of the different alloys coated with coatings with and with Li-carbonate before and after NSS exposure: (a)AA2024, (b) AA7075, (c) AA5083, (d) AA6014.

The unexposed AA6014 sample shows a low R_{oxide} (10 kΩ.cm^2) and R_{pol} (6 kΩ.cm^2) and a high C_{dl} (735 µF/cm^2), which indicates susceptibility to corrosion. However, the alloy shows significantly increased R_{oxide} and R_{pol} values of respectively 70 kΩ.cm^2 and 440 Ω.cm^2 for both samples AA6014WO and AA6014W after the NSS exposure. The cross-sectional analysis of AA6014W showed the formation of a protective layer in the defect area when the sample was exposed to NSS. The layer provides a R_{oxide} of 145 kΩ.cm^{2}which is double of the R_{oxide} of the sample AA6014WO. The polarisation resistance (R_{pol}) of the exposed samples increased dramatically compared to the unexposed sample to values of approximately 450 kΩ.cm^2 and the double layer capacitance (C_{dl}) of the samples dropped to 70 µF/cm^2 which indicates improved corrosion protection. These results imply that AA6014 has a kind self-passivating property after initial corrosion phenomena and the protective layer generated in the defect area of the AA6014W sample provides additional corrosion protection without local corrosion phenomena at the alloy surface.

9.3.5 Active corrosion protection on different alloys with Li-leaching coatings

Fast and effective corrosion inhibition is an essential requirement for active protective coatings. Especially, for the protection of aluminium alloys that are carefully engineered to fulfil specific industrial requirements by alloying and tempering. The electrochemical properties or corrosion susceptibility of an aluminium alloy are determined by the type, concentration and distribution of intermetallic or second phase particles in the matrix and the temper. Addition of alloying metals such as copper, magnesium, silicon, and zinc to the aluminium influence the mechanical properties of the aluminium alloy but also change the electrochemical behaviour of the alloys as well. For example, the addition of copper and silicon shifts the corrosion potential of an alloy to more noble corrosion potentials increasing cathodic reaction kinetics.[13] The alloys studied in this work were selected because of their inherent different electrochemical activity. AA2024-T3 (Al-Cu-(Mg)) and AA7075-T6 (Al-Zn-Mg(Cu)) were selected as alloys with a high corrosion susceptibility and AA5083-H111(Al-Mg-(Mn)), and AA6014-T4 (Al-Mg-Si-(Cu)) for their low corrosion susceptibility.[31] The intrinsic corrosion susceptibility of these alloys was confirmed by electrochemical means and the microscopy evaluation. . There are many corrosion tests available to evaluate the corrosion resistance of aluminium alloys. Amongst them, continuous neutral salt spray, cyclic salt spray acidified or copper assisted salt spray methods using a wide range of concentrations and electrolytes. The selection of the corrosion test depends on the application and industry. In this work the coated aluminium samples were exposed to continuous salt spray conditions using the neutral salt spray (NSS) accelerated corrosion test according to ASTM B-117 to compare the active corrosion protection of the Li-leaching coatings on other alloys than AA2024-T3 under equivalent test conditions. All aluminium alloys coated with the coating without Li-carbonate showed local corrosion phenomena due to their microstructure and second phase particles.[4, 13, 32, 33] As expected, both the high strength aluminium alloys, AA2024-T3 and AA7075-T6, showed

significantly more corrosion in the defect area compared to the other alloys. However the "corrosion resistant" aluminium alloys AA6014-T4, and AA5083-H111 were not free of localized corrosion either.

In contrast to this, the Li-leaching coatings were able to suppress these localized corrosion phenomena by the formation of a protective aluminium oxide/hydroxide layer as a result of the competitive growth-dissolution reaction at the aluminium/solution interface under alkaline conditions (pH 9-10).[11] A similar protective layer was formed on the aluminium substrate in the defect areas providing additional corrosion protection for all aluminium alloys, independent of their different electrochemical activity. The layer thickness and morphology of the protective layer was similar for all alloys but the magnitude of the resulting electrochemical properties are different. The corrosion inhibiting effect of the Li-leaching coatings seems to be more pronounced on the alloys with relative large amounts of alloying constituents and higher electrochemical activity (corrosion susceptibility), AA2024-T3 (4-5% Cu), AA7075-T6 (5-6% Zn and 1-2 % Cu) and AA5083-H111 (4-5% Mg). The corrosion inhibiting effect on AA6014 seems relatively small between the samples with Li-carbonate and no inhibitor after NSS exposure, this implies a certain self-passivating property of the AA6014-T4 alloy when exposed to a corrosive environment.

The work in this paper shows that all the studied aluminium alloys can be affected by (local) corrosion phenomena when the coating is damaged and the substrate is exposed to a corrosive environment such as the NSS corrosion test. Therefore, it is essential that the active corrosion protection mechanism provides a fast and effective protection by the formation of an irreversible layer on the exposed substrate in the defect, which will act as a new barrier to prevent further corrosion. It demonstrated that the active protective nature of the Li-carbonate leaching coatings is not limited to AA2024-T3 and that it is possible to effectively protect the defect areas from local corrosion effects by the generation of a corrosion protective layer in the defect areas of AA7075-T6, AA5083-H111, and AA6014-T4 samples after 168 h NSS exposure by using a Li-carbonate loaded coating for active corrosion protection. No other chromate-free corrosion inhibitor has demonstrated such an active protective behaviour independent of the metallurgy of the aluminium alloy. These results demonstrate that Li-salts can be considered as a promising and new class of environmentally-friendly corrosion inhibitors for the protection of a wide range of aluminium alloys even for applications outside the aerospace industry.

9.4 Conclusions

The active protective properties of the Li-leaching coatings on different aluminium alloys were investigated using scanning electron microscopy and electrochemical techniques. Li-carbonate leaching coatings provided effective corrosion inhibition on a range of aluminium alloys independent of their metallurgy and electrochemical activity. The largest

corrosion inhibiting effects were observed on high strength aluminium alloys, AA2024-T3, AA7075-T6, which are known for their active and corrosion susceptible behaviour. The Li-leaching coatings also suppressed localized corrosion and provided additional corrosion resistance on more corrosion resistant aluminium alloys such as AA5083-H111 and AA6014-T4. Planar view and cross-sectional SEM-analysis revealed that the characteristic three-layered protective layer was generated with a similar thickness and morphology on all investigated alloys. Complementary electrochemical impedance spectroscopy measurements demonstrated the corrosion protective properties of the generated layer in the defect area of the different alloys. Further analysis of the EIS data enabled the quantification of electrochemical properties associated with the protective layer on the different aluminium alloys.

References

1. R. G. Buchheit, A compilation of corrosion potentials reported for intermetallic phases in aluminum-alloys, *Journal of the Electrochemical Society*, 1995, 142, 3994-3996.
2. N. Birbilis and R. G. Buchheit, Electrochemical characteristics of intermetallic phases in aluminum alloys - An experimental survey and discussion, *Journal of the Electrochemical Society*, 2005, 152, B140-B151.
3. Z. Szklarska-Smialowska, Pitting corrosion of aluminum, *Corrosion Science*, 1999, 41, 1743-1767.
4. K. A. Yasakau, M. L. Zheludkevich, S. V. Lamaka and M. G. S. Ferreira, Role of intermetallic phases in localized corrosion of AA5083, *Electrochimica Acta*, 2007, 52, 7651-7659.
5. J. Gui and T. M. Devine, Influence of lithium on the corrosion of aluminum, *Scripta Metallurgica*, 1987, 21, 853-857.
6. R. G. Buchheit, Bode, M.D., Stoner, G.E., Corrosion-Resistant, Chromate free Talc Coatings for Aluminum, *Corrosion*, 1994, 50, 205-214.
7. P. Visser, Y. Liu, H. Terryn and J. M. C. Mol, Lithium salts as leachable corrosion inhibitors and potential replacement for hexavalent chromium in organic coatings for the protection of aluminum alloys, *Journal of Coatings Technology and Research*, 2016, 13, 557-566.
8. O. Gharbi, S. Thomas, C. Smith and N. Birbilis, Chromate replacement: what does the future hold?, *npj Materials Degradation*, 2018, 2, 12.
9. P. Visser, Y. Liu, X. Zhou, T. Hashimoto, G. E. Thompson, S. B. Lyon, L. G. J. van der Ven, A. J. M. C. Mol and H. A. Terryn, The corrosion protection of AA2024-T3 aluminium alloy by leaching of lithium-containing salts from organic coatings, *Faraday Discussions*, 2015, 180, 511-526.
10. P. Visser, A. Lutz, J. M. C. Mol and H. Terryn, Study of the formation of a protective layer in a defect from lithium-leaching organic coatings, *Progress in Organic Coatings*, 2016, 99, 80-90.
11. P. Visser, Y. Gonzalez-Garcia, J. M. C. Mol and H. Terryn, Mechanism of Passive Layer Formation on AA2024-T3 from Alkaline Lithium Carbonate Solutions in the Presence of Sodium Chloride, *Journal of The Electrochemical Society*, 2018, 165, C60-C70.
12. P. Visser, M. Meeusen, Y. Gonzalez-Garcia, H. Terryn and J. M. C. Mol, Electrochemical Evaluation of Corrosion Inhibiting Layers Formed in a Defect from Lithium-Leaching Organic Coatings, *Journal of The Electrochemical Society*, 2017, 164, C396-C406.
13. W. J. Liang, P. A. Rometsch, L. F. Cao and N. Birbilis, General aspects related to the corrosion of 6xxx series aluminium alloys: Exploring the influence of Mg/Si ratio and Cu, *Corrosion Science*, 2013, 76, 119-128.
14. J. G. Kaufman, in *Introduction to Aluminum Alloys and Tempers*, ASM International, ch. 6, pp. 87-117.
15. T. A. A. Inc., *International Alloy Designations and Chemical Composition Limits for Wrought Aluminum and Wrought Aluminum Alloys*, The Aluminum Association Inc.: Arlington, VA, USA, 2015.
16. M. Stern and A. L. Geary, Electrochemical Polarization: I . A Theoretical Analysis of the Shape of Polarization Curves, *Journal of The Electrochemical Society*, 1957, 104, 56-63.
17. T. A. Zawodzinski, JES Classics, *Electrochemical Society Interface*, 2009, 59.
18. D. Mata, M. Serdechnova, M. Mohedano, C. L. Mendis, S. V. Lamaka, J. Tedim, T. Hack, S. Nixon and M. L. Zheludkevich, Hierarchically organized Li-Al-LDH nano-flakes: a low-temperature approach to seal porous anodic oxide on aluminum alloys, *RSC Advances*, 2017, 7, 35357-35367.
19. Y. Zhang, J. Liu, Y. Li, M. Yu, S. Li and B. Xue, Fabrication of inhibitor anion-intercalated layered double hydroxide host films on aluminum alloy 2024 and their anticorrosion properties, *Journal of Coatings Technology and Research*, 2015, 12, 293-302.
20. Y. Liu, P. Visser, X. Zhou, S. B. Lyon, T. Hashimoto, M. Curioni, A. Gholinia, G. E. Thompson, G. Smyth, S. R. Gibbon, D. Graham, J. M. C. Mol and H. Terryn, Protective Film Formation on AA2024-T3 Aluminum Alloy by Leaching of Lithium Carbonate from an Organic Coating, *Journal of The Electrochemical Society*, 2016, 163, C45-C53.
21. F. C. Campbell, Elements of metallurgy and engineering alloys, 2008.
22. G. O. Ilevbare and J. R. Scully, Mass-transport-limited oxygen reduction reaction on AA2024-T3 and selected intermetallic compounds in chromate-containing solutions, *Corrosion*, 2001, 57, 134-152.
23. D. K. Xu, N. Birbilis and P. A. Rometsch, The effect of pre-ageing temperature and retrogression heating rate on the strength and corrosion behaviour of AA7150, *Corrosion Science*, 2012, 54, 17-25.
24. B. Van der Linden, H. Terryn and J. Vereecken, Investigation of anodic aluminium oxide layers by electrochemical impedance spectroscopy, *Journal of Applied Electrochemistry*, 1990, 20, 798-803.

25. J. Tedim, M. L. Zheludkevich, A. C. Bastos, A. N. Salak, A. D. Lisenkov and M. G. S. Ferreira, Influence of preparation conditions of Layered Double Hydroxide conversion films on corrosion protection, *Electrochimica Acta*, 2014, 117, 164-171.
26. M. L. Zheludkevich, K. A. Yasakau, S. K. Poznyak and M. G. S. Ferreira, Triazole and thiazole derivatives as corrosion inhibitors for AA2024 aluminium alloy, *Corrosion Science*, 2005, 47, 3368-3383.
27. C.H. Hsu and F. Mansfeld, Concerning the conversion of the Constant Phase Element Parameter Yo into a Capacitance *Corrosion*, 2001, 57, 747.
28. Y. Liu, P. Visser, X. Zhou, S. B. Lyon, T. Hashimoto, A. Gholinia, G. E. Thompson, G. Smyth, S. R. Gibbon, D. Graham, J. M. C. Mol and H. Terryn, An investigation of the corrosion inhibitive layers generated from lithium oxalate-containing organic coating on AA2024-T3 aluminium alloy, *Surface and Interface Analysis*, 2016, 48, 798-803.
29. B. Hirschorn, M. E. Orazem, B. Tribollet, V. Vivier, I. Frateur and M. Musiani, Determination of effective capacitance and film thickness from constant-phase-element parameters, *Electrochimica Acta*, 2010, 55, 6218-6227.
30. Y. B. Amor, E. M. M. Sutter, H. Takenouti, M. E. Orazem and B. Tribollet, Interpretation of Electrochemical Impedance for Corrosion of a Coated Silver Film in Terms of a Pore-in-Pore Model, *Journal of The Electrochemical Society*, 2014, 161, C573-C579.
31. J. R. Davis, *Corrosion of aluminum and aluminum alloys*, ASM International, 1999.
32. R. G. Buchheit, R. P. Grant, P. F. Hlava, B. McKenzie and G. L. Zender, Local dissolution phenomena associated with S phase (Al2CuMg) particles in aluminum alloy 2024-T3, *Journal of the Electrochemical Society*, 1997, 144, 2621-2628.
33. F. Andreatta, H. Terryn and J. H. W. De Wit, Corrosion behaviour of different tempers of AA7075 aluminium alloy, *Electrochimica Acta*, 2004, 49, 2851-2862.

Chapter 10

Conclusions & Recommendations

10.1 Introduction

The aerospace industry has been relying on chromate-based processes for the protection of aircraft structures for many decades. However, the use of these chromate-based processes is not acceptable anymore from a health and environmental perspective. Legislations, such as REACH, are being implemented and are forcing the industry to replace chemical substances of very high concern with environmental friendly and safe alternatives.

Chapter 2 of this thesis explained the philosophy of corrosion control in the aerospace industry, the concept of active corrosion protection, and discussed the state of the art, progress and challenges in chromate replacement over the recent years. One of the largest remaining challenges is the chromate replacement in active protective coatings used for the protection of aircraft structures. Chromate compounds are widely used as leachable corrosion inhibitors in organic coatings. They are versatile corrosion inhibitors that are active at low concentrations, work in a wide pH range and are suitable in different electrolytes. Chromates act as cathodic and anodic inhibitors, limiting both the oxygen reduction and metal dissolution reactions. When chromates leach from the coating matrix into a defect area they provide fast, effective and long-term corrosion protection by the formation of a protective film on the aluminium surface. A combination that, most of the current available alternative chromate-free corrosion inhibitors do not have.

Usually four key criteria are put forward, when considering leachable inhibitors in active protective coatings. The inhibitor must be (sparsely) soluble, provide fast and effective inhibition and the inhibition must be irreversible. Many different corrosion inhibitors have been proposed and evaluated as leachable corrosion inhibitor in coatings over the last three decades. However, up to now no viable candidate has been identified that performs as good as chromates and meets all the aerospace requirements.

In 2010, Li-salts have been identified as a promising alternative for chromates when used as leachable inhibitor in organic coatings. However, industrial implementation in the aerospace industry requires fundamental understanding of the corrosion protection mechanism of aerospace aluminium alloys. Hence, the scientific objective of this PhD thesis was to unravel the active protection mechanism of the Li-leaching coating technology. First, it was important to characterize the morphology and composition of the protective layer that is locally formed in a coating defect when Li-salts are released from the coating matrix. Secondly, it was crucial to understand the underlying mechanism under which conditions the formation of a protective film initiates and evolves, and what provides the layer its corrosion protective properties. Eventually, the versatility of the Li-leaching coating technology was demonstrated, by investigating the chemical throwing power of the Li-leaching inhibitor technology and its ability to provide irreversible protection. The last part of the thesis discusses the active corrosion protective properties of the Li-leaching coatings on a range of Al alloys with different intrinsic electrochemical activity.

10.2 The effect of Li-leaching coatings in a coating defect

Organic coatings loaded with Li-salts as leachable corrosion inhibitor demonstrated effective corrosion inhibition when they were exposed to corrosive conditions. It was found that, coatings without Li-salts showed severe (localized) corrosion phenomena after only 168 h NSS exposure, whereas the coatings loaded with Li-salts showed clean defect areas without corrosion products. Further analysis revealed that a layer was formed throughout the defect area.

The first aim of the work was to characterize morphology and composition of this layer that locally forms in the defect area when Li-salts leach from the organic coating. A very specific morphology composed of three distinct regions, comprising a columnar outer region, a porous middle region and a dense inner region at the aluminium substrate was observed (Fig. 10.1). It can be stated that this morphology was identified as being characteristic for the Li-leaching technology and the formation of the layer is regarded as the basic concept for the active protection mechanism throughout this entire study. The different phases of the formation were further analysed and linked with the local electrochemical protection mechanism.

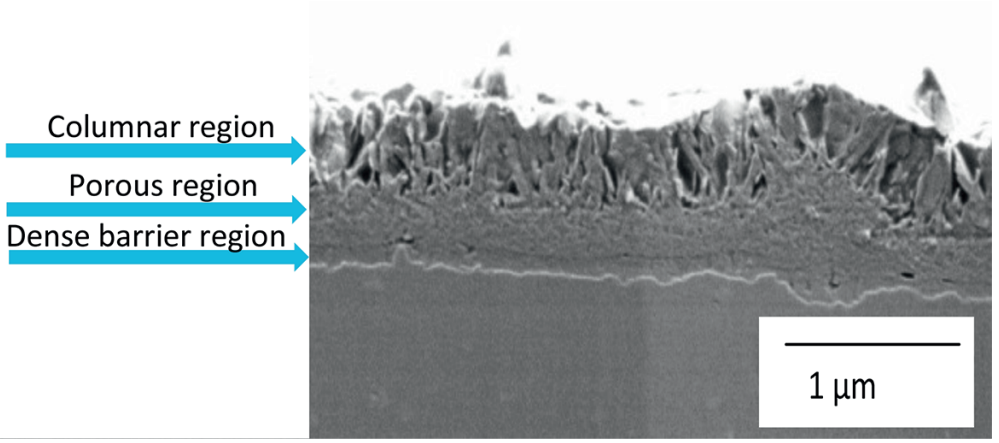

Figure 10.1 *SEM cross-sectional micrograph of the typical three-layered morphology of a protective layer generated from a Li-leaching coating.*

The compositional analysis of the protective layer showed that the layer mainly comprised aluminium, oxygen, lithium and some traces of magnesium and copper. TEM-EELS analysis revealed that lithium was distributed throughout the layer. These observations indicate that the protective layer is essentially an aluminium oxide/hydroxide layer and that Li-ions were able to leach from the organic coating matrix and were involved in the formation of the protective layer.

10.3 The formation mechanism of the protective layer

After the first observations reported in Chapter 3, a multi-stage mechanism was proposed for the formation of the protective layer based on the available literature of the behaviour of aluminium in (moderate) alkaline solutions.

With this hypothesis, the initiation and growth of the protective layer from an organic coating in a defect area was studied in more detail to understand the formation of this three-layered layer (Chapter 5). It was found that Li-salts were able to leach rapidly from the organic coating matrix and generated moderate alkaline conditions with a pH of 9 to 10 in the defect area. The formation of the layer in the defect area was followed with SEM as function of exposure time to the NSS test. Different stages of formation were observed, the initial formation started at the walls of the defect. This was followed by the lateral coverage of the defect and finally, the layer grew as a function of exposure time in the NSS test. Complementary XPS and AES depth profiles revealed that the formation in the defect involves a coverage and a subsequent growth phase. The observations also clearly indicate that the formation of the layer have the characteristics comparable to a conversion coating process.

Therefore, it was decided to investigate the formation of these protective layers in a more controlled manner by mimicking the aqueous conditions of a defect area in an electrochemical cell. Similar protective layers, as observed in coating defects, were generated under conversion conditions using moderate alkaline conditions (pH ≈ 10.6). Characterization studies of the layer at different stages of the formation provided an enhanced view on the formation of these protective layers, supporting the proposed hypothesis of a multi-step mechanism.

The investigation revealed that the formation mechanism involves three stages (Fig. 10.2):

- Stage I oxide thinning
- Stage II anodic dissolution and initial film formation
- Stage III growth through a competitive film formation and dissolution process

Stage I, the oxide-thinning step, occurs quickly under the alkaline conditions and the presence of chloride ions. This creates the conditions for Stage II, resulting in the anodic dissolution of aluminium from the alloy matrix resulting in the formation of an aluminium hydroxide gel layer on the aluminium substrate due to the alkaline conditions. It is known that the thickness of this aluminium hydroxide gel layer depends on the pH of the electrolyte present because under alkaline conditions, aluminium hydroxide is known to react with hydroxyl ions (OH^-) and chemically dissolves at the aluminium hydroxide gel/electrolyte interface. As a consequence, this dissolution of the aluminium hydroxide layer will trigger further anodic dissolution of aluminium from the aluminium matrix. This mechanism leads to Stage III of the formation mechanism, the competitive growth and dissolution process at the outer region of the layer.

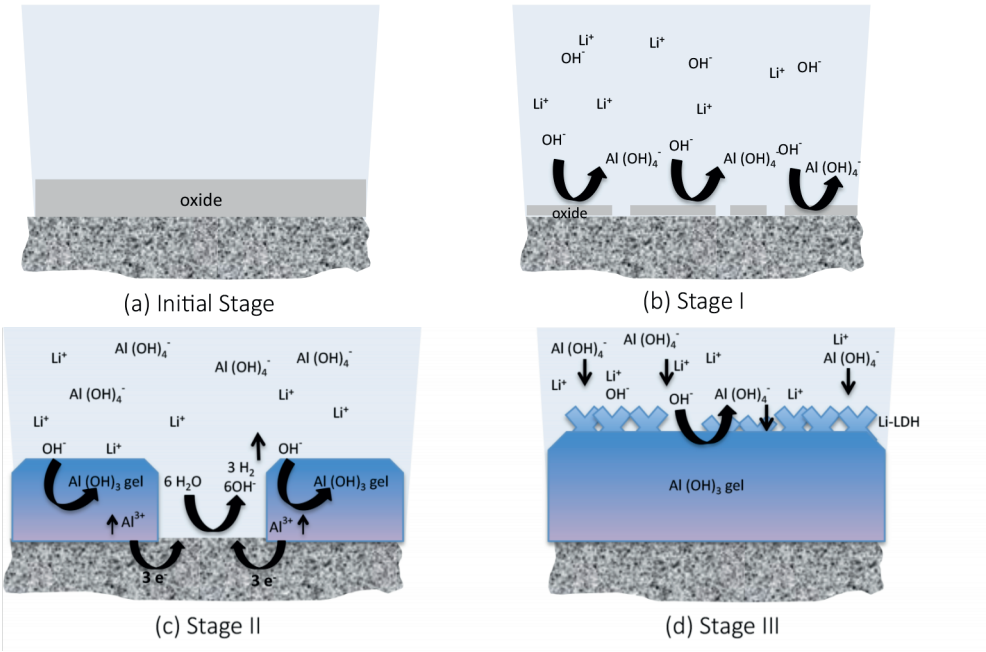

Figure 10.2 Schematic representation of the formation of the passive layer: (a) native oxide; (b) oxide thinning process; (c) Initial aluminium hydroxide layer formation (anodic dissolution); (d) competitive growth/dissolution process and Li intercalation

Based on the available literature on the behaviour of alkaline lithium solutions on aluminium, it was assumed that the formation of Li-LDH was an essential part in the formation of this protective layer. However, from the experiments in this thesis it appeared that Li-LDH was not always formed and in some cases the outer layer had the characteristics of a hydrated aluminium oxide (pseudoboehmite) containing some lithium. It is well known that Li-LDH is formed under very alkaline conditions (pH>10) but amorphous aluminium hydroxides are known to transform into a pseudoboehmite due to an ageing process under moderate alkaline conditions.

The compositional analysis of the protective layers with XPS and ToF-SIMS revealed that in general three different species can be identified at the surface layer depending on the relative concentration of lithium available in the defect area: Li-LDH is formed at high concentrations of lithium, Li-PB at lower concentrations of lithium and PB at very low concentrations. It was found that Li-LDH was only formed in specific situations like: preparation of the reference samples (pH> 11), during the controlled conversion process in an electrochemical cell at pH 10.6, and in narrow defects with fast leaching Li-leaching coatings. Further analyses, showed that in wider defect areas protective layers were formed which were identified as Li-PB, a lithium containing pseudoboehmite. In the mechanistic study, it was observed that the intercalation of lithium (>1 at.%) only occurred

in Stage III, the growth and dissolution process. Thus it can be concluded that the final composition of the outer layer depends on the pH of the electrolyte and the concentration of lithium present. High pH, (pH>10) and high lithium concentration will lead to Li-LDH and moderate pH (pH 9-10) and lower concentrations lead to Li-PB. This implies that the formation Li-LDH is a side-reaction which is not always desirable because layered double hydroxides are very porous materials. Furthermore, there is no evidence found of active intercalation of carbonate, oxalate or other ions in the protective layers, which makes them more or less buffering compounds to achieve the alkaline conditions in the defect area.

10.4 The protective properties of the Li-leaching technology

Enhanced insight in the physical morphology was an important step to determine the origin of the corrosion protection properties of the layer and the electrochemical analysis of the system. Considering the three-layered morphology of the protective layer, it was logical to postulate that the dense inner-layer provides the protective nature of the layer. A combined approach of microscopy and EIS analysis was used to link the electrochemical properties with the physical properties of the protective layer during the formation of the layer. An electrochemical model allowed attributing the corrosion protective properties of the layer to the dense inner layer. The corrosion protective effect of the inner barrier layer was also demonstrated by the work during the formation in the electrochemical cell.

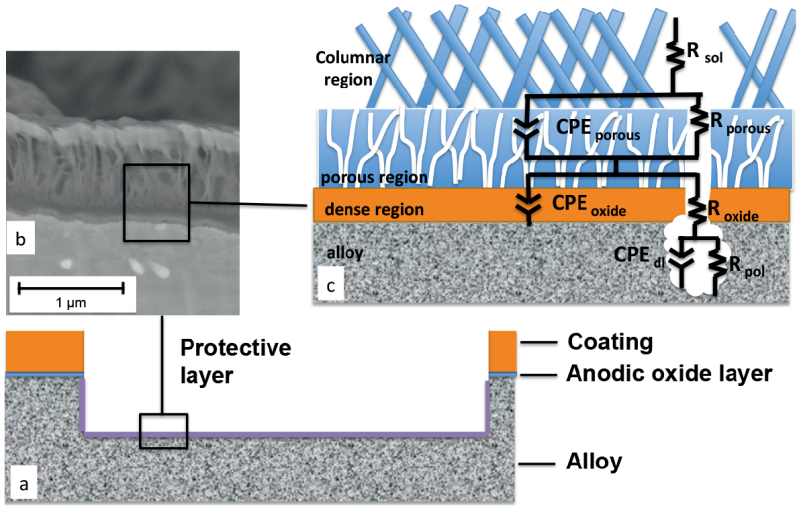

Figure 10.3 SEM cross-sectional micrograph of the typical three-layered morphology of a protective layer generated from a Li-leaching coating.

The fast formation of the protective properties of layer was demonstrated using EIS in combination with (local) potentiodynamic measurements revealing effective corrosion inhibition after only 2 hours exposure. Once the protective layer is formed it is able to provide long-term corrosion protection. This was demonstrated in industrial accelerated exposure tests but also by SVET analysis.

10.5 On the importance of irreversibility.

A comparison of the active protective properties of Li-salts and organic corrosion inhibitors by a combined approach of electrochemical methods, leaching profiles, optical observations, surface roughness and weight-loss measurements, revealed the fast, effective and irreversible corrosion inhibition behaviour of Li-salts on aluminium, whereas the organic corrosion inhibitors demonstrated a reversible behaviour.
The organic corrosion inhibitors are very efficient inhibitors when available at a sufficient concentration in an electrolyte, but they were not able to protect the defect area when incorporated in a coating matrix. The Li-salts were able to provide good corrosion protection from a coating and in an electrochemical cell.

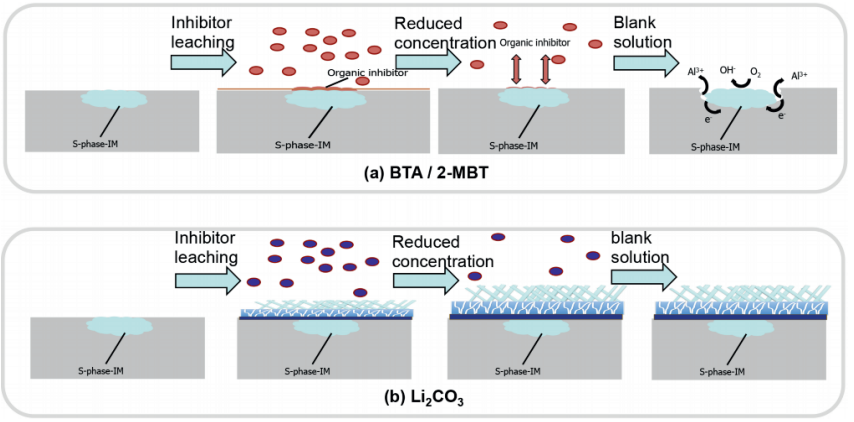

Figure 10.4 The schematic illustration on the importance of irreversibility of the corrosion inhibition mechanism comparing (a) organic corrosion inhibitors and (b) Li_2CO_3 *as leachable inhibitor*

The formation of the irreversible protective aluminium oxide/hydroxide layer, covering both cathodic and anodic areas of the aluminium matrix, limiting the reduction and oxidation reactions is from a mechanistic perspective very different from the inhibiting mechanism of organic corrosion inhibitors such as benzotriazole and 2-mercapto-benzothiazole. These organic corrosion inhibitors are well known for their efficient corrosion inhibitive properties on AA2024-T3 and AA7075-T6 through their ability to complex with the copper-containing intermetallic particles. The coverage of these copper containing intermetallic particles with organic corrosion has been one of the main strategies to prevent corrosion on AA2024-T3 and AA7075. However, this study revealed that this

corrosion mechanism appears to be reversible when the inhibitor concentrations decreased resulting in severe corrosion of the aluminium matrix.
These investigations showed that the irreversible behaviour of the corrosion inhibitor is an important factor in addition to fast and effective inhibition. Li-salts are soluble and inhibitor-leaching experiments demonstrated that Li-salts could leach rapidly from the coating matrix. The type of Li-salt and or the loading into the coating matrix can influence the rate of release. The corrosion inhibition in the defect area occurs fast and effective by the formation of a protective layer providing the Li-leaching coating technology all essential criteria needed for active protective coatings that rely on inhibitor leaching for the protection of aluminium alloys.

10.6 Versatility of Li-based inhibitors in organic coatings

Corrosion inhibitors need to be versatile to perform under different conditions. Therefore, the performance of Li-salts as leachable corrosion inhibitor in organic coatings was investigated on samples with defect areas with increasing widths and on aluminium alloys with different electrochemical activity. It was found that the corrosion protection of the Li-leaching coatings is not limited to only small defects or one specific aluminium alloy. This demonstrated the versatile character of Li-salts when used as leachable inhibitor in organic coatings.

The chemical throwing power, known as the distance over which a corrosion inhibitor is able to protect a defect, was investigated. This parameter is strongly connected to the leach rate of the inhibitor and the critical concentration needed to obtain effective inhibition. Therefore, Li-leaching coatings were formulated with different Li-salts as leachable corrosion inhibitor and different loadings to obtain coatings with fast and slow leaching kinetics. The chemical throwing power was assessed by evaluating the distance Li-inhibitors are able to protect using coating defects with increasing widths from 0.5 up to 6 mm. Depending on the inhibitor concentration in the organic coating, the Li-leaching coatings were able to effectively protect defect areas with a width up to 6 mm in industrial accelerated exposure tests (NSS ASTM B-117). The coatings with fast leaching kinetics (high loading) were able to protect defects with a width up to 6 mm and the coatings with slower leaching kinetics (low loadings) were able to effectively protect defects up to 3 mm. SEM analyses showed that the defects were effectively protected with a protective layer.

ToF-SIMS was used to map the lithium spread (distribution and relative concentration) in the defect areas with increasing widths. From this analysis it was observed that the lithium leached quickly and distributed evenly throughout the defect areas. In addition, the surface composition of the protective layer was unravelled using an NMF analysis on the ToF-SIMS data sets. This analysis revealed that Li-PB is the main surface component encountered in the protected defect areas and that Li-LDH appears to be a side-product, which is generated in situations with high lithium concentrations (e.g. small defect areas and fast leaching kinetics (Fig. 10.5)). This work also demonstrated that only a low amount of leached lithium-ions is needed to obtain effective corrosion inhibition.

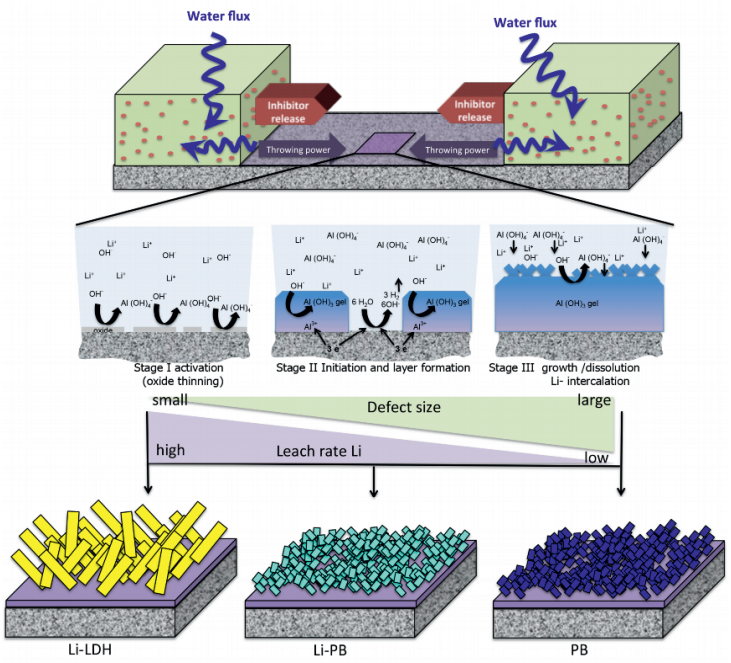

Figure 10.5 Chemical throwing power: the surface composition of the protective layer in the defect related to the Li leach rate and the size of the coating defect.

Alloying elements such as Cu, Mg, Zn or Si are added to the aluminium to influence the physical and mechanical properties of the alloys to make them suitable for their specific applications. However, the additions of these alloying elements and the subsequent treatments (tempering) have a large influence on the microstructure and corrosion resistance of the aluminium alloy. It is known that chemical conversion coatings (e.g. Zr/Ti conversion coatings) can be very sensitive to different alloys and their surface chemistry and electrochemistry. Since the formation of the layer in the defect area has the characteristics of a conversion layer, the active protective properties of the Li-leaching coatings were investigated on different aluminium alloys with a different electrochemical activity using microscopy and electrochemical techniques. The results show that Li-leaching coatings were able to effectively provide corrosion inhibition on a range of aluminium alloys independent of their metallurgy and electrochemical activity. The largest corrosion inhibiting effects were observed on high strength aluminium alloys, AA2024-T3 and AA7075-T6, which are known for their active and corrosion susceptible behaviour. The Li-leaching coatings also suppressed localized corrosion and provided additional corrosion resistance on more corrosion resistant aluminium alloys such as AA5083-H111 and AA6014-T4. These results provided a further insight into the aspects of the corrosion protective mechanism and indicate the versatile nature of this novel corrosion inhibiting technology.

10.7 The role of lithium

From the work in this thesis it can be concluded that the Li-leaching coatings provide very fast, effective, and irreversible corrosion inhibition by the formation of a protective layer on the aluminium substrate through a multi-step mechanism, which is comparable to a chemical conversion process. Li-salts are relatively soluble and able to leach rapidly from the coating matrix. The Li-salts are involved in the alkalinisation of the electrolyte in the defect area, which initiates the oxide thinning process. The mechanistic study of Chapter 6 suggests that the lithium-ion does not play a prominent role in the initial stages of the formation of the protective layer (Stage II). However, lithium is clearly involved in Stage III of the formation, the competitive growth and dissolution process. High concentrations of leaching Li-salt can lead to the formation of Li–LDH and low concentrations lead to the formation of Li-PB. These observations provide an enhanced insight of the composition of the porous outer layer and the different morphologies that have been observed. In addition it suggests that the inhibitive mechanism does not need the formation of Li-LDH, but the composition of the outer layer is a result of the lithium concentration involved in the inhibiting process.

That leaves us with a remaining question, what is the role of lithium in the stabilization of dense amorphous aluminium hydroxide layer at the aluminium substrate that provides the corrosion inhibiting properties to the protective layer. Lithium was detected throughout the protective layer and especially in the dense aluminium hydroxide layer using the TEM-EELS analysis. No significant amounts of lithium were observed in the inner layers with XPS, this might indicate that the concentration of lithium in the dense layer is less than 1 at %.

There must be a role for lithium there because in absence of Li-salts as leachable inhibitor, no protective layers are formed in the coating defects. Amorphous aluminium hydroxides are known as effective sorbents of Li-salts Therefore, it can be hypothized that lithium-ions are able to intercalate with the aluminium hydroxide gel to generate very small grain size particles or even an amorphous structure that can result in a dense impermeable protective layer. However, in order to investigate this overall hypothesis, additional research with inorganic chemistry disciplines is required.

10.8 Connecting science with product development.

The transition towards chromate-free coating technology provides a major challenge for the aerospace industry. The chromated coating technology is deeply embedded in the current design, specifications, corrosion management and maintenance programs. Chromates have a proven track record and scientists only started to investigate the corrosion inhibitive mechanism when it became apparent that chromates had to be replaced. For a long time, efforts focused on mimicking chromates. Many different

corrosion inhibitors were investigated but the performance of the alternative corrosion inhibitors did not meet the same performance as the trusted chromates. This raises the question whether it will ever be possible to provide the same corrosion protection as chromates and to what extend is the performance of the current chromate-leaching primers over-engineered? By fact, new chromate-free corrosion inhibitors will provide a different performance compared to chromates. Therefore, it is important to provide as much as possible information about these new chromate-free corrosion inhibiting technologies to increase the confidence to stakeholders in the aerospace industry to make the decision to start the transition to chromate-free coating technology and eliminate chromates as leachable corrosion inhibitor from the aerospace industry.

The knowledge and understanding of the corrosion inhibiting mechanism of the Li-leaching coating technology generated in this research is of key importance for the further development of this new chromate-free coating technology and instrumental to increase the confidence of the stakeholders in the aerospace industry concerned with the implementation of chromate-free active corrosion protective coating systems for aerospace aluminium alloys.

The work presented in this thesis was derived from model coating systems. It must be considered that the formulations of industrial coating concepts are more complicated in order to obtain a coating with a complete set of properties (e.g. adhesion, chemical resistance, flexibility) to protect the structure of an aircraft during its service life. In this work is was demonstrated that, despite their relatively high solubility, lithium salts can be formulated into a coating matrix similar to a chromated primer used today. Further work demonstrated that Li-leaching technology can be formulated in industrial coating systems and demonstrated their ability to meet the industrial corrosion resistance requirements in a direct comparison with a chromate loaded primer after 3000 h NSS exposure.[1] The successful implementation and active protective properties underline the potential of the Li-leaching coating technology.

One of the most important remaining challenges to address is to understand how the performance of the Li-leaching corrosion inhibiting primer under accelerated test conditions relates to long-term in-service performance. Therefore it is important to gain more insight on how the coatings age under in-service conditions and what leaching kinetics are needed to provide optimal corrosion protection during 30 years of service life. Leaching is a complex process that involves the dissolution of corrosion inhibitors via interconnected pathways from the coating matrix and it is important to understand which parameters control the dissolution rate of Li-salts from the organic coating matrix. Leaching kinetics can be influenced by the coating formulation: Cervellera et al. are studying the effect of different coating formulation parameters (e.g. PVC, inhibitor content, inhibitor solubility and the polymer matrix chemistry) on the leaching kinetics in relation to the active corrosion protective properties of the Li-leaching coatings.[2] Leaching and aging of the coatings will result in lithium depletion from the coating which is currently studied by Hughes et al.[3]

The knowledge and understanding from these studies can provide new insights and the connection on how to formulate with Li-salts in industrial coatings for long-term corrosion protection.

10.9 Reflections and recommendations

"The world as we have created it, is a process of our thinking. It cannot be changed without changing our thinking." as stated by Albert Einstein can be applied on the endeavour to replace chromates as leachable inhibitor in organic coatings. When we define "the world as we created " as the current status of chromate-free corrosion research, there is clearly a need to change our thinking. The chromate-leaching systems of today are embedded in processes, specifications, have a very good track record, provide confidence and are the benchmark for the current performance of active protective coatings. Since more than 30 years, the scientific world has been searching for alternative leachable corrosion inhibitors considering a range of inorganic and organic corrosion inhibitors. Over the years, promising candidates such as cerium and benzotriazole and 2-mercaptobenzothiazole have been and are still investigated. Although, no real breakthrough has been achieved to date, which can be considered as a concern. From the inhibitor perspective for the protection of aluminium alloys, it seems that research community started to run into circles and ran out of ideas for new corrosion inhibitors. In addition, it can be observed that the focus, interest and funding opportunities of the academic research community shifts to the corrosion protection of magnesium alloys at the expense of aluminium alloys.

The discovery of the corrosion inhibiting properties of Li-salts, when used as leachable inhibitor in organic coatings, is a new promising lead that provides a refreshed view on the concept of corrosion protection of aluminium alloys. However, not all aspects of the exact role of lithium in the stabilization of protective layer are fully clear yet and the Li-leaching technology is not the Holy Grail that solves all the issues and challenges to consider it as a drop-in technology for chromates. More research is needed but it can be stated that the technology provides a new opportunity for corrosion protection of aluminium alloys and the understanding obtained in this thesis can spark new ideas and even lead to a new class of corrosion inhibitors. It is interesting and encouraging to observe that other researches have picked up the concept of Li-salts as corrosion inhibiting technology for aluminium. For example by using Li-salts for sealing of anodic films[4], incorporation of Li-salts as leachable inhibitor in nano-porous diatom algae exoskeletons[5], Li-salts in embedded electrospun inhibiting nanonetworks[6] and in hybrid sol gel coatings.[7]

It is important change the way how to consider corrosion inhibition: the fast and effective formation of an irreversible layer via a conversion (or corrosion) process is very much different from the traditional cathodic inhibiting or copper inhibiting approaches using organic corrosion inhibitors. The Li-leaching technology initiates a general corrosion process to generate a protective layer on the aluminium alloy by the dissolution of the

aluminium matrix. The corrosion inhibition mechanism in not new in nature but can be a new avenue in future corrosion research.

We should change the view how to evaluate corrosion inhibitors for active corrosion protection. It is of great importance to look beyond the results in the electrochemical cell. Processes in an electrochemical cell can be totally different compared to the thin film processes when considering atmospheric corrosion. When corrosion inhibiting activity is observed, aspects such as irreversibility leach rate and inhibition from a coating matrix should become standard practice.

For future work, it is sensible to take a step back and consider what has been learned from previous approaches and the Li-leaching corrosion inhibiting mechanism and we should change again our thinking on how to evaluate future chromate-free inhibitor technologies, looking at the role of leaching, corrosion protective properties, and how to generate stable corrosion protective layers and inhibitor irreversibility in order to make the next steps forward to provide a new corrosion inhibiting technology to the industry.

The view on testing the corrosion inhibiting activity of coatings should be changed or at least reconsidered. It is known that there is no relationship between accelerated testing data and field performance data and long lifetime behaviour under real environmental conditions can not be simulated with the current accelerated testing procedures and service-life performance testing takes too much time (5-10 years). This is a major obstacle for the product development of new coatings in general but as well for new active protective coating concepts. Therefore the development of alternative accelerated test methods is of great importance and service life prediction tools are of great importance. [8, 9]

In this thesis it was demonstrated that Li-leaching coatings possess all the key criteria, such as inhibitor solubility, fast, effective, and irreversible corrosion inhibition. The results demonstrate that the Li-leaching technology is a promising technology, which potentially can provide a new class of corrosion inhibitors for the protection of aluminium alloys and change the current philosophy of corrosion protection.

References

1. P. Visser, Y. Liu, H. Terryn and J. M. C. Mol, Lithium salts as leachable corrosion inhibitors and potential replacement for hexavalent chromium in organic coatings for the protection of aluminum alloys, *Journal of Coatings Technology and Research*, 2016, 13, 557-566.
2. A. Cervellera-Dominguez, X. Zhou, P. Visser, C. Avendano and S. R. Gibbon, Effect of pigment volume concentration on the leaching behaviour of active corrosion inhibitor in a model aerospace primer, *Aluminium Surface Science and Technology Symposium (ASST), 27-13 May, 2018, Helgingør, Denmark*, 2018.
3. A. Hughes, J. Laird, C. Ryan, P. Visser, H. Terryn and A. Mol, Particle Characterisation and Depletion of Li2CO3 Inhibitor in a Polyurethane Coating, *Coatings*, 2017, 7, 106.
4. D. Mata, M. Serdechnova, M. Mohedano, C. L. Mendis, S. V. Lamaka, J. Tedim, T. Hack, S. Nixon and M. L. Zheludkevich, Hierarchically organized Li-Al-LDH nano-flakes: a low-temperature approach to seal porous anodic oxide on aluminum alloys, *RSC Advances*, 2017, 7, 35357-35367.
5. P. J. Denissen and S. J. Garcia, Exploring long-term protection at large damage sites in aerospace coatings using inhibitor and carrier synergies, *EuroCorr Conference*, 2018, Krakow, Poland.
6. C. D. Dieleman, P. J. Denissen and S. J. Garcia, Long-Term Active Corrosion Protection of Damaged Coated-AA2024-T3 by Embedded Electrospun Inhibiting Nanonetworks, *Advanced Materials Interfaces*, 2018, 5, 1800176.
7. A. Trentin, S. Vargas Harb, C. Valentim Santilli, P. Hammer, K. Marcoen, A. Lutz, T. Hauffman and H. Terryn, Improved corrosion resistance and lifespan of silica-PMMA hybrid coatings modified with cerium and lithium ions, *Eurocorr Conference*, 2018, Krakow, Poland.
8. D. Thierry, A common industrial approach towards the development of a reliable corrosion test in the aerospace industry, *Eurocorr Conference*, 2018, Krakow, Poland.
9. D. Pecko, D. De Wilde, A. Hubin, T. Hauffman, G. Van Assche, N. Van Den Steen, H. Simillion, M. Rohwerder, J. Deconinck and H. Terryn, Knowledge and technology platform for prediction of durability and lifetime of organic coated metals under long-term environmental corrosion, *EuroCorr Conference*, 2018, Krakow, Poland.

&

Acknowledgments,
List of publications,
and
About the author

Acknowledgments

This dissertation is the result of an exciting journey and an unforgettable experience. Many people asked me how I could achieve such a piece of work next to my responsibilities within my private life and AkzoNobel. First of all, I consider it as a great privilege to have received the opportunity to study my invention in an academic setting. It was a dream for me to pursue a PhD and to leave a footprint in the aluminium corrosion community. At the start of such an adventure you do not really know what you are getting yourself into. First, there is the plan, then the start of the journey, initially, you flow like a vessel on a river, later you gain control and set direction and you can influence the flow. During the journey, I have encountered some obstacles and also some rapids, I have learned a lot from others but also about myself, I have visited very nice places and I have met new colleagues and friends along the way. With this dissertation, the journey comes to an end but also marks a new beginning. During the journey there were many persons that contributed to the work that resulted in this dissertation and I would like to express my gratitude to all who helped me to complete this journey.

First of all, I would like to thank Hans Polak for challenging and supporting me to start this endeavour getting the funding and time from the AkzoNobel Aerospace Coatings management team to do this research alongside my AkzoNobel responsibilities. Also. I would like to thank Leo van der Ven for setting up the contacts with Delft University of Technology and guiding me through the academic environment in the first years.

Furthermore, I would like to thank my promotors Professor Arjan Mol and Professor Herman Terryn for accepting me into their research group. It was a pleasure to work with you. Thank you for your support, patience and scientific input during our discussions and balancing between in the force field of the academic and industrial interests. Both of you were always available for discussions, questions and setting the right scientific direction. I am greatly impressed how you manage to support your PhD students in such a positive way next to your busy schedule. After 16 years in industry, I really felt as a student again and thank you for introducing me into the scientific community of aluminium and corrosion. I really enjoyed the elaborate process of writing our publications. Arjan, thank you for your detailed and analytical way of reviewing my papers. I never noticed that I use so many double spaces in my writing. Herman, thank you for your valuable suggestions to rearrange the set-up of my manuscripts to come to the best scientific message. With this great team work I was able to succeed in the peer review process and publish in high profile journals. Thank you both for the great times at conferences and outings. I really enjoyed the informal atmosphere of the group and friendship between the groups in Delft and Brussels, this is a true strength of the group and have provided really fun memories and revived my passion for Belgian tripel beers.

Thank you to the co-authors that contributed to my papers. Your interest in my research, your efforts, our valuable discussions and your contributions really made a

enormous difference. Thank you to the team of the University of Manchester, especially Yanwen Liu for revealing the three layered morphology of the protective layer, Alexander Lutz (VUB) for the SIET measurements, Kristof Marcoen (VUB) for your dedication and endurance with the ToF-SIMS analysis, and Mats Meeusen (TUD) for all the discussions about the impedance data and fitting.

I would like to express my gratitude to the entire SURF team of the Vrije Universiteit Brussel where I performed most of the surface analytical measurements, thank you for making me feel welcome and the fun times. Especially, I would like to thank Oscar Steenhaut for helping me to work with the XPS and Auger, Marc Raes for his assistance with the SEM and for the enjoyable hours after work in the koffie-kot.

I also would like to thank all my colleagues of the corrosion technology and electrochemistry (CTE) group for over the years: Shoshan, Jose, Axel, Peyman, Laura-Lynn, Majid, Mats, Joost, Ali. Special thanks to Yaiza for getting me started in the beginning, Agniezska for your help in the lab and all micro-cell measurements and Zeynep for your work on the reversibility of the corrosion inhibitors

Thank you to all my AkzoNobel colleagues, who sometimes suffered due to my absence but kept the projects running when I was at the University, Especially: Marc, Gerrit, Richard, Wilfried, Emmanuelle, Floor and all interns who supported my project during the years. Furthermore, I would like to thank my other and former AkzoNobel colleagues, Dimitri and Lennaert in Deventer and Simon Gibbon, Derek Graham from Felling for the fruitful discussions. Special appreciation for Wilma Ravesloot and Lennaert Klerk for the numerous amounts of ion-milled samples.

Finally and most of all, I would like to thank my friends and family for their unconditional support over the years. I tried to balance the work to the best of my abilities but I realize that it was not always easy for you. Voor mijn jongens, Rik and Sem: bedankt voor jullie ongelofelijke geduld over de laatste jaren. Volg je hart, doe wat je leuk vindt en waar je goed in bent. Als je iets heel graag wilt kan je het bereiken. Blijf je verbazen over misschien de kleinste en normaalste dingen en dan komt het wel goed. Ik hou van jullie.

Lieve Jolanda, zo onverwacht maar gegroeid tot iets speciaals en heel dierbaars. Dank je wel voor je liefde, steun, geduld, het luisteren, aanmoedigen maar vooral de gezellige tijden en avonturen. Jij bent mijn rustpunt en soulmate en dat is een heerlijk gevoel. Je bent een fantastische vrouw. I love you to the moon and back!

I would like to dedicate my thesis to my parents who always supported me unconditionally with all my endeavours.

Lieve Mam: Dank je wel voor je steun en je hulp in huis met de jongens. Ik weet dat je trots bent, maar ik ben nog veel trotser op jou! Ik vind je zo verschrikkelijk dapper en een enorme doorzetter. Ik hou van jou.

Lieve Pap: Je vond het razend interessant en je wilde er alles van weten. Je kon meer vragen dan Herman en Arjan. We konden uren praten en je was positief kritisch en je wilde altijd van de hoed en de rand weten. Ik weet dat je trots was en ik ben super trots op jou. Niets is vanzelfsprekend, ik zal me blijven verbazen. Ik mis je…….

List of publications

Book chapter

1) P. Visser , H.A. Terryn, J.M.C. Mol, Aerospace Coatings, in: A.E. Hughes, J.M.C. Mol, M.L. Zheludkevich, R.G. Buchheit (Eds.) Active Protective Coatings, New-Generation Coatings for Metals, Springer, Netherlands, (2016) pp. 315-372.

Peer reviewed articles

1) P. Visser, Y. Liu, X. Zhou, T. Hashimoto, G.E. Thompson, S.B. Lyon, L.G.J. van der Ven, J.M.C. Mol, H.A. Terryn, "The corrosion protection of AA2024-T3 aluminium alloy by leaching of lithium-containing salts from organic coatings", *Faraday Discussions*, 180 (2015) 511-526.

2) P. Visser, Y. Liu, H. Terryn, J.M.C. Mol, "Lithium salts as leachable corrosion inhibitors and potential replacement for hexavalent chromium in organic coatings for the protection of aluminum alloys", *Journal of Coatings Technology and Research*, 13 (2016) 557-566.

3) P. Visser, A. Lutz, J.M.C. Mol, H. Terryn, "Study of the formation of a protective layer in a defect from lithium-leaching organic coatings", *Progress in Organic Coatings*, 99 (2016) 80-90.

4) P. Visser, M. Meeusen, Y. Gonzalez-Garcia, H. Terryn, J.M.C. Mol, "Electrochemical Evaluation of Corrosion Inhibiting Layers Formed in a Defect from Lithium-Leaching Organic Coatings", *Journal of The Electrochemical Society*, 164 (2017) C396-C406.

5) P. Visser, Y. Gonzalez-Garcia, J.M.C. Mol, H. Terryn, "Mechanism of Passive Layer Formation on AA2024-T3 from Alkaline Lithium Carbonate Solutions in the Presence of Sodium Chloride", *Journal of The Electrochemical Society*, 165 (2018) C60-C70.

6) P. Visser, H. Terryn and J. M. C. Mol, "On the importance of irreversibility of corrosion inhibitors for active coating protection of AA2024-T3", *Corrosion Science*, 140 (2018) 272-285.

7) P. Visser, H. Terryn, J.M.C. Mol, "Active corrosion protection of various aluminium alloys by lithium- leaching coatings." *Surface and Interface Analysis*. (2019);1–12. https://doi. org/10.1002/sia.6638.

8) P. Visser, K. Marcoen, G.F. Trindade, M.L. Abel, J.F. Watts, T. Hauffman, J.M.C. Mol, H. Terryn, "The chemical throwing power of lithium-based inhibitors from organic coatings on AA2024-T3", *Corrosion Science*, 150 (2019) 194-206.
.

Co-authored papers:

1) Y. Liu, P. Visser, X. Zhou, S.B. Lyon, T. Hashimoto, M. Curioni, A. Gholinia, G.E. Thompson, G. Smyth, S.R. Gibbon, D. Graham, J.M.C. Mol, H. Terryn, "Protective Film Formation on AA2024-T3 Aluminum Alloy by Leaching of Lithium Carbonate from an Organic Coating", *Journal of The Electrochemical Society*, 163 (2016) C45-C53.

2) Y. Liu, P. Visser, X. Zhou, S.B. Lyon, T. Hashimoto, A. Gholinia, G.E. Thompson, G. Smyth, S.R. Gibbon, D. Graham, J.M.C. Mol, H. Terryn, "An investigation of the corrosion inhibitive layers generated from lithium oxalate-containing organic coating on AA2024-T3 aluminium alloy", *Surface and Interface Analysis*, 48 (2016) 798-803.

3) A. Hughes, J. Laird, C. Ryan, P. Visser, H. Terryn, A. Mol, "Particle Characterisation and Depletion of Li2CO3 Inhibitor in a Polyurethane Coating", *Coatings*, 7 (2017) 106.

4) J.S. Laird, A.E. Hughes, C.G. Ryan, P. Visser, H. Terryn, J.M.C. Mol, "Particle induced gamma and X-ray emission spectroscopies of lithium-based alloy coatings", *Nuclear Instruments and Methods in Physics Research Section B: Beam Interactions with Materials and Atoms*, (2017)

5) K. Marcoen, P. Visser, G. F. Trindade, M. L. Abel, J. F. Watts, J. M. C. Mol, H. Terryn and T. Hauffman, "Compositional study of a corrosion protective layer formed by leachable lithium salts in a coating defect on AA2024-T3 aluminium alloys", *Progress in Organic Coatings*, 119 (2018) 65-75.

6) M. Meeusen, P. Visser, L. Fernández Macía, A. Hubin, H. Terryn and J. M. C. Mol, "The use of odd random phase electrochemical impedance spectroscopy to study lithium-based corrosion inhibition by active protective coatings", *Electrochimica Acta*, 278 (2018) 363-373.

Conference presentations

1) P. Visser, J.M.C. Mol, H. Terryn, "Active protective properties of lithium-leaching coatings for aluminium alloys", *EuroCorr 2018*, 9-13 Sept 2018, Krakow, Poland

2) P. Visser, J.M.C. Mol, H. Terryn, "Characterization and Performance of lithium-leaching coating technology for the protection of aluminium alloys", *VIII Aluminium Surface Science and Technology (ASST)*, 27-31 May 2018, Helsingør, Denmark

3) P. Visser, Z. Devecioglu, H. Terryn, J.M.C. Mol, "Active protection of aluminium alloys: a comparative study of lithium-based and organic corrosion inhibitors", EuroCorr 2017, 3-7 Sept 2017, Prague, Czech Republic

4) P. Visser, H. Terryn, J.M.C. Mol, "Corrosion protection of coated aluminium alloys by lithium-based inhibitor technology", *10th International Workshop on Application of Electrochemical Techniques to Organic Coatings (AETOC)*, 25-28 April 2017, Billerbeck, Germany

5) P. Visser, J.M.C. Mol, H. Terryn, "The corrosion protective properties and inhibitor throwing-power of lithium-based coating technology on AA2024-T3", *EuroCorr 2016*, 11-15 Sept 2016, Montpellier, France

6) P. Visser, H. Terryn, J.M.C. Mol, "Performance and Mechanism of Lithium–based Coating Technology for the Protection of High Strength Aluminium Alloys", *21th International Conference on Surface Treatments in the Aeronautics & Aerospace Industries (SurfAir)*, 24-26 May 2016, Biarritz, France

7) P. Visser, J.M.C. Mol, H. Terryn,"Lithium-salts as a new class of corrosion inhibitors for the protection of aluminum alloys." *the FOCUS Conference of The Detroit Society for Coatings Technology*, 5 May 2016, Troy, Illinois, USA (Invited lecture)

8) P. Visser, H. Terryn, J.M.C. Mol, "Lithium-doped organic coatings for the protection of aerospace aluminum alloys", *Smart Coatings 2016*, 24-26 February, 2016 Orlando, USA (Invited lecture)

9) P. Visser, Y Liu, X. Zhou, Y. Gonzalez-Garcia, A. Kooijman, L.G.J. van der Ven, H. Terryn, J.M.C. Mol, "Lithium-based corrosion inhibiting coating technology for the protection of AA2024-T3", *EuroCorr 2015*, 6 - 10 September 2015, Graz, Austria

10) P. Visser, Y. Gonzalez-Garcia, H. Terryn, J.M.C. Mol, "Lithium-salts for the protection of aluminum alloys, a new class of corrosion inhibitors for chromate-free coating technology", *11th Coatings Science International Conference (CoSi)*, 22 -26 June 2015, Noordwijk, The Netherlands

11) P. Visser, Y. Gonzalez-Garcia, F. Andreatta, A. Kooijman, L.G.J. van der Ven, H.Terryn, J.M.C. Mol, "Corrosion inhibition of AA 2024-T3 by lithium-based coating technology", *VII Aluminium Surface Science and Technology (ASST)*, 17-21 May 2015, Madeira, Portugal

12) P. Visser, Y. Liu, X. Zhou, T. Hashimoto, G.E. Thompson, S.B. Lyon, L.G.J. van der Ven, J.M.C. Mol, H.A. Terryn, " The corrosion protection of AA2024-T3 aluminium alloy by leaching of lithium-containing salts from organic coatings", *Faraday Discussions Corrosion Chemistry*, 13-15 April 2015, London, United Kingdom

13) P. Visser, J.M.C. Mol, H Terryn,"*Characterization and performance of passive layers generated from lithium-based inhibitors for corrosion protection of AA 2024-T3"*, *EuroCorr 2014*, 8 - 12 September 2014, Pisa, Italy

Awards

The Innovation Award, for the presentation: "Lithium-salts for the protection of aluminium alloys, a new class of corrosion inhibitors for chromate-free coating technology", *11th Coatings Science International Conference (CoSi), 22-26 June 2015*, Noordwijk, The Netherlands

The Award for Technique, for the presentation: "Performance and Mechanism of Lithium–based Coating Technology for the Protection of High Strength Aluminium Alloys", *21th International Conference on Surface Treatments in the Aeronautics & Aerospace Industries (SurfAir)*, 24-26 May 2016, Biarritz, France

AkzoNobel Scientist of the Year Award (2018), in recognition for his efforts to understand the corrosion of aluminium alloys and connecting science with product development.

About the author

Peter Visser was born in February 1972 in Vlaardingen the Netherlands. In 1996, Peter completed his study organic chemistry at the Hoge School Rotterdam & Omstreken and joined AkzoNobel Aerospace Coatings in 1997. In the global development group, he was responsible for the development of several high solids primers and topcoats for the aerospace industry. In 2007, Peter shifted his focus and started to work on chromate-free primer technology for the protection of high strength aluminium alloys. Since then, he was responsible for the search, assessment and development of new chromate-free coating technology for active protective coatings and developed several chromate-free products for exterior applications. In addition to his work in AkzoNobel, Peter joined Delft University of Technology as PhD researcher in 2013. He has been working in the Corrosion Technology & Electrochemistry group of Professor Arjan Mol and Professor Herman Terryn to investigate the lithium-leaching chromate-free coating technology that was developed by AkzoNobel. In this project Peter investigated the lithium-leaching coating technology to obtain fundamental knowledge and understanding about the active protective mechanism when lithium salts are used as leachable corrosion inhibitor. In this project Peter has been collaborating with AkzoNobel, Vrije Universiteit Brussel, CSIRO and the University of Manchester. In 2018, Peter received the AkzoNobel Scientist of the Year for his efforts connecting the science from his academic work with the product development activities in AkzoNobel, resulting in a range of chromate-free primers for the aerospace industry. Currently, Peter is innovation project leader in the Expertise Centre Corrosion of AkzoNobel in Sassenheim, The Netherlands.

ACTIVE CORROSION PROTECTION OF AEROSPACE ALUMINIUM ALLOYS BY LITHIUM-LEACHING COATINGS

PETER VISSER